

Observational study of urban aerosols: Long range transport and estimation of their radiative forcing

A thesis submitted to

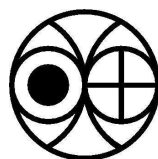
Gujarat University

for the degree of

Doctor of Philosophy in Physics

By

Dilip Ganguly



Space and Atmospheric Sciences Division
PHYSICAL RESEARCH LABORATORY,
AHMEDABAD - 380 009, INDIA

June, 2006

CERTIFICATE

I hereby declare that the work presented in this thesis is original and has not formed the basis for the award of any degree or diploma by any University or Institution.

Dilip Ganguly
(Author)

Certified by :

Prof. A.Jayaraman

(Thesis Supervisor)

Space and Atmospheric Sciences Division,

Physical Research Laboratory,

Navrangpura, Ahmedabad, INDIA

For
Ma and Baba

Contents

Acknowledgements	ix
Abstract	xi
1 Introduction	1
1.1 Atmospheric Aerosols	1
1.2 Radiation Budget of the Earth and Climate Change	3
1.2.1 Role of Aerosols	5
1.3 Importance of South Asian Region	6
1.4 Urban Aerosols	7
1.5 Present Study	9
2 Seasonal and inter-annual variations in aerosol characteristics over Ahmedabad	11
2.1 Site Description and Meteorology	12
2.2 Instrumentation and Measurements	16
2.2.1 Sun-Photometer	16
2.2.2 QCM cascade impactor	18
2.2.3 Aethalometer	19
2.2.4 Nephelometer	20
2.2.5 Aerosol Size Spectrometer	21
2.2.6 Micro Pulse Lidar	22
2.3 Results and Discussion	27
2.3.1 Aerosol optical depth	27
2.3.2 Aerosol mass concentration	32
2.3.3 Aerosol number size distribution	36
2.3.4 Black Carbon mass concentration	38

2.3.5	Aerosol absorption coefficient	43
2.3.6	Aerosol scattering coefficient	46
2.3.7	Single scattering albedo	49
2.3.8	Aerosol vertical profiles	53
2.4	Summary	56
3	Ship cruise study of aerosol characteristics over Bay of Bengal	59
3.1	Cruise track and Meteorology	60
3.2	Measurements and data analysis	61
3.3	Results and Discussion	64
3.3.1	Aerosol optical depth	64
3.3.2	Aerosol mass concentration	67
3.3.3	Aerosol number size distribution	70
3.3.4	Relationship between columnar and surface level aerosol characteristics . . .	75
3.4	Summary	79
4	Spatial variation in aerosol characteristics over Central India	81
4.1	Experiment and Meteorological Condition	82
4.2	Results and Discussion	85
4.2.1	Aerosol Optical Depth	85
4.2.2	Aerosol Mass Concentration and Size Distribution	87
4.2.3	Aerosol Scattering Coefficient	89
4.2.4	BC mass concentration	91
4.2.5	Aerosol Absorption Coefficient	92
4.2.6	Single Scattering Albedo	94
4.3	Summary	95
5	Aerosol-Fog interaction study over New Delhi	97
5.1	Measurement Site and Meteorology	99
5.2	Results and Discussion	102
5.2.1	Aerosol optical depth	102
5.2.2	Aerosol number size distribution	105
5.2.3	Black Carbon mass concentration	109
5.2.4	Aerosol absorption coefficient	113
5.2.5	Aerosol scattering coefficient	115
5.2.6	Single scattering albedo	118
5.2.7	Aerosol vertical profiles	120
5.3	Alterations in aerosol properties during a fog episode	123

5.4	Summary	128
6	Model estimates of aerosol radiative forcing and its sensitivity to various parameters	131
6.1	Methodology and Approach	132
6.2	Model estimates and Aerosol Radiative Forcing	139
6.2.1	ARF over Ahmedabad	139
6.2.2	ARF over Bay of Bengal	156
6.2.3	ARF over Central India	159
6.2.4	ARF over New Delhi	161
6.3	Summary	162
	Summary and Scope for Future Work	165
	References	171
	List of Publications	187

Acknowledgements

It is a pleasure to thank all those who helped me in various ways and made this thesis possible.

First and foremost I would like to thank and gratefully acknowledge Prof. A. Jayaraman for his enthusiastic supervision and excellent guidance throughout the duration of my thesis work. His understanding of the subject, encouraging attitude and personal guidance has been the source of inspiration for me. I have immensely benefited from the discussions with him and his critical evaluations for which I shall always be obliged to him.

I express my sincere thanks to Vinchi bhai and Rajesh for their help and support in maintaining various instruments in the laboratory and during field campaigns. I am also indebted to Late Prof. Kulkarni and Dr. Angom for teaching various skills in Fortran during my graduate course work which turned out to be very useful in my study.

I would like to thank Prof. Shyam Lal for coordinating the ISRO-GBP's Land Campaign I & II which became an important part of my present research. I express my sincere gratitude to Prof. M. M. Sarin for his involvement in the Land Campaign experiments and also being the chief scientist in one of my ship cruise studies over Bay of Bengal.

I thank Prof. S. K. Bhattacharya, Prof. S. D. Rindani and all other members of academic committee for critically reviewing the progress of my work and giving valuable suggestions at various stages of my research in this laboratory.

I acknowledge the Air Resources Laboratory, NOAA, USA for providing the HYSPLIT model and the wind data used in the air back-trajectory analysis and NOAACIRES Climate Diagnostic Center, USA for providing NCEP reanalysis data over various study regions. The Land Processes Distributed Active Archive Center (LPDAAC) of EOS, NASA is ac-

knowledgeed for proving the land surface reflectance data used in the study.

I take this opportunity to thank my friend Harish who has been my partner in most of the studies undertaken during the present research work. All kinds of discussions with him were always very interesting and entertaining. I shall always remember the excellent hospitality shown by his family during our memorable trip to Bhuj.

My special thanks to all members of our aerosol group Rama, Amit, Neeraj, Sudheer and Sanat as scientific discussions with all of them have always been rewarding for me.

I accord my thanks to all other members of Space and Atmospheric Sciences Division: Bhavesh, Vandana, Uma, Shilpy, Nabi, Kushwaha, Venkat, Sunil, Modh bhai, Suchita ben, Dipu da, Som Sharma, Dr. Varun Sheel, Dr. Bapat, Dr. Subramanian, Dr. Y.B. Acharya, Dr. Sekar, Dr. Haider, Prof. Harish Chandra and Prof. H.S.S. Sinha for providing a pleasant working atmosphere in the division during the entire course of my research.

Journey of research would not have been so wonderful without the company friends like Nagar, Jayesh, Morthekai, Sanjoy, Murli, Bhavesh and Murari who have always been a source of strength and refreshment. I still cherish the memory of fun made on our frequent visits to Lal Darwaza with my close friends Manish, Preeti and Nagar during our early days in PRL. I wish to thank my seniors Alok Taori, Jitti, Anirban, Tarak, Lokesh, Sarika, Jayendra, Sudeshna, Soumen da, Alam bhai, Shubhrangshu, Asoka, Santosh, Sanjeev, Manoj and Prasanta who helped me on numerous occasions during my stay in PRL and gave me valuable suggestions and support at difficult times. I express my heartiest gratitude to all other friends in PRL Satya, Shreyas, Utpal, Suranjana, Antra, Subimal, Gowda, Charan, Kaushik da and Sashadhar for making my stay worthwhile and enjoyable. My special thanks to Satya for preparing such delicious chicken curry during our party in Anirban's quarter.

I thank all members of PRL football club, specially Ravi, Harish ji and Jyoti, for providing regular weekend refreshment in all these years.

Perhaps words are inadequate to express any kind of acknowledgement for parents and family members because without their support and encouragement I stand nowhere.

Dilip.

Abstract

The work presented in this thesis deals with the characterization of physical and optical properties of aerosols that are mainly produced over urban regions and which get transported to long distances as well as investigation of their impact on the regional scale aerosol radiative forcing. *Chapter-1* of the thesis gives a brief introduction to atmospheric aerosols, their production sources, size distribution, chemical nature and removal mechanisms. This is followed by a short description of radiation budget of the Earth-Atmosphere system and potential climate change mechanisms occurring on our planet. There is discussion on the role of aerosols in perturbing the radiative balance of the Earth-Atmosphere system, emphasizing the need for observational, modelling and laboratory studies to improve our present understanding of climate change and reducing uncertainties involved in future projections of how aerosols influence climate. The air pollution problems currently occurring in South Asia, associated with increased production of aerosols due to rapidly growing industrialization and expanding urbanization across various parts of this region is of great concern. The importance of research on urban aerosols is emphasized as there are limitations with most of the climate models, such as the aerosol-cloud-rainfall relationship is not fully understood. Finally, the chapter describes the importance of the present research work in the context of above discussions.

Chapter-2 presents results from continuous measurements of physical and optical parameters of aerosols made over Ahmedabad, an urban location in western India, from early 2002 till the end of 2005. A brief description of various instruments used during the present study along with their measurement techniques and working principles are also included. Important aerosol parameters studied over this location are column AOD

spectra, aerosol mass concentration, number size distribution, black carbon (BC) mass concentration, wavelength dependency in absorption, scattering coefficient, single scattering albedo and vertical distribution of aerosols. All data have been classified in terms of four major seasons viz. Dry, Pre-Monsoon (PrM), Monsoon (Mon) and Post-Monsoon (PoM). Seasonal and inter-annual variabilities in meteorological parameters play an important role in shaping the observed patterns of seasonal variations in different aerosol parameters. Results from several complimentary measurements reveal the dominance of smaller size particles during Dry and PoM seasons while an increase in the concentration of coarser particles during PrM and Mon seasons. Single scattering albedo at $0.525 \mu m$ are found to be 0.73 ± 0.1 , 0.84 ± 0.04 , 0.81 ± 0.03 and 0.73 ± 0.08 during Dry, PrM, Mon and PoM seasons respectively. Vertical distribution of aerosol for Dry and PoM seasons are characterized by high values of extinction coefficients in the first few hundred meters from the surface which decreases sharply with increasing altitude, whereas during Monsoon a thick and stable aerosol layer between 0.5 and 2.0 km is observed.

Chapter-3 presents results obtained from a ship cruise experiment conducted over the Bay of Bengal (BoB) in February 2003 to study the transport of aerosols from highly populated urban and industrialized areas of Indo-Gangetic plain to this oceanic region and study their impact on regional radiative forcing. Daily mean AOD at $0.5 \mu m$ is found to be in the range of 0.29 to 0.60. AOD values were particularly high over northern BoB and along the east coast of India. Average values of near surface aerosol mass concentration over the entire cruise region are 50, 37 and $13 \mu g/m^3$ for the coarse, accumulation and nucleation modes respectively. Measured aerosol size distributions exhibit four distinct modes, all of which could be fitted using log-normal curves with mode radii in the range of $0.025 - 0.036 \mu m$ for mode 1, between $0.15 - 0.165$ for mode 2, between $0.39 - 0.55$ for mode 3 and between $2.2 - 3.5$ for mode 4. The columnar aerosol size distribution derived using an inversion technique is used to estimate the aerosol scale height, whose values are found to be low over northern BoB showing larger contribution of boundary layer aerosols to the total columnar AOD values.

In *Chapter-4*, results obtained from a detailed study on aerosol characteristics over the central Indian region during February 2004 are presented. Observations were conducted at selected stations between Ahmedabad and Hyderabad as a part of ISRO-GBP's Land-Campaign-I. Results from complimentary measurements show that aerosols over the

northwestern parts of the study region are dominated by surface derived dust particles, whereas we find a relative increase in the amount of secondary aerosols over the south-central parts of Indian peninsula. Single scattering albedo at $0.525 \mu\text{m}$ is in the range of 0.75 to 0.9 and exhibit an overall increasing trend towards the end of dry winter season. Spectral dependence of light absorption by aerosols showed an excess absorption of up to 30% in the shorter wavelength range, less than $0.88 \mu\text{m}$. Our results have emphasized the fact that measurement of spectral dependence of light absorption by aerosols is more important than mere knowledge about the mass concentration of BC aerosols as absorption by aerosols can exhibit different wavelength characteristics at locations where major source of BC is not fossil fuel but biofuel/biomass burning.

Chapter-5 presents results from complimentary measurements of physical and optical properties of aerosols carried out at Delhi, as part of the ISRO-GBP's Land Campaign-II in December-2004, a period characterized by intermittent foggy, hazy and clear sky conditions over the entire Indo-Gangetic belt. Average AOD at $0.5 \mu\text{m}$ is found to be 0.91 ± 0.48 . Increase in AOD on hazy and foggy days are spectrally non-uniform with percentage increase in AOD at shorter wavelengths being higher on hazy days compared to clear days. Diurnally averaged BC mass concentration varied from a low value of $15 \mu\text{g}/\text{m}^3$ measured on clear days to a high value close to $65 \mu\text{g}/\text{m}^3$ on hazy days. Single scattering albedo at $0.525 \mu\text{m}$ varied from 0.6 to 0.8 with an average value around 0.68. Our results show that carbonaceous aerosols over Delhi has its source from both fossil fuel and biomass burning activities. A sudden anticyclonic movement triggered a fog event when aerosol scattering and absorption exhibited nearly two fold increase. Almost all conditions remaining same, a slightly higher relative humidity helped in the activation of droplets and formation of fog on 18th, while it remained hazy the next day. Lidar observations reveal a total collapse of the vertical distribution of aerosols in an extremely dense and shallow atmospheric layer of merely 200 m height from the surface. Presence of aerosol layer at elevated altitudes is also detected.

Chapter-6, presents implications of observed variabilities in aerosol parameters for the regional scale aerosol radiative forcing. A discrete ordinate radiative transfer model, SB-DART, is used to carry out radiative transfer calculations in the SW and LW regions. Two different approaches are followed to generate spectral values of various aerosol parameters required as input for the radiative transfer model and the computed values of aerosol

radiative forcing are found comparable in both methods. Over Ahmedabad, magnitude of surface forcing are found to be the highest during Post-Monsoon ($-63 \pm 10 W/m^2$), followed by Dry season ($-54 \pm 6 W/m^2$) and lower values during Pre-Monsoon ($-41.4 \pm 5 W/m^2$) and Monsoon ($-41 \pm 11 W/m^2$) seasons. In the case of TOA, aerosol forcing are found to be negative during Dry ($-26 \pm 3 W/m^2$) and Post-Monsoon ($-22 \pm 3 W/m^2$), while positive values of forcing are obtained during Monsoon ($14 \pm 4 W/m^2$) and Pre-Monsoon ($8 \pm 2 W/m^2$) seasons. Different properties of aerosols and differences in their vertical distribution give rise to different heating rates within the atmosphere during different seasons. Results from several sensitivity studies have emphasized the importance of diurnal variations in the amount of insolation, solar zenith angle and other related factors in modulating the values of aerosol radiative forcing over Ahmedabad. Average value of net ($LW + SW$) direct aerosol radiative forcing over Bay of Bengal region, computed using the measured values of AOD, are in the range of -30.6 to $-26.6 W/m^2$ at the surface and -8.4 to $10.6 W/m^2$ at the TOA. Magnitude of LW forcing is found to be less ($\sim 10\%$) compared to its SW counterpart, both at the surface and TOA. Result of a sensitivity test shows that LW aerosol forcing decreases with the increase in column water vapor. Over Central India, we find the diurnally averaged SW forcing at the surface to be negative in the range of -15 to $-40 W/m^2$ and $+0.7$ to about $-11 W/m^2$ at the TOA. Our results indicate towards a possible gradient in the atmospheric forcing due to aerosols during Indian winter season from Arabian Sea in the west, peninsular India in the middle and Bay of Bengal in the east. During a field campaign over New Delhi, we find a large negative forcing at the surface, in the range of -40 to $-86 W/m^2$, while forcing at the TOA varied between -2 and $+3 W/m^2$.

CHAPTER 1

Introduction

1.1 Atmospheric Aerosols

Atmospheric aerosols are tiny solid particles or liquid droplets which remain suspended in the atmosphere, with large differences in their size, chemical nature and production sources. Aerosols are produced by natural processes as well as due to anthropogenic activities. On a global scale, anthropogenic sources contribute a small fraction in the range of 10–15 % to the total production from various sources [Kiehl and Rodhe, 1995; Andreae, 1995]. However, this ratio is true only for the global average and the figures are quite different on regional scales eg. in the vicinity of major industrial areas or urban locations, contribution from anthropogenic sources are found to be much higher than the global average value. Moreover, the statistics presented by *Satheesh and Moorthy* [2005] shows that although on a global scale, naturally produced aerosols contribute nearly 81% of the total columnar mass burden but their contribution to the aerosol optical depth is only about 52%.

Some aerosols such as wind blown dusts, pollen grains, sea salt particles, soot from combustion of fossil fuel or biomass burning emissions are directly injected into the atmosphere as particles and hence they are known as primary aerosols. Whereas there are several inorganic species in the atmosphere such as sulfates, nitrates etc. produced from precursor gases released into the atmosphere which gets converted into particles and these are known as secondary aerosols. Usually aerosols in the atmosphere vary over a wide size range starting from a few nanometers to several tens of micrometers. In terms of size,

aerosols are generally classified into three categories viz. (i) Nucleation mode particles ($0.001 - 0.1 \mu\text{m}$ radius), (ii) Accumulation mode particles ($0.1 - 1.0 \mu\text{m}$ radius) and (iii) Coarse mode particles (greater than $1.0 \mu\text{m}$ radius). The terms nucleation and accumulation refer to the mechanical and chemical processes by which aerosol particles in those size ranges are produced. The smallest aerosols, belonging to nucleation mode, are mostly produced by gas-to-particle conversion processes occurring in the atmosphere. Usually, nucleation mode particles are the most predominant in terms of number, however due to their smaller size, these aerosols constitute only a few percent of the total mass concentration of bulk aerosols in the atmosphere. Aerosols in the accumulation mode size range are usually produced either by coagulation of smaller particles or by heterogeneous condensation of gas vapor onto existing smaller nucleation mode particles. Coarse mode aerosols are mainly formed by mechanical processes such as wind blown dusts, sea salt aerosols produced due to breaking of sea waves etc. Chemical nature of aerosols is mainly decided by their production source while the size distribution of aerosols depends on their production mechanism.

Once suspended in the atmosphere, aerosols move along with air currents for short or long distances before they are finally removed from the atmosphere. Removal processes of aerosols can be broadly classified into two categories viz. dry and wet deposition mechanisms. Dry deposition occurs when an aerosol settles on the Earth's surface under the action of gravitational force or impacts on a surface because of its inertia or due to their Brownian motion arising from constant collision with other particles and the surrounding gas molecules. Wet deposition mechanism can be further classified into three closely related categories viz. rainout, washout and sweepout. Rainout describes the removal of aerosols acting as cloud condensation nuclei as some of these drops grow to such a large size that they start falling gravitationally to the surface as rain drops. If an aerosol is incorporated into an already existing cloud drop, and that drop grows large enough to fall as rain, the particle is said to have been washed out. Aerosols which are present below the base of a raining cloud are often impacted by the falling raindrops and if such an impact leads to incorporation of the aerosol into the drop, the aerosol is deposited with the raindrop and is considered to be swept out from the atmosphere. During the course of transport, aerosols can grow due to coagulation among themselves or by condensation of vapors on them. However, there can also be evaporation taking place from particles con-

taining water or volatile organic compounds in them. The processes of formation, coagulation removal and transformation affect the residence times of aerosols in the atmosphere [Jaenicke, 1993]. The residence time of a particle depends on its size as well as its location in the atmosphere. Nucleation mode particles being more subject to Brownian motion, experience higher rate of coagulation and get transformed into larger agglomerates. Larger particles having higher settling velocities exhibit higher sedimentation rate and hence they too have smaller residence time in the atmosphere. Residence time of aerosols is higher in the stratosphere compared to troposphere. One important reason for this is the negligible amount of water vapor present in the stratosphere which prevents cloud formation and renders the wet removal of aerosols completely ineffective. In general, the residence time of aerosols in the lower troposphere is about a week which increases to about a month in the upper troposphere and in the stratosphere aerosols can reside even upto two years [Jayaraman *et al.*, 1995].

1.2 Radiation Budget of the Earth and Climate Change

The climate system of our Earth is defined as an interactive system consisting of several components such as the atmosphere, the hydrosphere, the cryosphere, the land surface and the biosphere [IPCC, 2001]. The ultimate source of energy that drives the climate system is the radiation received from the Sun. About 50% of the Solar radiation is in the visible range of the electromagnetic spectrum and the rest is in the ultra violet (UV) and near infrared (NIR) regions. Each square meter at the top of the Earth's atmosphere receives on an average around 1368 W of Solar radiation. Nearly one third of it is reflected back to space collectively by the clouds, the atmosphere and the Earth's surface. The remaining is absorbed by the atmosphere and largely by the land and the ocean regions on the Earth's surface. In response to this insolation, Earth's surface re-emits energy to the atmosphere, partly as thermal infrared radiation, partly as sensible heat and the remaining in the form of latent heat released by water vapor as it condenses higher up in the atmosphere as well as during evapotranspiration. Much of this infrared radiation emitted by the Earth is absorbed by molecules in the atmosphere, important ones being water vapor, carbon dioxide, ozone etc. and by clouds. All these components in turn radiate infrared energy in all directions, a fraction of which is directed towards the Earth. As a

consequence of these processes, radiation is trapped in the lower atmosphere, so that the global and annual average radiative flux available at the surface is about 390 W/m^2 , which exceeds the corresponding incident flux at the top of the atmosphere. This phenomenon gives rise to the well known greenhouse effect in the atmosphere and helps in maintaining the average temperature of the Earth's surface at around 288°K . On an annual mean and for the Earth as a whole, flux of incoming Solar radiation is balanced by the outgoing solar and terrestrial radiations at the top of the atmosphere (TOA).

In an equilibrium climate state, the average net radiation at the top of the atmosphere is zero. Any factor that alters the radiation received from the Sun or the amount which is lost from the atmosphere to space or that changes the redistribution of energy within the atmosphere or between atmosphere, land and ocean can affect climate. The corresponding imbalance in the net irradiance (down minus up and solar plus terrestrial) at any level in the atmosphere quantified in units of watts per square meter is known as 'radiative forcing'. A positive radiative forcing tends to warm the atmosphere while negative forcing tries to cool it. There can be natural as well as human induced variations in climate. For example, if the Solar radiation reaching the Earth's atmosphere changes or when a large volcanic eruption takes place, large quantities of aerosols are dumped in the atmosphere which can disturb the climate system on our Earth. Besides these factors, climate on Earth can also change because of continuous ongoing non-linear interactions between the various components of the climate system having different response time to any kind of perturbation. Examples of such internal factors causing variations in climate are El Nino Southern Oscillation (ENSO) and North Atlantic Oscillation (NAO). In addition to these natural factors, there are human induced variabilities of climate. Human activities involving combustion of fossil fuels for industrial or domestic usage, and biomass/biofuel burning, produce significant quantities of greenhouse gases and aerosols which affect the composition of the atmosphere and hence impact climate. Although human beings have always influenced their environment, but after the industrial revolution (1750) there has been a substantial increase in the amount of greenhouse gases in the atmosphere. For example, the concentration of CO_2 alone has increased by more than 30% compared to its pre-industrial values and is still increasing at an unprecedented rate. Thus human activities have caused large perturbation to the atmospheric composition and have resulted in the enhanced greenhouse effect. Besides these, land-use changes, due to urbanization, de-

forestation and agricultural practices, affect the physical and biological properties of the Earth's surface. Such effects change the radiative forcing and produce potential impact on regional and global climate.

1.2.1 Role of Aerosols

Atmospheric aerosols from both natural and anthropogenic sources directly affect the radiative balance of the Earth by scattering and absorbing the incoming Solar and outgoing terrestrial radiation besides producing other indirect effects such as modifying the cloud properties etc. [IPCC, 2001 and references therein]. Study of aerosol properties across various places on the Earth is essential to understand climate change occurring on our planet during the post-industrial era (after 1750) [IPCC, 2001]. The largest source of uncertainty in predicting climate change, even by the best available General Circulation Models (GCM), is due to uncertainties involved in the estimation of aerosol radiative forcing [Ramaswamy *et al.*, 2001]. This uncertainty arises mainly due to lack of adequate information on temporal and spatial distribution of aerosols and their associated properties across the globe [Pilinis *et al.*, 1995; Ramanathan *et al.*, 2001a]. Moreover, due to shorter residence time and diverse aerosol types of varying optical properties which are not uniformly distributed around the globe, their radiative forcing also exhibits significant regional variations [Kiehl and Briegleb, 1993; Chung *et al.*, 2005]. Variations in aerosol composition affect climate through variations in the abundance and distribution of these radiatively active species which alter the energy balance of the Earth-Atmosphere system at various levels in the atmosphere. Different aerosols interact with radiation in different ways, eg. soot is highly absorbing while sulfate is highly scattering. However, their combined impact on global climate need not be additive because of inhomogeneity in the distribution of different aerosol types over both space and time, differences in their mixing states, differences in albedo of the underlying surface, differences in the vertical distribution of aerosols in the atmosphere and several other factors [Haywood and Ramaswamy, 1998; Haywood and Boucher, 2000; Jacobson, 2001; Ramaswamy *et al.*, 2001; Chung *et al.*, 2005].

1.3 Importance of South Asian Region

The South Asian region, comprising of India, Pakistan, Bangladesh, Nepal, Bhutan, Sri Lanka and Maldives, is one of the most densely populated areas in the world with present population density in the range of 100 – 500 persons per square kilometer. Although, in terms of land area, this region constitutes merely 3% of the world's total land mass, currently it sustains nearly 20% of the global population and this percentage is expected to reach about 25% by the year 2025 [UNEP, 2002]. Due to large human population residing in this region, South Asia is considered to be a potentially strong source region for the production of various anthropogenic aerosols such as sulfates, nitrates, black carbons etc. [Kaufman *et al.*, 2002; Menon *et al.*, 2002; Akimoto, 2003; Ramanathan and Crutzen, 2003; Ramanathan *et al.*, 2005]. One major reason for the increased production of anthropogenic aerosols is related to rapidly growing industrialization and expanding urbanization in various parts of this region, without much stringent control over different emissions. The type of air pollution problems and anthropogenic production of aerosols, currently occurring in South Asia had already taken place in the western countries of Europe and America at early stages of their economic development around middle of the last century [Grey *et al.*, 1986; Pearce, 1992]. Apart from industrial emissions and fossil fuel combustion, another major anthropogenic source of aerosols in South Asia is related to biomass burning (open burning of dry leaves, shrubs etc.) and usage of biofuels for domestic purposes [Reddy and Venkataraman, 2002; Ganguly *et al.*, 2005b; Ganguly *et al.*, 2006]. In another study, Venkataraman *et al.* [2005] have shown that in India about 44% of the total black carbon (BC) emission comes from biofuel combustion.

The South Asian region is characterized by tropical climate and influenced by two contrasting monsoon systems in a full annual cycle. There is a seasonal alteration of wind pattern and latitudinal movement of the inter-tropical convergence zone (ITCZ) associated with the monsoon system. During southwest monsoon period or summer season (June to September), ITCZ moves northward across India and a strong south westerly wind flow in the lower troposphere brings large supply of moisture from the Indian Ocean region and causes rainfall almost over the entire region. On the other hand, during Northeast monsoon period or winter season (December to March), ITCZ moves southward and even crosses the equator when the surface level wind pattern within this region is predomi-

nantly from the continent towards the ocean. During this time large quantities of aerosols and other gaseous pollutants, mostly produced due to various anthropogenic activities over the populous and industrialized parts of the Indian sub-continent are dumped onto the otherwise pristine Indian ocean region. Over most of South Asia, rainfall occurring during the summer monsoon accounts for almost the total annual rainfall and serves as a source of fresh water for agriculture and other activities in the region. However, monsoon rainfall in South Asia is characterized by large spatial and inter-annual variability. Moreover, within South Asia, there are some anomalous regions such as the arid and semi-arid regions of Pakistan and northwest India comprising of states like Rajasthan and Gujarat experience frequent droughts whereas the eastern Himalayan regions like Assam are subjected to frequent flood events.

For semi-arid region of Pakistan and northwest India, rainfall amount and aerosol loading in the atmosphere are very intricately related to each other. Unfortunately, very few long term records and that too on limited aerosol parameters are available from land areas within this region [Moorthy *et al.*, 1999; Singh *et al.*, 2004]. There is a strong need for high quality, consistent and scientifically useful data on aerosol characteristics from various parts of this region [Ramanathan and Crutzen, 2003].

1.4 Urban Aerosols

Currently about 50% of the total human population live in urban locations, which constitute even less than 2% of the total land area available on our planet Earth [UNDP, 2001]. Progressive living standards and increasing demand for energy by the urban population has resulted in unprecedented production of aerosols and other gaseous pollutants due to various anthropogenic activities during the post-industrial era [IPCC, 2001]. Urban aerosols consist of primary particulate matter produced from automobiles, industries, power plants and natural sources apart from several secondary aerosols produced from gas-to-particle conversion processes. Over land areas, urban centers and particularly mega-cities appear as hot islands with higher concentrations of fine mode (sub-micron) aerosols produced due to various anthropogenic activities compared to background atmosphere which is mostly dominated by naturally produced coarse aerosols [Crutzen, 2004]. The number size distribution of urban aerosols is dominated by nucleation mode parti-

cles smaller than $0.1 \mu\text{m}$, while the surface area distribution is dominated by accumulation mode particle in the range of 0.1 to $1.0 \mu\text{m}$. Contrary to these, mass size distribution of urban aerosols is characterized by two equally dominating modes, one in the accumulation mode regime and the other one corresponding to coarse mode particles of size greater than $1.0 \mu\text{m}$ [Seinfeld and Pandis, 1998]. Although shape of the distribution remains the same, absolute concentration of aerosols could be variable within an urban location with higher concentration of smaller particles near source regions which fall off rapidly with distance from these sources. Another important characteristic feature of urban aerosols is the presence of higher concentration of soot particles in the mixture of composite aerosols. Soot aerosols are produced from incomplete combustion of fossil fuels like coal and diesel [Bond, 2001; Jacobson, 2001], residential biofuels and outdoor burning of dry leaves and other organic waste materials [Reddy and Venkataraman, 2002; Venkataraman et al., 2005; Ganguly et al., 2006].

Presently there are limitations with most of the climate models in assessing the actual impact of urban aerosols. These limitations arise mainly because the aerosol-cloud-rainfall relationship is not fully understood as controversial results are available on this subject [Jin et al., 2005]. Some of the earlier studies have shown that the atmospheric heating by absorbing aerosols, mainly produced over urban locations, can evaporate some of the low level clouds resulting in a decrease in cloud cover and planetary albedo. This may in turn lead to a net warming at the surface and reduction in rainfall [Hansen et al., 1997; Ackerman et al., 2000]. In another study, Ramanathan et al. [2001b] report that aerosols produced from urban areas can result in reduction of rainfall due to cloud microphysics modification. Contrary to both these results, two other independent studies by Menon et al. [2002] and Shephard et al. [2002] have shown that urban environment dominated by absorbing soot aerosols can significantly enhance the intensity of storms and result in downwind rainfall. According to Menon et al. [2002] when soot aerosols from various industrial emissions and fossil fuel combustion absorbs sunlight, it heats the air and reduces the amount of sunlight reaching the surface. This heated air makes the atmosphere unstable, creating rising air due to convection, which forms cloud and brings rainfall to regions that are heavily polluted.

Urban environment provides a natural laboratory to study the characteristics of these anthropogenic aerosols close to their source region that are capable of producing large

perturbation to the radiation budget of the Earth-Atmosphere system.

1.5 Present Study

The present study has been carried out to characterize the physical and optical properties of aerosols that are mainly produced over urban regions and get transported to long distances by wind. This study is largely motivated by the rising concern of the global scientific community during the post-INDOEX (Indian Ocean Experiment) period to know more about aerosols prevalent over the South Asian region as some of the earlier studies have shown that aerosols over this region can even slow down the hydrological cycle and lead to severe consequences not only for this region but can produce global impacts [Ramanathan *et al.*, 2001a, 2001b, 2005]. Major part of this research work is devoted to understand the seasonal and inter-annual variations of various aerosol parameters measured over Ahmedabad, an industrialized urban location in western India, studied during the four year period from 2002 to 2005. Several interesting results on seasonal and inter-annual variabilities of aerosol parameters measured over Ahmedabad are discussed in *Chapter-2* of this thesis. Besides the long term characterization of aerosol parameters over Ahmedabad, the present work also involves several campaign based measurements conducted over different parts of the Indian subcontinent to study the characteristics of aerosols pertaining to these specific regions and transport of aerosols to distant regions and estimate their radiative impacts. In order to study the transport of aerosols, their physical characteristics, their chemical nature and the effect of these diverse aerosols on the regional climate forcing in greater detail, a ship cruise study was conducted over Bay Of Bengal (BoB) in February-2003. Results from this ship cruise study are discussed in *Chapter-3* of the thesis. The present work includes another intensive field campaign over the Central Indian region, organized in February 2004, to understand and quantify the spatial heterogeneity in the distribution of aerosols and study their impact on the regional climate system. Various results obtained from the campaign based study over Central India are discussed in *Chapter-4* of the thesis. Another major research work carried during the present study involves the characterization of aerosols constituting the infamous wintertime haze over North India, occasionally resulting in the formation of notorious fog within various parts of Indo-Gangetic plain. As a part of ISRO-GBP's (Geosphere Biosphere programme of

Indian Space Research Organization) Land-Campaign-II, complementary measurements of physical and optical parameters of aerosols were made from New Delhi, a highly industrialized megacity in South-Asia during December 2004. Results from this aerosol-fog interaction study conducted over New Delhi are discussed in *Chapter-5*.

Two types of long range transport of aerosols are prevalent over the South-Asian region. First one is transport of naturally produced dust aerosols from various arid and semi arid regions of west Asia, Northern Africa and North West India to our study location which is an urban site in western India. This provided us a unique opportunity to study the behavior of urban aerosols, mainly characterized by presence of anthropogenic aerosols such as soot, sulfates etc., which get influenced by the transported dust particles from western arid regions. Other transport pathway which has been studied during the present work involves transport of anthropogenic aerosols from highly populated urban and industrialized areas of Indo-Gangetic plain to the otherwise pristine oceanic region of Bay of Bengal, and the transport of pollutants from North Indian regions to central India during the Dry winter season.

With an attempt to estimate the implications of the observed variabilities in aerosol parameters in terms of their potential capability to perturb the radiative balance of the Earth-Atmosphere system, measured aerosol parameters have been used as input in a radiative transfer model to make estimates of aerosol radiative forcing for all the study locations. We have carried out further model estimates to know the sensitivity of aerosol radiative forcing to various parameters required as input for the radiative transfer calculations. Model estimates of aerosol radiative forcing and its sensitivity to different parameters are presented and discussed in *Chapter-6*.

Seasonal and inter-annual variations in aerosol characteristics over Ahmedabad

The Asian region, comprising of China, India and other East-Asian countries is a rapidly developing region with increasing levels of pollution caused by industries, vehicles and other anthropogenic activities [Menon *et al.*, 2002; Akimoto, 2003]. Our present study is largely motivated by the rising concern of the global scientific community during post-INDOEX (Indian Ocean Experiment) period to know more about aerosols over the South Asian region in greater detail, as some of the earlier studies have shown that aerosols over this region can even slow down the hydrological cycle thereby resulting in severe consequences not only for this region but can produce global impacts [Ramanathan *et al.*, 2001*a*, 2001*b*]. This chapter presents results on various physical and optical parameters of aerosols continuously measured over Ahmedabad, an urban location in western India, from early 2002 till the end of 2005 and discusses their seasonal and inter-annual variabilities which has implications for aerosol radiative forcing over the region. Important aerosol parameters that have been studied over this location include: aerosol optical depth (AOD) spectra, aerosol mass concentration, size distribution, BC mass concentration, wavelength dependency in aerosol absorption, aerosol scattering coefficient, single scattering albedo and aerosol vertical distribution. All measured parameters have been classified in terms of four major seasons prevailing over the region, viz. Dry, Pre-Monsoon, Monsoon and Post-Monsoon season. For the first time continuous measurements of such large number of aerosol parameters are being presented from Ahmedabad and the results presented are of

special importance for all researchers interested in investigating the role of aerosols prevalent over this region on regional scale climate forcing and their possible global impacts.

2.1 Site Description and Meteorology

The measurement site is at the campus of the Physical Research Laboratory [23.03⁰N, 72.55⁰E, 50 m amsl], located in the western edge of the Ahmedabad city. The city has a population of about 5.5 million and has several small and large scale industries, mostly located on its eastern and northern outskirts. There is also a rapid increase in the number of vehicles (about 10% per year) in the city which includes buses, cars, two-wheelers (motorbikes, scooters) and three-wheelers (Indian auto-rickshaws) all of which contribute significantly to the production of various kinds of pollutants including aerosols. Moreover, since the city is located in the south-east direction of Thar desert and the entire region being semi-arid, the anthropogenically produced sub-micron aerosols get mixed with the naturally produced coarser mineral dust aerosols over the measurement location.

In the present work, the data are grouped in terms of four major seasons viz. Dry (December to March), Pre-Monsoon (April-May), Monsoon (June-September) and Post-Monsoon (October-November), primarily based on different meteorological conditions prevailing over this site during different months of the year. Figure 2.1 shows the seasonal variation of major meteorological parameters over Ahmedabad during last four years (2002 – 2005). Vertical lines on top of each bar in all the four panels represent $\pm 1\sigma$ variation about mean value of the corresponding parameter in that season. The inter-annual variability in most of the meteorological parameters has been much less over the period of our study except the rainfall amount which is different for different years. Also we find that within a year, the pattern of seasonal variation in different meteorological parameters has remained similar in all four years. Average daily mean temperature is minimum, in the range of 22 – 24° C, during Dry season and maximum of about 32° C during Pre-Monsoon season. In general, relative humidity is found to be less than 30% during Dry season while it ranges between 30 and 40% during both Pre-Monsoon and Post-Monsoon seasons. The season which markedly differs from all other seasons in any year is the Monsoon season, spread over four months from June to September, when average relative humidity over this site is more than 70% and surpasses 90% mark quite a few times within this season.

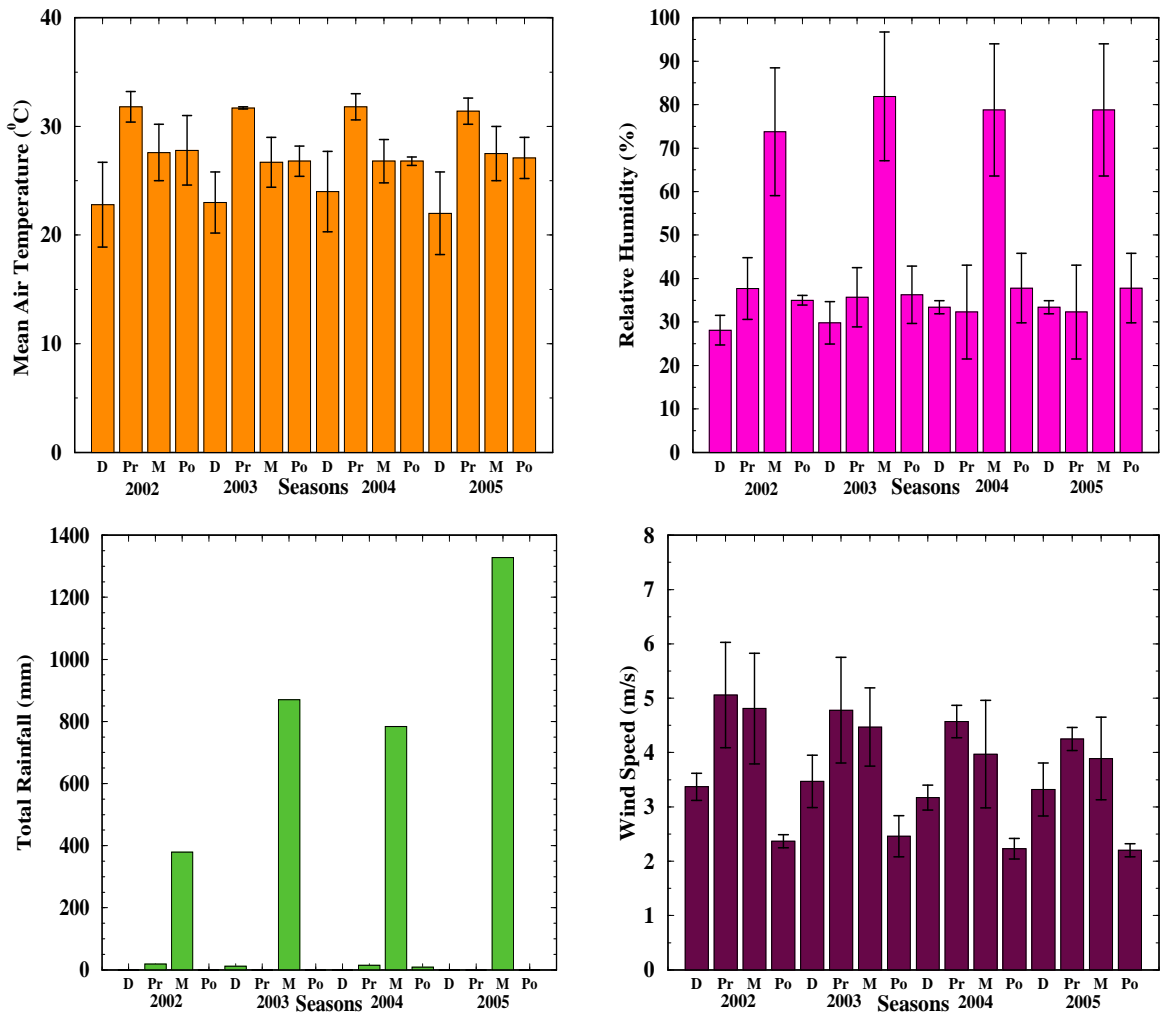


Figure 2.1: Seasonal variations of four important surface meteorological parameters measured over Ahmedabad during the four year period from 2002 to 2005

The Indian summer Monsoon, active during this season is part of a large scale circulation pattern which develops in response to the thermal gradients between the warm Asian continent in the north and cooler Indian Ocean in the south. A strong south westerly flow in the lower troposphere brings a substantial supply of moisture into India which is released as precipitation almost across the entire country. Ahmedabad receives most of the rainfall only during this season (Figure 2.1). In the year 2002, total annual rainfall over Ahmedabad was much lower than the climatological mean, which is about 700 mm, whereas during 2003 and 2004 though the total rainfall was within the climatological mean, its day to day variability was quite large during the Monsoon months. On the other hand, in the

year 2005, not only the total annual rainfall over Ahmedabad was more than the climatological mean but also it was distributed over the entire Monsoon period from June to September. For semi-arid region like Ahmedabad, amount of rainfall and aerosol loading in the atmosphere are very intricately related to each other. This is because on the one hand, amount and type of aerosols which act as cloud condensation nuclei (CCN) together with the available moisture in the atmosphere decides the amount of rainfall that occurs over a region, while on the other, more frequent rainfall leads to moist soil and more vegetation, which curtails the amount of soil derived dust aerosol loading in the atmosphere and possibly can have impact on subsequent weather pattern. Although, establishing an exact relation between aerosol loading in the atmosphere and rainfall occurring in the region is beyond the scope of the present work, nevertheless, since aerosols are key to the formation of CCN required for rainfall, seasonal and inter-annual variabilities of major aerosol parameters measured over this site will be very useful for future studies on the role of aerosols in monsoon rainfall over the region.

Near surface wind speeds over Ahmedabad are the highest during Pre-Monsoon season (~ 4.8 m/s) which is closely followed by during Monsoon season (~ 4.3 m/s), whereas winds are usually calm during Post-Monsoon season (~ 2.3 m/s) and increases slightly by the end of Dry season (~ 3.3 m/s). Seasonal variation in wind speed remained the same in all four years. However, we noticed a slightly decreasing trend in the maximum wind speed during Pre-Monsoon and Monsoon seasons over the period of our study from 2002 to 2005 (Figure 1). Apart from speed, wind direction can also play a role in determining the type of aerosols present over a location as they help in bringing aerosols from different neighboring regions to the measurement site. For example, figure 2.2 shows the wind speed and direction prevailed over Ahmedabad during all the four seasons for the year 2003. The seasonal wind directions can be considered representative for all the four years. During Dry season, surface winds over Ahmedabad are either north easterly or north westerly, making the lower level air masses reaching our measurement site mostly of continental origin and hence they are rich in land derived dust particles apart from other sub-micron aerosols produced due to anthropogenic activities. Surface wind vectors slowly change their direction to become north westerly or south westerly during Pre-Monsoon and Monsoon seasons. Therefore during these seasons, aerosols over Ahmedabad will have a possible influence of the marine air masses reaching this region from

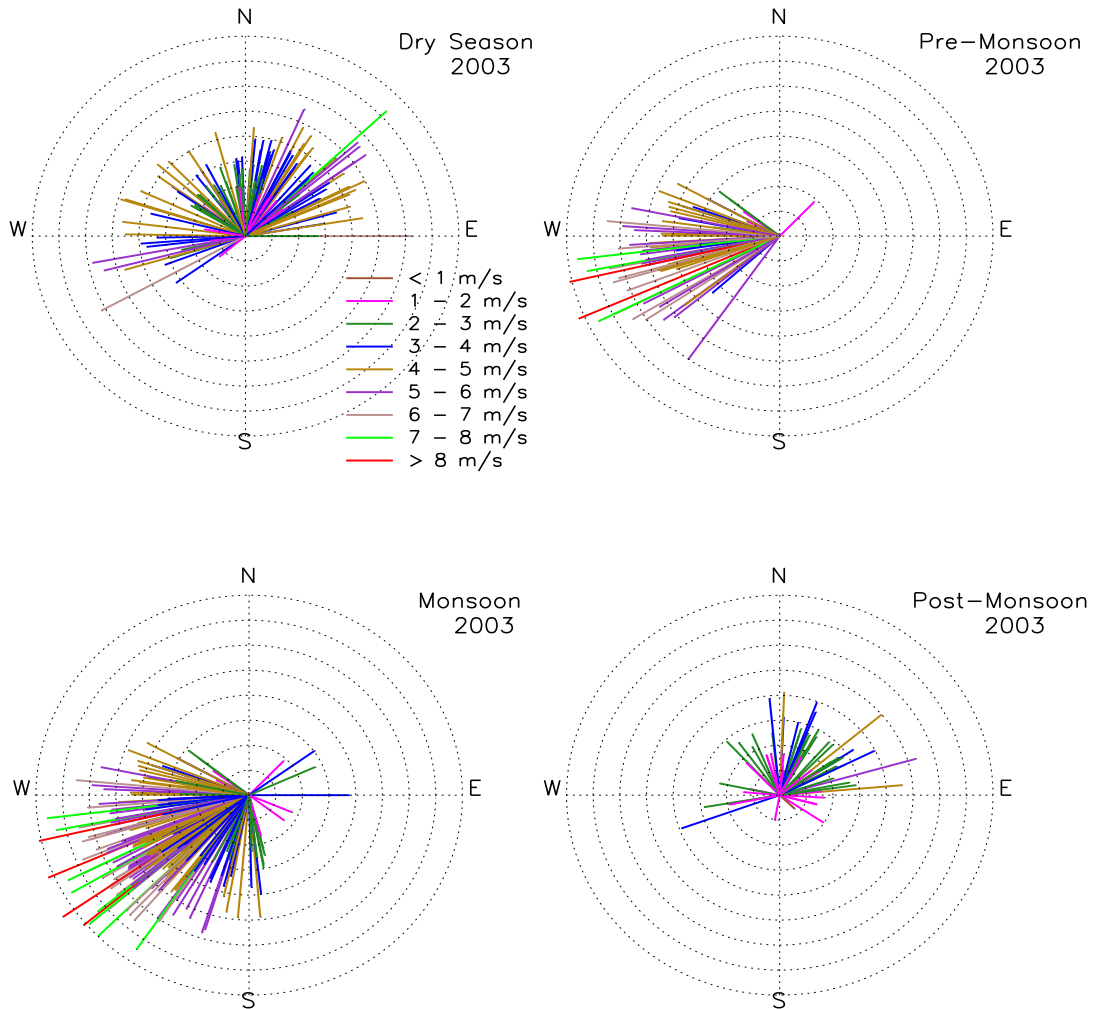


Figure 2.2: Daily average values of surface level wind speed and wind direction measured over Ahmedabad during all four seasons for the year 2003

Arabian Sea in the south. However, even during these seasons, when the surface winds are dominated by south westerly flow from the Arabian sea, air back-trajectory analysis using NOAA HYSPLIT-4 (Hybrid Single-particle Lagrangian Integrated Trajectory) model shows that air parcels reaching over our measurement site at higher heights (> 2 km), could be completely of land origin in the west. Thus, there are high chances of coarser mineral dust aerosols getting transported along these trajectories while they cross through large areas of arid and semiarid regions in northern Africa, west Asia and north western India [Figure 2.6(a)]. During Post-Monsoon season, winds are not only calm but wind directions are also found to be random. Primarily, due to lower wind speed prevailing

during this season, amount of land derived dust aerosols are expected to be less in the atmosphere compared to other seasons of the year.

2.2 Instrumentation and Measurements

Physical and optical parameters of aerosols have been studied in detail by observational means using a variety of techniques. The instruments used in the present study along with a brief description of their measurement techniques and working principles are presented below. As the same instruments have been used for the measurement of aerosol parameters over other study locations, discussions on methodology and working principle of these instruments are not repeated in subsequent chapters.

2.2.1 Sun-Photometer

Measurements of aerosol optical depth (AOD) have been carried out using a hand held multichannel sun-photometer named Microtops-II (Solar Light Co. U.S.A.), capable of measuring AOD at five wavelength bands centered around 0.380, 0.440, 0.500, 0.675 and 0.870 μm [Morys *et al.*, 2001]. Field of view of each collimator is about 2.5° and band-width of each filter is about 0.01 μm . A second Microtops is also used to measure AOD at 1.02 μm along with total columnar concentrations of ozone and water vapor in the atmosphere. AOD values are derived from the direct measurement of solar radiance at each channel and using a calibration constant corresponding to that channel. Derivation of AOD is based on Beer-Lambert-Bouguer law as follows:

$$\tau_\lambda = \frac{-1}{m} \left[\ln\left(\frac{I_\lambda}{I_{0\lambda}}\right) - 2\ln\left(\frac{r_0}{r}\right) \right] \quad (2.1)$$

where τ_λ is the total columnar optical depth of the atmosphere at wavelength λ , I_λ is the instantaneous solar radiation intensity recorded by the Microtops and $I_{0\lambda}$ is the solar radiation intensity reaching the top of the atmosphere derived using Langley plot technique, m is the relative air mass, r is the instantaneous sun-earth distance and r_0 is the sun-earth distance when $I_{0\lambda}$ is evaluated. Young [1994] gave an empirical relation for the relative air mass as follows:

$$m = \frac{1.002432\cos^2 z + 0.148386\cos z + 0.0096467}{\cos^3 z + 0.149864\cos^2 z + 0.0102963\cos z + 0.000303978} \quad (2.2)$$

where z is the Solar zenith angle at the time of measurement. This expression takes care of atmospheric refraction and Earth's curvature effect to provide better accuracy at all zenith angles. However, for smaller zenith angles ($< 60^\circ$), equation 2.2 simplifies into $m = \sec z$. From the total optical depth, aerosol optical depth $\tau_{a\lambda}$ is obtained by subtracting the contribution due to Rayleigh scattering ($\tau_{R\lambda}$) and molecular absorption ($\tau_{M\lambda}$).

$$\tau_\lambda = \tau_{a\lambda} + \tau_{R\lambda} + \tau_{M\lambda} \quad (2.3)$$

Air column density of 2.16×10^{25} molecules cm^{-2} applicable for tropical atmosphere has been used for the estimation of $\tau_{R\lambda}$. Molecular absorption has been taken into account for the air molecules O_3 , H_2O as well as O_2 and N_2 based on their concentrations valid for the tropical atmosphere. Regular calibration of this instrument is important [Ichoku *et al.*, 2002], which otherwise could lead to erroneous values of AOD computed by this user friendly instrument. In the present study, both Microtops have been regularly calibrated at least twice a year and fresh up-to-date values of calibration constants obtained from Langley plot analyses carried out from Mount Abu ($26.6^\circ N$, $72.7^\circ E$), a relatively pristine site at a height of about 1.7 km above the mean sea level, are used for every subsequent period of about six months. Figure 2.3 shows the Langley plot analysis for the 0.38 and 0.87 μm

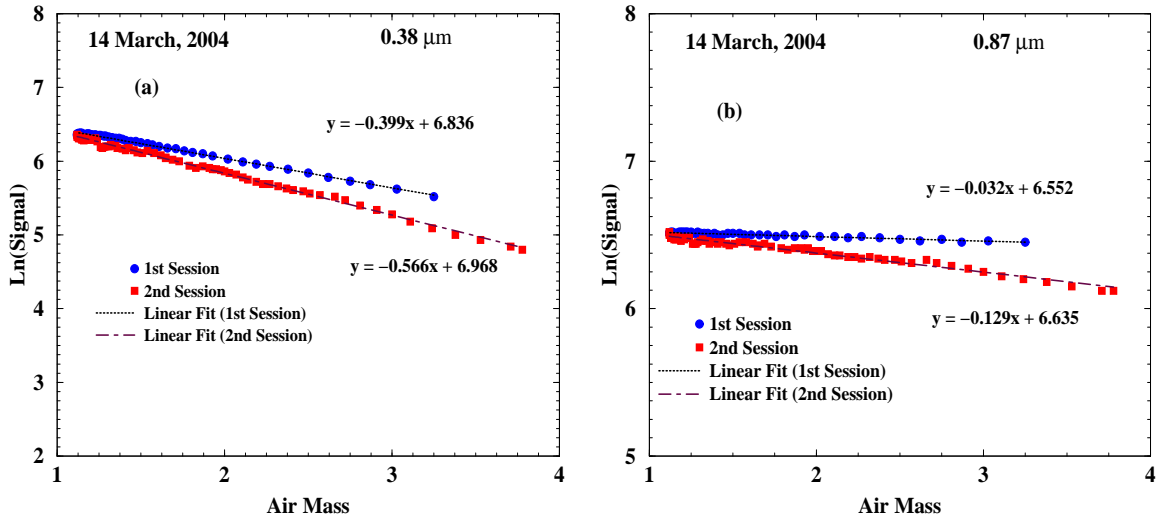


Figure 2.3: Langley plots for the (a) 0.38 and (b) 0.87 μm channels of Microtops carried out from Mount Abu on 14 March 2004. Radiance data measured during forenoon (1st session) and afternoon (2nd session) hours of the day are separately fitted with different straight lines to obtain the value of $I_{0\lambda}$

channel carried out from Mount Abu on 14 March 2004. Radiance data measured during

forenoon and afternoon hours of the day are separately fitted with different straight lines to obtain the value of $I_{0\lambda}$ (equation 2.1) for all the channels of Microtops. Table 2.1 lists the calibration constants ($I_{0\lambda}$) for the 6 AOD channels of Microtops obtained from separate Langley plot analysis carried out during the period 2002 – 2005. Also, most of the time,

Table 2.1: Calibration constants ($I_{0\lambda}$) for the 6 AOD channels of Microtops obtained from separate Langley plot analysis carried out during the period 2002 – 2005.

Date	Calibration constant, $I_{0\lambda}$					
	0.38 μm	0.44 μm	0.50 μm	0.675 μm	0.87 μm	1.02 μm
03 March, 2002	7.03	6.47	6.64	7.23	6.60	
10 November, 2002	7.15	6.47	6.70	7.27	6.67	6.88
13 February, 2003	6.87	6.27	6.54	7.16	6.56	6.88
09 December, 2003	6.92	6.27	6.50	7.16	6.60	6.85
14-15 March, 2004	6.88	6.26	6.48	7.16	6.58	6.83
22 November, 2004	6.96	6.30	6.49	7.20	6.64	6.85
17 May, 2005	6.85	6.20	6.43	7.12	6.54	6.83

the measurements are repeated for three times and the one with lowest AOD is considered for further analysis. The absolute uncertainty in the AOD values are less than 0.03 at all wavelengths.

2.2.2 QCM cascade impactor

Aerosol mass concentrations are measured using a Quartz Crystal Microbalance (QCM) cascade impactor (model PC-2, California Measurements Inc. U.S.A.) [Ganguly *et al.*, 2005a]. It draws the ambient air at a constant flow rate of 0.24 $l \text{ min}^{-1}$ and segregates aerosols present according to their aerodynamic diameters into ten different size ranges viz. 25, 12.5, 6.4, 3.2, 1.6, 0.8, 0.4, 0.2, 0.1, 0.05 μm from stages 1 to 10 respectively. Typical sampling duration is kept as 5 minutes. In this instrument, aerosol concentration is determined from the relative change in frequency between a pair of sampling and reference quartz crystal sensors employed for each stage. Filtered air is flushed through the instrument prior to actual measurement to facilitate the crystals to attain stability. During actual measurements, relative frequency between the sampling and reference crystal are recorded, thereby ensuring that the changes in air temperature and relative humidity does not affect our measurement. Jayaraman *et al.* [1998] and Ramachandran and Jayaraman [2002] have estimated a maximum overall uncertainty of about 25% in the mass measurement

for all stages of QCM. Higher chances of error in the mass measurements by QCM occurs under high relative humidity conditions during Monsoon season. This is because, during the measurement time of about 5 to 10 minutes, there could be an evaporation loss of the adsorbed water from the water soluble particles which are being collected under low pressure condition inside the impactor stages [Jayaraman *et al.*, 1998]. Aerosol mass concentrations obtained at different size ranges are then used to retrieve aerosol number size distributions using appropriate mass density applicable for an urban environment [Hess *et al.*, 1998].

2.2.3 Aethalometer

Black carbon mass concentration and absorption coefficient of aerosols (β_{abs}) are obtained using a seven channel Aethalometer (model AE-42, Magee Scientific, USA). This instrument measures attenuation of light beam at seven different wavelengths viz. 0.37, 0.47, 0.52, 0.59, 0.66, 0.88 and 0.95 μm , transmitted through the aerosols deposited continuously on a quartz fiber filter [Hansen *et al.*, 1982, 1984] that acts as a perfect diffuse scattering matrix with light absorbing particles embedded in it. The difference in light transmission through the particle-laden sample spot and a particle free reference spot of the filter is attributed to the absorption caused by the aerosol. The attenuation data are converted into BC mass loading using a set of wavelength dependent calibration factors [see http://mageesci.com/Aethalometer_book_2009.pdf]. The instrument was operated at a flow rate of 3 $l\ min^{-1}$ and with a data averaging time set to 5 minutes. 0.88 μm channel is considered as the standard channel for BC measurement because at this wavelength, BC is the principle absorber of light and other aerosol components have negligible absorption. Data obtained from other channels can be considered as *equivalent BC* mass that will produce the same absorption. If the absorbing component of the aerosols being sampled consists only of black carbon then the BC values obtained from all the channels of Aethalometer would be identical.

Absorption coefficient of the aerosols at all the seven channels of Aethalometer are calculated using the following relation [Bodhaine, 1995, Weingartner *et al.*, 2003; Ganguly *et al.*, 2005b]

$$\beta_{abs}(\lambda) = -\frac{1}{C.R} \frac{A \cdot \ln(I_2/I_1)}{Q \cdot \Delta t} \quad (2.4)$$

where I_1 and I_2 are the ratios of the intensities recorded by the detector for the sensing

beam to the reference beam before and after each sampling time interval Δt . Q is the volumetric flow rate of air sampled through the filter during interval Δt and A is the area of the spot where aerosols are collected. C is a correction factor applied to account for any change in absorption occurring in the filter embedded aerosols over that of the airborne particles while R is an empirical correction factor describing the change in instrumental response with increased particle loading on the filter. Finally Aethalometer calculates the aerosol black carbon concentration [Gundel *et al.*, 1984, Bodhaine, 1995, Weingartner *et al.*, 2003] using the following relation

$$M_{BC}(\lambda) = \frac{\beta_{abs}(\lambda)}{\sigma_{abs}(\lambda)} = \frac{\beta_{abs}(\lambda) \cdot C}{\sigma_{atn}(\lambda)} \quad (2.5)$$

where $\sigma_{abs}(\lambda)$ and $\sigma_{atn}(\lambda) = \sigma_{abs}(\lambda) \cdot C$ are the mass specific absorption and attenuation cross-sections respectively. The values of $\sigma_{atn}(\lambda)$ used are $14625/\lambda \text{ nm m}^2 \text{ g}^{-1}$ [Weingartner *et al.*, 2003]. Knowledge about the correction factors C and R is very important for the determination of the absorption coefficient [Weingartner *et al.*, 2003 and Kirchstetter *et al.*, 2004]. In the present study we have used the wavelength dependent values $C(\lambda)$ obtained from the work of Bodhaine, [1995] and assumed R to be equal to unity. Our calculation shows that the error in the estimation of absorption coefficient due to various instrumental artifacts such as flow rate, filter spot area, detector response is about 1%. However, maximum error can come due to empirical factors C and R . Previously Moosmuller *et al.* [1998] found the difference in absorption coefficient and BC mass from Aethalometer with those from Photoacoustic instrument, PSAP, Integrating Plate etc. to be in the range of 2 – 6%.

2.2.4 Nephelometer

Scattering coefficient of aerosols (β_{sca}) are measured using an Integrating Nephelometer (Model M903, Radiance Research, California, USA) [Ganguly *et al.*, 2005c]. This instrument draws the ambient air through a temperature controlled inlet, which is then illuminated by a flash lamp and the scattered light intensity is measured at 530 nm by a photomultiplier tube. Pressure and temperature measurements are made in the scattering chamber which are further used to calculate the scattering by air molecules and is subtracted from the total scattering to get the scattering by aerosols. Figure 2.4 shows the block diagram of the Nephelometer, model M903 of Radiance Research, USA, used in the present study.

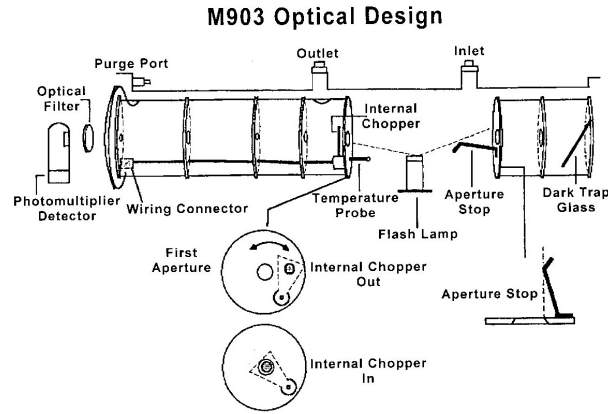


Figure 2.4: Block diagram of the Nephelometer (model M903 Radiance Research, USA) used in the present study for the measurement of aerosol scattering coefficient.

The instrument is regularly calibrated in laboratory according to the procedure described by Charlson *et al.* [1968], in which the Nephelometer is adjusted to read zero by passing particle free air and span calibration is done by passing the gases of high scattering coefficient such as CO_2 . The instrument has been operated in a continuous mode with data averaging time of 5 minutes.

2.2.5 Aerosol Size Spectrometer

Number size distribution of near surface aerosols is measured using an aerosol size spectrometer (model 1.108, Grimm aerosol technik, Germany) giving particle count for all aerosols in the size range of 0.3 to 20 μm by grouping them into 14 different size bins [see <http://www.grimm-aerosol.com/index.htm>]. This instrument constantly draws the ambient air using a volumetric pump at a flow rate of 1.2 $l\ min^{-1}$, passes them through a laser beam and records the scattered signal from particles at an angle of approximately 90° . Strength of each recorded signal carries information on particle size while number of such signals above a set threshold is proportional to the number of particles in that size range. Continuous data are recorded by this instrument at 5 minute interval.

2.2.6 Micro Pulse Lidar

We have used a co-axial mono-static Micro Pulse Lidar (MPL) system (SES Inc., USA) to get the vertical distribution of aerosols in the atmosphere and retrieve their extinction profiles. Lidar is based on active remote sensing principle in which backscattering of laser radiation is used to retrieve information on the structure and composition of the atmosphere. Usually a Lidar employs a pulsed laser as light source and the time delay between the transmitted pulse and the backscattered signal is used to derive information about the range of the scatterer from the lidar system.

Micro Pulse Lidar used in the present study uses an AlGaAs diode laser pumped Nd:YLF laser to get a frequency doubled output at 523.5 nm. This Lidar can be operated with a laser pulse repetition frequency varying anywhere from 1 Hz to 10000 Hz and pulse duration of 10 nS. However, in order to optimize the power associated with individual laser pulses and the signal to noise ratio, we have operated the MPL system with a pulse repetition frequency of 2500 Hz. High pulse repetition frequency is advantageous for averaging large number of low energy pulses in shorter time as it helps in achieving high signal to noise ratio [Welton *et al.*, 2000]. Pulse repetition frequency decides the maximum range detection limit for the Lidar system according to the relation

$$R_{max} = \frac{c}{2 \times PRF} \quad (2.6)$$

where c is the velocity of light and PRF is the pulse repetition frequency of the laser. The output energy for each pulse is in the range of 2 – 4 μJ . The MPL uses a common beam expansion configuration with a Schmidt-Cassegrain telescope serving as both transmitter of the outgoing laser beam as well as receiver of the backscattered photons. Diameter of the telescope is 20 cm and it has a field of view of about 50 μrad . In order to reduce the background noise, photons received by the optical transceiver are passed through an interference filter whose peak transmission is centered around 523.5 nm and a FWHM (Full Width at Half Maxima) of 0.1 nm. The MPL system uses a Si avalanche diode (Si-APD) based photon counting detector. The photon counting detector generates electrical pulses according to the photon numbers reaching the active element of the detector with a quantum efficiency of about 45% at 523.5 nm. The electrical pulses are counted by a *Multi Channel Scaler* (MCS) as time gated signal. Synchronization between multi channel scaler and the outgoing laser pulse is achieved by triggering the MCS with the laser pulse itself.

Currently allowed bin widths for our MPL system are 200, 500, 1000 and 2000 ns which correspond to the spatial resolution of 30, 75, 150 and 300 m respectively. In the present study MPL was operated with a bin width of 200 ns, corresponding to a range resolution of 30 m. Bin width of Lidar corresponds to the time for which backscattered signals are counted and recorded in a buffer of the multi channel scaler unit. In the present configuration of MPL, the first bin records the electrical pulses generated by photons scattered from the first 30 m of the atmosphere. Second bin holds the number of pulses generated by the scattered photons from the atmosphere between 30 and 60 m, third bin holds the number of pulses for 60 to 90 m and so on. For all practical purposes, each bin is designated by the central value of the corresponding range. Lidar signals are averaged and stored at 1 minute interval during data collection, which are averaged for longer periods of 5 minutes to one hour at the time of data analysis. Figure 2.5 shows the Micro Pulse Lidar system fitted inside the Mobile Lidar Observatory of Physical Research Laboratory and also a block diagram of MPL system. For the above geometry of the MPL, raw signal intensity can be

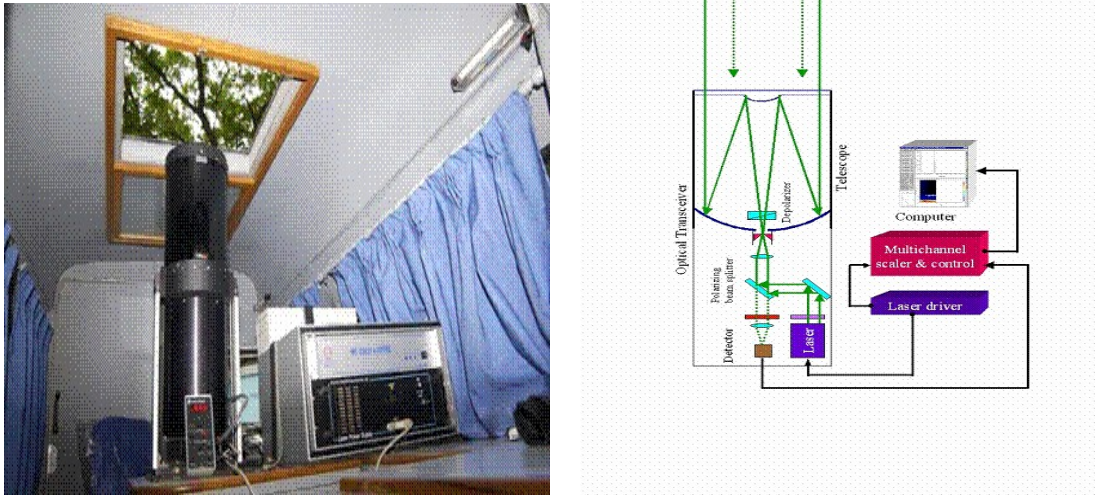


Figure 2.5: Left panel shows the Micro Pulse Lidar system fitted inside the Mobile Lidar Observatory of the Physical Research Laboratory, Ahmedabad. Right side panel shows the block diagram of the Micro Pulse Lidar system.

expressed in terms of Lidar equation of the following form

$$P(r) = \frac{CO(r)E\beta(r)T^2(r)}{r^2} + N_b + A(r) \quad (2.7)$$

In the above equation $P(r)$ represents the instantaneous signal intensity recorded by the

system, arriving from an altitude r . C is the MPL system constant which depends on the transmitter and receiver efficiencies and is a function of the MPL optics, $O(r)$ is the overlap correction factor (discussed later) and E is proportional to the output energy of the laser pulse. $\beta(r)$ is the volume backscattering coefficient of the atmosphere at laser wavelength and at range r . This gives the fractional amount of the incident energy scattered per steradian in the backward direction per unit atmospheric path length and has a unit of $m^{-1}Sr^{-1}$. N_b is the background noise signal, primarily due to sunlight during daytime, at laser wavelength (523.5 nm in the present case). $A(r)$ is the after-pulse correction signal (discussed later). $T(r)$ is the transmission of atmosphere from Lidar to range r and is given by

$$T(r) = \exp\left\{-\int_0^r \sigma(\hat{r})d\hat{r}\right\} \quad (2.8)$$

where $\sigma(\hat{r})$ is the extinction coefficient of the atmosphere and has a unit of m^{-1} . Replacing $T(r)$ of equation 2.7 by the above expression, equation 2.7 takes the following form

$$P(r) = \frac{CO(r)E\beta(r)\exp\left\{-2\int_0^r \sigma(\hat{r})d\hat{r}\right\}}{r^2} + N_b + A(r) \quad (2.9)$$

In this equation, the terms β and σ contain the required information of the atmospheric properties in which we are interested. However, β and σ values depend on a number of interacting physical processes as both these terms represent the sum of contribution from air molecules and aerosols. Also, it can be seen from equation 2.9 that the raw signals obtained from the Lidar need to be subjected through several correction procedures such as dead time correction, after pulse correction, overlap correction, background correction etc. before proceeding any further towards the evaluation of extinction coefficient of aerosols [Campbell *et al.*, 2002; Welton *et al.*, 2002]. Some of the correction factors applied to the raw signal from MPL are described below, however, the actual procedures followed to make the signals free from any instrumental artifact are described in Gadhavi [2005].

Detector dead-time correction: This correction is needed because the silicon avalanche photodiode detectors do not respond perfectly linearly under high incident rate of photons. Incident rate of photons being high for the first few bins, detector underestimates the actual count rate of photons for these bins. Usually the manufacturer supplies a correction table relating the actual incident count rate and the detected count rate, from which the dead-time correction factor can be calculated for all the bins of MPL.

After-pulse correction: This correction is needed because the internal reflection of the laser pulse within the MPL system, saturates the Si-APD detector at the beginning of the sampling period and an exponentially decaying leakage signal is recorded along with the actual signal. As the signal from different altitudes takes different times to reach the detector after the laser pulse is fired, after-pulse noise is a function of range. Correction for this after-pulse noise is determined by measuring the normalized signal when the returning photons are completely blocked beyond the first range bin. In this situation, the signal does not contain any return from the atmosphere and the measured signal is completely due to the after-pulse effect. In the after-pulse correction procedure, this beam-blocked after-pulse profile is subtracted from all actual atmospheric profiles at the time of post-processing the raw data. After-pulse noise being dependent on the energy of the laser pulse, the corresponding correction factor is normalized with the laser energy.

Background subtraction: When the MPL is operated in daytime, sky background is much stronger than the actual signal. Since the backscattered signal (both Rayleigh and Mie scattering) returning from high altitudes (more than 25 km) are negligible, counts recorded in the bins corresponding to such long distances are mainly due to sky background or to a small extent due to after-pulse effect. Based on this assumption, photon counts measured in the last 5 km (between 25 to 30 km) has been averaged and subtracted from the photon counts measured at all bins.

Overlap correction: Overlap correction is needed because due to a small difference existing between the field of view of the transmitter and receiver (detector) in MPL, there is an overspilling effect of the focused image of backscattered photons from the near vicinity of the detector which could be upto 5 km. At near-range, closer than about 3-5 km, the spot size of the outgoing laser pulse yields an image larger than the detector field of view, which results in an under-representation of near-range signal. In order to correct for this near-field instrumental artifact, MPL is operated with the beam oriented horizontally. Under appropriate well-mixed atmospheric conditions, the Lidar profile is expected to display an exponential dependence on range and show a linear relationship with it when plotted on a semi-log plot. The measured profile shows a straight line behaviour at far range, but due to imperfect overlap, it shows a kind of roll-off tending towards zero signal at near range. The overlap correction factor is evaluated for each bin in the near range by taking the ratio of expected signal strength obtained by extrapolating the straight line behaviour from far

range to near range bins and the measured signal for the corresponding bins.

After incorporating all the correction factors listed above, Lidar equation 2.9 takes the following form:

$$r^2 \dot{P}(r) = \dot{C} \beta(r) \exp \left\{ -2 \int_0^r \sigma(\dot{r}) d\dot{r} \right\} \quad (2.10)$$

where \dot{P} is the Lidar count at range r and \dot{C} is called as the calibration constant of the Lidar. The above equation is made system independent by taking a relative calibration approach and the same equation 2.10 takes the following form:

$$S - S_0 = \ln \frac{\beta}{\beta_0} - 2 \int_0^r \sigma(\dot{r}) d\dot{r} \quad (2.11)$$

where $S = \ln[r^2 \dot{P}(r)]$, $S_0 = S(r_0)$, $\beta_0 = \beta(r_0)$ and r_0 is a reference distance. Above equation can be written in the form of a differential equation of the following form:

$$\frac{dS}{dr} = \frac{1}{\beta} \frac{d\beta}{dr} - 2\sigma \quad (2.12)$$

There are two unknowns in the above equation viz. β and σ and a solution of the above equation is possible only if we have a relation between these two parameters. For all practical purposes, a linear relationship of the following form is assumed between these two quantities

$$\sigma = L\beta \quad (2.13)$$

where L is known as Lidar ratio. *Klett* [1985] gave a solution of equation 2.12 for $r < r_m$ of the following form

$$\sigma(r) = \frac{\exp[S - S_m]}{\left\{ \sigma_m^{-1} + 2 \int_r^{r_m} \exp[S - S_m] d\dot{r} \right\}} \quad (2.14)$$

Extinction values obtained using the above relation contains contribution due to both air molecules and aerosols ($\sigma(r) = \sigma_M(r) + \sigma_R(r)$, where suffix M and R stand for contribution due to aerosols and air molecules respectively). However, extinction due to aerosols can be calculated by subtracting the extinction values due to air molecules derived using tables of *McClatchey et al.* [1972] for standard tropical atmosphere from $\sigma(r)$ of equation 2.14.

In the present study, extinction coefficient due to aerosols is determined using a solution of equation 2.10 for the range $r < r_m$ of the following form

$$\sigma_M(r) = -L_M(r)\beta_R(r) + \frac{Z(r)}{N(r)} \quad (2.15)$$

with

$$Z(r) = L_M(r)r^2P(r)\exp\left\{2\int_r^{r_m}[L_M(\acute{r}) - L_R]\beta_R(\acute{r}d\acute{r})\right\} \quad (2.16)$$

$$N(r) = \frac{L_{Mm}r_m^2P_m}{L_{Mm}\beta_{Rm} + \sigma_{Mm}} + 2\int_r^{r_m}Z(\acute{r})d\acute{r} \quad (2.17)$$

where index m refers to the value of the corresponding quantity at the maximum range r_m . Also, Lidar ratio for the air molecules denoted as L_R is a constant and is equal to $8\pi/3$. Usually Lidar ratio for aerosols lie in the range from 20 to 80 Sr over different environments [Young *et al.*, 1993; Voss *et al.*, 2001; Welton *et al.*, 2002]. For our study, we have assumed Lidar ratio to be independent of altitude of the aerosol layer.

Meteorological data discussed in the present study are obtained from the meteorological center of Indian Meteorological Department (IMD) at Ahmedabad.

2.3 Results and Discussion

In order to study the characteristics of aerosols present over the urban location Ahmedabad, understand their behavior and estimate their effect on the radiative balance of the Earth-Atmosphere system on a regional scale, continuous measurements of various physical and optical parameters of aerosols are being made since early 2002. In this chapter, we present results on seasonal and inter-annual variabilities of these aerosol parameters studied over Ahmedabad during the period 2002 to 2005. Implications of the observed variabilities in various aerosol parameters are discussed separately in *Chapter-6*.

2.3.1 Aerosol optical depth

The time series of seasonal variation in AOD at two representative wavelengths viz. 0.38 and 1.02 μm , measured over the entire period of our study from 2002 to 2005 are shown in figure 2.6(b). Vertical lines on top of each bar represents $\pm 1\sigma$ variation about the mean value measured during that season. AOD values corresponding to both these wavelengths are higher for the year 2002 than during 2005, indicating higher total columnar loading of aerosols during 2002 than compared to 2005. Annual patterns of seasonal variability in AOD shows more consistency at longer wavelengths than at smaller wavelengths (0.38 μm). In all four years, AOD at 1.02 μm has been lower and comparable (within $\pm 1\sigma$ variation) during Dry and Post-Monsoon seasons, while higher values are obtained during

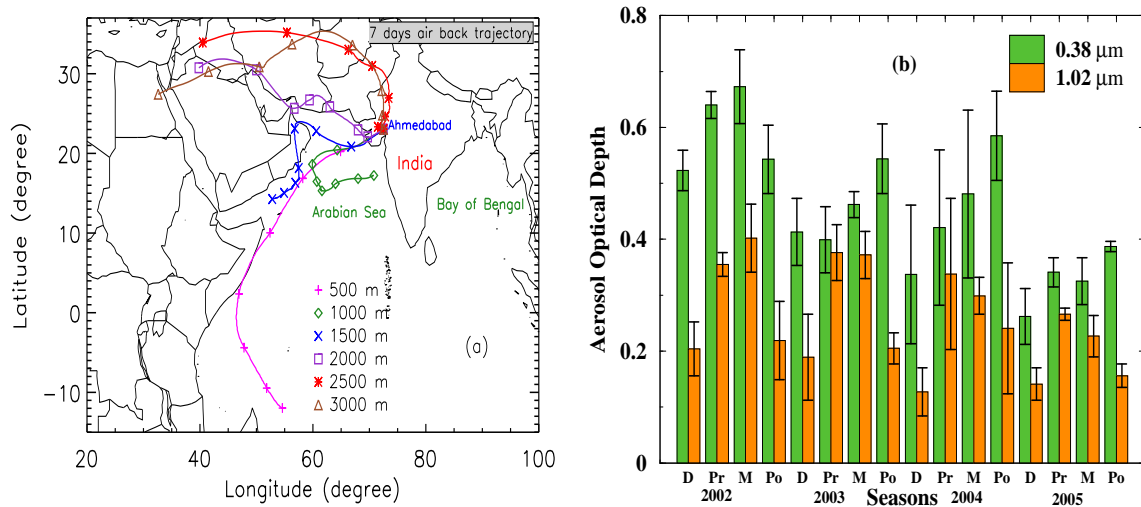


Figure 2.6: (a) Seven days air back trajectories for 6th June, 2002 from six different altitude levels over Ahmedabad. (b) Seasonal variation of AOD at 0.38 and 1.02 μm wavelengths measured over the period of our study from 2002 to 2005.

Pre-Monsoon and Monsoon seasons of the same year. Also, from Dry to Pre-Monsoon season, we notice an increase in AOD at all wavelength channels. This happens because of two reasons: first, due to increased wind speed during Pre-Monsoon season, large quantities of soil derived dust aerosol gets lifted in the atmosphere from the dry lands of semi-arid region all around our measurement location. Secondly, boundary layer height or the mixed layer thickness increases from Dry to Pre-Monsoon season, which provides a larger room for all kinds of natural and anthropogenic aerosols to get accommodated into it. Also, AOD values at higher wavelengths are more affected by naturally produced coarser aerosols, while the sub-micron sized aerosols produced mostly due to various anthropogenic activities contribute maximum to AODs at smaller wavelengths. While there is no significant variation occurring in the local production of aerosols from anthropogenic activities such as fossil fuel combustion or industrial emissions, there is always an increase of dust aerosols in the atmosphere from Dry to Pre-Monsoon season. Thus both these factors cause AOD values at all wavelength channels to increase over the first half of the year, the trend being much stronger and consistent at higher wavelengths. Further, AODs at almost all wavelength channels continue to maintain higher values during Monsoon season because not only winds, which are capable of lifting dust aerosols remain high during

this season, but also the higher relative humidity facilitates hygroscopic growth of several water soluble aerosols in the atmosphere. Although Monsoon season spans from June to September and Ahmedabad gets almost all of its total annual rainfall during this period, it is expected to see a decrease in AOD values due to wet removal of aerosols during rain events. However, this decrease does not seem to be always taking place primarily because even during Monsoon, rainfall in Ahmedabad is not very uniformly distributed over the entire season but occurs in certain spells with large intermittent gaps. Moreover as shown in figure 2.6(a), although the surface level wind flow is predominantly south-westerly, transport of dust aerosols from distant regions of West Asia and Northern Africa to this region continue to occur at higher altitudes during this season. Also, since the rainfall amount as well as its distribution over the Monsoon season has been quite different in different years, we observe different trends in AOD at different wavelengths and in different years. In the year 2002, when total annual rainfall itself was very scarce, AODs at 0.38 and 1.02 μm both show a continuously increasing trend from Dry to Monsoon season. In 2003, when Ahmedabad received more rainfall during Monsoon, AOD at higher wavelengths remained similar to their Pre-Monsoon values, but AOD at 0.38 μm increased further to reach still higher values. This trend is reversed in the year 2004, when AOD at 1.02 μm decreases from Pre-Monsoon to Monsoon season while AOD at 0.38 μm increased during the same period. This observed decrease in AOD at higher wavelengths from Pre-Monsoon to Monsoon period occurred primarily due to decline of dust loading during Monsoon season. As a result of good rainfall occurring this year, surface remained damp and offered sufficient resistance to lifting of soil dust by wind. However, increasing trend in AOD at lower wavelengths suggest that the effect due to increase in boundary layer height dominated over any loss due to wet removal processes in case of smaller aerosols of sub-micron size. But unlike all previous years, not only greater amount of rainfall occurred in the year 2005 but also it was more uniformly distributed over the entire Monsoon period. Due to such frequent spells of rainfall continuing throughout the Monsoon time, level of every aerosol type decreased in the atmosphere, which is evident from lower values of AOD at all wavelength channels measured during intermittent cloud free skies available during Monsoon season of 2005. Total aerosol loading in the atmosphere over any location depends on the differences between production of aerosols from all possible sources (either locally produced or transported to that location by wind) and their sinks (either gravita-

tional settling, rain wash or transported to other locations by wind). This means that even if there is no difference in source strength of aerosols, any weakening of the sink mechanisms can result in pile up of aerosols in the atmosphere which may manifest itself in terms of higher aerosol optical depth. This is what happens during Post-Monsoon season of all the years studied. Due to much weaker wind speeds during Post-Monsoon, dispersal of aerosol becomes much slower and those produced within city are not properly ventilated or get transported to other downwind locations. This causes AODs to attain much higher values during Post-Monsoon compared to following Dry season.

Although a time series of AOD at any single wavelength helps to study changes in total columnar aerosol loading, comparison of spectral AOD measured during different seasons can provide further insight on relative changes in columnar aerosol size distribution occurring at different times of a year. Figure 2.7(a) shows a comparison of mean AOD spectrum for different seasons, averaged over four years. Vertical lines in the figure represent $\pm 1 \sigma$ about the mean AOD value for a particular season and corresponding to a particular wavelength channel. Another important parameter estimated from multi-spectral measurement of aerosol optical depths is Angstrom wavelength exponent α , which is the slope of a plot between logarithm of AOD verses logarithm of wavelength in micron units. Angstrom parameter α is useful to compare and characterize the wavelength dependence of AOD and columnar aerosol size distribution [Eck *et al.*, 1999; Cachorro *et al.*, 2001]. For example, a relative increase in the number of larger sized particles with respect to the smaller ones result in a decrease in the value of α and vice-versa. However, α estimated from sun-photometer measured AOD depends on the wavelength pair used for the computation. In a separate study, Reid *et al.* [1999] have shown that α computed using shorter wavelength pair is more sensitive to changes in the amount of nucleation and accumulation mode sized particles than when estimated using longer wavelength pairs. In order to know the dominating factor which causes α to change from one season to another, we have computed this parameter for different wavelength intervals. Figure 2.7(b) shows the seasonal variation of α computed for three different wavelength intervals, each one of which is averaged over four years of AOD data from 2002 to 2005. Vertical lines on top of each bar represents $\pm 1 \sigma$ variation about the mean value for that season during the entire period of study. First, Angstrom parameter α is calculated using AOD values for all the channels (from 0.38 to 1.02 μm) and is also computed for two different wavelength pairs viz. 0.38 – 0.5 and

0.5 – 1.02 μm . In the present study, we find that α value computed using the complete spectrum of measured AOD are almost same when computed for the longer wavelength pair of 0.5 – 1.02 μm in all seasons, except during Dry and Post-Monsoon seasons, when α value derived for the shorter wavelength pair is found to be smaller than its corresponding value derived for larger wavelengths. Nevertheless, the pattern of seasonal variation of α computed using all the three wavelength pairs are similar.

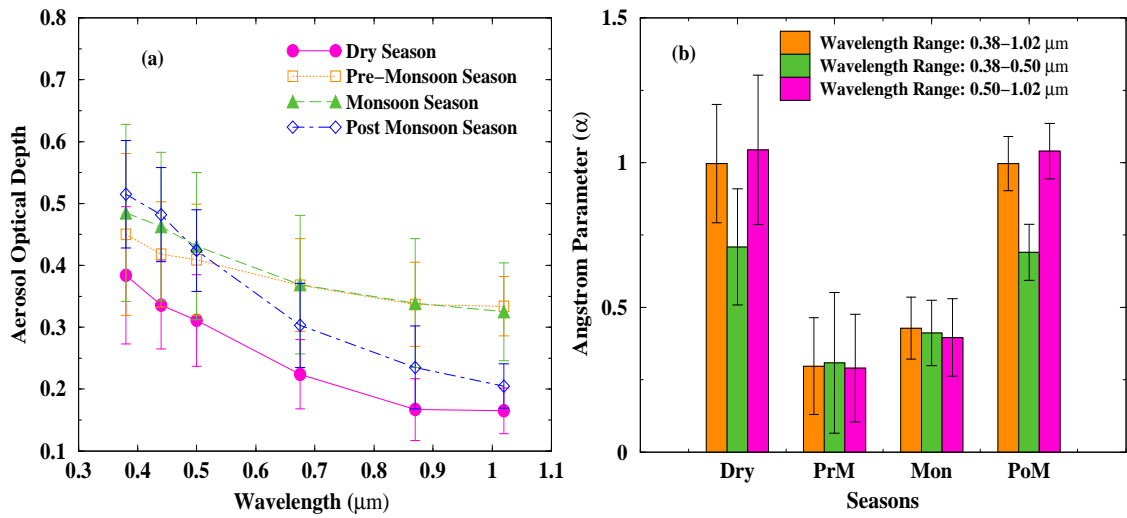


Figure 2.7: (a) Comparison of mean AOD spectrum for different seasons, averaged over four years of data available from 2002 to 2005. (b) Seasonal variation of Angstrom parameter α computed for three different wavelength intervals, each one of which is averaged over four years from 2002 to 2005.

Lower AODs for the entire spectrum obtained during Dry season suggest that total aerosol loading in the atmosphere is usually low during this season compared to all other seasons. When Dry season changes to Pre-Monsoon, we notice an increase in AOD values at all wavelength channels. However, importantly, this increase is found to be spectrally non-uniform as percentage increase in AOD at 1.02 μm during this seasonal transition is more than 100% while the corresponding increase in the case of AOD at 0.38 μm is merely 17%. On the other hand, we find a large drop in α values over the same period. As mentioned earlier, decrease in α can occur either due to a relative decrease in number of smaller sized particles with respect to larger ones or due to an increase in coarser particles with respect to smaller ones. It can be seen from figure 2.7(b) that α values computed using the longer wavelength pair, which is more sensitive to changes in the amount of coarse particles, exhibit maximum decrease while changing from Dry to Pre-Monsoon season.

Also, since AODs at higher wavelengths are more sensitive to changes in coarser particles while those at smaller wavelengths are susceptible to changes in smaller sized particles, this suggests that an increase in the amount of coarser particles (mostly super-micron) relative to other smaller (mostly sub-micron) aerosols is the dominating factor responsible for the observed non-uniform shift in AOD spectrum during this change of season from Dry to Pre-Monsoon. No significant change in the average AOD spectrum is observed from Pre-Monsoon to Monsoon season except some marginal increase in the AOD values at wavelengths shorter than $0.625 \mu\text{m}$, with a marginal increase in the α value estimated using all the wavelength pairs. These observations suggest that there is an increase in the total amount of sub-micron aerosols in the atmosphere from Pre-Monsoon to Monsoon season. It will be shown later using lidar data that the observed increase actually occurs due to increased volume being available to these aerosols to distribute themselves vertically in the atmosphere. During Post-Monsoon season, AOD spectrum takes different shape with further increase in AOD values at wavelengths shorter than $0.5 \mu\text{m}$ while a large drop is seen in the AOD values at longer wavelengths, with a simultaneous increase in α values computed using all the three wavelength pairs [figure 2.7(b)]. Once again we find that the percentage increase in α value derived using the longer wavelength pair is maximum, suggesting that as the season changes from Monsoon to Post-Monsoon period, amount of smaller particles increase and coarser particles decrease in the total atmosphere. The decrease in the amount of coarser particles play a dominating role in shaping the AOD spectrum during Post-Monsoon season. This decrease in the amount of coarser particles is expected as the wind speeds are minimum during this season and also after the monsoon rainfall, the growth of vegetation and grass offers resistance to the production mechanism of wind derived dust aerosols.

2.3.2 Aerosol mass concentration

Aerosol mass concentrations measured separately in 10 different size bins have been further classified into three categories viz. coarse mode particles with size ranging between 1 and $10 \mu\text{m}$ (total mass collected in stages 2, 3 and 4 of the QCM), accumulation mode particles in the size range of 0.1 to $1 \mu\text{m}$ (total mass collected in stages 5, 6, 7 and 8) and the nucleation mode particles with size less than $0.1 \mu\text{m}$ (total mass collected in stages 9 and 10). Aerosol mass obtained from stage 1 of the QCM device is not included in this

classification, as it integrates all particles of size greater than $12.5 \mu m$ and no meaningful mean radius could be assigned to this stage.

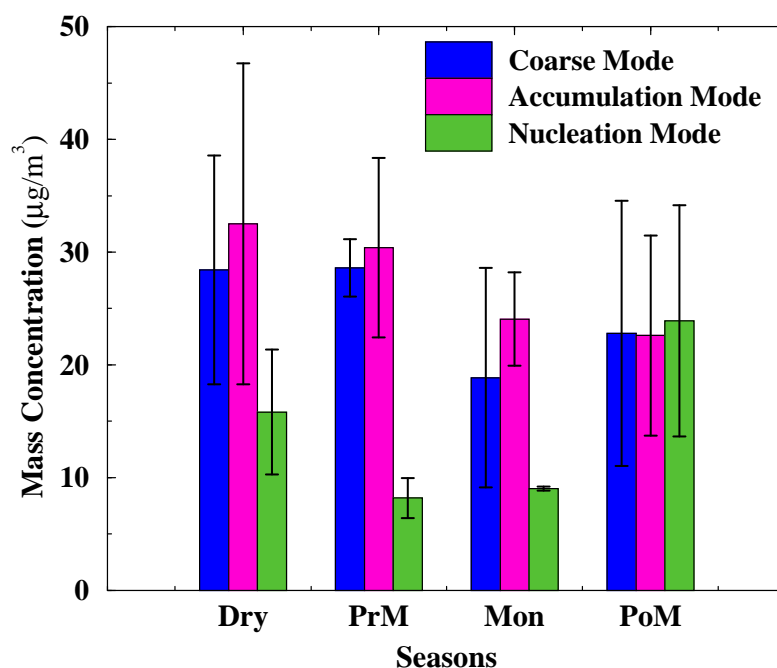


Figure 2.8: Seasonal variation of near surface aerosol mass concentration classified into three categories viz. coarse mode, accumulation mode and nucleation mode particles, averaged for three years of data available from 2002 to 2004.

Figure 2.8 shows the seasonal variation of near surface aerosol mass concentrations for all the three size modes and averaged over a period of three years from 2002 to 2004. Measurements of aerosol mass concentration could not be continued during 2005 due to technical problem with the QCM device. Though the problem could be rectified during late 2005 and regular measurements were resumed the data are not considered in the present study. Over the period for which data is available, PM_{10} (particulate matter of size less than $10 \mu m$) concentration mostly varied from low values close to $40 \mu g/m^3$ to high of about $106 \mu g/m^3$ with an average value of around $66 \mu g/m^3$. Lower values for PM_{10} mass concentration are observed during Monsoon season. This is contrary to the trend seen in the case of columnar AODs which exhibit higher values during Monsoon season (except for the year 2005). This condition could arise only if changes occur in the vertical distribution of aerosols in such a way that a significant contribution of extinction to the column AOD comes from aerosols present at higher altitudes. In an earlier study conducted

over another tropical Indian station, Gadanki ($13.5^{\circ}N$, $79.2^{\circ}E$), *Krishnan and Kunhikrishnan* [2004] observed the atmospheric boundary layer height to become maximum during Pre-Monsoon period and minimum during Dry months. Over Ahmedabad we find a summer-time increase in atmospheric boundary layer, as a result of which, a larger volume becomes available for the aerosols to get distributed in the atmosphere during this period. Because of this increased boundary layer height, a larger mixing of aerosols occurs within this layer, which in turn dilutes the aerosol concentration near surface level. It will be shown later in the chapter that using a simultaneously operated Micro Pulse Lidar system we have observed such changes occurring in boundary layer height and aerosols are detected upto much higher heights in summer, contributing significantly to AOD.

In general, nucleation mode aerosols contribute least to the total mass, except during Post-Monsoon season when the contribution by all the modes are found to become almost equal. Also, since most of the nucleation mode aerosols (soot, sulfate etc.) are associated with anthropogenic sources (fossil fuel or biomass/biofuel burning), their concentration is found to increase when the surface level wind flow is observed from the north, north-east or north-west. During Pre-Monsoon and Monsoon seasons, surface level wind flow is from the Arabian sea in south and hence the air masses reaching Ahmedabad at lower levels are relatively less polluted compared to air masses which are of purely continental origin during other seasons. During Dry and Post-Monsoon seasons, aerosols which are either locally produced or transported from other regions are constrained within a shallow boundary layer having smaller ventilation coefficient and this causes their surface level concentration to rise. High values of mass concentration for the nucleation mode aerosols are obtained during Post-Monsoon and Dry season. One of the reasons is that during the months from November to January (winter months) we observe a lot of waste burning activities in the open, such as burning dry leaves and shrubs in various parts of the city. In addition, another important source which contributes significantly to the production of aerosols and precursor gases is burning of wood, paper or other solid wastes in the open by population dwelling in the city slums, to keep themselves warm during cold winter nights. It will be shown later in the chapter that signatures of such anthropogenic activities are very well captured in the data from other two surface based aerosol instruments viz. Aethalometer and Nephelometer.

The accumulation mode aerosols are produced by the condensation growth and co-

agulation of nucleation mode aerosols. In general, we have found accumulation mode aerosols contributing maximum to the total PM_{10} mass. On an average, their mass varied from a low concentration of about $22 \mu g/m^3$ recorded during Monsoon or Post-Monsoon seasons to a high concentration of about $33 \mu g/m^3$ during Dry season. Over the period of our study, accumulation mode aerosols have shown minimum variability in their mass concentration during all seasons and over the entire period of measurement (a maximum of 34% departure from the mean). Except for the nucleation mode, we have seen large inter-annual differences in the seasonal variation of aerosol mass concentration as specific patterns are obtained in different years. The intricacies behind such inter-annual differences in the pattern of seasonal variation of surface level aerosol mass concentration is difficult to explain and we restrict our discussion only to the average pattern of seasonal variation over the entire period of study.

Coarse mode aerosols over land are mainly soil derived dust particles produced by wind blowing over land surfaces, particularly when it is dry and has less vegetation cover. Most of these particles are mineral aerosols made up of materials derived from the Earth's crust and are therefore rich in iron and aluminium oxides and calcium carbonate [Rastogi and Sarin, 2005]. The North Indian Ocean is surrounded by several arid and semi-arid areas which are the major sources of these particles. The largest one being the Rub Al Khali desert in central Saudi Arabia but there are several other sources located in Iran, Pakistan, Afghanistan and north-west India [Leon and Legrand, 2003].

During the period of our study, average value of coarse mode aerosol mass measured over Ahmedabad is around $25 \mu g/m^3$. This amount varied anywhere from low values close to $12 \mu g/m^3$ measured during Monsoon season to high values around $40 \mu g/m^3$ measured during Dry or Pre-Monsoon seasons. Higher values of coarse mode aerosol mass are recorded during Dry season because during this time surface level wind flow over Ahmedabad is mainly from north-west direction (figure 2.2) and there are high possibilities of dust particles being carried to the city from vast areas of arid and semi-arid regions in north-west India including Thar Desert. This transport of dust aerosols from arid and semi-arid regions in the west of Ahmedabad continues even during other seasons of the year but those occurring at higher levels [figure 2.6(a)] are not detected in surface measurements. Near surface values of coarse mode aerosol mass decreases during Monsoon season because during this time surface level wind flow is from the Arabian Sea in south

and south-west of Ahmedabad and therefore it is depleted in dust content but could bring in some amount of sea salt aerosols. Also, during Monsoon season, occasional spells of rain keeps the surface damp and availability of loose soil to be lifted by the wind becomes less. Most of the dust aerosols measured during Monsoon season are locally produced and higher values of coarse mode aerosol mass are measured in the years when rainfall amount is less and soil remains dry. Lower values of coarse mode aerosol mass are also measured during Post-Monsoon season because of two reasons, firstly lower wind speed during this season is not very efficient in lifting dust from the surface and secondly rainfall occurring during previous Monsoon increases grass and other vegetation cover over the surface, which offers resistance to lifting of soil dust by wind.

2.3.3 Aerosol number size distribution

QCM observations have been further used to obtain the number size distribution for the near surface aerosols. Mass concentrations measured in the 10 size ranges are used to derive the aerosol number distribution using appropriate mass density valid for the urban atmosphere and prevailing relative humidity conditions [d'Almeida, 1991; Hess *et al.*, 1998]. We have observed maximum seasonal variation in the number concentration data corresponding to nucleation mode aerosols, with nearly 60% spread in its value about the mean for the entire study period. This is followed by accumulation and coarse mode data showing about 26 and 17 % spread in their values respectively. The size distribution of aerosols at any location is mainly governed by the relative strengths of different production and removal mechanisms [Jaenicke, 1993]. Several authors [Porter and Clarke, 1997; Bates *et al.*, 1998; Koponen *et al.*, 2003; Ramachandran and Jayaraman, 2002; Ganguly *et al.*, 2005a] have shown that the size distribution of tropospheric aerosols is a combination of many log-normal distributions, where different modes represent different production sources. Figure 2.9 shows the aerosol number size distribution for two typical seasons of the study period with vertical bars in the figure representing $\pm 1 \sigma$ variation about the average number concentration for different size bins. All size distribution plots obtained during the study period exhibited presence of three distinct modes and hence they could be fitted using three log-normal modes of the form:

$$\frac{dn(r)}{d\log r} = \frac{N}{\sqrt{2\pi}\log\sigma} \exp\left[-\frac{\log^2\left(\frac{r}{r_m}\right)}{2(\log\sigma)^2}\right] \quad (2.18)$$

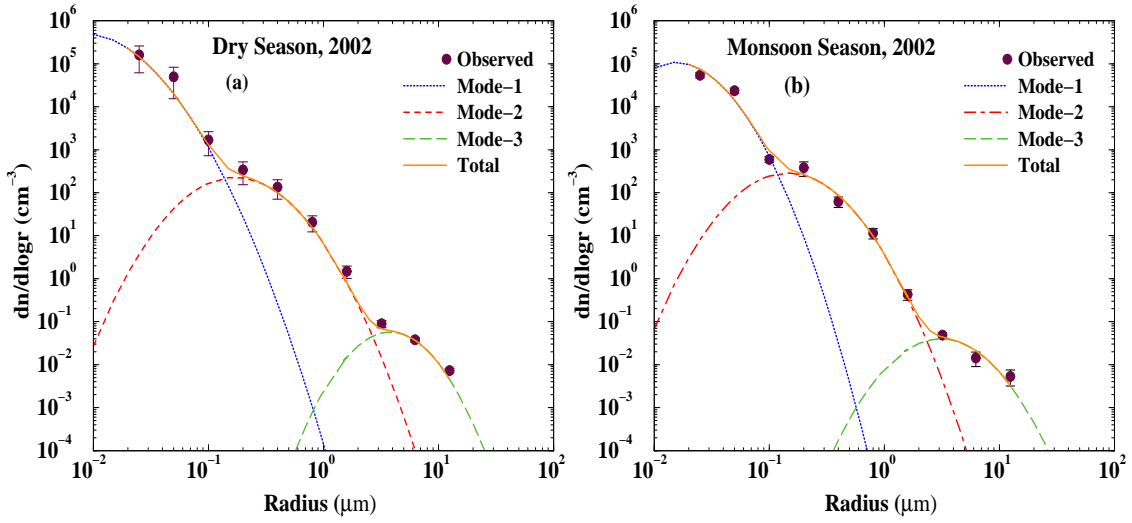


Figure 2.9: Aerosol number size distribution for two typical seasons of the study period with vertical bars in the figure representing $\pm 1 \sigma$ variation about the average number number concentration for different size bins.

where N is the number concentration (cm^{-3}), σ is the width of the distribution and r_m is the mode radius for a particular mode. We find that the shape of the aerosol size distribution remained same over the study period while number concentration changed in all the three modes during different seasons of different years. This indicates that the amount of aerosols as well as their in situ production strengths changed while various physical processes responsible for their distribution in the atmosphere remained unaltered. Table 2.2 gives the average values of various modal parameters obtained by log-normal curve fitting carried out on the measured distribution. Mode radii of the distribution corresponding to mode-1 lie in the range of $0.009 - 0.018 \mu m$ and the number concentration values for this mode are found to be highest during Pre-Monsoon season while low values are obtained in Monsoon period. Similarly, mode radii of the distribution corresponding to mode-2 and mode-3 lie in the range of $0.08 - 0.18 \mu m$ and $2.2 - 3.8 \mu m$ respectively. Comparing the modal parameters of Table 1 with those of various aerosol types classified by *Hess et al.* [1998], we find that water soluble aerosols and soot particles constitute mode-1 aerosols while the r_m value of mode-2 matches with those of sulfate aerosols or some of the accumulation mode mineral aerosols. These sulfate aerosols are mostly produced by chemical reactions in the atmosphere by gaseous precursors, mainly sulfur dioxide (SO_2) emitted from various anthropogenic sources [*Charlson et al.*, 1992]. Finally, possible aerosol types

constituting mode-3 of the measured size distribution are either insoluble particles such as soil dusts getting transported from arid and semi-arid regions of surrounding areas or coarser mineral aerosols of desert origin. It can be seen from table 2.2 that there is an increase in the number concentration of particles in mode-3 during Post-Monsoon season, which is contrary to the trend seen in the case of coarse mode aerosols [figure 2.8]. However, the seasonal variation of mode radii corresponding to mode-3 shows a maximum during Dry and Pre-Monsoon seasons and minimum during Monsoon and Post-Monsoon periods. Although number concentration of mode-3 aerosols is less during Dry and Pre-Monsoon compared to Monsoon and Post-Monsoon seasons, it contributes maximum towards the mass concentration of coarse mode aerosols due to their larger mode radii during Dry and Pre-Monsoon seasons. One possible reason for getting larger mode radii for mode-3 aerosols during Dry and Pre-Monsoon seasons is that during these seasons, surface level winds coming from north-west direction of Ahmedabad can bring in coarser desert dust particles to the measurement location (figure 2.2). On the other hand particles constituting mode-3 aerosols during Monsoon and Pre-Monsoon seasons being locally produced soil dust, their mode radii are found to be less compared to other desert dust mineral aerosols prevalent during other seasons.

Table 2.2: Average values of size distribution parameters obtained by fitting log-normal curves to the measured aerosol number size distribution over Ahmedabad

Season	Mode-1			Mode-2			Mode-3		
	N (cm^{-3})	σ (μm)	r_m (μm)	N	σ	r_m	N	σ	r_m
Dry	410000	1.95	0.009	180	1.95	0.157	0.034	1.79	3.47
PrM	230000	2.03	0.009	157	1.99	0.160	0.040	1.78	3.77
Mon	60000	1.81	0.017	203	1.93	0.143	0.040	1.83	3.03
PoM	380000	1.89	0.012	280	2.04	0.112	0.045	1.83	2.87

2.3.4 Black Carbon mass concentration

In the present day global scenario, one of the crucial climate forcing agents is black carbon (BC) aerosols, mostly produced from the incomplete combustion of fossil fuels such as coal, diesel, petrol etc. as well as due to usage of biofuel and biomass burning across various parts of the world [Novakov *et al.*, 2000; Jacobson, 2001; Venkataraman *et al.*, 2005]. Although BC aerosols have been recognized as crucial climate forcing agents contributing

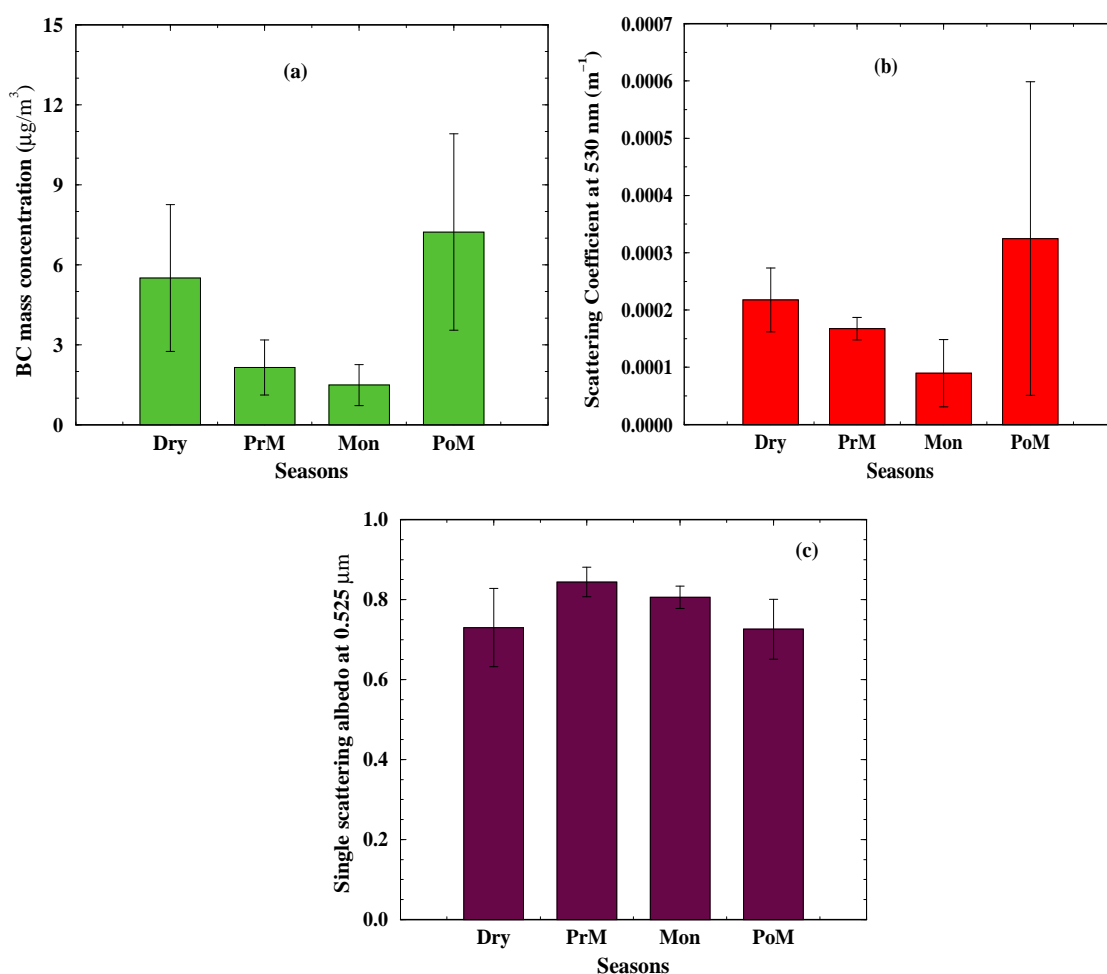


Figure 2.10: Seasonal variation of (a) BC mass concentration, (b) aerosol scattering coefficient at $0.53 \mu\text{m}$ and (c) single scattering albedo at $0.525 \mu\text{m}$, averaged over all data available from 2003 to 2005. Vertical lines on top of each bar represent $\pm 1 \sigma$ variation about the mean value for the corresponding parameter in that season.

significantly to the present day global warming [Jacobson, 2002], they occupy special importance over populous regions of the world like India and China because of their large local production and possible impact on regional climate [Ramanathan *et al.*, 2001b; Menon *et al.*, 2002]. Jacobson [2002] has shown that large positive radiative forcing produced by BC aerosols makes it second most important agent for global warming after CO_2 in terms of direct radiative forcing estimates. Total BC emissions from India including all sources such as fossil fuel, open burning and biofuel combustion is around $610 \pm 200 \text{ Gg year}^{-1}$ [Venkataraman *et al.*, 2005]. This constitutes a large fraction of total global emission and

therefore demands regular monitoring of BC aerosols across various parts of India to know their radiative impacts not only on a regional scale but also to study their global climatic effects.

BC measurements over Ahmedabad started during Monsoon 2003 and since then almost continuous data are available over this location till date. Figure 2.10(a) shows the seasonal variation of BC mass concentration averaged over 2003 to 2005. Vertical lines on top of each bar represent $\pm 1 \sigma$ variation about the mean mass concentration available for that season. Observed seasonal variation in BC mass is similar to that observed in the case of nucleation mode aerosols [figures 2.10(a) and 2.8]. This shows that BC aerosols constitute a major fraction of nucleation mode aerosols over Ahmedabad. Highest value of BC mass is obtained during Post-Monsoon season (mean value $7.3 \pm 3.7 \mu\text{g}/\text{m}^3$). This amount decreases slightly during Dry season ($5.5 \pm 2.8 \mu\text{g}/\text{m}^3$) and comparatively much lower values of BC mass are measured during Pre-Monsoon ($2.2 \pm 1.0 \mu\text{g}/\text{m}^3$) and Monsoon seasons ($1.5 \pm 0.8 \mu\text{g}/\text{m}^3$). It is also found that not only the absolute values of BC mass concentration are high in Post-Monsoon and Dry seasons, mass fraction of BC in the total aerosol concentration also remains high during these seasons. On an average, we find BC mass fraction over Ahmedabad is around 10% during Post-Monsoon season while this percentage changed to 7, 3 and 3 during Dry, Pre-Monsoon and Monsoon seasons respectively. Previously *Babu et al.* [2002] have reported the BC concentrations over Bangalore (13°N , 77°E) for the month of November to be in the range of $0.4 - 10.2 \mu\text{g}/\text{m}^3$. Also, from a month long campaign in December 2004, *Tripathy et al.* [2005] have reported BC concentrations over Kanpur city (23.43°N , 80.33°E) to be in the range of $6 - 20 \mu\text{g}/\text{m}^3$ and BC mass fraction to vary from 7 to 15%. *Ganguly et al.* [2005b] found the daytime (10 – 16 hrs) average BC mass over another urban location, Hyderabad (17.47°N , 78.45°E) to be around $4.8 \mu\text{g}/\text{m}^3$. *Venkataraman et al.* [2002] have reported the BC concentrations for Mumbai (19.38°N , 72.83°E) during INDOEX-IFP (Jan-Mar, 1999) as $12.5 \pm 5 \mu\text{g}/\text{m}^3$. At another coastal urban station, Trivandrum (8.55°N ; 77°E), *Babu and Moorthy*, [2002] found the mean BC concentration to vary from 5 to $1.5 \mu\text{g}/\text{m}^3$ from Dry to Monsoon seasons. Also, during an intensive field campaign in December 2004, our group found the average BC mass over Delhi to be $29 \pm 14 \mu\text{g}/\text{m}^3$ (highest among all above mentioned values) [*Ganguly et al.*, 2006]. Comparing results from the present study and BC measurements conducted over other urban locations in India, we find that BC mass over Ahmedabad is

lower than the two urban cities viz. Delhi and Kanpur located in the Indo-Gangetic belt while it is higher than coastal locations like Trivandrum and comparable with two other urban cities viz. Bangalore and Hyderabad both located in peninsular India.

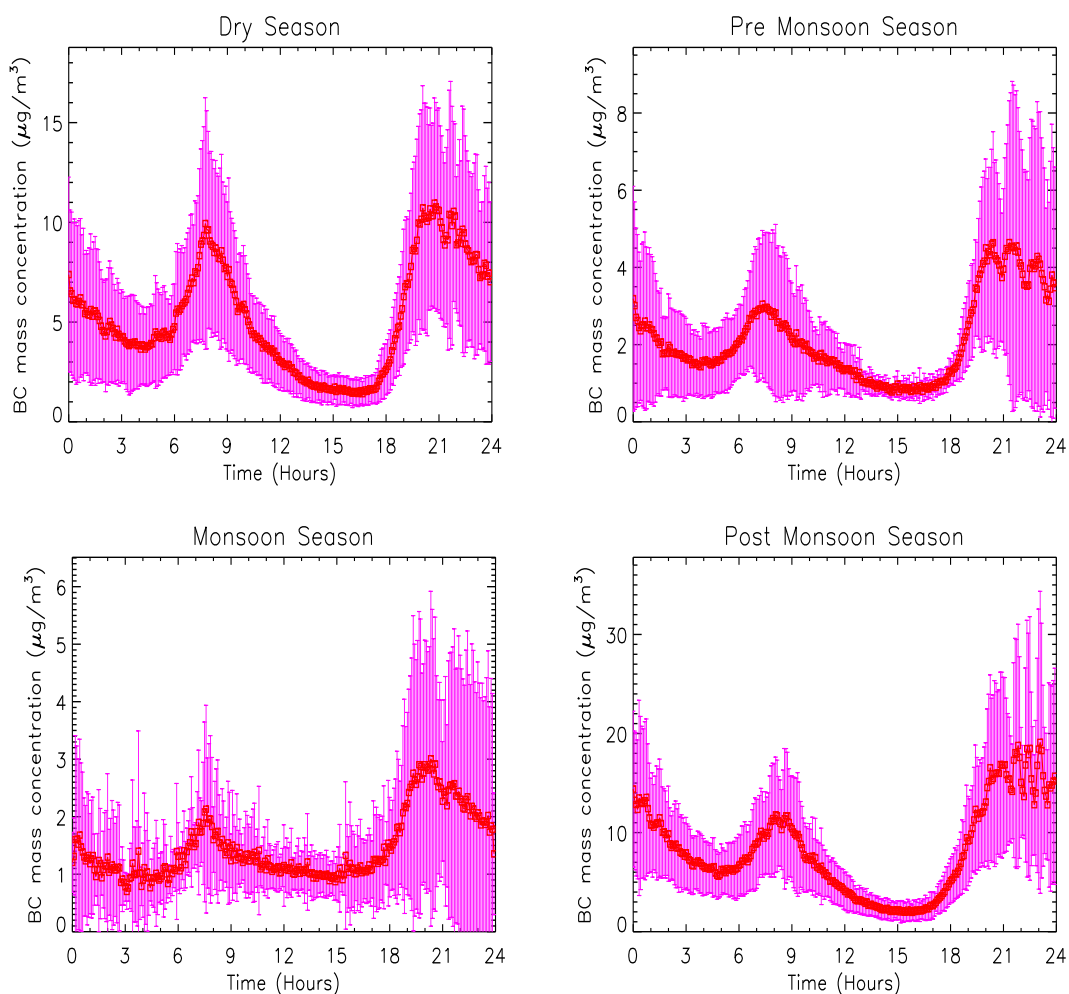


Figure 2.11: Average patterns in diurnal variation of BC aerosol mass concentration for different seasons of a year, with vertical lines representing $\pm 1\sigma$ variation about the mean value of BC at a particular time on different days of a particular season.

High values of BC mass and its mass fraction in the total aerosol concentration measured over Ahmedabad during Post-Monsoon and Dry seasons have serious implications on regional aerosol radiative forcing as these soot particles are strong absorber of both incoming solar radiation as well as outgoing terrestrial infrared radiation, and alter the radiation budget of the Earth by trapping heat within the atmosphere [Jacobson, 2001]. Figure 2.11 shows the average patterns in diurnal variation of BC aerosol for different sea-

sons of the year. These patterns are actually combined outcome of various factors such as production source of aerosols, their source strengths, their removal mechanisms and also the surface meteorology. Vertical lines in all the panels represent $\pm 1 \sigma$ variation about the mean BC value measured at a particular time on different days of a particular season. Most common feature in the diurnal variation of BC mass during all seasons is the presence of two maxima and two minima in all these plots. During Dry and Post-Monsoon seasons, first maxima of the day is observed in the morning hours, sometime between 08 – 09 hrs, while this peak shifts to earlier period between 07 – 08 hrs during Pre-Monsoon and Monsoon seasons. Second maxima in the diurnal variation of BC mass concentration is recorded in the late evening or nighttime between 20 – 21 hrs. First minima in BC mass concentration is observed in the early morning between 03 – 04 hrs, while second minima corresponding to the lowest concentration of a day occurs in the afternoon, sometime between 15 – 17 hrs depending on the season. Identical patterns appearing in all seasons suggest that the diurnal variation of BC is mainly governed by the diurnal evolution of atmospheric boundary layer which remains low during morning hours then gradually increases and reaches a higher value at noontime and starts decreasing in the evening [Krishnan and Kunhikrishnan, 2004]. This cycle is repeated on all clear sky days throughout any year. However, seasonal variations in absolute magnitude of BC largely occurs due to differences in the extent of contraction and expansion of the atmospheric boundary layer primarily due to differential Solar heating of the Earth's surface as well as differences in production sources and their source strengths in different seasons. Increased production of BC aerosols and gradual formation of a surface based inversion opposing vertical mixing in the atmosphere cause BC concentrations to escalate from around 16 hrs and reach maxima in the evening after 20 hrs. One important reason for the increased production of BC aerosols in the evening time is related to road traffic and open burning of solid wastes such as dry leaves and other garbage materials, particularly during Dry and Post-Monsoon seasons. In addition to waste burning, wood and shrubs are also burnt at night by several people to keep themselves warm during cold winter months. Maxima in BC concentrations between 07 – 09 hrs is primarily due to morning peak in traffic level and several small scale industrial activities spread around the city. After around 09 hrs, BC concentrations start decreasing as some of the sources are not very active during this time while boundary layer height of the atmosphere start rising with increased insolation of

the Earth's surface which kicks off convective mixing of air capable of lifting aerosols to higher levels in the atmosphere and causing a dilution of their concentration at the surface level [Krishnan and Kunhikrishnan, 2004]. BC values reach lowest concentrations between 15 – 17 hrs due to minima in traffic levels in the afternoon hours and higher boundary layer height. After around 20 hrs, the city traffic decreases by a large extent, making one of the main production sources of BC over this urban location weaker while removal of particles from the atmosphere by gravitational settling process continues, which give rise to a minima in BC concentration during early morning between 03 – 04 hrs.

2.3.5 Aerosol absorption coefficient

Although measurements of BC concentration itself is important over populous parts of the world to assess the air quality, but the parameter required to calculate the impact of light absorbing particles on the regional and global climate forcing is the absorption coefficient (β_{abs}) of these aerosols. In the present study, absorption coefficient of aerosols are calculated using the raw absorbance data recorded at all the seven wavelength channels of Aethalometer viz. 0.37, 0.47, 0.52, 0.59, 0.66, 0.88 and 0.95 μm . Measurements on spectral dependence of aerosol absorption is very useful because it contains some characteristic features of the sources producing these absorbing species [Kirchstetter *et al.*, 2004]. This fact is particularly important over the Indian region where contribution of BC from biomass/biofuel burning is as important as fossil fuel combustion and the same amount of BC from biofuel can exhibit stronger absorption characteristics [Venkataraman *et al.*, 2005; Ganguly *et al.*, 2005b]. Wavelength dependence of absorption by aerosols have been investigated using a power law relationship of the form $\beta_{abs}(\lambda) = K \cdot \lambda^{-\alpha}$ where K and α are the absorption Angstrom coefficients and α is a measure of spectral dependence of aerosol absorption [Kirchstetter *et al.*, 2004; Ganguly *et al.*, 2005b]. Figure 2.12 shows the spectra of aerosol absorption coefficient for different seasons, averaged over all available data from 2003 to 2005. Vertical lines in this figure represent $\pm 1 \sigma$ about the mean value β_{abs} for a particular season and corresponding to a particular wavelength channel of Aethalometer. As reported earlier, BC mass concentration over Ahmedabad during Post-Monsoon and Dry seasons are higher than those obtained during Pre-Monsoon and Monsoon seasons. Figure 2.12 clearly shows that not only mass concentration of these soot particles but also the absorbing capability of the aerosols in general increases enormously, particularly at

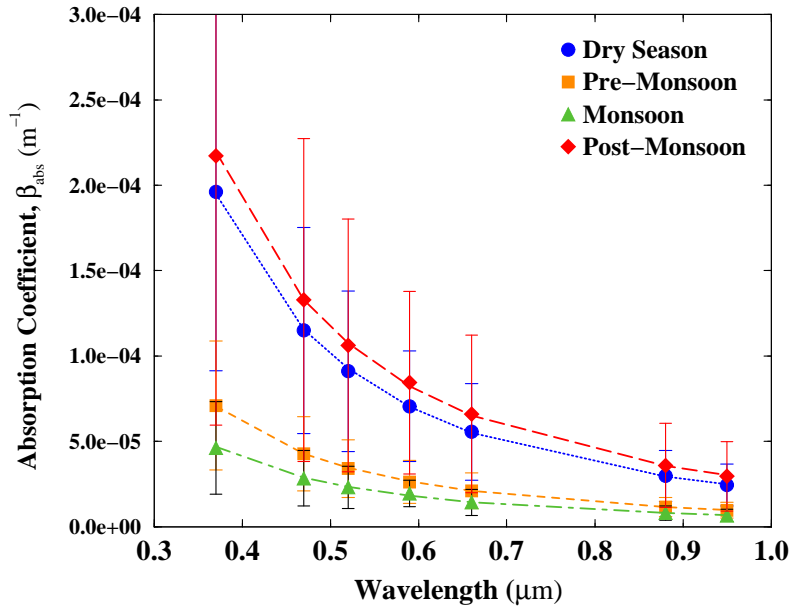


Figure 2.12: Mean spectra of aerosol absorption coefficient for different seasons of a year, which are best fitted using power law curves.

shorter wavelengths, during Post-Monsoon and Dry seasons. In order to quantify these relative changes in absorption characteristics of aerosols, spectra of absorption coefficients for each season are fitted using the power law relation mentioned earlier and α values have been estimated. We find the average values of absorption Angstrom parameter α to be 2.2, 2.0, 1.9 and 2.1 for Dry, Pre-Monsoon, Monsoon and Post Monsoon seasons respectively. Although, differences in absolute values of absorption coefficient are not very large in different seasons, large differences occur in the values of β_{abs} at shorter wavelengths due to exponential relation of β_{abs} with λ . *Kirchstetter et al.* [2004] reported stronger spectral dependence in absorption ($\sim \lambda^{-2.5}$) shown by biomass/firewood aerosols from the Southern African Regional Science Initiative (SAFARI) experiment while a much weaker spectral dependence ($\sim \lambda^{-1}$) exhibited by roadway samples from Berkeley consisting of motor vehicle aerosols produced due to fossil fuel burning. *Kirchstetter et al.* [2004] also observed that extraction of biomass burning aerosols with acetone, removed significant amount of organic carbon (OC) from the sample, reduced spectral dependency in absorption and brought down the α value close to 1.2. Other studies [eg. *Jacobson et al.*, 2000; *Bond*, 2001; *Bergstrom et al.*, 2002] have also shown that mixture of aerosols in which absorption is mainly due to BC, exhibit a weak spectral dependence (λ^{-1}). Wavelength dependency

of aerosol absorption obtained over Ahmedabad shows signatures for the presence of absorbing aerosols produced from sources other than burning of fossil fuel. Comparison of our finding with the results published by other researchers shows that there are significant amounts of absorbing aerosols in the atmosphere produced from biomass/biofuel burning occurring in all seasons. Higher values of absorption Angstrom parameter α during Dry and Post-Monsoon season shows that activities related to biomass/biofuel burning increase during these seasons which produces larger amounts of such absorbing species in the atmosphere. These activities mainly include open burning of dry leaves or other waste materials which serves as a rather easy way of getting rid of such garbage materials. Other source of carbonaceous aerosols is the usage of biofuel such as wood, animal-dung cakes etc. for cooking by a large population living in slums of the city [Reddy and Venkataraman, 2002]. Also a detailed work by Venkataraman *et al.* [2005] have shown that in India about 44% of the total BC emission comes from biofuel combustion. Most of the sources of carbonaceous aerosols discussed so far involve low temperature and incomplete combustion processes which release sufficient amount of organic carbon (OC) apart from soot or BC. Kirchstetter *et al.* [2004] have shown that presence of OC in addition to BC in biomass/biofuel smoke aerosols affects spectral dependence in absorption by aerosols, contributing significantly to the measured light absorption in visible and ultraviolet regions. However, it is a subject for investigation whether OC from biomass burning, which is considered to be the scattering component of carbonaceous aerosols [Novakov *et al.*, 2005], itself contributes to absorption in addition to BC or it forms some kind of coated shell around BC aerosols that increases the absorption efficiency of these complex mixtures [Jacobson, 2000; Jacobson, 2001]. Further laboratory experiments under controlled conditions with known aerosol types as well as modelling studies are required to confirm the exact reason which causes the observed increase in spectral dependence of absorption by aerosols at places where biomass/biofuel burning are major sources of carbonaceous aerosols in the atmosphere. Nevertheless, high values of BC mass with increased absorption efficiency measured over Ahmedabad is expected to produce higher values of aerosol radiative forcing.

2.3.6 Aerosol scattering coefficient

Measurements of aerosol scattering coefficient (β_{sca}) started during Monsoon 2003, along with the BC measurements. Figure 2.10(b) shows the seasonal variation of aerosol scattering coefficient at $0.53 \mu m$, averaged over all data available from the year 2003 to 2005. Vertical lines on top of each bar represent $\pm 1 \sigma$ variation about the mean of all data on β_{sca} available for that season. Aerosol types which contribute maximum to the scattering coefficient include water-soluble inorganic species such as sulfates, nitrates etc., arising from emissions of SO_2 and NO_x associated mainly with fossil fuel combustion, ammonium from fertilizers and biological sources and some organic aerosols arising from biomass combustion [Charlson *et al.*, 1992; Penner *et al.*, 1994]. In addition to these, nitrates and organic aerosols from industrial emissions also contribute significantly to the scattering characteristics of aerosols. Comparing the results presented in figure 2.10(a) and 2.10(b), we find that the seasonal variation in aerosol scattering coefficient is very much similar to that of BC mass concentration. This shows that majority of absorbing and scattering type aerosols prevalent over Ahmedabad have common production sources. Also, similarity of both these plots with the seasonal variation of nucleation mode aerosols (figure 2.8) shows that most of these scattering and absorbing type aerosols fall in the nucleation mode size range, which are mostly produced due to various anthropogenic activities. Highest values of β_{sca} are measured during Post-Monsoon season and this is followed by values obtained during Dry, Pre-Monsoon and Monsoon seasons respectively in the decreasing order of their magnitudes. Higher values of β_{sca} measured during Post-Monsoon and Dry seasons is an outcome of the combined effect of several favorable factors. During these seasons, there is an increase in waste burning activities, such as burning dry leaves, shrubs etc. in various parts of the city and all these contribute significantly to the emission of both scattering and absorbing type species in the atmosphere. Unlike Pre-Monsoon and Monsoon seasons, when the surface level wind flow is from the Arabian sea in south or south-west, relatively pristine air masses with less continental influence reach our measurement location, while air masses reaching Ahmedabad during Post-Monsoon and Dry seasons are mostly of continental origin contributing more aerosols from surrounding locations to the already high level of aerosols produced within the city. Moreover, during Dry and Post-Monsoon seasons, aerosols which are either locally produced or transported from other regions are constrained within a shallow boundary layer having smaller ventilation coefficient and

this causes their concentration to rise near the surface level. Also, as will be shown later while discussing the vertical profiles of aerosols, during Pre-Monsoon and Monsoon seasons, atmospheric boundary layer height increases, making more volume available for the aerosols to get distributed and this results in a dilution of their concentration near surface level.

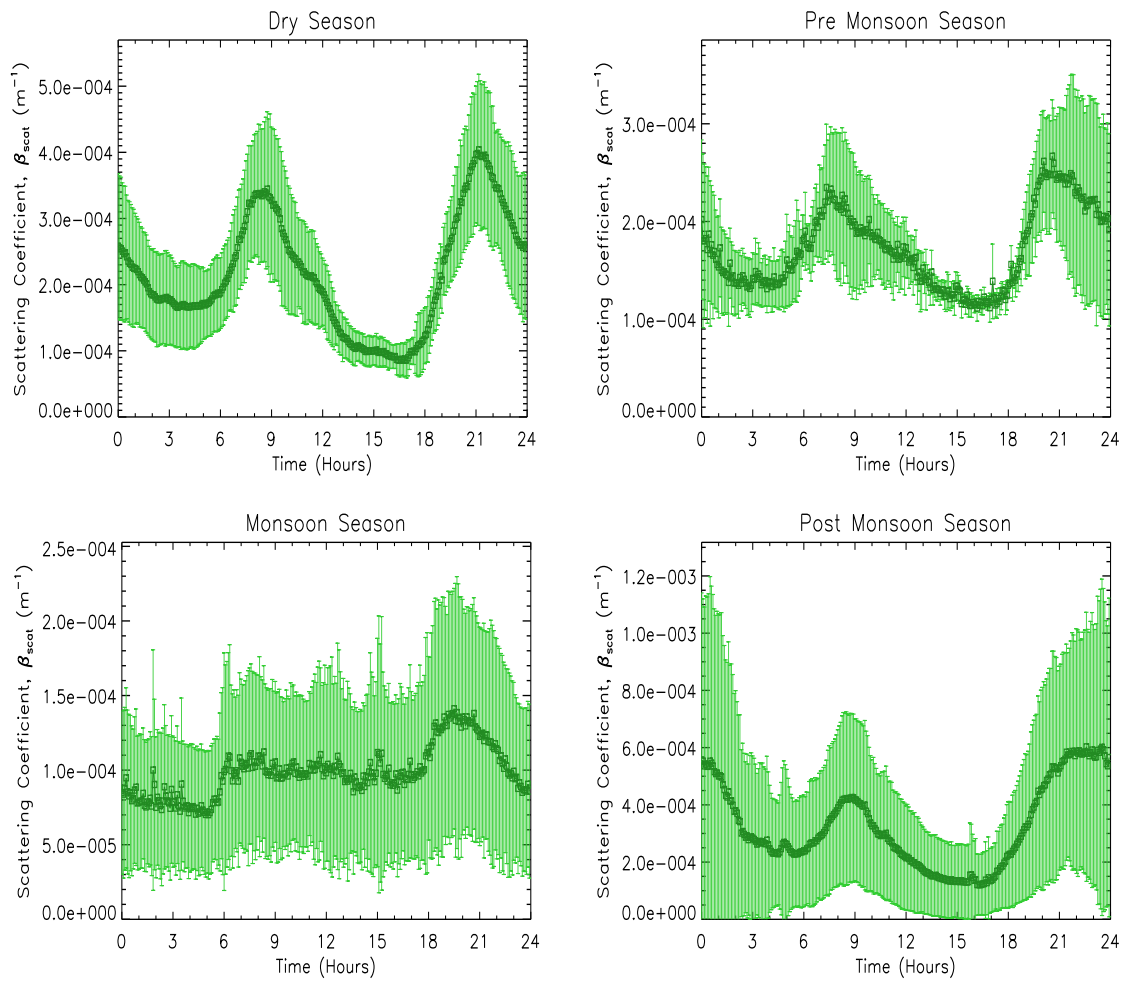


Figure 2.13: Average patterns in diurnal variation of aerosol scattering coefficient (β_{sca}) at $0.53 \mu\text{m}$ for different seasons of a year, with vertical lines representing $\pm 1\sigma$ variation about the mean value of β_{sca} at a particular time on different days of a particular season.

Figure 2.13 shows the average patterns in diurnal variation of β_{sca} for different seasons of the year. Vertical lines represent $\pm 1\sigma$ variation about the mean value of β_{sca} measured at a particular time on different days of a particular season. Most striking similarity among the plots on diurnal variation of β_{sca} and BC mass concentration is the occurrence

of twin maxima and minima within a day in all seasons, except the first maxima and second minima are not resolvable as both appear at a same level during Monsoon season (Figures 2.11 and 2.13). Highs and lows in the diurnal variation of β_{sca} are governed by several factors such as production source of these scattering type aerosols, variations in their source strength, removal mechanisms, boundary layer height variations and also the surface meteorology. First maxima in β_{sca} is observed between 08 – 09 hrs. during Dry and Post-Monsoon seasons while this occurs little early between 07 – 08 hrs. during Pre-Monsoon season. Evening peak in scattering coefficient is reached around 21 hrs during Dry and Post-Monsoon season while it shifts little early, between 20 – 21 hrs during Pre-Monsoon and Monsoon seasons. This peak is a result of increased production of aerosols in the evening hours due to various anthropogenic activities such as peak in traffic level after 17 hrs, burning of waste materials (dry leaves, shrubs, papers etc.), usage of biofuel in the slums of the city etc. All these result in piling up of aerosols produced during evening hours which continue up to late night, in the surface layer of the atmosphere. In addition to increased production of aerosols, formation of inversion layer in the evening hours inhibits convective mixing of air and therefore aerosols present in it. However, after around 21 hrs, production of aerosol particles from most of these sources start declining but their removal from the atmosphere, mostly by gravitational settling process, remains still active. This removal process continues for the whole night and β_{sca} reaches a minima between 04 – 05 hrs in the early morning. However, various human activities start from the morning itself and release many precursor gases for the production of these scattering aerosols. These activities start when the boundary layer height continues to be low and therefore aerosols produced during this time get very less volume in the atmosphere to distribute themselves causing β_{sca} to rise and reach a maxima between 07 – 09 hrs depending on the season. After 09 hrs, due to increased insolation of the Earth's surface, atmospheric boundary layer height starts rising along with an entrainment at the top of the inversion layer. This kicks off convective mixing of air capable of lifting aerosols to higher levels in the atmosphere and causing a dilution of their concentration at the surface level. This mixing of air continues upto afternoon hours when we see a minima in the traffic level. As a result of this, β_{sca} measured for near surface aerosols reaches a minima between 16 – 17 hrs. Under favorable conditions such as increasing relative humidity, collapsing boundary layer and increased production of aerosols in the evening hours, scattering coefficient of aerosols starts rising

after 17 hrs to reach the evening maxima. This cycle in the diurnal variation of β_{sca} is repeated on all clear sky days throughout the year, except with some abnormalities during Monsoon season. During Monsoon season, boundary layer height mostly remains high and shows a very weak diurnal variation. Also, the formation of surface based inversion layer and nocturnal boundary layer are not very strong and distinct during this season as a result of which we do not get a well defined peak of β_{sca} in the morning hours and even the second maxima during evening hours is not very prominent as observed in other seasons.

2.3.7 Single scattering albedo

As scattering and absorbing type aerosols are present together in the atmosphere, their effect in terms of cooling or warming of the atmosphere depends on the single scattering albedo (ω) of the mixture of aerosols, which is the ratio of scattering to extinction coefficient of aerosols. The magnitude of ω is considered as an index for the relative dominance of scattering with respect to absorbing type of aerosols, which can range from 0 (purely absorbing) to 1 (purely scattering). Exact knowledge of single scattering albedo is very crucial as small error in its magnitude can produce large difference in the estimated values of aerosol radiative forcing [Takemura *et al.*, 2002]. Ganguly *et al.* [2005a] have shown that for the same aerosol optical depth (AOD) and mass loading over Bay of Bengal, atmospheric forcing by aerosols is very sensitive to ω . Over land areas, knowledge of ω is even more critical and any small change its value can have larger impact resulting from errors in the estimated flux changes within and below the aerosol layer such as differential heating rates, changes in atmospheric stability and cloud formation [Ackerman *et al.*, 2000; Russell *et al.*, 2002]. Even satellite retrieval of aerosol optical depth (AOD) is also intricately dependent on the assumption of ω in the aerosol model for any study region [Ignatov *et al.*, 1995; Stowe *et al.*, 1997]. Although there are some reports on measurements of BC mass concentration over the Indian mainland [Babu *et al.*, 2002; Babu and Moorthy, 2002; Venkataraman *et al.*, 2002; Tripathy *et al.*, 2005; Latha and Badrinath, 2005], reports on measurement of single scattering albedo over Indian mainland is almost nil, except during a field study over central India in February 2004 by Ganguly *et al.* [2005c] and during another campaign at New Delhi in December 2004 by our group [Ganguly *et al.*, 2006]. Moreover, most of these studies [Babu *et al.*, 2002; Venkataraman *et al.*, 2002; Ganguly *et al.*, 2005c; Tripathy *et al.*, 2005]

are part of intensive campaigns organized for short periods. What is needed for proper assessment of possible impacts produced by these aerosols prevalent over the Indian sub-continent is to make long term measurements of these important aerosol parameters at various stations spread all across the country.

In this particular study, we have estimated the single scattering albedo of aerosols from the ratio of scattering coefficient at $0.53 \mu m$ using Nephelometer and its sum with the absorption coefficient at $0.52 \mu m$ measured using Aethalometer. Measured values of scattering coefficient are associated with some angular truncation loss which is an inherent and unavoidable problem for all Nephelometers [Heintzenberg and Charlson, 1996]. Detailed Mie theory calculation using the simultaneously measured aerosol size distribution shows that, an angular truncation of 8° each in the forward and backward direction could result in an underestimation of scattering coefficient by about 15%. However, this causes a maximum error of about 3 – 4 percent (in the extreme case) in the estimated values of ω for the range of absorption and scattering coefficient values measured over Ahmedabad. Similarly, a maximum error of 10% in the estimation of absorption coefficient using Aethalometer causes about 2% error in the estimated values of ω in the extreme case. Taking into account all possible sources of error, overall uncertainty in the estimated value of ω during the present study is around 6%. Nevertheless, for estimation of aerosol radiative forcing, presented in Chapter-6, diurnally averaged values of ω are used which have a spread of about 13%.

Figure 2.10(c) shows the seasonal variation of single scattering albedo at $0.525 \mu m$, averaged over all data available from the year 2003 to 2005. Vertical lines on top of each bar represents $\pm 1 \sigma$ variation about the mean value of ω for that season. Over the period of our study, single scattering albedo at $0.525 \mu m$ are found to be 0.73 ± 0.1 , 0.84 ± 0.04 , 0.81 ± 0.03 and 0.73 ± 0.08 during Dry, Pre-Monsoon, Monsoon and Post-Monsoon seasons respectively. Although patterns of seasonal variation in β_{abs} and β_{sca} appear almost identical [figures 2.10(a) and 2.10(b)], small differences in the percentage variation of individual parameters (β_{abs} and β_{sca}) from one season to other cause the observed pattern in seasonal variation of ω . Relatively lower values of ω obtained during Dry and Post-Monsoon season shows that although both BC mass and β_{sca} exhibit higher values during these seasons, effect of increase in BC mass dominates in terms of contribution to the total extinction caused by all aerosols present near the surface level. This happens primarily

because during these seasons, there is an increase in the activities related to burning of waste materials such as dry leaves, shrubs, papers etc. which are mainly collected as part of cleanliness drives in various parts of the city and putting them on fire serves as an easy way for getting rid of these garbage materials. As discussed earlier and also seen in some of the earlier studies, aerosols emitted due to biomass/biofuel burning exhibit stronger absorption characteristics than those produced due to fossil fuel burning [Kirchstetter *et al.*, 2004; Ganguly *et al.*, 2005b, 2006]. Therefore it is a matter of concern from the climate point of view as such practices are not only loading large quantities of aerosols of various kinds in the atmosphere but they are also producing soot particles with increased absorption efficiency, bringing down the single scattering albedo to lower values, thereby trapping heat within the atmosphere which can lead to climate forcing [Ramanathan *et al.*, 2001b; Menon *et al.*, 2002].

Comparing results from Ahmedabad with previously published values of single scattering albedo for other regions [Anderson *et al.*, 1999; Jayaraman *et al.*, 2001a; Russel *et al.*, 2002, Bergstrom *et al.*, 2003; Han *et al.*, 2003; Qiu *et al.*, 2004], we find that ω values estimated over Ahmedabad are much lower indicating the dominance of absorbing aerosols. Babu *et al.* [2002] estimated ω at $0.5 \mu\text{m}$ over Bangalore for the month of November, based on measurements of BC mass fraction and using the OPAC model developed by Hess *et al.* [1998], to be around 0.73. Following the same method, Singh *et al.* [2005] and Tripathy *et al.* [2005] reported ω ($0.5 \mu\text{m}$) value for Delhi and Kanpur to be 0.67 and 0.76 during Pre-Monsoon period and December month respectively. Also, by inverting sun/sky radiometer data, Pandithurai *et al.* [2004] estimated ω ($0.5 \mu\text{m}$) value for Pune (18.53°N , 73.85°E) to be around 0.81. Unlike previous examples, Ramana *et al.* [2004] estimated ω ($0.5 \mu\text{m}$) value for Kathmandu (27.67°N , 85.31°E) to be in the range of 0.7 – 0.9, combining the actual measurements of scattering and absorption coefficient using a Nephelometer and a Particle Soot Absorption Photometer (PSAP). Similar to present study, Ganguly *et al.* [2005c] reported the single scattering albedo ($0.525 \mu\text{m}$) values estimated using simultaneously operated Nephelometer and Aethalometer measuring scattering and absorption coefficient of aerosols respectively for different locations (mostly rural) over the central Indian region to be in the range of 0.75 – 0.90. Also, during an intensive campaign at New Delhi in December 2004, our group estimated single scattering albedo at $0.525 \mu\text{m}$ following the same method as the present study and found ω to vary between 0.6 and 0.8 with an average

value close to 0.68 for the entire period of campaign [Ganguly *et al.*, 2006].

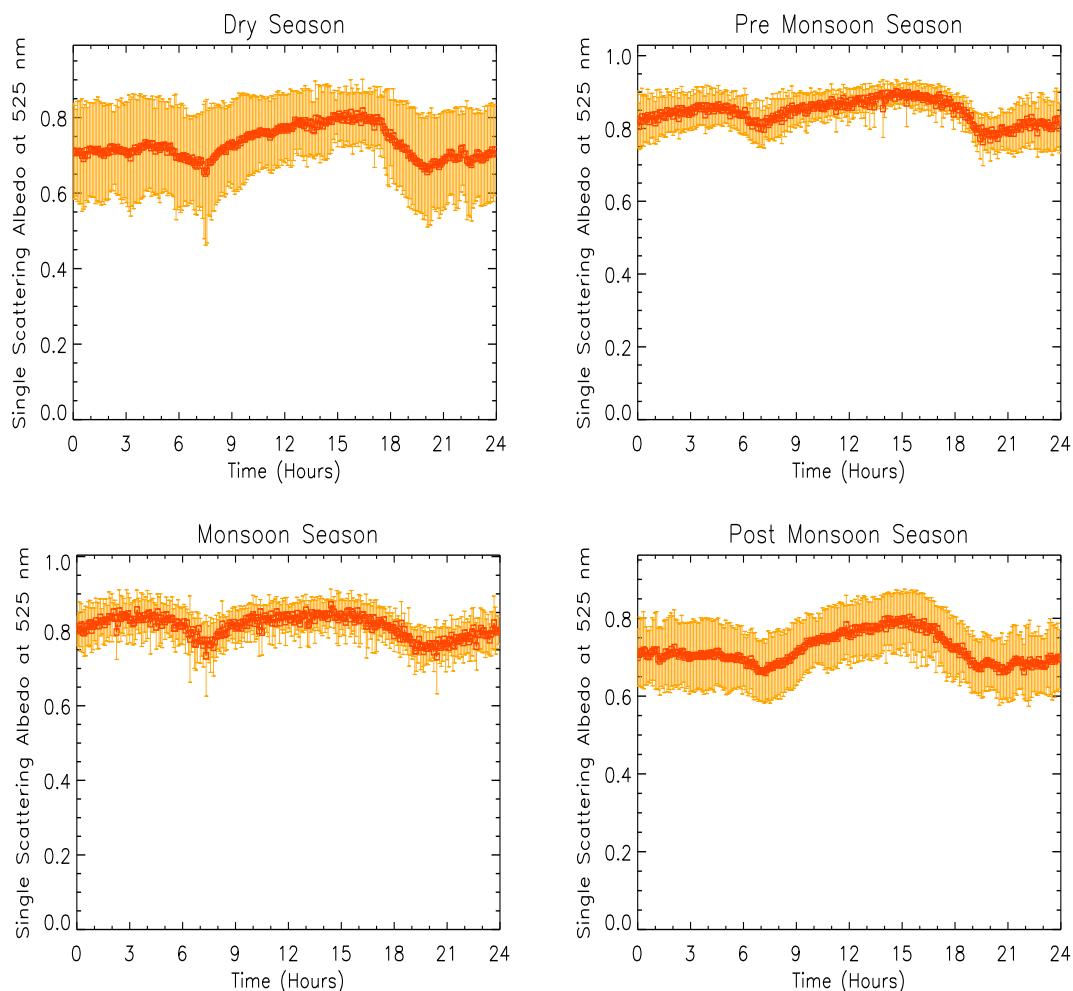


Figure 2.14: Average patterns in diurnal variation of single scattering albedo (ω) at $0.525 \mu\text{m}$ for different seasons of a year, with vertical lines representing $\pm 1\sigma$ variation about the mean value of ω at a particular time on different days of a particular season.

Figure 2.14 shows the average patterns in diurnal variation of ω ($0.525 \mu\text{m}$) for different seasons of the year. Vertical lines represent $\pm 1\sigma$ variation about the mean value of ω estimated for a particular time on different days of a particular season. Among the most common features, notable in all four panels of figure 2.14 include occurrence of two dips and an afternoon maxima in the diurnal cycle of ω observed in different seasons. Since the single scattering albedo is a combined effect of scattering and absorption by aerosols, diurnal pattern in the variation of ω is determined by the contemporary behavior of scattering and absorption coefficient of aerosols. We find that ω values attain a minima sometime

between 07 – 09 hrs, almost coinciding with the peak in BC mass concentration (figures 2.11 and refAhmddiurnalssa). After this dip, ω starts rising very slowly upto a time when BC concentration reaches a minima in the afternoon time between 15 – 17 hrs. Main reason for getting the observed trend in ω is the presence of a very small phase lag between the diurnal variation of BC mass and aerosol scattering coefficient (figures 2.11 and 2.13). This phase lag exists because while soot particles from vehicular exhausts or biomass/biofuel burning are directly released as particles in the atmosphere, most of the scattering type aerosols viz. sulfates and nitrates are secondary aerosols formed by gas-to-particle conversion processes. Therefore, although most of the precursor gases are released at the same time together with absorbing soot particles, it takes slightly longer time for the precursor gases to get converted into sub-micron particles. Also, as long as concentration of these precursor gases are sufficient and conditions in the atmosphere remain conducive, their transformation into particles continues. After about 15 hrs when traffic level starts rising along with increase in other types of burning activities, BC mass and absorption coefficient values start increasing in response to increased production of aerosols from these sources. Although scattering coefficient increases after 15 hrs, a faster increase shown by BC aerosols causes ω value to decrease up to a time when both scattering and absorption coefficient values reach a more or less steady state after around 20 hrs.

2.3.8 Aerosol vertical profiles

A Micro Pulse Lidar (MPL) system (SES Inc., USA) has been used to get the vertical distribution of aerosols in the atmosphere and retrieve their extinction profiles. Earlier, several researchers emphasized the importance of measuring vertical distribution of aerosols as they have pointed out that one major contributor to the uncertainty in atmospheric forcing comes from uncertainty in the vertical distribution of aerosols and their single scattering albedo [Haywood and Ramaswamy, 1998; Chung *et al.*, 2005]. MPL observations at Ahmedabad started in February 2002 and continuous data on vertical distribution of aerosols over our measurement site are available upto February 2005. Due to technical problem with the MPL system, vertical profile measurements could not be continued beyond March 2005. Throughout our study period, a significant day to day variability in the vertical profiles of aerosol extinction coefficient is observed. For the sake of simplicity and for the purpose of the present work, we have grouped the aerosol extinction profiles in terms of four

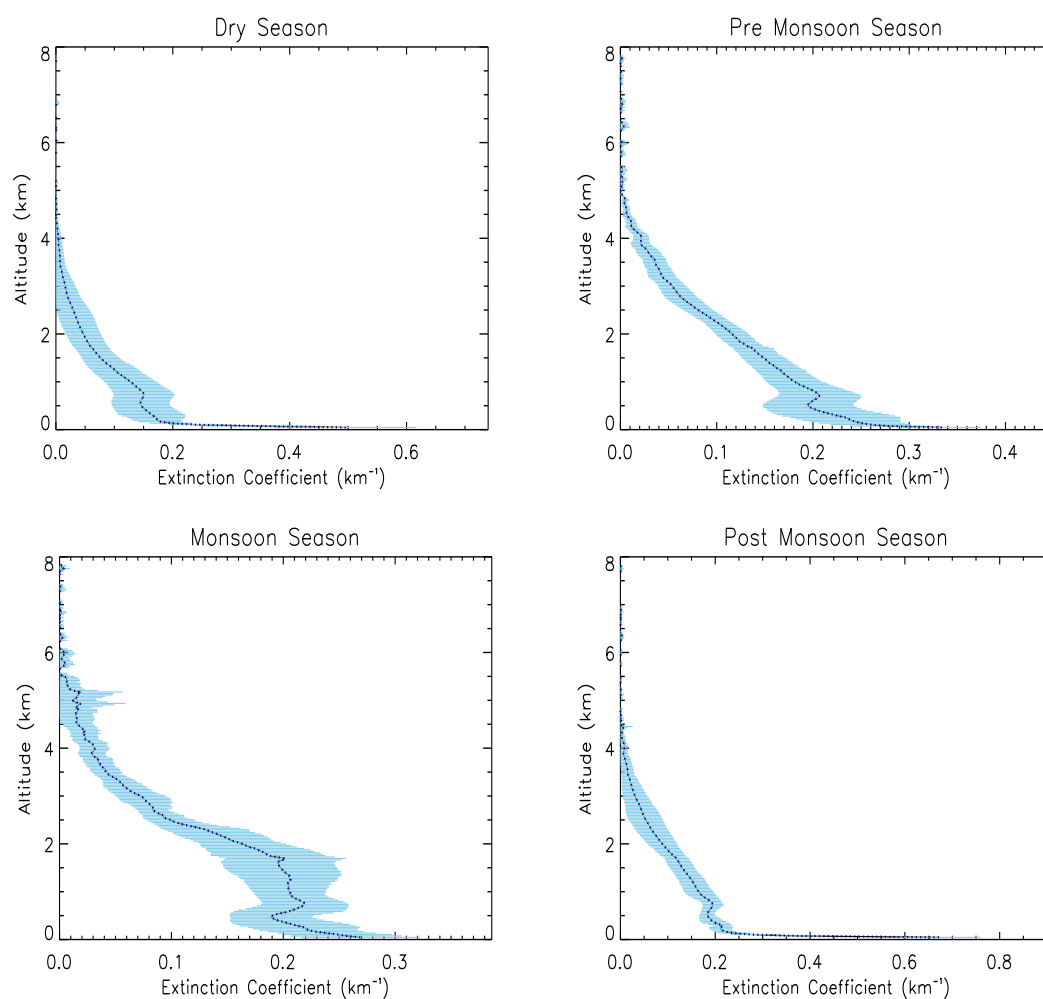


Figure 2.15: Clear sky aerosol extinction profiles for different seasons, averaged over all data available for the years 2002 to 2005. Horizontal bars represent $\pm 1 \sigma$ variation about the mean value of extinction coefficient retrieved for a particular altitude on different days of a particular season.

different seasons (as discussed earlier) and for all years. We have further averaged the data on aerosol extinction profiles available for same season but in different years. Figure 2.15 shows the seasonal variations in clear sky aerosol extinction profiles, averaged over all data available from the year 2002 to 2005. Horizontal bars represent $\pm 1 \sigma$ variation about the mean value of aerosol extinction coefficient retrieved for a particular altitude on different days of a particular season. In the present work, we restrict our discussions to the four seasonally averaged profiles shown in figure 2.15. Seasonal variabilities in the shape of these extinction profiles explain reasons for observing relatively opposing trends in seasonal variation of surface aerosol parameters [Figure 2.10] and the columnar aerosol

optical depths [Figure 2.6(b)]. These profiles clearly show the kind of evolution of the atmospheric boundary layer height occurring during different seasons of any year. Area under all these curves represent the average aerosol optical depth for that season. We find the extinction profiles for Dry and Post-Monsoon seasons to be much similar to each other while the profiles obtained during Pre-Monsoon seasons appear intermediary between the two extreme type of profiles obtained during Dry and Monsoon seasons. Aerosol vertical profiles for Dry and Post-Monsoon seasons are characterized by very high values of extinction coefficient within first few hundred meters (~ 200 m) from the surface where we find a sharp decrease in the extinction values with increasing height. The reason for observing such high values of aerosol extinction coefficient at lower heights is the formation of a surface based inversion layer during Dry and Post-Monsoon seasons. This layer being very stable, opposes vertical mixing of various constituents in the atmosphere which results in piling up of aerosols within the layer and pushes extinction values towards higher side [Krishnan and Kunhikrishnan, 2004]. During Dry and Post-Monsoon seasons, atmospheric boundary layer height remains low, primarily due to less insolation at the Earth's surface. It can be seen from figure 2.15 that extinction values from the top of this surface layer (~ 200 m) decrease rather slowly and approach zero level, almost asymptotically, at an altitude of about 4 km. On the other hand, no such surface layer is observed during Pre-Monsoon and Monsoon seasons but in these seasons, height of the atmospheric boundary layer goes up due to increased insolation at the Earth's surface on cloud free days. This provides a larger room for the aerosols to distribute themselves in the atmosphere, assisted by stronger convective circulations in lower parts of the atmosphere. Vertical distribution of aerosols in Pre-Monsoon season appears to follow a combination of two exponentially decreasing profiles connected through a small inversion layer between them (base of the inversion layer occurs at ~ 0.6 km). During Monsoon season, we find an exponentially decreasing type of distribution in the first ~ 0.5 km, above which rests an inversion layer with its peak close to 1.0 km. Most striking feature in the vertical distribution of aerosols during Monsoon season is the presence of a thick and stable aerosol layer between 0.5 and 2.0 km. This layer contributes significantly to the columnar aerosol optical depth values but its effect is not felt in any of the surface level measurements. This is the main reason why higher AODs are observed on clear sky days during Monsoon season while surface measurements of BC mass and aerosol scattering coefficient shows low value in the same

season. Vertical profiles of aerosol distribution shows finite contribution of extinction coefficients almost up to 5 km from the surface during Pre-Monsoon and this reaches close to 6 km during Monsoon season.

Large seasonal variabilities are observed in all aerosol parameters measured over Ahmedabad during the period from 2002 to 2005. These are bound to produce large differences in radiative forcing due to aerosols in different seasons of the year. All results on different aerosol parameters measured over Ahmedabad are used as inputs in a radiative transfer model and implications of the observed variabilities have been studied in terms of regional scale aerosol radiative forcing. Several interesting results on model estimates of aerosol radiative forcing and its sensitivity to the observed variabilities in aerosol parameters are discussed separately in *Chapter-6*.

2.4 Summary

Results from continuous measurements of physical and optical parameters of aerosols made over Ahmedabad, an urban location in western India, from early 2002 till the end of 2005 are presented. Important aerosol parameters studied over this location include: column AOD spectra, aerosol mass concentration, number size distribution, BC mass concentration, wavelength dependency in absorption, scattering coefficient, single scattering albedo and vertical distribution of aerosols in the atmosphere. All parameters showed large variability in their values during different seasons and in different years. All available data are classified in terms of four major seasons observed over Ahmedabad viz. Dry (December to March), Pre-Monsoon (April-May), Monsoon (June-September) and Post-Monsoon (October-November), primarily based on different meteorological conditions prevailing during different months of the year. Seasonal and inter-annual variabilities in meteorological parameters played an important role in shaping the observed patterns of seasonal variations for different aerosol parameters. AOD at all wavelength channels show an increasing trend over first half of the year, which is found to be stronger and consistent at higher wavelengths. Angstrom parameter α , estimated for three different wavelength pairs showed almost same pattern of seasonal variation in all years with higher values obtained during Dry and Post-Monsoon seasons and lower values during Pre-Monsoon and Monsoon seasons. We find a dominance of smaller size particles during Dry and

Post-Monsoon seasons while an increase in coarse mode particle concentration during Pre-Monsoon and Monsoon seasons. Over the period of our study, PM_{10} mass concentration varied between low values close to $40 \mu g/m^3$ upto high of about $106 \mu g/m^3$ with an average value of around $66 \mu g/m^3$. Lower values of PM_{10} mass concentrations are usually measured during Monsoon season. QCM observations have been further used to obtain the number size distribution of near surface aerosols. We have seen maximum seasonal variation in the number concentration of nucleation mode aerosols, with nearly 60% spread in their value about the mean concentration for entire period. This is followed by accumulation and coarse mode data showing about 26 and 17 % spread in their values respectively. Aerosol size distribution for all seasons exhibit presence of three distinct modes each one of which could be fitted using a log-normal curve. The shape of the aerosol size distribution remained more or less same over the study period while number concentration changed in all three modes during different seasons, indicating that the amount of aerosols as well as their in situ production strengths changed while various physical processes responsible for their distribution in the atmosphere remained unaltered. High values of BC mass are obtained during Post-Monsoon season ($7.3 \pm 3.7 \mu g/m^3$). This decreased slightly during Dry season ($5.5 \pm 2.8 \mu g/m^3$) and comparatively much lower values of BC mass are measured in Pre-Monsoon ($2.2 \pm 1.0 \mu g/m^3$) and Monsoon season ($1.5 \pm 0.8 \mu g/m^3$). Diurnal variation of BC mass shows the presence of two maxima and two minima in all seasons. Wavelength dependency of aerosol absorption shows signatures of presence of significant amount of absorbing aerosols produced from biofuel/biomass burning. Average values of absorption Angstrom parameter α are found to be to be 2.2, 2.0, 1.9 and 2.1 for Dry, Pre-Monsoon, Monsoon and Post Monsoon seasons respectively. Highest values of aerosol scattering coefficient are measured during Post-Monsoon which is followed by values measured during Dry, Pre-Monsoon and Monsoon seasons respectively in the decreasing order of their magnitude. Over the period of our study, single scattering albedo at $0.525 \mu m$ is found to be 0.73 ± 0.1 , 0.84 ± 0.04 , 0.81 ± 0.03 and 0.73 ± 0.08 during Dry, Pre-Monsoon, Monsoon and Post-Monsoon seasons respectively. A Micro Pulse Lidar (MPL) has been used to get the vertical distribution of aerosols in the atmosphere and retrieve their extinction profiles. MPL observations at Ahmedabad started in February 2002 and continuous data on vertical distribution of aerosols over our measurement site are available upto February 2005. Aerosol vertical profiles for Dry and Post-Monsoon seasons are

characterized by very high values of extinction coefficient within first few hundred meters ($\sim 200m$) from the surface where we find a sharp decrease in the extinction values with increase in height. MPL observations during Pre-Monsoon and Monsoon season shows the presence of aerosols upto higher levels in the atmosphere, contributing significantly to the columnar aerosol optical depth values.

Ship cruise study of aerosol characteristics over Bay of Bengal

In the South Asian region, comprised of Indian subcontinent and its surrounding ocean territories, the Bay of Bengal (BoB) occupies a special importance because every year during the winter months (December to February), large quantities of aerosols and gaseous pollutants, mostly produced due to various anthropogenic activities over the populous and industrialized regions in the Indo-Gangetic belt, are dumped onto this otherwise clean oceanic region. BoB provides an ideal location for the investigation of natural marine aerosols as well as their interaction with continental pollution. Focus of the study during previously conducted INDOEX (Indian Ocean Experiment) campaigns was mostly confined to the Arabian Sea and the tropical Indian Ocean [*Krishnamurti et al.*, 1998; *Rajeev et al.*, 2000; *Jayaraman et al.*, 2001a; *Ramanathan et al.*, 2001a] and not many in-situ ship cruise aerosol observations were made over the Bay of Bengal region. BoB is surrounded by densely populated and industrialized areas on its north, east and west, where sufficient amount of soot and sulfate aerosols are produced which get transported into this oceanic region. Particles like sulfate can decrease the surface reaching solar radiation by scattering while the soot component present in aerosols can absorb radiation and contribute to atmospheric heating. Some of the recently conducted observations [*Satheesh et al.*, 2001; *Li and Ramanathan*, 2002; *Ramachandran and Jayaraman*, 2003a, 2003b; *Moorthy et al.*, 2003; *Vinoj et al.*, 2004] have shown higher values of aerosol optical depth(AOD) over the BoB region compared to Arabian sea and other parts of the Indian Ocean. Apart from the knowledge of AOD, other key properties of aerosols which must be accurately accounted for in any

chemical transport and transformation model include aerosol size distribution and their size dependent chemical composition.

In order to study the transport of aerosols, their physical characteristics, their chemical nature and the effect of these diverse aerosols on the regional climate forcing in greater detail, a ship cruise study was conducted over BoB in February 2003. Simultaneous measurements of surface level aerosol mass concentrations, their size distribution and aerosol optical depths (AOD) were made during the ship cruise study over BoB, when the prevailing surface level wind flow is predominantly from the continent towards the ocean, using a ten stage QCM cascade impactor and Microtops sun-photometer. To the best of our knowledge, for the first time simultaneous observation of surface level aerosol size distribution and columnar aerosol optical depth have been made over this region. The obtained aerosol size distribution has been used to calculate the aerosol optical properties and are validated with the measured AOD values and further used for obtaining the aerosol radiative forcing over this region.

3.1 Cruise track and Meteorology

All observations were carried out onboard the Indian Oceanographic Research Vessel, *Sagar Kanya* from 19 to 28 February 2003. The period of observations was when the prevailing surface level wind flow is predominantly from polluted continents towards the ocean. Figure 3.1 shows the average pattern of the surface level wind vectors and the ship track during the cruise period. The cruise started on 19 February at around 0030 hrs UT from Chennai port (13.09° N, 80.30° E) on the eastern coast of Indian peninsula. The ship cruised towards free ocean in the east upto 87° E and then turned north to travel along 87° E longitude upto 19.5° N latitude, which was less than about 100 km from the Indian coast. In the return leg, the ship sailed towards south almost parallel to the Indian coastline upto 13° N, maintaining a distance within 100 to 200 km from the east coast of India. From 13° N, the ship moved further south along 82.16° E longitude, took a turn around Sri Lanka and reached Tuticorin (8.75° N, 78.22° E) in India on 28 February 2003.

During the cruise, meteorological parameters such as relative humidity (RH) and air temperature have been measured on an hourly basis from the ships' deck at a height of about 15 m above the sea level. Daily mean surface air temperature during the cruise

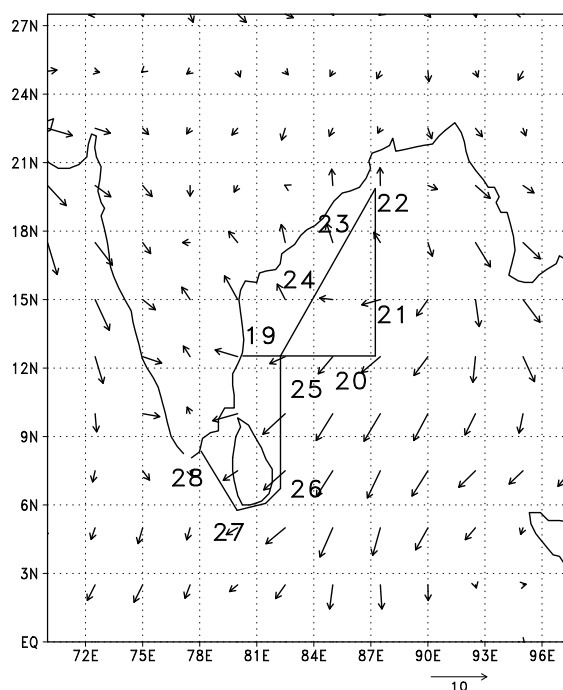


Figure 3.1: Surface level wind vectors averaged for 19th to 28th February, 2003 and the ship track for the cruise SK188 over the Bay of Bengal.

varied from 26° to 30° C while the relative humidity was mostly in the range of 60 to 75%. Wind speed and direction have been obtained from the weather station installed in the ship and maintained by the National Institute of Oceanography, Goa. Wind speed showed variation from a low value of 2 m s^{-1} to a maximum of about 6 m s^{-1} . Surface level wind flow was predominantly from North and North-East directions (Figure 3.1).

3.2 Measurements and data analysis

Surface level aerosol mass concentration is measured using a quartz crystal microbalance (QCM) cascade impactor which draws the ambient air at a constant flow rate of 0.24 l min^{-1} and segregates the aerosols according to their aerodynamic diameters into ten different size ranges (discussed earlier in section 2.2.2 of Chapter-2). Typical sampling duration was kept as 5 min. Aerosol sampling was done from a height of about 15 m above the sea level. The instrument was kept inside the ship cabin and air samples were drawn from the front bow region and along the right side (starboard side) of the ship. The instrument was operated manually and prior to actual measurements, filtered outside air was

flushed through the instrument so as to facilitate the crystals to attain temperature stability. During actual measurements, the relative frequency difference between the sampling and reference crystal are recorded, thereby ensuring that the changes in air temperature and relative humidity do not affect the measurement. The measurements were taken only when the ship was cruising at its maximum speed so as to avoid any contamination from ship exhaust and other local contamination. *Jayaraman et al.* [1998] and *Ramachandran and Jayaraman* [2002] have estimated a maximum overall uncertainty of about 25% in the QCM measurement for all the stages. The major source of error in the mass measurements by QCM is due to high relative humidity of the ambient air. This is because during the measurement duration of about 5 – 10 minutes, there could be an evaporation loss of the adsorbed water from the water soluble particles which are being collected under low pressure condition inside the impactor stages [*Jayaraman et al.*, 1998]. Observations were taken at nearly hourly intervals on all days of the cruise. Aerosol mass concentrations measured at different size ranges are then converted into aerosol number distributions using appropriate mass density valid for marine environment.

Aerosol optical depth (AOD) observations were carried out using a hand held multi-channel sun-photometer Microtops-II (Solar Light Co. U.S.A.), capable of measuring AOD at five wavelength bands centered around 380, 440, 500, 675 and 870 nm (discussed earlier in section 2.2.1 of *Chapter-2*). A second Microtops was used to measure the AOD at 1020 nm as well as total columnar concentrations of ozone and water vapor in the atmosphere.

In order to trace the sources of aerosols reaching the measurement location we have used the air back-trajectory analysis by NOAA HYSPLIT-4 (Hybrid Single-particle Lagrangian Integrated Trajectory) model. These trajectories basically give information about the path traversed by air parcels back in time, before reaching the particular site, which help in identifying the possible source regions [*Krishnamurti et al.*, 1998]. The background aerosols within the boundary layer over ocean regions are mostly of marine origin. Hence the total particle concentration of these background aerosols is expected to be quite uniform throughout the tropical trade wind regions [*Fitzgerald et al.*, 1991]. However, high winds can result in localized higher concentration of sea salt aerosols. The extra loading of aerosols over and above the prevalent background aerosols not only depends on the contributions of the continental source regions which the air parcels at different altitudes cross before finally reaching over the measurement site but also on the time taken by them

to reach these sites.

Air back-trajectories were computed for 7-days starting from local noon ($UT + 5 : 30$ hrs) of each day, taking the typical residence time of aerosols in the troposphere as about a week. As the observations included both columnar AOD values as well as surface level aerosol mass concentration, four trajectories in the marine boundary layer (at 10 m, 100 m, 500 m and 1000 m above the mean sea level) are considered, which are mainly linked to short range transport and two trajectories above the boundary layer height (at 3000 m and 5000 m), which are capable of long range transport of dust and mineral aerosols.

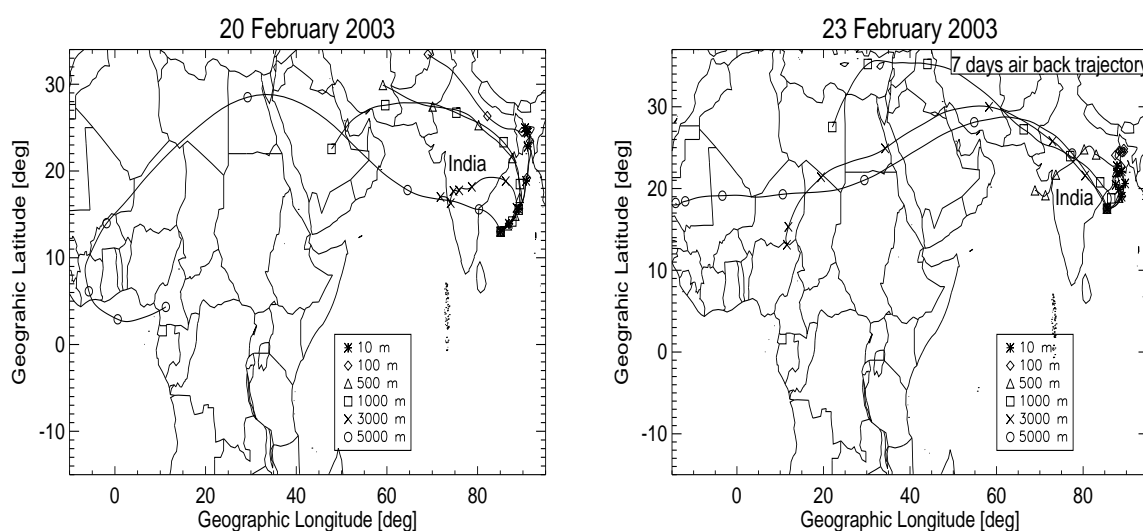


Figure 3.2: Seven days air back trajectories plotted for two representative days of the cruise and at six altitude levels.

It is found that on all nine days of the cruise, air parcels at all the above selected altitude levels are coming either from west or from north-west direction. The air parcels at all these heights cross a significant portion of the Indian subcontinent before finally reaching over BoB. Thus the chances of land derived dust aerosols as well as anthropogenic aerosols getting transported along these trajectories are quit high. These air parcels after reaching BoB, turn around in a clockwise fashion and move towards south India and the southern Indian Ocean.

We observe that almost on all the days, air parcels reaching the measurement site at low altitudes originated either from the West Bengal (in India) region or from Bangladesh. Both these regions have a population density among the highest in the world. Two out of top

15 megacities in the world viz. Kolkata ($22.57^{\circ}N$, $88.4^{\circ}E$) having a Population of about 13.1 million and Dhaka ($23.85^{\circ}N$, $90.4^{\circ}E$) which has a Population of about 12.7 million reside in this region. Large consumption of fossil fuels and biomass burning are the major sources of anthropogenic aerosols produced from this region [Reddy and Venkataraman, 2002]. On 19, 20 and 21 February, the air parcels at 10 and 100 m altitudes took about four days to reach over the measurement sites, whereas air parcels at the same altitudes took just one day to reach the cruise location on 22 and 23 February. Again on 24 and 25 February the air parcels at the same altitudes took nearly four days to reach the cruise location. Similarly on 19, 20 and 21 February, the air parcels at 500 and 1000 m altitude travelled for nearly 3 days over the ocean before finally arriving over the measurement sites but the corresponding air parcels took only about a day to reach the measurement location on 22 and 23 February. The transport time for the air parcels at 500 m and 1000 m to reach the observation sites after leaving the continental boundaries once again increased to 3 and 4 days on 24 and 25 February respectively. Almost on all the days the air parcels reaching at 3000 m and 5000 m originated either in northern or central Africa and crossed a significant portion of desert before finally arriving over the study area. So the possibility of desert dust and mineral aerosols getting transported to the BoB region can not be completely ruled out though there could be sufficient loss of these relatively heavy particles during transport. On 27 February, air parcels at 10, 100 and 500 m originated over BoB, south of Bangladesh and crossed a large portion of Sri Lankan island before reaching the measurement site. On this day the air parcels at all the altitudes mentioned earlier, except the one at 5000 m, crossed the island on their way. Similar to other days, on 27 February, air parcels at 3000 and 5000 m originated somewhere in northern Africa and reached the cruise location via the Arabian Sea. Consequences of these different air trajectories and the traversal time of the air parcels on the measured columnar AOD and surface level aerosol mass concentration are discussed in the following sections.

3.3 Results and Discussion

3.3.1 Aerosol optical depth

Figure 3.3(a) shows the variation of aerosol optical depth (AOD) observed at 6 wavelengths (380, 440, 500, 675, 870, 1020 nm) on different days of the cruise. The vertical bars repre-

sent $\pm 1\sigma$ variation about the daily mean AOD. The daily mean values for 380 nm are in the range of 0.34 – 0.75 and those at 1020 nm varied between 0.09 and 0.25. During the entire cruise highest values of AOD were recorded over northern BoB and along the east coast of India. AOD values showed a decreasing trend with increasing distance from the coast and towards lower latitudes. Lowest AOD was observed near the central portion of BoB. Higher values of AOD, particularly at shorter wavelengths, indicate the dominance of sub-micron size aerosols over BoB. A large fraction of these aerosols based on model estimates (discussed latter) have continental origin which gets advected over the marine atmosphere in this season due to the prevailing meteorology. The AOD data over Bay of Bengal region retrieved by MODIS (Moderate Resolution Imaging Spectroradiometer) instrument, on-board the Terra and Aqua satellites of NASA also shows higher values of aerosol optical depth in the downwind of Bangladesh, West Bengal and Orissa coast in India and there is a decreasing gradient in the AOD values from north to south [Figure 3.3(b)]. AOD val-

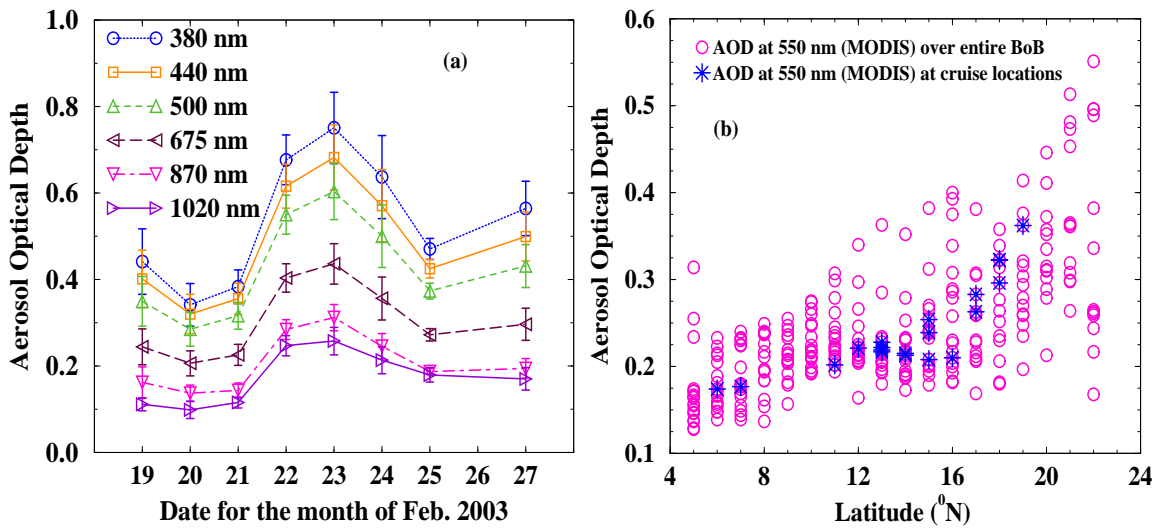


Figure 3.3: (a) Variation of daily mean AOD values observed at 6 wavelength channels of Microtops, on different days of the cruise over Bay of Bengal. (b) Decreasing gradient in AOD values over Bay of Bengal region from north to south as retrieved by MODIS instrument during February 2003.

ues over Bay of Bengal are much higher when compared with those observed over other marine regions across the globe. The mean AOD at 500 nm reported for the month of February over Coastal India, Arabian sea and Tropical Indian Ocean (classifications based on Jayaraman *et al.* [2001a] during INDOEX cruises conducted in the period 1996 – 1999) was around 0.25, 0.20 and 0.05 respectively while it is in the range of 0.04 – 0.25 for the

wavelength range of 440–880 nm, measured over the Atlantic Ocean by Hoppel *et al.* [1990]. Villevalde *et al.* [1994] observed the AODs at 551 nm over Pacific Ocean to be in the range of 0.04 – 0.24 and that over North Atlantic Ocean to be in the range of 0.07 – 0.19. AOD at 500 nm reported by Ramachandran *et al.* [2003a] observed during a cruise conducted over Bay of Bengal in February 2001 are in the range of 0.2 – 0.7. These values although comparable, show higher variation than our observations made in 2003. This could be possibly because of the differences in the cruise track for these two years. Li and Ramanathan [2002] have reported the AOD value for the month of February averaged over a period of 5 years from 1996 to 2000 for the Bay of Bengal region ($10^\circ \sim 77^\circ N$, $77^\circ \sim 100^\circ E$) derived using the NOAA14-AVHRR in the wavelength band of 580 – 680nm to be around 0.25.

In order to estimate the relative dominance of sub-micron size aerosols in the total aerosol loading of the atmosphere over the study area, we analyzed the AODs using the power law expression [Angstrom, 1964]:

$$\tau_a(\lambda) = \beta\lambda^{-\alpha} \quad (3.1)$$

where $\tau_a(\lambda)$ is AOD and λ is wavelength in units of micron. α and β are referred to as Angstrom parameters. The exponent α describes the spectral characteristics of the AOD values and is related to the slope of aerosol size distribution curves. Large value of α indicates higher ratio of smaller to larger particles. Parameter β equals to AOD at 1 μm and is proportional to the total columnar loading of aerosols in the atmosphere. The Angstrom power law is valid for the entire wavelength range only if the aerosol size distributions follow the Junge power law function [Hess *et al.*, 1998]. However our own observations show that at the surface level, the aerosol size distributions could be fitted by more than two lognormal curves (discussed latter). Hoppel *et al.* [1990] and Ramachandran and Jayaraman [2002] have also shown that the measured aerosol size distributions in the lower troposphere are combinations of two or more lognormal distributions. Under such conditions, the value of α is not constant, but depends on the wavelength range considered. We determined α and β for the wavelength ranges 380 – 675 nm (α_1, β_1) and 500 – 1020 nm (α_2, β_2). During the entire cruise, α_1 is found to be less than α_2 and they have a mean value of 0.99 and 1.31 respectively while the corresponding values of β_1 and β_2 are 0.21 and 0.18 respectively. Ramachandran and Jayaraman [2002] found the mean wavelength exponent α for the wavelength range 0.40 – 0.85 μm to be around 1.80 and the turbidity parameter, β

to be 0.1. Based on cruise track *Satheesh et al.* [2001] classified their data into three groups and the estimated values of α for Bay of Bengal, Arabian Sea and Indian Ocean regions are found to be 1.2, 0.8 and 0.5 respectively while the value of β for Bay of Bengal region is 0.2. *Villevaude et al.* [1994] have reported the mean value of the parameter α measured over Pacific Ocean and North Atlantic Ocean for the wavelength range 461 – 1016 nm to be around 0.56 and 0.99 respectively. *Tomasi and Prodi* [1982] measured AOD over equatorial areas of Indian Ocean and reported the average values of α and β to be 0.60 and 0.19. Higher values of α over Bay of Bengal compared to other ocean regions prove the abundance of smaller size aerosols over this region.

We found that although the observed AODs at lower wavelengths are comparable with those reported by *Ramachandran and Jayaraman* [2003a], the α values derived by them are higher than our present values. This is possible because either an increase in the number of smaller size particles or a decrease in the larger size particles can increase the value of α and vice-versa. *Villevaude et al.* [1994] have shown that if the relative humidity is quite high and relatively uniform across a large part of the aerosol layer in the atmosphere, then this could lead to the particle growth which in turn may bring down the value of α . Higher value of β and AODs at higher wavelengths with respect to those of *Ramachandran and Jayaraman* [2003a], reflects the coexistence of significant number of bigger size particles along with sub-micron aerosols which increased the total columnar aerosol loading over Bay of Bengal in February 2003.

3.3.2 Aerosol mass concentration

Aerosol mass concentrations measured separately in 10 different size bins have been grouped into three categories as coarse mode particles with size ranging between 1 and 10 μm (sum of mass collected in stage 2, 3 and 4 of the QCM), accumulation mode particles in the size range of 0.1 to 1 μm (sum of mass collected in stage 5, 6, 7 and 8) and the nucleation mode particles with size less than 0.1 μm (sum of mass collected in stage 9 and 10). Aerosol mass obtained from stage 1 of the QCM device is not included in this classification as it integrates all particles of size greater than 12.5 μm and no meaningful mean radius could be assigned to this stage.

Figure 3.4(a-c) shows the variation of daily average mass concentration for the three modes. Nucleation mode aerosols contributed the least to the total mass, with amount

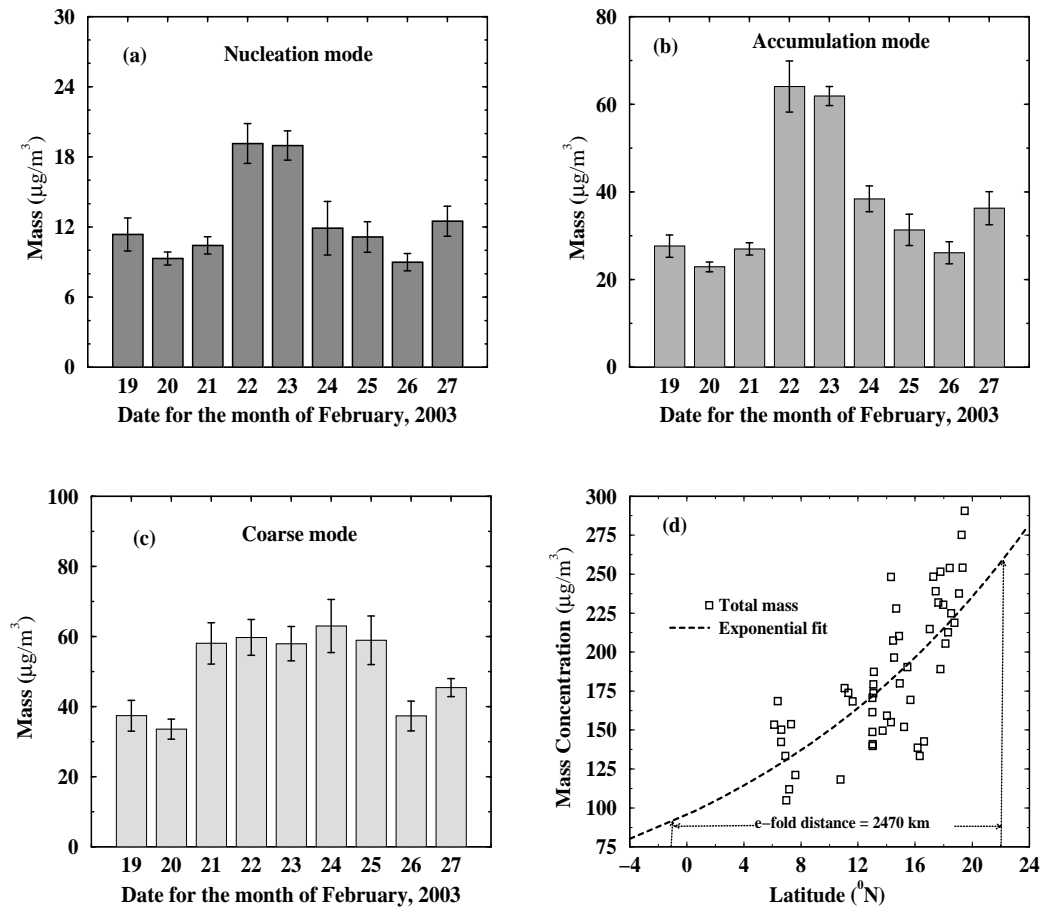


Figure 3.4: Surface level aerosol mass concentrations measured individually in 9 stages of the Q.C.M. device have been grouped into three categories viz. (a) nucleation mode particles with size less than $0.1 \mu\text{m}$, (b) accumulation mode particles in the size range of 0.1 to $1 \mu\text{m}$ and the (c) coarse mode particles with size ranging between 1 and $10 \mu\text{m}$ and (d) Latitudinal gradient in the total aerosol mass concentration (sum of all 10 stages).

varying between a low value of $8 \mu\text{g}/\text{m}^3$ to the highest value of about $20 \mu\text{g}/\text{m}^3$. Since most of the precursors involved in the formation of nucleation mode aerosols have continental origin [Quinin *et al.*, 1996], their concentration increases at places where the air parcels, coming from surrounding continents, take shorter time to reach. Higher values of aerosol mass were observed for this mode on 22 and 23 February where the air parcels at lower altitudes came from some of the most polluted areas and it took about a day to reach the location of our cruise, as shown in the air back-trajectory analysis (Figure 3.2). The accumulation mode aerosols are in general produced by the condensation growth and coagulation of nucleation mode aerosols. Due to this reason, spatial variation of accumu-

lation mode aerosols is found to be similar to those of nucleation mode aerosols. In the present cruise, accumulation mode aerosols varied from a low concentration of about $20 \mu\text{g}/\text{m}^3$ at places far away from the land in the southern BoB to a high concentration of about $60 \mu\text{g}/\text{m}^3$ near the coastal areas in the northern BoB. Coarse mode aerosols found over oceans are mainly constituted by sea spray particles and their mass concentration varied between 35 and $60 \mu\text{g}/\text{m}^3$. A maximum 20% variation in the coarse mode aerosol mass is observed with respect to its average value for the entire cruise while that for accumulation and nucleation modes are about 40% and 30% respectively. The spatial variation in aerosol mass is found to be maximum for the accumulation mode particles followed by the nucleation and coarse modes.

Aerosols collected in stage 1 of the QCM device are either sea salt particles produced by breaking of sea waves or wind blown coarse particles reaching from the surrounding land masses. Since the particles collected in this stage are bigger in size, most of the time the total mass measured in this stage is very high. Mass concentration for the particles collected in the first stage of QCM and the coarse mode mode aerosols depend on the surface level wind speed and relative humidity of the ambient atmosphere. In order to study the dependence of aerosol mass collected in stage 1 of QCM and coarse mode aerosols on meteorological parameters such as wind speed and relative humidity, we analyzed their scatter diagrams with these parameters. While the aerosol mass collected in stage 1 showed a positive correlation ($R^2 \sim 0.65$) with the surface level wind speed they were not much affected by changes in relative humidity ($R^2 < 0.2$). On the other hand coarse mode(sum of stages 2, 3 and 4) aerosol mass concentrations showed only a weak positive correlation with the surface level wind speed ($R^2 < 0.2$) but it exhibited a relatively stronger positive correlation with relative humidity ($R^2 \sim 0.65$), indicating that the mass concentration of coarse mode aerosols are relatively more sensitive to changes in relative humidity than to changes in the observed wind speed. This observation shows that the hygroscopic growth is more effective in increasing the mass concentration of marine aerosols only upto a certain size range of about $20\mu\text{m}$. For aerosols above this size range, a kind of balance is reached between those entering into this range by hygroscopic growth and the ones which are undergoing gravitational settling due to their increased weight. Many researchers [Exton *et al.*, 1985; Gong *et al.*, 1997; Ramachandran and Jayaraman, 2002] have shown that the dependence of aerosol mass concentration on wind speed could be

fitted using the following exponential relation:

$$M = a \exp(bU) \quad (3.2)$$

where, M is the aerosol mass concentration at wind speed U (ms^{-1}), b is a coefficient, often called the wind index and a is the background aerosol mass concentration when wind speed reaches zero. The values of the coefficients a and b estimated for the aerosols collected in stage 1 of QCM in the present cruise are 38.67 and 0.17 respectively. The corresponding values reported by *Exton et al.* [1985] for North Atlantic Ocean are 14.30 and 0.17. *Ramachandran and Jayaraman* [2002] studied the dependence of coarse mode aerosol mass on wind speed using the same relation for the QCM data collected during 1996–2000 over the Arabian Sea and the Tropical Indian Ocean and found a value of $15 \mu gm^{-3}$ for a and 0.35 for b . Higher value of a obtained in the present cruise reflects that the background aerosol mass over BoB is quite high and it includes a large fraction of non sea salt particles.

In the present cruise, average value for the total mass concentration (including the 1st stage) was found to be about $170 \mu g/m^3$. We also observed a north-south gradient in the total aerosol loading at the surface level over the study region. In order to model the transport of aerosols from their source regions in Indian subcontinent towards BoB, we assumed a simple exponential relation to represent the aerosol dispersion as a function of distance from northern coastal areas as follows:

$$M(D) = M(D_0) \exp\left(-\frac{D}{D_e}\right) \quad (3.3)$$

where $M(D)$ and $M(D_0)$ are the mass concentrations of aerosol at a distance D and at $D = 0$ ($22^\circ N$, in this case) respectively. D_e is the *e-fold distance* or the distance at which the concentration decreases to $1/e$ of the concentration at $22^\circ N$. The *e-fold distance* for aerosols comes out to be approximately 2460 km (Figure 3.4). Earlier *Satheesh et al.*, [1998] have reported a mean *e-fold distance* of 2446 km, calculated using the AOD data over Indian Ocean and Arabian Sea region.

3.3.3 Aerosol number size distribution

QCM observations have been further used to obtain the surface level aerosol size distributions. Mass concentrations measured in the 10 size ranges were used to derive the aerosol

Table 3.1: Size distribution parameters obtained from fitting log-normal modes to the observed aerosol number size distribution over BoB

Date	Mode-1			Mode-2			Mode-3			Mode-4		
	N, cm^{-3}	$\sigma, \mu m$	$r_m, \mu m$	N, cm^{-3}	$\sigma, \mu m$	$r_m, \mu m$	N, cm^{-3}	$\sigma, \mu m$	$r_m, \mu m$	N, cm^{-3}	$\sigma, \mu m$	$r_m, \mu m$
19 Feb 03	30000	1.72	0.027	340	1.41	0.150	5.5	1.50	0.47	0.099	2.43	2.36
20 Feb 03	23000	1.68	0.029	330	1.38	0.150	5.5	1.58	0.39	0.102	2.15	2.20
21 Feb 03	20000	1.58	0.034	340	1.38	0.150	5.8	1.50	0.43	0.149	1.94	2.43
22 Feb 03	31000	1.58	0.036	655	1.38	0.165	8.4	1.43	0.48	0.175	1.94	2.40
23 Feb 03	41000	1.54	0.033	685	1.38	0.163	8.5	1.43	0.53	0.190	1.97	2.16
24 Feb 03	28000	1.62	0.027	475	1.38	0.163	8.5	1.43	0.53	0.130	1.78	3.00
25 Feb 03	23000	1.58	0.028	390	1.38	0.160	7.6	1.43	0.54	0.097	1.68	3.54
26 Feb 03	26500	1.58	0.025	285	1.38	0.163	6.8	1.45	0.56	0.067	2.11	2.71
27 Feb 03	30000	1.62	0.026	450	1.45	0.160	7.4	1.48	0.54	0.100	1.93	2.37

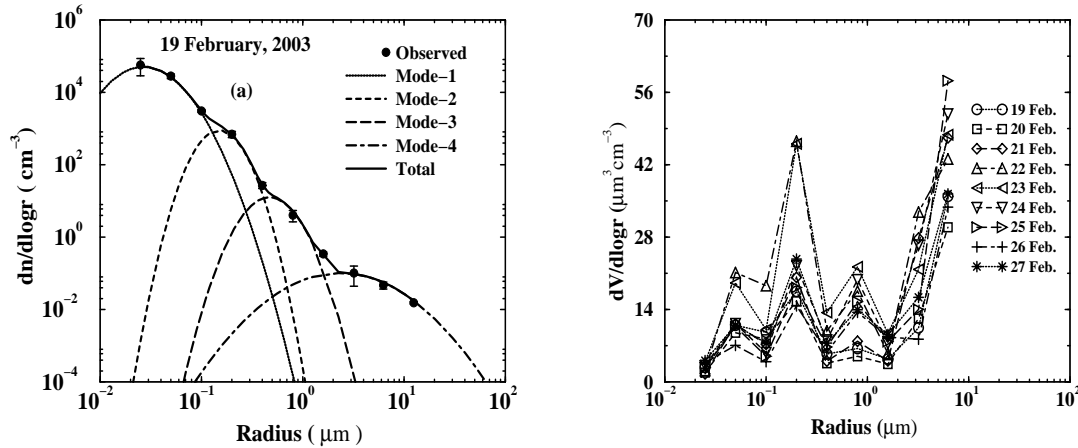


Figure 3.5: (a) The observed aerosol number size distribution is fitted using four individual log-normal curves and for example a typical data obtained on 19 February is shown. (b) Daily average aerosol volume size distributions obtained during the cruise period.

Table 3.2: Size distribution parameters for some of the aerosol types obtained from Hess et al. 1998.

Type	σ (μm)	R_m (μm) at R.H.				
		0%	50%	70%	80%	90%
Insoluble	2.51	0.471	0.471	0.471	0.471	0.471
Water Soluble	2.24	0.021	0.026	0.029	0.031	0.035
Soot	2.00	0.012	0.012	0.012	0.012	0.012
Sea salt (Acc)	2.03	0.209	0.336	0.378	0.416	0.497
Sea salt (coa)	2.03	1.750	2.820	3.170	3.490	4.180
Mineral (Acc)	2.00	0.390	0.390	0.390	0.390	0.390
Mineral (Coa)	2.15	1.900	1.900	1.900	1.900	1.900
Sulfate Drops	2.03	0.070	0.098	0.109	0.118	0.135

number distribution using appropriate mass density valid for the prevailing relative humidity conditions. Similar to the variation found in the mass concentration values, number concentrations of accumulation mode particles showed maximum spatial variation, with about 47% spread from its mean value over the entire study area, followed by nucleation mode and coarse mode particles with about 30% and 35% variations. Figure 3.5(a) shows the aerosol number size distribution for one typical day of the cruise with vertical bars representing $\pm 1 \sigma$ variation about the average number density values, while Figure 3.5(b) shows the daily average volume size distributions for different days of the cruise. The size distribution of aerosols at any location is mainly governed by the relative strengths

of different production and removal mechanisms [Jaenicke, 1993]. Many authors [Porter and Clarke, 1997; Bates et al., 1998; Koponen et al., 2002, 2003; Ramachandran and Jayaraman, 2002] have shown that the total size distribution of tropospheric aerosols is actually a combination of many log-normal distributions, where each mode represents different production sources. All size distributions measured during the present cruise exhibited the presence of four distinct modes and hence they could be fitted using up to four log-normal modes (equation 2.18). The shape of the derived aerosol size distribution remains same over the study region while the number concentration of aerosols changed in all the four modes, indicating that the amount of influx of particles as well as their in situ production changed while the physical processes responsible for their distribution remained unaltered. Mode radii for the distribution lie in the range of $0.025 - 0.036 \mu\text{m}$ for mode-1,

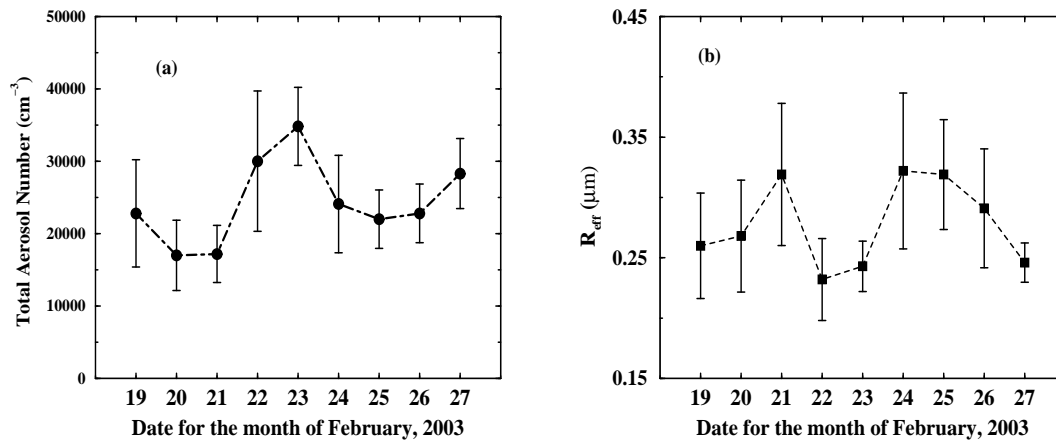


Figure 3.6: Variations of (a) total aerosol number concentration N (cm^{-3}) and (b) effective radius r_{eff} (μm) derived (using equations 3.4 and 3.5) from the observed aerosol size distribution.

between $0.15 - 0.165$ for mode-2, between $0.39 - 0.55$ for mode-3 and between $2.2 - 3.5$ for mode-4. Table 3.1 gives a summary of various modal parameters obtained from the log-normal curve fitting carried out on the daily average number distribution for the cruise period. We found that the number concentration for particles of all the four modes increased on 22 and 23 February when the ship was cruising in the northern BoB and coastal areas of India. Size distribution parameters for some of the aerosol types classified by Hess et al. [1998], at different relative humidity conditions is shown in Table 3.2. Comparing the modal parameters of Table 3.1 with those of Table 3.2, we find that water soluble and soot

particles constitute the mode-1 aerosols while the r_m value of mode-2 closely matches with those of sulfate aerosols. These sulfate aerosols are mostly produced by chemical reactions in the atmosphere by gaseous precursors such as sulfur dioxide (SO_2) from anthropogenic sources and dimethyl sulfide (DMS) from marine biogenic sources [Charlson *et al.*, 1992]. On similar arguments, possible aerosol type for mode-3, could be either sea salts in the accumulation size range and (or) insoluble particles such as soil dusts which get transported from arid and semi-arid regions of surrounding land masses [Prospero, 1979]. Similarly the large sized sea salt particles and mineral dusts constitute the aerosols in mode-4.

Two more parameters derived from the observed number size distribution are (i) total aerosol number concentration N (cm^{-3}) and (ii) effective radius r_{eff} (μm) which are defined as:

$$N = \int_{r_1}^{r_2} \frac{dn(r)}{dr} dr \quad (3.4)$$

$$r_{eff} = \frac{\int_{r_1}^{r_2} r^3 \frac{dn(r)}{dr} dr}{\int_{r_1}^{r_2} r^2 \frac{dn(r)}{dr} dr} \quad (3.5)$$

Here N is the integral number of aerosols of all size bins but is more sensitive to the number of smaller size particles (mode-1) and effective radius (r_{eff}) is a measure of total volume to the surface area of the distribution. Relative increase in the number of larger particles with respect to the smaller ones results in an increase in r_{eff} and vice-versa. Thus, together the value of N and r_{eff} give an indication of the relative dominance of smaller particles in the total size distribution. Figure 3.6 shows that there exists an anti-correlation between the total aerosol number concentration and the effective radii derived for all the size distributions measured during the cruise. We found that whenever the ship moved towards more open ocean regions, the value of N decreased and r_{eff} increased whereas over northern and coastal regions of BoB, increase in total aerosol concentration was accompanied by a decrease in the effective radii for the aerosol distribution. As discussed earlier, during winter season, large amount of gaseous pollutants and aerosols enter into BoB from Bangladesh and coastal areas of India like West Bengal, Orissa and Andhra Pradesh. These aerosols are dominated by smaller particles produced due to anthropogenic activities in these areas. As the distance from these source regions increases, total aerosol concentration decreases and the relatively bigger sea salt aerosols start dominating the distribution thereby increasing the value of r_{eff} .

3.3.4 Relationship between columnar and surface level aerosol characteristics

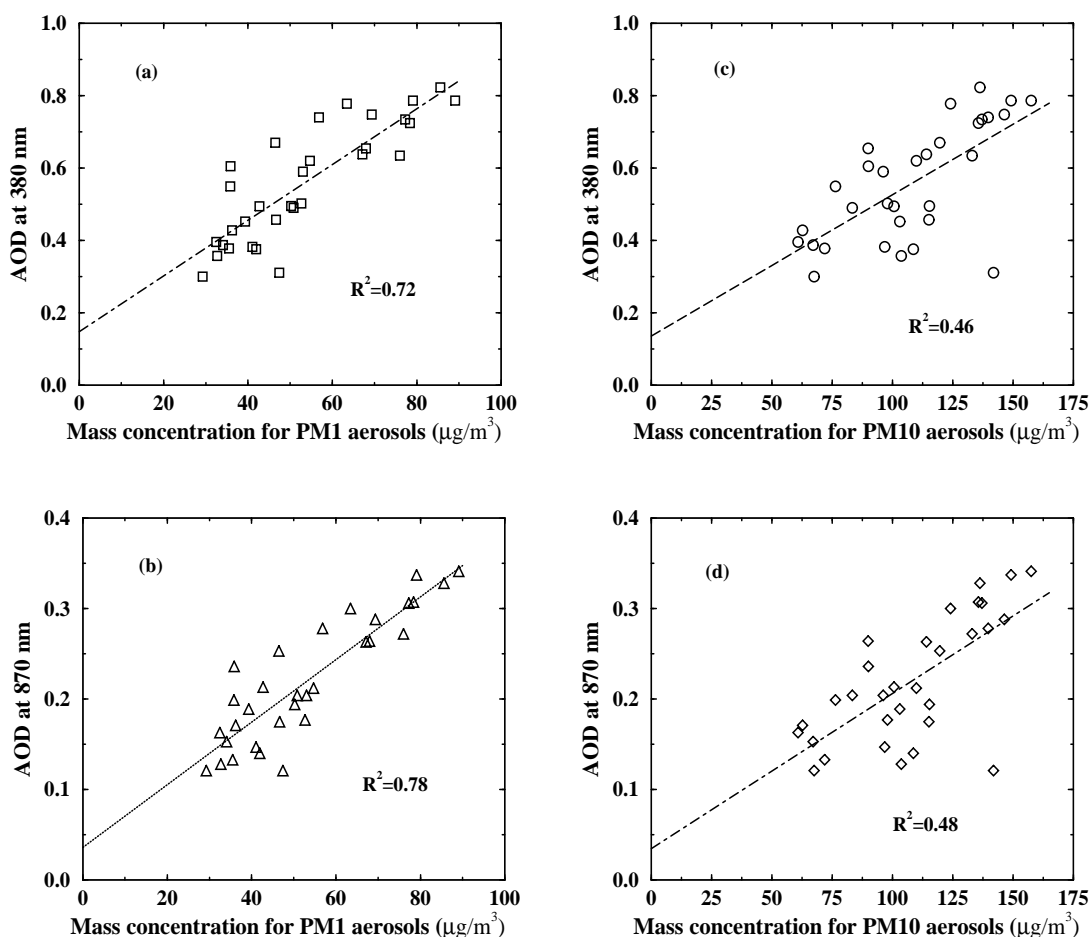


Figure 3.7: Scatter diagrams between column AOD values for two selected wavelengths of 380 and 870 nm and surface level aerosol mass concentration for PM1 and PM10 particles.

In order to investigate the correlation between columnar and surface level aerosol characteristics, a linear regression relation between the values of aerosol optical depth and mass concentration is attempted. Such relation is useful as they can be used for the estimation of optical depth within a given accuracy, when only mass concentration measurements are available and vice-versa. Figures 3.7 and 3.8 show the scatter diagram between AOD values at two different wavelengths and the PM10 (aerosols of size less than $10 \mu\text{m}$) and PM1 (aerosols of size less than $1 \mu\text{m}$) mass concentrations measured during the cruise. Figures 3.7(a) to 3.7(d) are obtained by correlating the simultaneously observed AOD data and the mass concentration measurements. In this correlation study only those data sets

have been considered for which both observations were conducted within a time gap of 15 minutes. The observed scatter in all these plots is due to the fact that while the mass concentration values are for the aerosols present within the relatively well mixed marine boundary layer (MBL), whereas AOD observations include the contribution from aerosols present not only within MBL but also from those lying in the free troposphere, immediately above it. Relative contribution from these two layers is dependent on the extent of vertical mixing between them, which in turn depends on other meteorological conditions. As evident from figures 3.8(a-d), there is a better correlation when the data is averaged for whole day rather than considering each individual observation. We also noticed that the correlation coefficients further increased in case of scatter plots involving smaller aerosols and shorter wavelengths. This reflects that the smaller particles are more well mixed in the atmosphere than the bigger ones. Most interesting observation to be noted in these scatter plots is that all the regression lines yield a positive non-zero intercept on the AOD axis. This comes from the contribution of background aerosols in the free troposphere towards the total columnar AOD value which is higher in the case of observations at smaller wavelengths. *Smirnov et al.* [2000] obtained a value of 0.04 as the intercept of the regression line for a similar scatter plot between AOD at 870 nm and dust concentrations measured over Barbados. Based on multi-wavelength LIDAR observations from Hulhule (4° N, 73° E) island in Maldives carried out during the INDOEX period, *Franke et al.* [2003] have shown that free tropospheric aerosol layers contributed 30 – 60% to the aerosol optical depth values measured at that site. Surface level aerosol number concentrations were further used to estimate the extinction caused by these aerosols following the Mie scattering theory. Wavelength dependent extinction coefficient (β_{ext}) is obtained using the following relation:

$$\beta_{ext}(\lambda) = \int_{r_1}^{r_2} \frac{dn(r)}{dr} Q_{ext}(m, r, \lambda) \pi r^2 dr \quad (3.6)$$

Here Q_{ext} is the extinction efficiency factor from Mie theory, which depends on the complex refractive index (m) of the aerosols, λ is the wavelength of the incident radiation and r is the radius of the particles. Since the columnar aerosol optical depth is the integrated value of the altitude dependent aerosol extinction coefficient, one can write:

$$\tau(\lambda) = \int_0^{z_{max}} \beta_{ext}(\lambda, z) dz \quad (3.7)$$

where z_{max} is the maximum altitude up to which aerosols are present. Based on the above

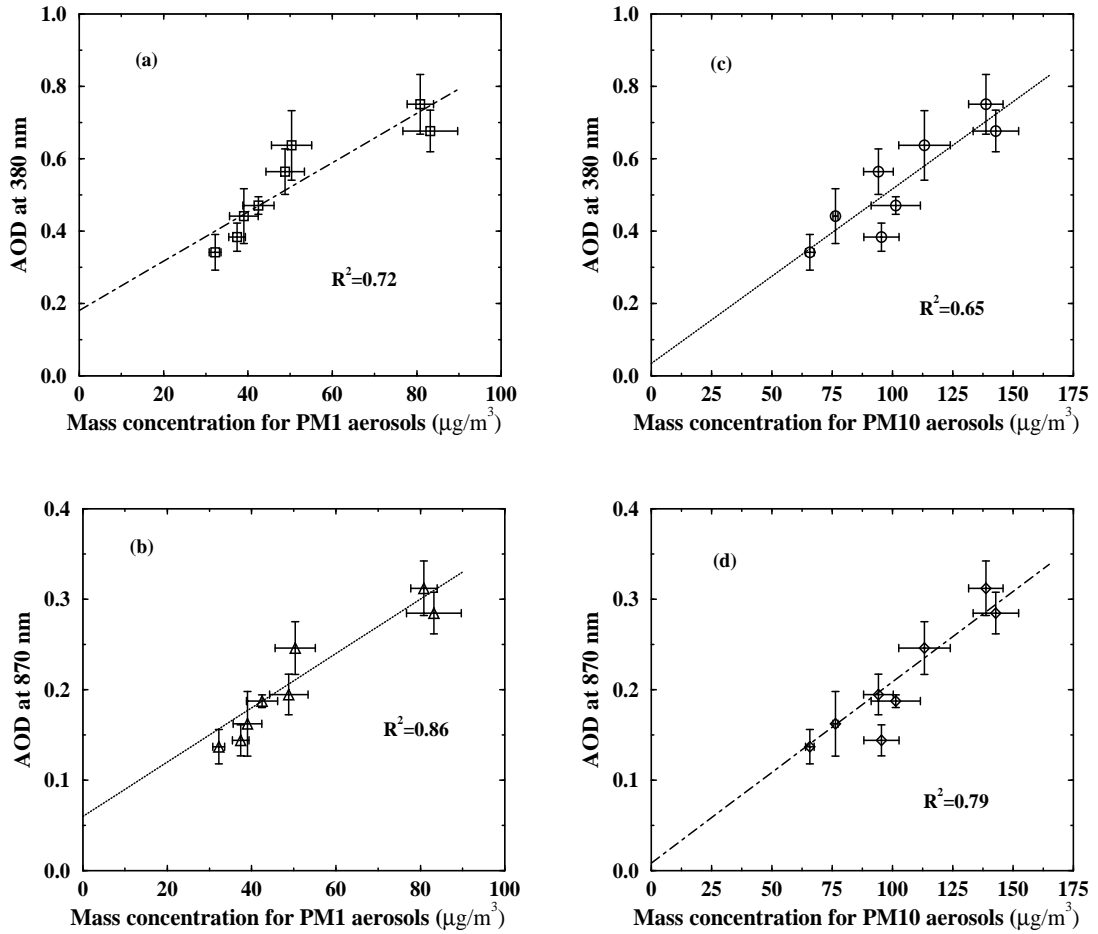


Figure 3.8: Same as figure 3.7 but the daily average values of AOD and surface level aerosol mass concentrations are correlated. The horizontal bar shows 2σ variation in the daily average mass concentration and the vertical bar shows the 2σ variation in the daily average AOD values.

equation, an estimate of aerosol scale height [$H(\lambda)$] is made for all the cruise days which may be defined as the altitude where the total columnar aerosol content could be brought down such that it still gives the same AOD value while maintaining a constant aerosol characteristics as that of the surface. So the wavelength dependent aerosol scale height, $H(\lambda)$ can be written as

$$H(\lambda) = \frac{\tau(\lambda)}{\beta_{ext}(\lambda, z = 0)} \quad (3.8)$$

Magnitude of this aerosol scale height tells about the contribution of surface level aerosols towards the integrated optical characteristics of aerosols present in the entire column of atmosphere. Higher value of scale height indicates a lesser contribution by surface level

Table 3.3: Aerosol scale heights calculated by using two different methods and for three different values of refractive index.

Refractive index at 500nm	Scale Height(H) in km	
	Method-1	Method-2
$1.465 \pm i0.0342$	2.92	4.11
$1.48 \pm i0.043$	2.74	4.16
$1.39 \pm i0.003$	3.35	5.53

aerosols towards the columnar properties of aerosols in the atmosphere and vice-versa. We found that the aerosol scale height estimated by this technique (Table 3.3) is not very much sensitive to the assumed values of aerosol refractive index.

Aerosol optical depth values have been further used to derive the columnar aerosol size distributions by applying the iterative inversion procedure described in *King et al.* [1978], *King* [1982] and latter on applied by several researchers [*Satheesh et al.*, 1998, 1999; *Devara et al.*, 1999; *Rao and Devara* 2001,]. A weighted refractive index for the BoB aerosols is used assuming them to be an internal mixture of various possible components as estimated using the OPAC model (discussed later) and procedure discussed by *Ramachandran and Jayaraman* [2002]. For the estimation of weighted refractive index, we have used the wavelength dependent refractive indices of various aerosol species given by *d'Almeida* [1991] and *Hess et al.* [1998]. Apart from using the weighted refractive index we have also derived the columnar number concentrations using the effective refractive indices proposed for the maritime polluted aerosols by *Hess et al.* [1998] and for the Indian Ocean aerosols by *Lubin et al.* [2002]. We found that the columnar size distributions derived by this technique is sensitive to the choice of refractive index values within 45%. From the ratio of the derived values of columnar number distribution and the measured aerosol number concentration at the surface level, aerosol scale height(H) are estimated for all the cruise days (Table 3.3). Figure 3.9 shows the comparison between columnar number distribution obtained by inverting the average AOD value and by using a refractive index value of $1.465 \pm i0.034$ for 25 February and simultaneously measured surface level aerosol number concentrations obtained using QCM on the same day. The aerosol scale height estimated using both the above methods are lower over northern BoB and higher at places away from the coast, indicating that the contribution of surface level aerosols towards their column integrated optical properties is more over northern BoB compared to those over free ocean regions. This also means that the free tropospheric aerosols have less variation over the cruise re-

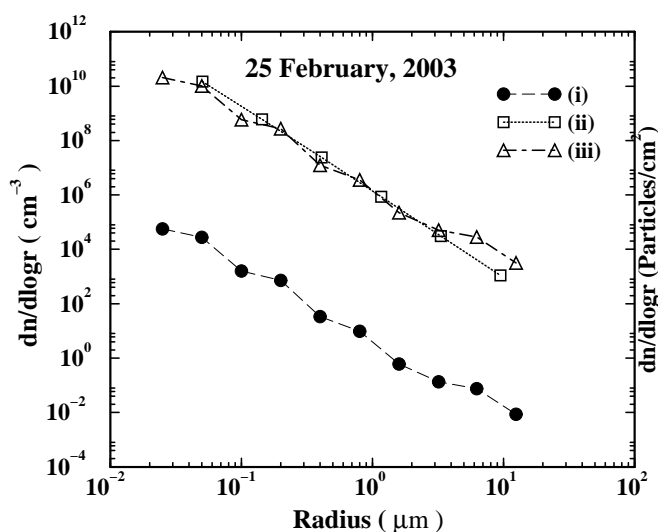


Figure 3.9: Aerosol size distribution for 25 February (i) measured using QCM is compared with (ii) columnar size distribution obtained by inverting the simultaneously measured AOD spectrum and (iii) obtained after multiplying curve (i) with a suitable scale height.

gion and the spatial differences in the columnar AOD values is mostly due to variations in aerosol loading at the surface level. Finally, all aerosol parameters measured over BoB are used to estimate the aerosol radiative forcing for this region. Details on methodology adopted for the estimation of aerosol radiative forcing and important results from the model estimates are discussed in *Chapter-6*.

3.4 Summary

A ship cruise experiment was conducted in February 2003 over the Bay of Bengal to study the transport of aerosols, their physical characteristics, optical properties and their effect on the regional scale radiative forcing. It is found that on all days of the cruise, air parcels at different altitude levels were coming either from west or from north-west direction of BoB and they cross significant portion of the Indian subcontinent before finally reaching the measured sites. Daily mean AOD values for 380 nm are found to be in the range of 0.34 to 0.75 and those at 1020 nm varied between 0.09 to 0.25. These values are much higher compared to that reported for other ocean regions of the world. AOD values were particularly high over northern BoB and along the east coast of India. Surface level aerosol mass concentrations averaged over the entire cruise region are 50, 37 and 13 $\mu\text{g}/\text{m}^3$ respectively

for the coarse mode ($> 1 \mu m$), the accumulation mode (between $1 \mu m$ and $0.1 \mu m$) and the nucleation mode ($< 0.1 \mu m$). The aerosol size distribution curves exhibit four distinct modes which could be fitted using four log-normal distributions, with mode radii in the range of $0.025 - 0.036 \mu m$ for mode-1, between $0.15 - 0.165$ for mode-2, between $0.39 - 0.55$ for mode-3 and between $2.2 - 3.5$ for mode-4. Total column aerosol optical depth and surface level aerosol mass concentrations show a good positive correlation amongst them. The aerosol extinction coefficients computed from the aerosol number concentrations are found to agree with the aerosol optical depth and both show higher values over northern and coastal areas of BoB. The computed extinction coefficients are further used to derive a wavelength dependent aerosol scale height by taking their ratio with the columnar AOD values. The columnar aerosol size distributions derived using the iterative inversion procedure described by *King et al.* [1978] and *King* [1982], is further used to estimate the aerosol scale height(H). Estimated value of scale height is found to be low over northern BoB due to relatively larger contribution of boundary layer aerosols to the total columnar AOD values.

Spatial variation in aerosol characteristics over Central India

Although several cruise experiments have been conducted over the ocean regions around the Indian subcontinent to assess the flux of aerosols getting transported into these regions from the surrounding land masses [Jayaraman *et al.*, 1998, 2001*a*; Ramachandran and Jayaraman, 2002, 2003*a*, 2003*b*; Ramanathan *et al.*, 2001*a*; Satheesh *et al.*, 2001; Ganguly *et al.*, 2005*a*], measurements of aerosol characteristics over land areas within the Indian subcontinent are very limited and confined to only specific locations [Moorthy *et al.*, 1999; Devara *et al.*, 2002; Niranjana *et al.*, 2004; Pandithurai *et al.*, 2004; Singh *et al.*, 2004;]. In order to understand and quantify the spatial heterogeneity in the distribution of aerosols as well as various trace gases and to study their impact on the regional climate system, an intensive field campaign was organized by the Indian Space Research Organization under its Geosphere Biosphere Program (ISRO-GBP) over the central and peninsular India in February 2004 [Ganguly *et al.*, 2005*b*, 2005*c*; Moorthy *et al.*, 2005; Niranjana *et al.*, 2005; Jayaraman *et al.*, 2006]. This field campaign was participated by more than a dozen experimental groups from different Institutes and Universities in India specializing in making measurements on aerosols, radiation and trace gases. As a part of this Land Campaign-I, we conducted aerosol measurements at selected locations between Ahmedabad and Hyderabad from 7 to 29 February 2004. Results obtained from this campaign provided the state of aerosol parameters in the background rural atmosphere, weakly influenced by growing number of urban agglomerations spread all across the country through long range transport. Measurements were conducted in two phases and observations were repeated at most of the

stations in order to see the temporal changes in the aerosol properties, if any over the period of this campaign.

4.1 Experiment and Meteorological Condition

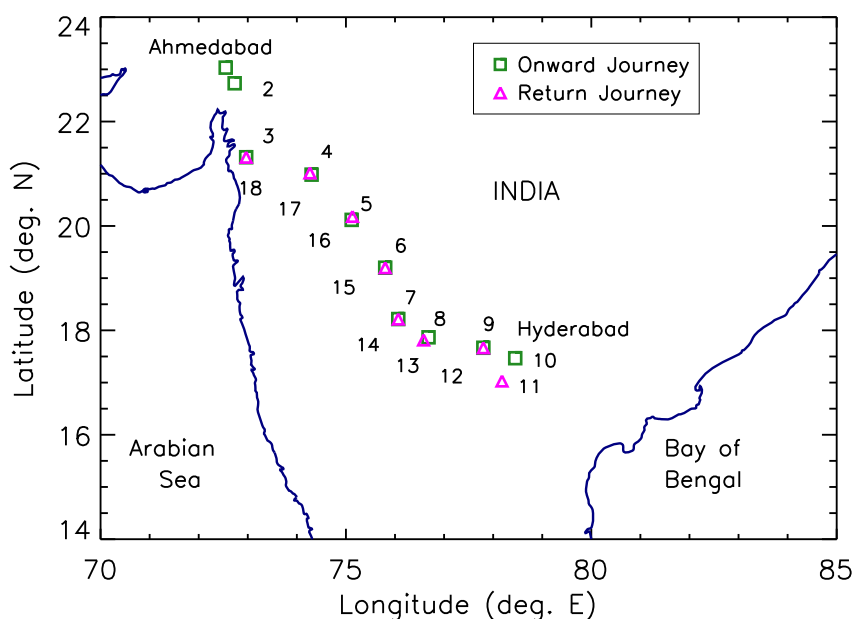


Figure 4.1: Stations where observations were made during the land campaign in February 2004 between Ahmedabad and Hyderabad. Locations marked as square are the stations used during the onward journey and the triangles are the stations used during return journey.

The campaign started on 7 February 2004 from Ahmedabad (23.03° N, 72.50° E) and observations were carried out on daily basis at selected locations (herein after referred to as stations) roughly at an interval of about 120 km enroute to Hyderabad (17.47° N, 78.45° E), in a total stretch of about 1200 km. The stations selected for this campaign are mostly rural sites, away at a distance of more than ~ 3 km from any major industry or highway to ensure that the measurements are not directly affected by any of the local sources and sampling is done for the well mixed air in the ambient atmosphere, representing the aerosol properties for each of these locations [Ganguly *et al.*, 2005b, 2005c; Jayaraman *et al.*, 2006]. According to a protocol adopted for the campaign, measurements conducted at each station from 10 : 00 to 17 : 00 Hrs (local time) have been considered for further data analysis

and the average values are treated as the daytime representative value for the corresponding station. Figure 4.1 shows the locations of various stations where extensive observations were made on a daily basis.

Table 4.1: Details of the locations and dates where measurements are made during the campaign.

Station	Station No.	Date	Lat. (° N)	Lon. (° E)	Alt (m) above MSL
Ahmedabad	1	6 Feb. 04	23.03	72.55	80
Kheda	2	7 Feb. 04	22.73	72.73	40
25 km from Surat	3	8 Feb. 04	21.32	72.97	26
Sakri	4	9 Feb. 04	20.98	74.30	446
50 km from Challisgaon	5	10 Feb. 04	20.12	75.12	590
20 km from Beed	6	11 Feb. 04	19.20	75.80	496
Osmanabad	7	12 Feb. 04	18.22	76.07	698
Omergaon	8	13 Feb. 04	17.82	76.58	566
36 km from Sangareddi	9	14 Feb. 04	17.67	77.80	630
NRSA, Hyderabad	10	15 Feb. 04	17.47	78.45	540
Sadhnagar	11	16-21 Feb. 04	17.03	78.18	628
36 km from Sangareddi	12	23 Feb. 04	17.67	77.80	637
Omergaon	13	24 Feb. 04	17.82	76.58	566
Osmanabad	14	25 Feb. 04	18.22	76.07	680
20 km from Beed	15	26 Feb. 04	19.20	75.80	495
50 km from Challisgaon	16	27 Feb. 04	20.18	75.13	602
Sakri	17	28 Feb. 04	21.02	74.27	475
25 km from Surat	18	29 Feb. 04	21.32	72.97	30

Table 4.1 gives the geographic information of the stations and dates where measurements were made during the campaign. An inter-calibration camp was organized at Shadnagar (17.03° N, 78.18° E) from 16 to 21 February, 2004 which is a relatively cleaner site located at a distance of about 80 km from the city of Hyderabad. During the inter-comparison campaign, observations were carried out for all 24 hrs of the day. The return leg of the campaign started from Hyderabad on 23 and ended on 29 February at Ahmedabad. In the return leg, observations were repeated at most of the stations visited during onward journey so as to study any systematic temporal variation in the parameters measured during the time interval of about two weeks between the onward and return legs of the campaign.

Along with aerosol properties, meteorological parameters such as air temperature, relative humidity, wind speed and wind direction were also measured at all the stations using a portable weather station. Figure 4.2 shows the daytime average values of surface air

temperature, relative humidity and wind speed for all the stations and for the period when aerosol observations were made. Surface air temperature shows a slight increase over the campaign period with its average value close to $29^{\circ}C$ during the onward leg while the corresponding value for the return leg was $33^{\circ}C$. The entire campaign period was mostly dry with relative humidity never exceeding 40%. NCEP reanalysis data shows that during the onward leg, surface level wind was coming from the north east direction at all stations while it was more randomized during the return leg. All along the campaign the winds were moderate with wind speed less than 10 km/h . The surface level wind was generally

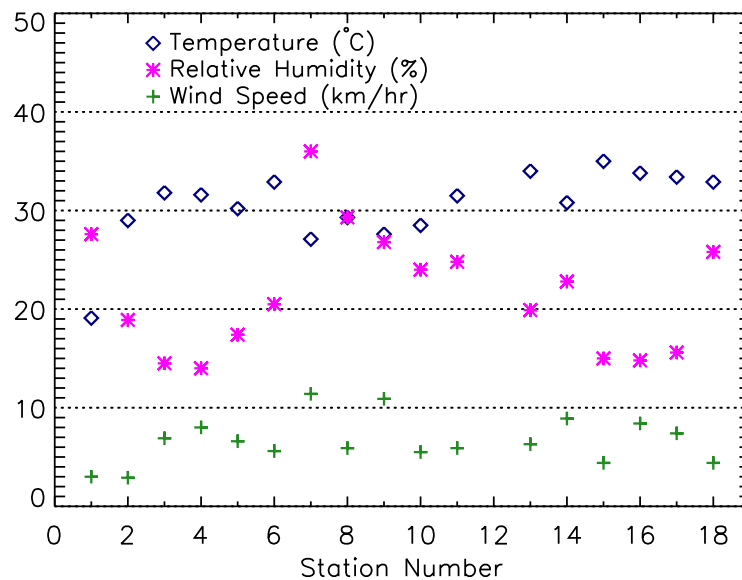


Figure 4.2: Daytime average meteorology data for each station. The values are averaged typically for the 10:00 to 17:00 h period during which other aerosol measurements are made.

from north and northwest direction at all high latitude stations (station above $19^{\circ}N$) while it was north and northeast at the low latitude stations (station below $19^{\circ}N$). In general, the observed meteorology is typical of the central India for the dry winter season for all the stations. Figure 4.3 shows the seven days air back trajectories plotted using the HYSPLIT-4 (Hybrid Single-particle Lagrangian Integrated Trajectory) model of ARL NOAA, showing the transport pathways of air parcels reaching at 10 m and 100 m altitudes over the measurement locations during the onward and return journey of the campaign. It can be seen from figure 4.3(a) that during the onward leg, all air trajectories at lower altitudes origi-

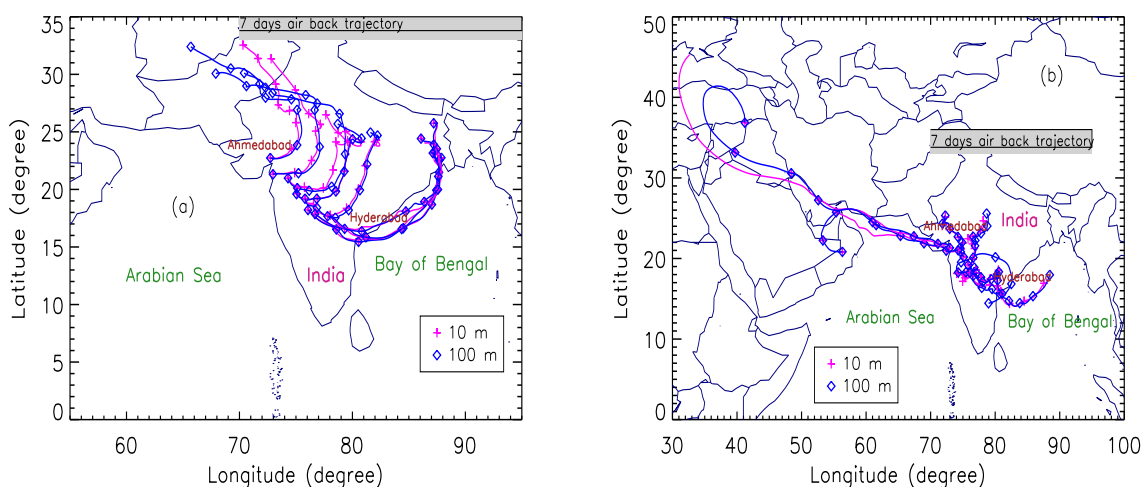


Figure 4.3: Seven days air back trajectories plotted using the HYSPLIT model showing the transport pathways of air parcels reaching at 10 m and 100 m altitudes over our measurement locations used during the (a) onward journey and (b) return journey of the campaign.

nated somewhere in North or North-West India, swept across large parts of North India and finally after taking a small turn reached the measurement locations from the North-East direction. These trajectories represent the possible transport pathways of aerosols from North Indian regions to central India during the Dry winter season. Unlike the systematic pattern observed during the onward leg, air back trajectories for lower altitudes are found to be random during the return leg of the campaign. This is seen because towards the end of February, over the central Indian region, wind vectors at lower altitudes start showing a reversal in their direction from previously North-East to South-West during the following Pre-Monsoon and Monsoon seasons.

4.2 Results and Discussion

4.2.1 Aerosol Optical Depth

Figure 4.4 shows the variation of AOD values at three selected wavelengths observed during the campaign period over different stations. During the onward leg of the campaign, AOD values increased almost monotonically from station-1 to station-10, indicating an overall increase in the columnar concentration of aerosols. AOD values for each station

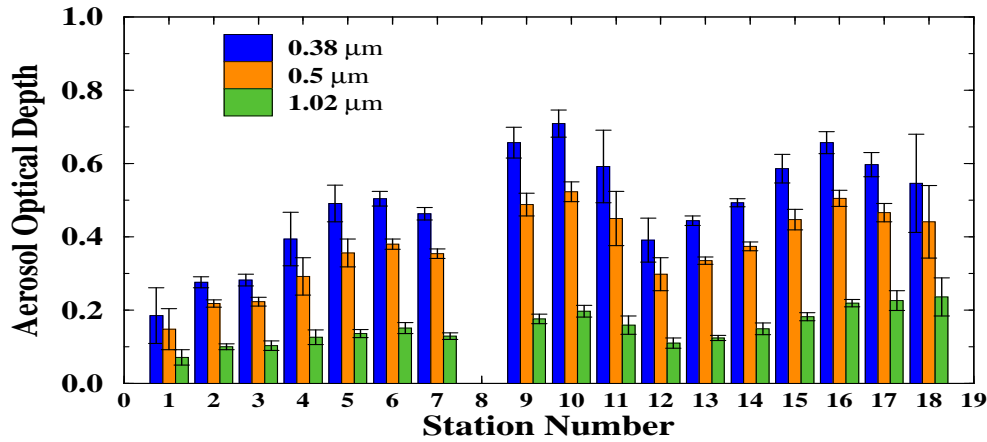


Figure 4.4: Aerosol optical depth values at three selected wavelength channels measured using Microtops-II sun-photometer for each station. AOD at intermediate wavelengths are found to lie within these values.

have been further used to estimate the Angstrom parameters α and β using the relation $\tau(AOD) = \beta\lambda^{-\alpha}$ [Angstrom, 1964]. Angstrom exponent α describes the spectral dependence of the AOD values and is related to the slope of aerosol size distribution curves. Large value of α is an indicator of higher ratio of smaller to larger particles in the total columnar atmosphere and vice versa. Parameter β represents the AOD at $1 \mu\text{m}$ and is proportional to the total columnar loading of aerosols in the atmosphere. During the en-

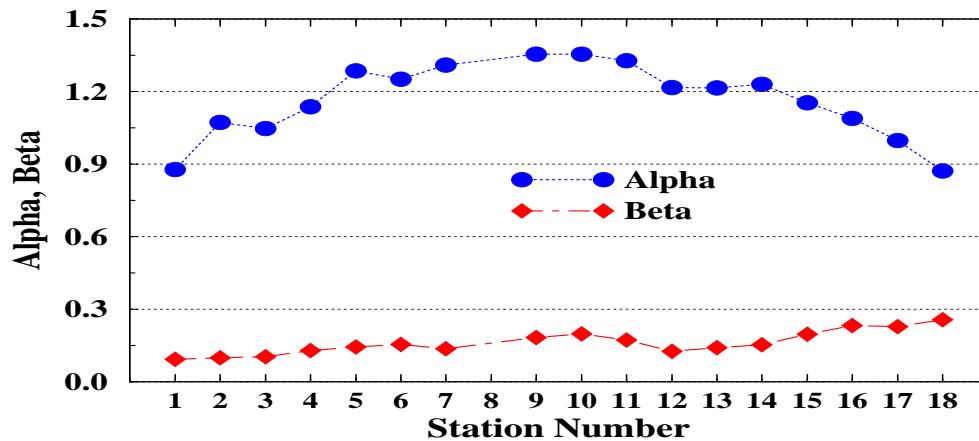


Figure 4.5: Angstrom coefficients α and β derived from the daily average AOD spectrum constructed for each station. Higher values of α indicates the presence of relatively larger number of smaller particles and vice versa.

tire campaign, Angstrom parameter α varied between 0.85 and 1.35 with highest values observed over station 10 and lowest values corresponding to station 18 [Figure 4.5]. The

observed variations in α and β shows that the concentration of surface-derived mineral particles over the northern stations are higher compared to the southern stations. Also, a further decrease in α and a corresponding increase in β over the northern stations during the return leg indicate an increase in the amount of coarser mineral particles in the atmospheric column as the season changes from winter to summer towards the end of the campaign. One of the reasons is the less vegetation cover and availability of more open fields at places closer to Ahmedabad. Secondly the soil type also changes from northern to southern stations. Soil type for stations closer to Ahmedabad are more of loose sand type whereas central India being a plateau region, its soil is not so loose and more of rocky type. Also as the summer progresses, in the northern plains, the dry continental winds uplift finely crushed dusty mineral particles from the land surface into the atmosphere and with increasing surface wind speed, they often result in dust-storm activities. A dust-storm like condition was also experienced on 29 February while measurements were made at station 18.

4.2.2 Aerosol Mass Concentration and Size Distribution

Surface level aerosol mass concentrations are measured at all stations using a quartz crystal microbalance (QCM) cascade impactor (model PC-2, California Measurements Inc., USA). Figure 4.6 shows the daily mean values of aerosol mass concentrations measured at all the stations. Mass concentration values measured individually from stage 2 to 10 are further grouped into three categories, viz., coarse mode ($110 \mu m$), accumulation mode ($0.11 \mu m$) and the nucleation mode ($0.010.1 \mu m$). Mass values measured in stage 1 of QCM device consist of all particles of size greater than $10 \mu m$ and are not included in the present classification. Average values of aerosol mass concentrations for the whole study region are $18.4 \pm 10.3 \mu g/m^3$ for coarse mode, $25.3 \pm 10.0 \mu g/m^3$ for accumulation mode and $16.1 \pm 6.7 \mu g/m^3$ for nucleation mode particles. The coarse mode particles, owing to their larger mass are not transported as effectively as accumulation and nucleation mode particles and hence they exhibit larger spatial variation, as indicated by the larger standard deviation with respect to its absolute value. Higher mass concentration for accumulation mode particles is due to their longer residence time in the atmosphere compared to other two modes.

Aerosol size distribution for all stations are constructed by merging the data obtained

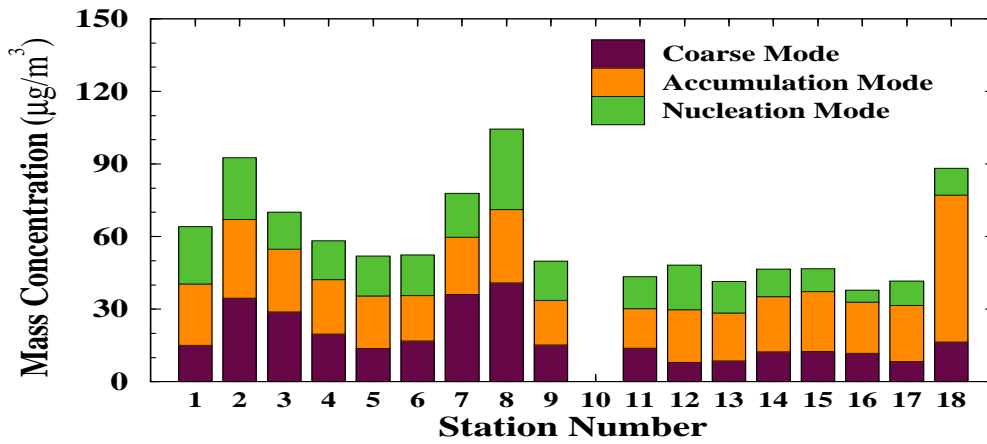


Figure 4.6: Daily average aerosol mass concentration measured using the Quartz Crystal Microbalance at 10 different size ranges are grouped into three categories, viz., coarse mode ($110 \mu\text{m}$), accumulation mode ($0.11 \mu\text{m}$) and the nucleation mode ($0.010.1 \mu\text{m}$).

from two different but simultaneously operated instruments, viz. the QCM cascade impactor, segregating the aerosols into ten different size ranges from 0.025 to $12.5 \mu\text{m}$ and an aerosol size spectrometer (Grimm aerosol technik, Germany) giving particle count for all aerosols in the size range of 0.3 to $20 \mu\text{m}$ by grouping them into 15 different size bins. Mass concentration values measured separately at 10 size ranges are used to derive the aerosol number size distribution, assuming a aerosol mass density of 2 g/cc . As shown in figure 4.7, the number size distribution for all stations show the presence of at least three different modes, each one being a representative of aerosols originating from different sources with different production mechanisms. All the measured size distributions are fitted using multiple log-normal distribution curves having different mode radii and width. The average mode radii for all stations, except station 18, are 0.024 ± 0.005 , 0.13 ± 0.02 and $0.70 \pm 0.16 \mu\text{m}$, respectively. Observed size distribution for station 18 could not be fitted using three modes as it exhibited the presence of an additional fourth mode at the coarse end of the size spectrum. Mode radii for the fitted modes corresponding to station 18 are 0.019 , 0.17 , 0.72 and $7.0 \mu\text{m}$, respectively. In general, the relative concentration of coarse size particles increases as one moves towards the northwest Indian region.

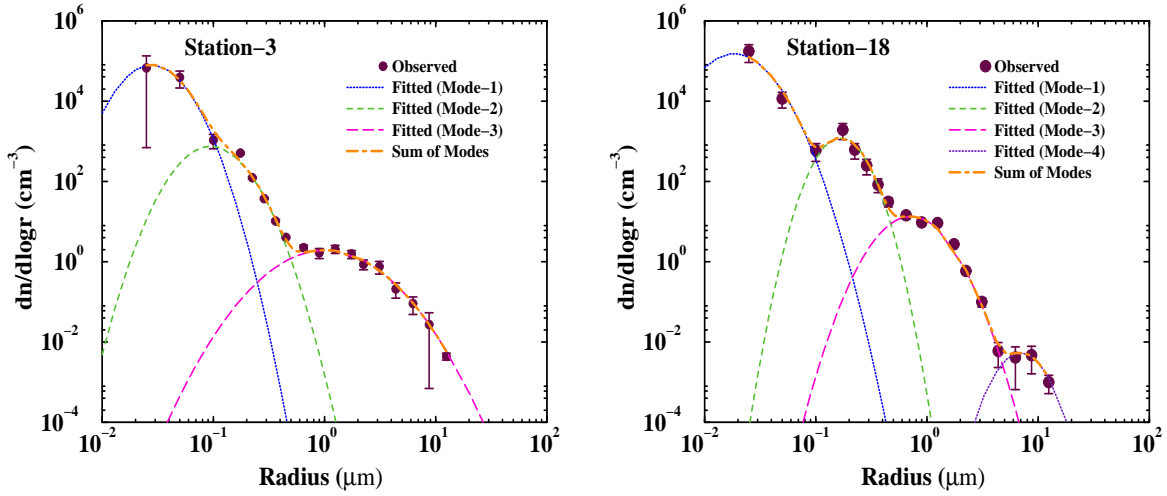


Figure 4.7: Observed aerosol size distribution for station 3 and 18 are fitted using multiple log-normal curves in such a manner that the sum of individual distributions best describes the observed pattern.

4.2.3 Aerosol Scattering Coefficient

Scattering coefficient of aerosol was measured using an Integrating Nephelometer (Model M903, Radiance Research, California, USA). Figure 4.8(a) shows the variation of scattering coefficient of aerosols at $0.53 \mu m$ at all stations where measurements were conducted during the campaign. Vertical lines represent $\pm 1\sigma$ variation about the mean values measured at different stations. Except for stations 10 and 18, the scattering coefficient values are found to vary between 0.08 and $0.20 km^{-1}$. Also, except for stations 1, 10 and 18, the observed variation in scattering coefficient between stations shows similarity with the variation of AOD values [Figures 4.4 and 4.8(a)]. This similarity between surface aerosol characteristics and its column integrated behaviour shows the well mixed state of aerosols in the atmospheric boundary layer for most of the stations. However, the exceptions are stations 1, 10 and 18. In these stations, although the scattering coefficient values are almost a factor of two higher compared to some other stations, columnar AOD values do not show an increase in the same proportion. Measurement location for station 10 is within the city of Hyderabad and surrounded by industries and large vehicular traffic. Proximity of these pollution sources is responsible for increasing the surface level aerosol scattering by nearly a factor of two compared to values obtained at other stations. In fact, not only the absolute values of scattering coefficients are higher in these stations, we also find large standard

deviations indicating strong short term variations in their values. Although AOD values are also high for station 10, corresponding increase is not proportionate with the increase in surface aerosol parameters. This observation shows that within the urban location, most of the locally produced aerosols are dispersed in the horizontal direction than in the vertical. Vertical distribution of aerosols obtained using simultaneously operated Micro Pulse Lidar (MPL) system also exhibited almost a factor of two higher extinction due to aerosols at lower altitudes (below 135 m) over station 10 compared to other rural stations. Highest value of aerosol scattering coefficient during the entire campaign was obtained at station number 18, a rural location 25 kms away from Surat. Interestingly, no such corresponding increase in the columnar AOD values shows that the observed increase in aerosol concentration over this station was confined to only up to about a few tens of meters from the surface. Unfortunately, the lidar system failed on 29 February and no vertical profile of aerosol could be obtained for station number 18. However, other surface level measurements such as aerosol mass concentration, size distribution, BC mass concentration etc. confirmed the large increase in aerosol concentration at the surface level in station number 18.

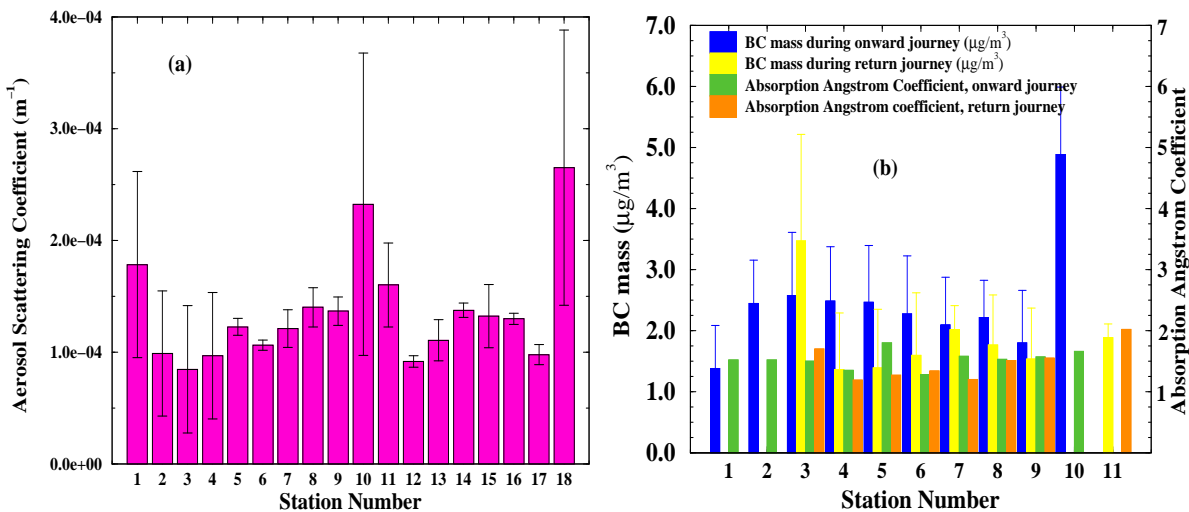


Figure 4.8: (a) Average values of the aerosol scattering coefficient for each station, measured using an Integrating Nephelometer. (b) Daily average BC mass concentration value measured at each station using Aethalometer

4.2.4 BC mass concentration

A seven-channel Aethalometer (model AE-42, Magee Scientific, USA) was used to measure the absorption coefficient of near surface aerosols at seven different wavelengths viz. 0.37, 0.47, 0.52, 0.59, 0.66, 0.88 and 0.95 μm along with mass concentration of black carbon aerosols. Out of the seven, 0.88 μm channel is considered as the standard channel for BC measurement because BC is the principle absorber of light at this wavelength and other aerosol components have negligible absorption at this wavelength. Data obtained from other channels can be considered as *equivalent BC* mass that will produce the same absorption. If the absorbing component of the aerosol consists only of black carbon then the BC values obtained from all the channels of Aethalometer would be identical, which is not the case in majority of the measurements during the present campaign.

Figure 4.8(b) shows the average value of BC mass concentration obtained from 0.88 μm channel of the Aethalometer for all observations made between 10 am to 5 pm of local time at different stations of the campaign. Since observations were repeated at most of the stations, BC values measured during onward and return journey are shown using different colors. The *equivalent BC* values from different channels are found to be much different from each other. This inconsistency indicates the presence of other absorbing aerosols in the atmosphere apart from black carbon. For example hematite mineral dust (Fe_2O_3) has absorption bands in the red region of the spectrum and hence abundance of this material can increase response of 660 nm channel [Lindberg *et al.*, 1993]. Also, aerosols produced in tobacco smoke [Lawless *et al.*, 2004] can increase the response of the yellow channel corresponding to 590 nm. However, at this stage it will be premature to conclude on this additional aerosol component. Nevertheless, this non-uniformity in the BC values obtained from different wavelength channels necessarily indicate the presence of absorbing aerosols other than BC at most of the locations. High value of BC was observed at station number 10 because unlike other stations, its location was inside the city of Hyderabad and surrounded by anthropogenic sources of BC like vehicular exhausts etc. Aircraft measurements [Moorthy *et al.*, 2004] conducted during the same campaign period reported the BC concentration at the surface level over Hyderabad to be around 3.5 $\mu\text{g}/\text{m}^3$. During the return leg of the campaign, a slight decrease in the BC values was observed at all the stations except at station number 18 which corresponds to station number 3 of the onward leg [Figure 4.8(b)]. Lower BC values obtained during the return leg is due to an increase

in the height of boundary layer as indicated by the difference in the surface temperature between the onward and return legs. Average ambient air temperature during the observation period in the onward leg of the campaign was 29.3°C while the corresponding value for the return leg was 33.3°C . The corresponding increased surface heating during the return leg of the campaign caused an increase in the height of surface boundary layer thereby facilitating an easier dispersion and dilution of aerosols into a larger volume.

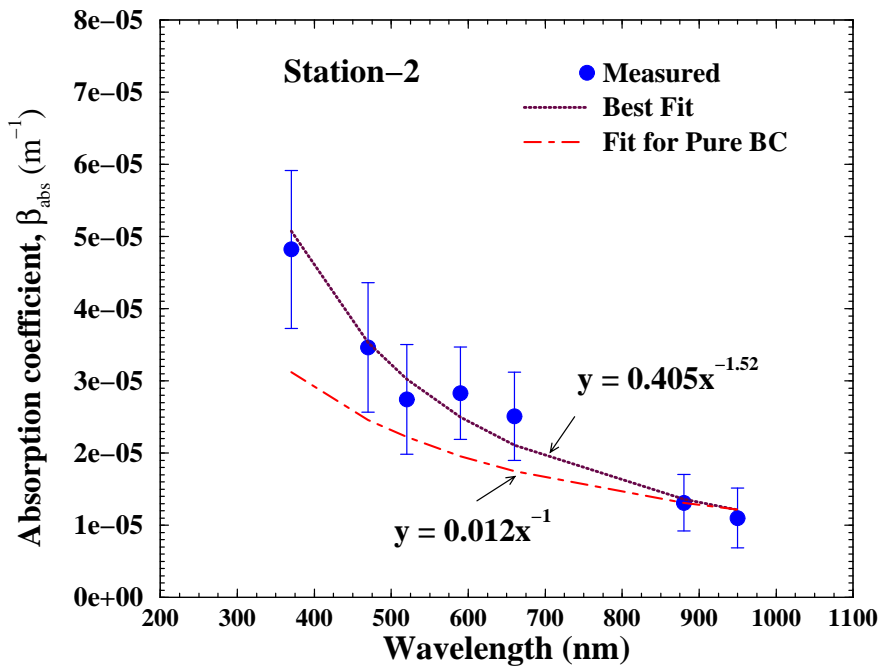


Figure 4.9: Spectrum for aerosol absorption coefficient observed at station 2 is best fitted using a power law and compared with the spectrum of a model atmosphere having BC from fossil fuel as the only absorbing aerosol component.

4.2.5 Aerosol Absorption Coefficient

The parameter which is required to assess the role of light absorbing particles on the regional and global climate forcing is the absorption coefficient of aerosols. In order to study the variation in spectral dependence of aerosol absorption at different stations, absorption coefficient of aerosols are derived from the raw radiance data recorded at all the seven wavelength channels using equation 4.1. Following the work of *Kirchstetter et al.* [2004] we investigated the wavelength dependence of light absorption by aerosols using a power

law relationship of the form

$$\beta_{abs}(\lambda) = K.\lambda^{-\alpha} \quad (4.1)$$

where K and α are the absorption Angstrom coefficients. The value α is a measure of spectral dependence of aerosols absorption. Figure 4.9 shows a typical spectrum for aerosol absorption coefficient observed at station 2. Absorption Angstrom coefficient α are estimated by least square fitting of equation 4.1 to the measured values of absorption coefficient and are found to vary between 1.2 to 2.0 over the study region [Figure 4.8(b)]. *Kirchstetter et al.* [2004] have shown that aerosols produced from biomass burning exhibit stronger wavelength dependence ($\sim \lambda^{-2}$) in absorption while those produced from fossil fuel burning such as motor vehicle exhausts etc. show a weaker dependence ($\sim \lambda^{-1}$). It was also observed that the extraction of biomass burning aerosol with acetone, which removed significant quantity of organic carbon (OC) from the sample, reduced the spectral dependency in absorption and brought down the α value close to 1.2. Several other researchers such as *Jacobson et al.* [2000], *Bond* [2001], *Bergstrom et al.* [2002] etc. have also shown that atmospheric aerosol mixtures in which absorption is mainly due to BC, exhibit a weak spectral dependence (λ^{-1}). Also *Schnaiter et al.* [2003] estimated a low content of Elemental Carbon (EC) in the spark discharge soot but they attributed the stronger spectral dependence in absorption by such aerosols to the specific bonding structures present in these type of soot. According to *Bond* [2001] the spectral dependence of light absorption by aerosols is mostly determined by the size of graphite clusters present within the absorbing material. *Bergstrom et al.* [2002] discussed that stronger absorption at shorter wavelengths could also arise due to the presence of mineral dusts in atmospheric aerosols.

Assuming BC to be the only absorbing aerosol component present, we estimated the absorption coefficient at all the seven wavelength channels using equation 4.1 with α value equal to unity and forcing the power law curve to cross the absorption coefficient value measured at 880 nm channel. Our result on spectral dependence of light absorption shows an excess absorption of upto 30% in the wavelength range of 0.4 to 1.0 μm [Figure 4.10]. This emphasizes the fact that measurement of spectral dependence of light absorption by aerosols is more important than mere knowledge about the mass concentration of BC as aerosol absorption can exhibit different wavelength characteristics at locations where major source of BC is not fossil fuel. While λ^{-1} dependence for aerosol absorption is typical of BC emitted from fossil fuel, deviation from λ^{-1} indicates contribution of absorbing parti-

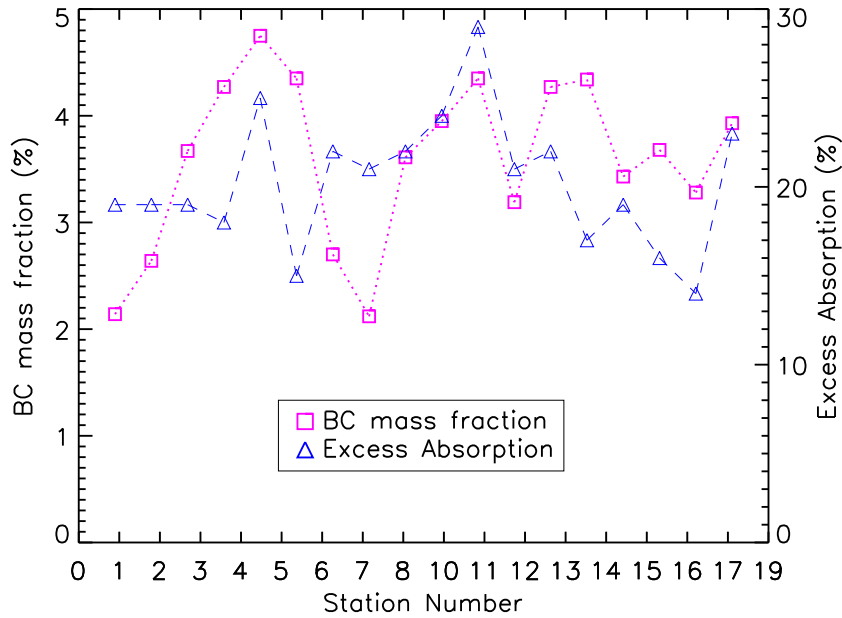


Figure 4.10: BC mass fraction in the total aerosol concentration and the excess absorption by aerosols in the wavelength range of 370 to 950 nm.

cles from biofuel/biomass burning or mineral dust. As there was no major biomass burning activity observed in the study region and also no specific enhancement in the amount of coarse mode particles measured using QCM device, we attribute the observed excess absorption to BC particles coming from biofuel burning [Reddy and Venkataraman, 2002; Venkataraman *et al.*, 2005] used for cooking in rural India. Figure 4.10 shows the BC mass fraction for all stations estimated by taking the ratio of BC mass from Aethalometer and the total aerosol mass from a QCM device, which varied between 2 to 5% over the study region.

4.2.6 Single Scattering Albedo

Single scattering albedo of aerosols are estimated by taking the ratio of β_{sca} measured at 530 nm and its sum with the β_{abs} at 520 nm. Although there is a difference of 10 nm between the wavelength of measurements of absorption and scattering coefficients, detail error analysis show that the error in ω will be less than 1% even in extreme case. Figure 4.11 shows the average value of ω at $0.525 \mu m$ and aerosol optical depth (AOD) at $0.5 \mu m$ for

all stations. AOD is measured using a hand held sun-photometer, and the average values from observations made between 10 am to 5 pm of local time is shown. Magnitude of ω can be considered as an index for the relative dominance of scattering with respect to absorbing aerosols whose value can range from 0 (purely absorbing) to 1 (purely scattering). It can be seen from figure 4.11 that during the entire period of the campaign, there was an overall increase in the measured value of ω with an average value for all the stations close to about 0.84. This indicates an unequal change in source strength or the removal process between absorbing and scattering type of aerosols over the region during the period of study. Black carbon (BC) mass concentration showed lower values during return leg of the campaign [Ganguly *et al.*, 2005b]. Interestingly, both minimum as well as maximum value of ω were observed at the same site (close to Surat (21.32° N, 72.97° E), a rapidly growing industrialized city of western India) which corresponds to station number 3 for the onward journey and station number 18 during the return journey of the campaign. Low value of ω was also observed at station number 10 because unlike other stations which were mostly rural, its location was inside the city of Hyderabad and surrounded by several anthropogenic sources of BC, mainly exhausts from vehicles.

Comparing our data with previously reported values of ω from other regions [Jayaraman *et al.*, 2001a; Russell *et al.*, 2002; Bergstrom *et al.*, 2003], we find that the ω values estimated during the present campaign are relatively low indicating the dominance of absorbing aerosols like BC over the study region.

4.3 Summary

A detailed study on aerosol properties has been made over the central Indian region during February 2004 as a part of the ISRO-GBP's Land-Campaign-I. During this campaign, observations were conducted at selected stations between Ahmedabad (23.03° N, 72.50° E) and Hyderabad (17.47° N, 78.45° E), which are mostly rural sites and away at a distance of more than ~ 3 km from any major industry or highway to ensure that the measurements are not directly affected by any of the local sources and sampling is done for the well mixed air in the ambient atmosphere truly characterizing the aerosol properties for each of these locations. Results from various complimentary measurements show that aerosols over the northwestern parts of the study region are dominated by surface derived dust particles

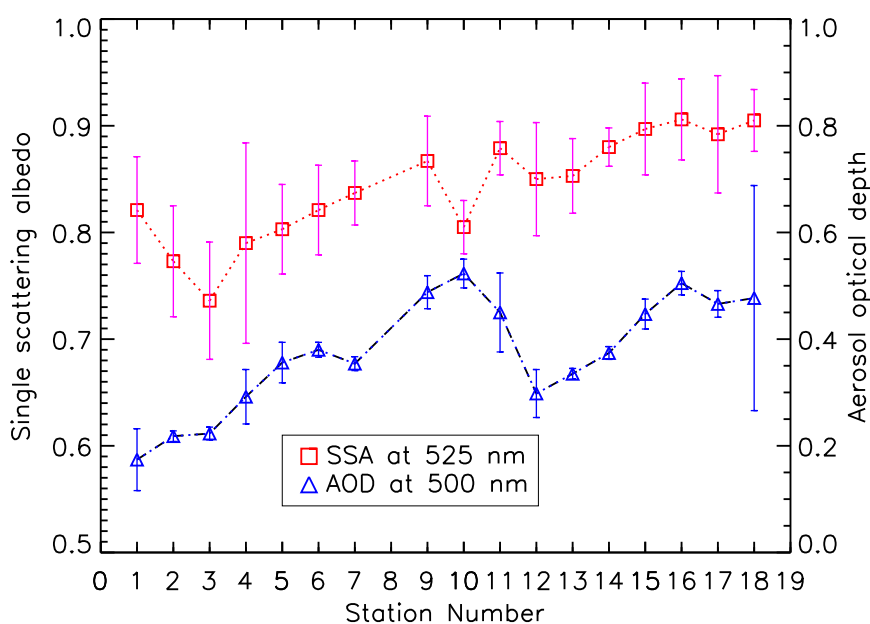


Figure 4.11: Average values of Single scattering albedo at $0.525 \mu\text{m}$ and aerosol optical depth at $0.5 \mu\text{m}$ obtained at different stations during the campaign. Vertical bars are the two standard deviation about the mean.

while there is an increase in the amount of secondary aerosols over the south-central parts of Indian peninsula. Relatively low values of single scattering albedo are obtained over the central Indian region, which shows an overall increasing trend towards the end of dry winter season, indicating unequal changes in source strength and/or removal processes of absorbing and scattering type aerosols. The spectral dependence of light absorption shows an excess absorption of up to 30% in the shorter wavelength range, less than $0.88 \mu\text{m}$. This emphasizes the fact that measurement of spectral dependence of light absorption by aerosols is more important than mere knowledge about the mass concentration of BC as aerosol absorption can exhibit different wavelength characteristics at locations where major source of BC is not fossil fuel. The observed excess absorption is attributed to particles coming from biofuel burning used for cooking in rural India.

Aerosol-Fog interaction study over New Delhi

Satellite imagery over North India shows the presence of aerosol haze along the southern edge of Himalayan region, over the Indo-Gangetic plain extending across Bangladesh and onto the Bay of Bengal during winter months (December to February) when there are minimal rainfall and shallow boundary layer over this region [Kaufman *et al.*, 2002]. This entire Indo-Gangetic belt is one of the densely populated areas in the world and is a source region for various anthropogenic aerosols such as sulfates, nitrates, black carbons etc. Over and above this prevailing hazy condition, situation becomes even worse at times when some of the areas within this region are affected by intense fog events. High concentration of aerosols help in the formation of early morning fog which also turns into production of smog (smoke+fog) causing severe reduction in visibility and leading to road accidents, health problems, delay in air traffic etc. Since the fog droplets are formed on aerosols which act as condensation nuclei, onset of fog very much depends on the properties of these aerosols [Pandis and Seinfeld, 1990], which also have an impact on the subsequent evolution of the fog layer. On the other hand, fog droplets can modify the characteristics of aerosols by aqueous-phase chemical reactions occurring within the fog droplets as well as resulting in their removal from the atmosphere by wet deposition [Frank *et al.*, 1998; Lillis *et al.*, 1999]. Left panel of Figure 5.1 shows the distribution of Modis (Moderate Resolution Imaging Spectroradiometer) derived aerosol optical depth at $0.55 \mu m$ for December 2004, indicating higher aerosol loading over the Indo-Gangetic plain. Right hand panel of Figure 5.1 is the Modis image from NASA's Terra satellite for 17 December 2004 showing haze

and smog (*smoke + Fog*) over North India. This persistent haze with frequent occurrence of fog is capable of producing large imbalance between the incoming solar and outgoing IR radiation which can have climate impacts not only on a regional scale but also globally [Ramanathan and Crutzen, 2003; Ramanathan et al., 2005].

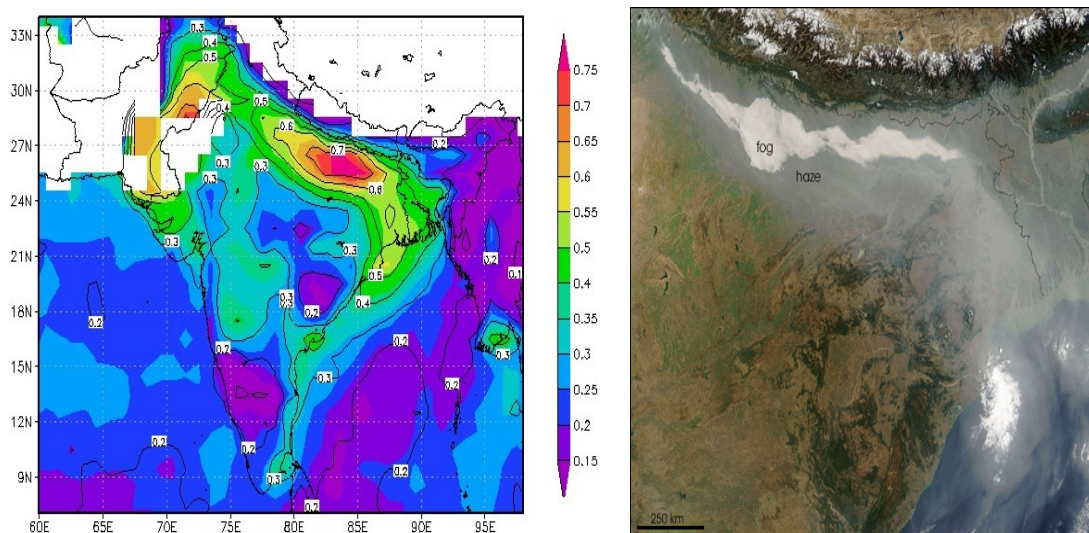


Figure 5.1: Left panel shows the distribution of Modis derived aerosol optical depth at $0.55 \mu\text{m}$ for December 2004. Right hand side panel is a Modis image from NASA's Terra satellite for 17 December 2004 showing haze and smog (*smoke + Fog*) over North India.

Unfortunately very few data records and that too on limited aerosol parameters are available from this potentially strong source region [Monkkonen et al., 2004; Singh et al., 2004; Tripathi et al., 2005]. In order to study the characteristics of aerosols constituting this infamous wintertime haze over north India which occasionally results in the formation of notorious fog in different parts of this region, an intensive field campaign was organized by the Indian Space Research Organization under its Geosphere Biosphere programme (ISRO-GBP) during December 2004, when observations were carried out at selected stations spread across the entire Indo-Gangetic plain. Broader objective of this campaign was to understand and quantify the spatial heterogeneity in the distribution of aerosols over the region, study their impact on the regional climate forcing and identify the transport pathways from one part of this region to another. As a part of this Land Campaign-II, complementary measurements of various optical and physical parameters of aerosols were made from New Delhi (one of the stations identified for this campaign), a highly industrialized megacity in South Asia. For the first time, ground truth values of several radiatively

important aerosol parameters such as aerosol optical depth spectra, size distribution, black carbon mass concentration, wavelength dependency in absorption, scattering coefficient, single scattering albedo, vertical distribution of aerosols in the atmosphere etc. are obtained. Several interesting features are observed in the behavior of these aerosol parameters under intermittent foggy, hazy and clear sky conditions, prevailed during the campaign period. We also observed alterations in physical and optical properties of aerosols during an intense fog episode which occurred in New Delhi during the period of our campaign in December 2004. Finally all results are combined and used to calculate the radiative forcing due to these aerosols which is necessary to understand their implications on the environment and climate on regional scale in a global perspective, details of which are discussed separately in *Chapter-6*.

5.1 Measurement Site and Meteorology

Measurements were carried out from the campus of the National Physical Laboratory, New Delhi (28.63° N, 77.17° E), an urban mega-city and national capital of India, between 1 to 31 December 2004. Period of observation was purposely chosen in the month of December so that measurements of aerosol parameters could be carried out during the prevailing hazy conditions over Delhi and also look for opportunities to study the changes in their behavior during occasional fog events occurring at several places over this region during this time of the year. Different days of the campaign period have been classified into certain categories viz. hazy, foggy and clear sky days based on general sky conditions, meteorological parameters and horizontal visibility for that day. Table 5.1 lists this classification done for all days and also for both halves of each day viz. forenoon and afternoon. Figure 5.2 shows the behavior of surface level meteorological parameters viz. temperature, relative humidity and wind speed during the campaign period. There was an overall decrease in the average surface temperature recorded for the entire month. As the winter started intensifying, surface temperature dropped by nearly 10° in the first 10 days of the campaign. After that there was some increase in temperature around 12 December and it remained fairly uniform during next couple of days. However, once again there was a continual drop in surface temperature after 18 December which increased slightly during the last two days of the campaign. Relative humidity (RH) exhibited large variations through-

out the campaign with an average value of about 66% for the entire month. On some of the days its value were very critical as with all other conditions remaining nearly identical, slightly elevated values of RH resulted in the formation of fog on one day while with small difference in its value, it remained hazy on another day. In general, winds were very calm throughout the campaign period with an average near surface wind speed of about 18 km/h. Previously, Singh *et al.* [2005] have reported higher values of wind speed (~ 5 m/s) measured over Delhi during the pre-monsoon months from April to June. Lower values of wind speed over Delhi and its surrounding regions during the present study period implies that the amount of land derived dust aerosols in the atmosphere must be much less in proportion compared to other seasons of the year. Thus majority of the aerosols present in the atmosphere over Delhi during this season of the year are dominated by locally produced particles from various anthropogenic activities.

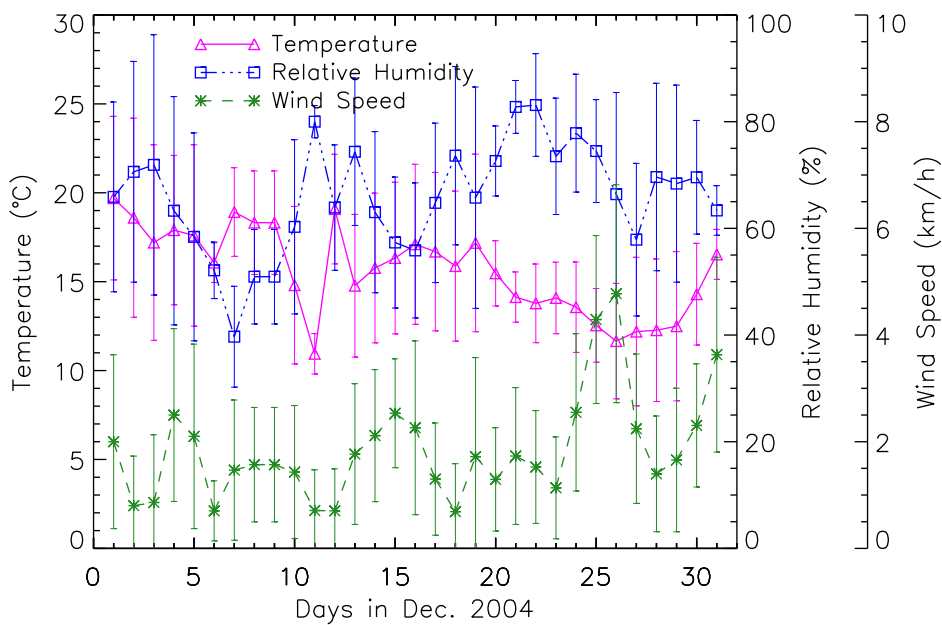


Figure 5.2: Daily variation of surface level meteorological parameters viz. temperature, relative humidity and wind speed during the campaign period. Vertical bars represent $\pm 1\sigma$ about the mean value for each day.

Table 5.1: Classification of days based on sky conditions and visibility

Days of December 2004	Forenoon	Afternoon
1	Hazy	Hazy
2	Clear	Clear
3	Clear	Clear
4	Hazy	Hazy
5	Clear	Clear
6	Clear	Clear
7	Clear	Hazy
8	Hazy	Hazy
9	Clear	Clear
10	Clear	Hazy
11	Foggy	Clear
12	Foggy	Hazy
13	Foggy	Clear
14	Clear	Clear
15	Clear	Clear
16	Clear	Clear
17	Clear	Hazy
18	Foggy	Hazy
19	Hazy	Clear
20	Hazy	Hazy
21	Foggy	Hazy
22	Hazy	Hazy
23	Hazy	Hazy
24	Foggy	Hazy
25	Clear	Clear
26	Clear	Clear
27	Clear	Clear
28	Clear	Hazy
29	Hazy	Hazy
30	Hazy	Hazy
31	Drizzle	Drizzle

5.2 Results and Discussion

Various physical and optical properties of aerosols have been studied during December 2004 when intermittent foggy, hazy and clear sky conditions prevailed over Delhi. In this section, we describe the important features observed in the behavior of aerosols during each of these conditions.

5.2.1 Aerosol optical depth

Figure 5.3(a) shows the time series of daily average values of AOD at $0.5 \mu m$ and the Angstrom wavelength exponent α estimated from the daily mean AOD spectra. Vertical bars in the figure represent $\pm 1\sigma$ variation about the mean AOD value for each day. Monthly mean value of AOD at $0.5 \mu m$ is about 0.91 with a standard deviation of 0.48. In particular, daily mean values of AOD as well as its standard deviation are found to be higher on hazy and foggy days. Table 5.2 shows a comparison of AOD values obtained at different urban locations in India during dry winter months. It can be noticed that the average AOD value over Delhi is higher than the maximum AOD value at most of other cities in India. Aerosol optical depth being an index for total columnar burden of aerosols, Delhi is at top in the list of most polluted cities in India in terms of total columnar amount of particulate matter during this season of the year. Another urban location which closely follows Delhi in terms of high AOD is Kanpur, situated at a distance of about 350 km south-east of Delhi, also lying in the Indo-Gangetic basin and experiencing similar conditions as of Delhi [Tripathi *et al.*, 2005]. Another important parameter estimated from multi-spectral measurement of aerosol optical depths is Angstrom wavelength exponent α , which is the slope of logarithm of AOD verses logarithm of wavelength (in micron units) plot. Angstrom's parameter α is useful to compare and characterize the wavelength dependence of AOD and columnar aerosol size distribution [Eck *et al.*, 1999; Cachorro *et al.*, 2001]. For example, a relative increase in the number of larger particles with respect to smaller ones result a decrease in the value of α and vice-versa. However, α estimated from sun-photometer measured AOD depends on the wavelength pair used for the computation. In a study Reid *et al.* [1999] have shown that α computed using shorter wavelength pair is more sensitive to changes in the amount of nucleation and accumulation mode sized particles than when estimated using longer wavelength pairs. However, we

find that α values estimated using two different wavelength pairs viz. $0.38 - 0.87 \mu\text{m}$ and $0.675 - 1.02 \mu\text{m}$ match within ± 0.2 except on 13 December when α estimated using the longer wavelength pair showed much lower values as there was a dense fog on that day. In the present study α values plotted in Figure 5.3(a) are estimated using the full AOD spectrum between 0.38 to $1.02 \mu\text{m}$. Mean value of α for the entire month is found to be around 1.12 . In general, Angstrom parameter α is found to be higher on hazy days such as on 8, 12, 28 etc. It will be shown later in this section that most of these hazy days are characterized by increased levels of sub-micron aerosols, mainly comprised of absorbing soot aerosols as well as other scattering type aerosols. Only exception is during 20 to 24 December which has been classified as hazy/foggy period with high values of AOD when estimated α values are found to be very low [Table 5.1 ; Figure 5.3(a)]. Such a decrease in the value of α indicates an increase in the population of coarse particles in the atmospheric column compared to smaller particles. However, aerosol size distribution measured at the surface level did not show a significant increase in the number concentration of coarser particles with respect to smaller ones, but aerosol vertical profiles obtained using the Micro Pulse Lidar showed presence of an aerosol layer at an elevated altitude of about 0.6 km. This will be further discussed while describing the nature of variation in the aerosol vertical distribution observed during the campaign period. Since size distribution measurements are not available at different altitudes, it is not possible to give any conclusive reason for the observed decrease in α value, but the observed aerosol layer at the elevated altitude could have a definite role.

Figure 5.3(b) shows the AOD spectrum for five representative days of the campaign period viz. 1, 5, 8, 18 and 24 December, comprising of at least one clear, hazy and foggy day. During the entire period of observation, lowest AOD was obtained on 5 December while the highest value was obtained on 24 December [Figure 5.3(a)] and for all other days the values remained between these two extremes. It is not only the average value of AODs are higher on hazy and foggy days [Figure 5.3(b)] but they are also characterized by large standard deviations compared to any clear day. Boundary layer height remains very low in the morning hours on hazy and foggy days, due to which various pollutants including aerosols remain trapped within a dense atmospheric layer and results in high values of AOD at all wavelength channels from 0.38 to $1.02 \mu\text{m}$. This is also reflected in other surface based measurements carried out using Grimm aerosol spectrometer, Aethalometer

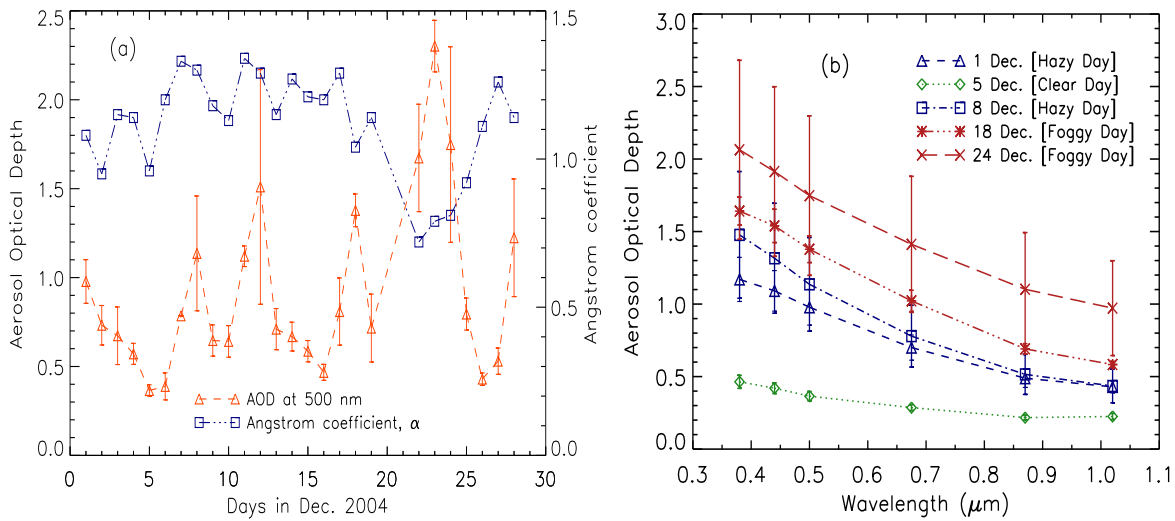


Figure 5.3: (a) Time series of daily average values of AOD at $0.5 \mu\text{m}$ measured during the campaign together with the variation of Angstrom wavelength exponent α estimated from the daily mean AOD spectra. (b) AOD spectrum for five representative days during the campaign period.

and Nephelometer. As the day progress, gradual increase in solar insolation causes a break up of this dense layer and the trapped aerosols are ventilated away both vertically and horizontally. As the aerosols reach little higher altitudes (\sim above 0.2 km), they get advected to distant places beyond the limits of the city and the haze layer originally formed over such urban centers spreads to surrounding regions. Due to this ventilation effect, a slight decrease in AOD values is observed during mid-day hours on such hazy and foggy days. Comparing the AOD spectra for 1 and 5 December, we find that although AOD values at all wavelength channels are higher on the hazy day of 1 December than on the clear day of 5 December, this increase is not spectrally uniform, rather percentage increase in AOD is larger at shorter wavelengths ($\sim 150\%$) than at longer wavelength channels ($\sim 90\%$ in this case). Comparison of the AOD spectra for 1 and 8 December, both hazy days, negligible difference in AOD value is found above $0.87 \mu\text{m}$ but at shorter wavelengths (eg. at $0.38 \mu\text{m}$) AOD on 8 December is higher than on 1st by nearly 26%. Both these observations show that, a hazy day is characterized by increased levels of sub-micron sized aerosols in the atmosphere and the AOD measurements at lower wavelengths are most affected. It is also found that even among hazy days, a more haziness is characterized by higher AOD at smaller wavelengths with no appreciable difference in longer wavelengths AOD. Compar-

Table 5.2: Comparison of AOD values measured at some of the urban locations in India.

Location	Period	AOD at 0.5 μm	References
Bangalore (13°N, 77°E)	November, 2001	0.236 \pm 0.005	Babu <i>et al.</i> [2002]
Chennai (13.04°N, 80.17°E)	February, 2001	0.58	Ramachandran and Jayaraman [2003a]
Pune (18.53°N, 73.85°E)	November-April 2001-02	0.4 \pm 0.2	Pandithurai <i>et al.</i> [2004]
Nainital (29.37°N, 79.45°E)	December, 2002	0.12 \pm 0.02	Sagar <i>et al.</i> [2003]
Kanpur (23.43°N, 80.33°E)	December 2001-2003	0.57 \pm 0.27	Singh <i>et al.</i> [2004]
Ahmedabad (23.03°N, 72.5°E)	December 2002-2003	0.44 \pm 0.09	Unpublished work
Kathmandu (27.67°N, 85.31°E)	Winter 2003	0.34	Ramana <i>et al.</i> [2004]
Hyderabad (14.47°N, 78.43°E)	Winter 2003	0.35	Latha and Badrinath [2005]
Kanpur (23.43°N, 80.33°E)	December 2004	0.77 \pm 0.29	Tripathi <i>et al.</i> [2005]
Delhi (28.63°N, 77.17°E)	December 2004	0.91 \pm 0.48	Present study

ing the AOD spectra of 8 December, a hazy day with those of 18 and 24 December which were foggy days, AOD values on foggy days are found higher than on any hazy day. Also, unlike between hazy and clear days, the increase in AOD values on foggy day compared to a hazy day is almost spectrally uniform between 0.38 to 1.02 μm . This happened because before the onset of fog, there is an increased concentration of sub-micron sized aerosols in the atmosphere and under high relative humidity prevailing during foggy period, some of these particles play the role of condensation nuclei and grow in size with increase in relative humidity [Frank *et al.*, 1998] thereby raising the AOD values at longer wavelengths.

5.2.2 Aerosol number size distribution

Size resolved aerosol number concentration were measured using Grimm particle size spectrometer. Figure 5.4 shows the daily mean values of number concentration for all aerosols in the size range of 0.3 – 20 μm . The vertical lines on top of each bar represent the standard deviation ($\pm 1\sigma$) in number concentration of aerosols for each day. Num-

ber concentration values are not available for 24 December due to malfunctioning of the instrument. Similar to AOD, surface level aerosol concentration also showed large variations during the campaign period. There are similarities as well as differences in the pattern of variations in columnar AOD and surface level number concentrations [Figures 5.3(a) and 5.4] with some days exhibiting maxima or minima for both of these parameters while there have been days when although higher values of AOD were observed but surface level number concentrations do not show a corresponding maxima. Hazy or foggy days of 8, 11, 18, 29 December, characterized by higher values of AOD has been captured in the surface measurements as well, with increased levels of aerosol concentration particularly in the smaller size range. Similarly when lower values of AOD were obtained on relatively clear days such as 5, 6, 16 and 26 December, surface level aerosol number concentration also showed lower values in almost all size ranges. However a clear discrepancy between surface based measurements and column integrated AOD is observed during the period of 20 – 24 December. Under normal condition, aerosol concentration is found to be high in the lower part of the atmosphere as it is close to most of the natural and anthropogenic sources of aerosols and contribute maximum in terms of aerosol extinction to the column integrated AOD. However, a condition with higher values of AOD and lower concentration of near surface aerosols is possible only if higher contribution of extinction comes from aerosols present at higher altitudes. During this period we detected using a simultaneously operated Micro Pulse Lidar system, an aerosol layer present at an elevated altitude in the atmosphere and contributing significantly towards columnar AOD values.

Surface level aerosol number concentration exhibited a strong and consistent diurnal variation throughout the campaign period. Figure 5.5(a) shows the monthly mean pattern for diurnal variation of aerosol number concentration measured continuously at every 5 minute interval. Vertical bars in the figure represent $\pm 1\sigma$ variation about the mean value for all measurements made around a particular time of each day during the entire month. This pattern is a combined effect of diurnal variation of surface meteorology as well as source strength of aerosols. Major sources of aerosols for an urban atmosphere are anthropogenic in nature and the important ones being vehicular exhausts, smokes from factories etc. However, one major factor which contributes significantly towards the production of aerosols in Delhi and other parts of Northern India during this season is the disposal of waste by burning, such as burning of dry leaves. Another source of aerosols which

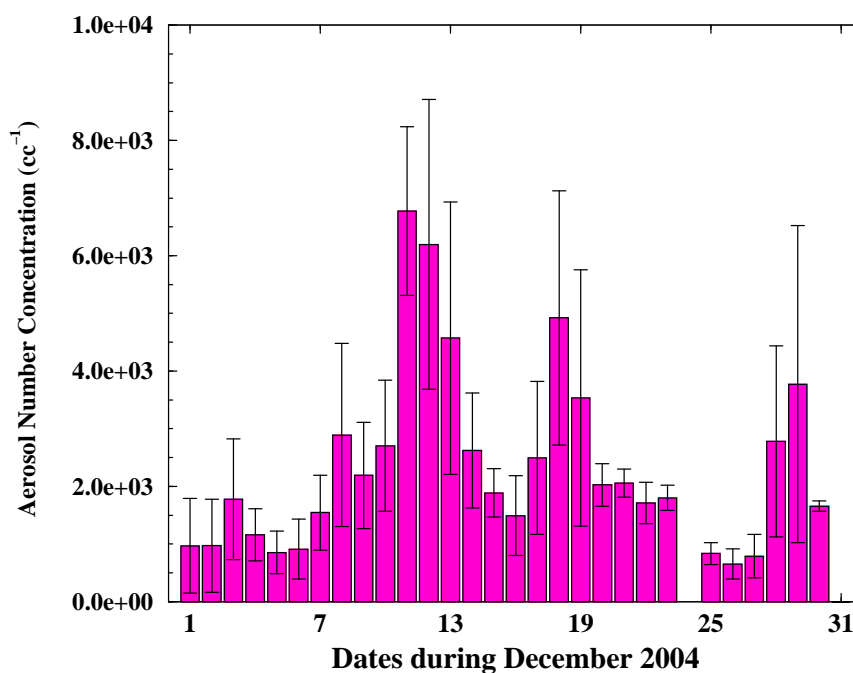


Figure 5.4: Daily mean values of aerosol number concentration in the size range $0.3 - 20 \mu\text{m}$ measured using Grimm particle size spectrometer.

has a relation with anthropogenic activity includes burning of wood, paper or other solid wastes by population dwelling in the city slums to keep themselves warm during cold winter nights.

Surface level aerosol number concentration was found to be maximum between 22 hrs and 03 hrs of local time [Figure 5.5(a)]. Most important reason for observing higher concentration of near surface aerosols during nighttime is due to formation of inversion layer at very low altitude which prevents convective mixing of air and acts as a barrier for the vertical transport and dispersion of aerosols produced near the Earth's surface. This results in piling up of particles produced during evening hours which continues up to late night, in the lower atmosphere. In Delhi, it is common to find dry leaves and other waste materials collected and put on fire which serves as an easy way for getting rid of these garbage materials. Most of these waste burning activities take place during evening hours when the boundary layer height of the atmosphere is already very low and formation of temperature inversion prevents vertical transport of these pollutants. However, after about 03 hrs, aerosol concentration starts declining because many anthropogenic sources of aerosols cease during this time while particle removal due to gravitational settling pro-

cess continues. Number concentration values reach a local minima just after Sunrise at around 07 hrs. But very soon with the beginning of a new day, road traffic starts rising and vehicular exhausts release lot of aerosols which includes black carbon and precursor gases for the production of other sub-micron aerosols such as sulfates, nitrates etc. This leads to an increase in aerosol number concentration which reaches maxima around 09 hrs and thereafter remains constant with some small fluctuations up to about 12 hrs. By noon, the nighttime inversion breaks down completely, boundary layer height goes up and increased insolation at the Earth's surface starts convective mixing of air thereby lifting aerosols from surface to higher levels in the atmosphere. Increased boundary layer height provides larger volume for the aerosols to distribute themselves in the atmosphere and this causes a dilution in their concentration at the surface level leading to a decrease in aerosol concentration which reaches the minimum value around 16 hrs. After this time, solar heating of the Earth's surface decreases while increasing traffic level combined with waste burning activities start loading the atmosphere with more aerosols. Thus on the one hand there is increase in production of aerosols after 16 hrs, on the other hand planetary boundary height starts lowering thereby providing smaller room for the distribution of aerosols in the atmosphere and also convective mixing of air ceases in the absence of insolation of Earth's surface. Due to all these factors, surface level aerosol concentration start increasing from its minimum value and this stride continues almost up to 22 hrs and stabilizes at high value till late night hours.

Although diurnal variation of aerosol number concentration is found to be consistent throughout the campaign period, we observe distinct differences in the aerosol size distribution measured on different days categorized as clear, hazy and foggy days [Figure 5.5(b)]. Although foggy days were marked with increased concentration of aerosols of all size ranges, we found this augmentation to be more pronounced in case of coarse particles of size greater than $1 \mu m$. Our observation shows that number concentration of coarse mode particles increased on foggy days by nearly two orders of magnitude compared to their corresponding values measured at the same site on clear days. Another observation made during this campaign was the distinction between a clear day and a hazy day in terms of aerosol number size distribution. We did not find any appreciable difference in number concentration of aerosols larger than $5 \mu m$ measured on a hazy day and on a normal day. However, this difference increased with decrease in particle size such that for

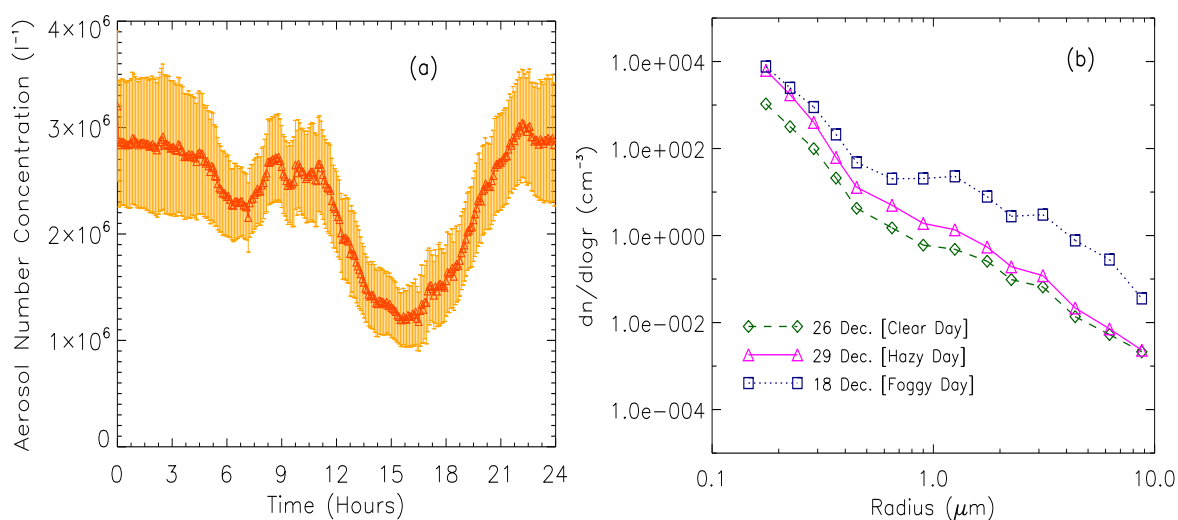


Figure 5.5: (a) Monthly mean pattern for diurnal variation of total aerosol number concentration ($0.3 - 20 \mu\text{m}$) measured continuously at every 5 minute interval. Vertical bars represent $\pm 1\sigma$ variation about the mean value for all measurements made around a particular time of each day during the entire month. (b) Different aerosol number size distributions obtained on typical clear, hazy and foggy days

aerosols smaller than $\sim 1.0 \mu\text{m}$, number concentrations are found to be higher on hazy days than on clear days, reaching almost an order of magnitude difference at $0.3 \mu\text{m}$ diameter (lower limit of the Grimm instrument used). However, for particles bigger than about $0.9 \mu\text{m}$, large differences in number concentration is observed between hazy and foggy days, as formation of fog mostly takes place in hazy atmosphere with increased concentration of aerosols and under favorable meteorological conditions [Frank *et al.*, 1998]. During fog formation process, some of the nucleation mode particles ($< 0.1 \mu\text{m}$) experiencing hygroscopic growth get activated under high relative humidity condition [Seinfeld and Pandis, 1998]. However, due to large differences in aerosol concentration of different size ranges, observed increase in the concentration of larger sized particles are not accompanied by a detectable decrease in the concentration of smaller size particles.

5.2.3 Black Carbon mass concentration

Black carbon (BC) aerosols produced as a result of incomplete combustion of coal, diesel, petrol, biofuels and biomass burning, is one of the crucial climate forcing agents globally but more importantly over populous countries like India and China [Novakov *et al.*, 2000].

Jacobson [2001] has shown that large positive radiative forcing produced by BC aerosols makes it second most important agent for global warming after CO_2 in terms of direct forcing estimates. Total BC emissions from India including all sources such as fossil fuel, open burning and biofuel combustion is around $610 \pm 200 \text{ Gg year}^{-1}$ [Venkataraman *et al.*, 2005]. This is nearly 8.5% of total global emission and therefore demands regular monitoring of BC aerosols across various parts of the country and study their climatic effects not only on a regional scale but also their global impacts. Throughout the campaign, we observed large variability in the values of BC mass concentration [Figure 5.6]. Due to some instrumental problem, data on BC mass concentration are not available for first ten days of the campaign. Nevertheless, instrument was repaired and BC measurements could be made during next twenty one days of campaign consisting of hazy, foggy and also one or two clear sky days. BC concentration exhibited almost identical day-to-day variability as observed in the case of particle number concentration [Figure 5.4], signifying that BC constitutes a large fraction of total aerosol concentration in the atmosphere of Delhi. Peak values of BC concentration used to surpass $60 \mu\text{g}/\text{m}^3$ for several hours of the day during hazy and foggy conditions. Highest value of diurnally averaged BC mass concentration ($65 \mu\text{g}/\text{m}^3$) was measured on the hazy day of 11 December, while lowest value ($11 \mu\text{g}/\text{m}^3$) was obtained on a relatively clear day of 26 December. Average value of BC mass concentration measured during the entire campaign period was around $29 \pm 14 \mu\text{g}/\text{m}^3$. Monkkonen *et al.* [2004] reported the PM_{10} concentration over Delhi during this season to be in the range of $276 - 422 \mu\text{g}/\text{m}^3$. Also during a meet for inter-comparison of instruments, as a part of ISRO-GBP's Land campaign-II, conducted just prior to its launch at our measurement site in New Delhi, total aerosol mass concentration was measured to be around $230 \mu\text{g}/\text{m}^3$. Considering our BC data and results published by Monkkonen *et al.* [2004], we infer the BC mass fraction over Delhi for this season to be in the range of 4-15%. Previously, Babu *et al.* [2002] have reported the BC concentrations over Bangalore for the month of November to be in the range of $0.4-10.2 \mu\text{g}/\text{m}^3$. While conducting parallel measurements of ISRO-GBP's Land campaign-II, BC concentrations over Kanpur city varied between $6-20 \mu\text{g}/\text{m}^3$ and BC mass fraction was in the range of 7-15% [Tripathy *et al.*, 2005]. During an earlier campaign in February 2004, Ganguly *et al.* [2005b] found the daytime (10-16 hrs) average BC mass over Hyderabad to be around $4.8 \mu\text{g}/\text{m}^3$. Also Venkataraman *et al.* [2002] reported the BC concentrations for Mumbai during INDOEX-IFP (Jan-Mar, 1999)

as $12.5 \pm 5 \mu\text{g}/\text{m}^3$. Comparing with measurements over other urban locations of Europe, America and Asia, *Tripathy et al.* [2005] found the BC mass concentration over Kanpur to be higher than any of the refereed locations. However, results from the present study shows that BC concentrations over Delhi is not only highest among megacities in India but also much higher than several other urban locations of the world. Such high values of BC mass and its mass fraction in the total aerosol concentration over Delhi is a matter of concern as these soot particles are strong absorber of both incoming solar radiation as well as the outgoing terrestrial infrared radiation and hence having tremendous potential to alter the radiation budget of the Earth by trapping heat within the atmosphere [*Jacobson, 2001*].

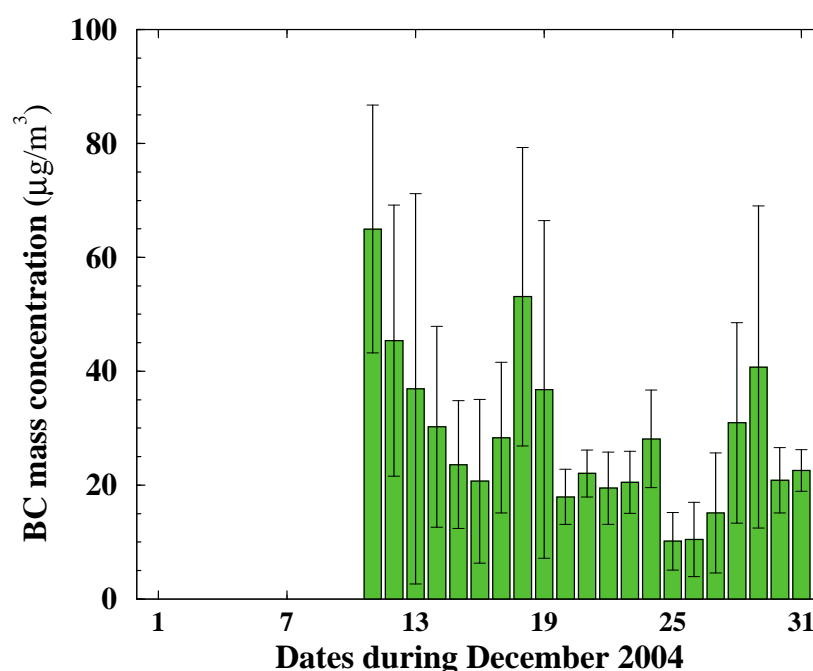


Figure 5.6: Daily mean values of BC mass concentration measured using an Aethalometer. Due to instrument problem, data are not available for first ten days of the campaign.

Long vertical lines on top of each bar in Figure 5.6 represent standard deviation ($\pm 1\sigma$) in the daily values of BC data indicating large variations occurring in BC concentration measured within a day. A consistent pattern in the diurnal variation of BC mass concentration [Figure 5.7(a)] is observed which is identical with that of near surface aerosol number concentration [Figure 5.5(a)]. This is an outcome of combined effect produced due to variation in aerosol production and surface meteorology. Diurnal variation of BC mass showed periods of two maxima, one in the late evening or nighttime (20-00 hrs) and the

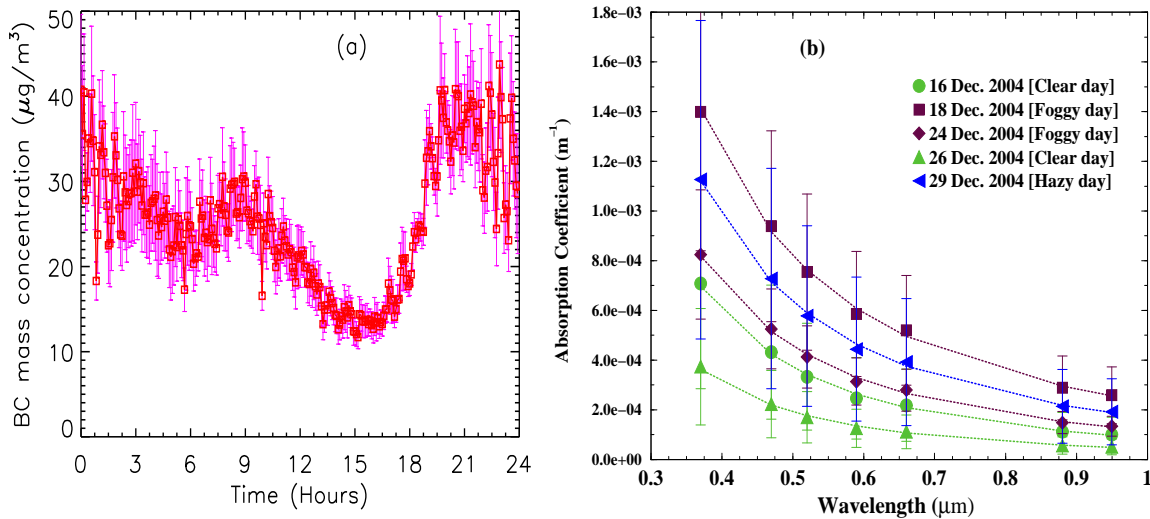


Figure 5.7: (a) Monthly averaged diurnal variation of BC mass concentration with vertical bars representing $\pm 1\sigma$ variation about the mean value. (b) Some typical spectra of aerosol absorption coefficient for five representative days of the campaign period. Spectrum for each day is best fitted using power law curves.

other during morning hours (08-09 hrs) while lowest concentrations were measured in the afternoon time between 15 – 16 hrs. Increased production of BC aerosols and gradual formation of a surface based inversion opposing vertical mixing in the atmosphere cause BC concentrations to escalate from around 16 hrs and reach maxima in the evening after 20 hrs. One important reason for the increased production of BC aerosols in the evening time is related to road traffic and open burning of solid wastes such as dry leaves and other garbage materials. Apart from waste burning, wood and shrubs are also burnt at night by several people living in slums to keep themselves warm during cold weather. Maxima in BC concentrations between 08-09 hrs is primarily due to morning peak in traffic level and several small scale industrial activities spread around the city. After around 09 hrs, BC concentrations start decreasing because some of the sources such as open burning of wastes are not very much active during this time while boundary layer height of the atmosphere starts rising with increased insolation of the Earth's surface which kicks off convective mixing of air capable of lifting aerosols to higher levels in the atmosphere and causing a dilution of their concentration at the surface level. BC values reach lowest concentrations between 15 – 16 hrs due to minima in traffic levels in the afternoon hours and higher boundary layer height.

5.2.4 Aerosol absorption coefficient

Measurements of BC concentration itself is important over populous and industrial parts of the world because they act as source regions for production of these absorbing species in the atmosphere. However, the parameter required to assess the role of light absorbing particles on the regional and global climate forcing is the absorption coefficient of these aerosols. In the present study, aerosol absorption coefficients were calculated using the raw absorbance data recorded at all the seven wavelength channels of Aethalometer viz. 0.37, 0.47, 0.52, 0.59, 0.66, 0.88 and 0.95 μm . Details on the working principle of Aethalometer and the methodology for the estimation of absorption coefficient of aerosols are mentioned earlier in *Chapter-2*. Knowledge on spectral dependence of aerosol absorption is very useful as it contains certain characteristic features of the sources producing these absorbing particles. This fact is particularly important over the Indian region where contribution of BC from biomass/biofuel burning is as important as fossil fuel combustion and the same amount of BC from biofuel can exhibit stronger absorption characteristics [Venkataraman *et al.*, 2005; Ganguly *et al.*, 2005b]. Wavelength dependence of absorption by aerosols have been investigated using a power law relationship of the form $\beta_{abs}(\lambda) = K \cdot \lambda^{-\alpha}$ where K and α are the absorption Angstrom coefficients and α is a measure of spectral dependence of aerosol absorption [Kirchstetter *et al.*, 2004]. Figure 5.7(b) shows some typical spectra of aerosol absorption coefficient for five representative days of the campaign period viz. 16 (Clear day), 18 (Foggy day), 24 (Foggy day), 26 (Clear day) and 29 December (Hazy day). Absorption coefficients for each day were fitted using power law curves following the earlier relation and α values have been estimated. Values of absorption Angstrom parameter α remained very much steady with only small variations during the campaign period, even under rapidly changing hazy, foggy or clear conditions. Average value of α for the entire period is found to be 1.9 ± 0.1 . This shows that although we observe large spread in the values of absorption coefficient, sources of production for these absorbing particles remained same over the period of our measurement. This fact is also evident from the non-intersecting nature of absorption coefficient curves of Figure 5.7(b) unlike the AOD spectra shown in Figure 5.3(b). Earlier Kirchstetter *et al.* [2004] have reported a stronger spectral dependence in absorption ($\sim \lambda^{-2.5}$) shown by biomass/firewood aerosols from the Southern African Regional Science Initiative (SAFARI) experiment while a much weaker spectral dependence ($\sim \lambda^{-1}$) exhibited by roadway samples from Berkeley consisting of motor ve-

hicle aerosols produced due to fossil fuel burning. It was also shown that the extraction of biomass burning aerosol with acetone, removed significant amount of organic carbon (OC) from the sample, reduced spectral dependency of aerosol absorption and brought down the α value close to 1.2. Other researchers [Jacobson *et al.*, 2000; Bond, 2001; Bergstrom *et al.*, 2002] have also shown that mixture of aerosols in which absorption is mainly due to BC, exhibit a weak spectral dependence (λ^{-1}). Thus wavelength dependency of aerosol absorption obtained during the present study shows signatures of the presence of absorbing aerosols produced from biofuel/biomass burning. This new finding goes against the expected mindset that over Delhi spectral dependency of aerosol absorption is of the type λ^{-1} , since fossil fuel burning is considered to be the principle source of BC over megacities [Gaffney and Marley, 2003; Monkkonen *et al.*, et al. 2004]. Stronger wavelength dependence in the absorption characteristics of aerosols over Delhi occurs due to presence of significantly large proportion of carbonaceous aerosols produced from open burning of dry leaves or other waste materials as well as burning of wood, shrubs etc. Another source of carbonaceous aerosols in Delhi is the usage of biofuel such as wood, cow-dung cakes etc. for cooking by a large population living in slums of the city [Reddy and Venkataraman, 2002]. Also in a recent work Venkataraman *et al.* [2005] have shown that in India about 44% of the total BC emission comes from biofuel combustion. Most of the sources of carbonaceous aerosols discussed so far involve low temperature and incomplete combustion processes which release sufficient amount of organic carbon (OC) apart from soot or BC. Kirchstetter *et al.* [2004] have shown that presence of OC in addition to BC in biomass/biofuel smoke aerosols affect spectral dependence in absorption by aerosols, contributing significantly to the measured light absorption in visible and ultraviolet regions. However, still it is a matter of debate and subject for further investigation whether OC from biomass burning, which is considered to be the scattering component of carbonaceous aerosols [Novakov *et al.*, 2005], itself contributes to absorption in addition to BC or it forms some kind of coated shell around BC aerosols that increases the absorption efficiency of these complex mixtures [Jacobson, 2000; Jacobson, 2001]. Further laboratory experiments under controlled conditions with known aerosol types as well as modelling studies are required to confirm the exact reason which causes the observed increase in spectral dependence of aerosol absorption at places where biomass/biofuel burning are major sources of carbonaceous aerosols in the atmosphere. Nevertheless, such high values of BC concentration over Delhi with increased

absorption efficiency is a matter of concern as it is bound to produce very high values of atmospheric forcing.

5.2.5 Aerosol scattering coefficient

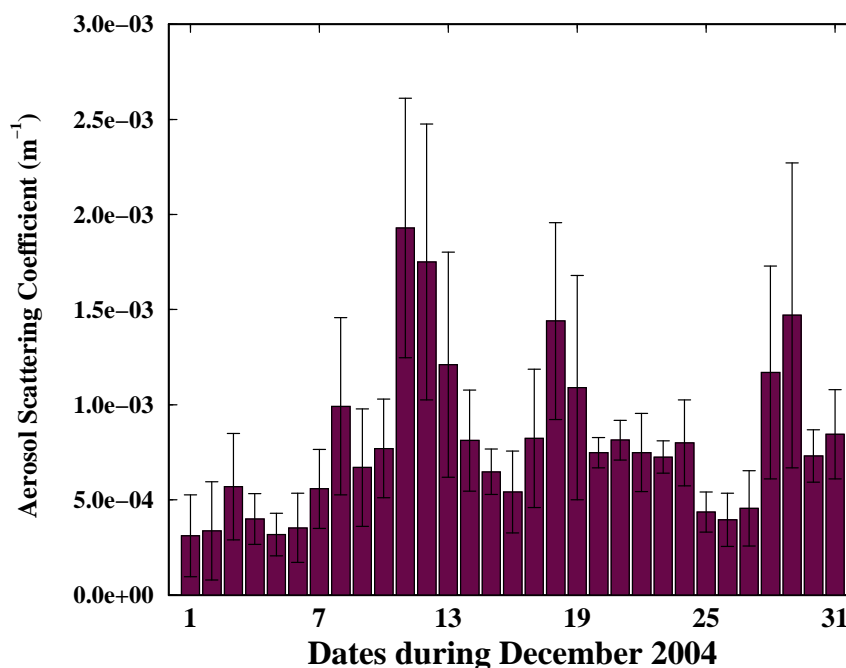


Figure 5.8: Time series of daily mean values of aerosol scattering coefficient at $0.525 \mu\text{m}$, measured over the entire month. Vertical lines in this figure represent $\pm 1 \sigma$ variation about the mean scattering coefficient for each day.

Figure 5.8 shows the time series of daily mean values of aerosol scattering coefficient at $0.525 \mu\text{m}$ measured over the entire month using the Integrating Nephelometer. Vertical lines represent $\pm 1 \sigma$ variation about the mean value for each day. Comparing this plot with Figure 5.4, we find that the day-to-day variation in aerosol scattering coefficient is exactly same as that of aerosol number concentration. Aerosol types which contribute maximum to the scattering coefficient include water-soluble inorganic species such as sulfates, nitrates etc., arising from emissions of SO_2 and NO_x associated mainly with fossil fuel combustion, ammonium from fertilizers and biological sources and some organic aerosols arising from biomass combustion [Charlson *et al.*, 1992; Penner *et al.*, 1994]. In addition to these, nitrates and organic aerosols from industrial emissions also contribute significantly to the scattering characteristics of aerosols. Again, comparing Figures 5.6 and 5.8, we

find a close similarity in the observed variation of BC mass concentration and scattering coefficient. This shows that most of the absorbing and scattering type aerosols had common production source, which is quite possible because during this season major sources of aerosols over Delhi are related with anthropogenic activities such as fossil fuel burning and open burning of dry leaves, garbage etc. during evening and night hours. Like other parameters discussed earlier, high values of aerosol scattering were measured on hazy and foggy days of 8, 11, 18, 29 December, characterized by increased levels of aerosol concentration particularly in the smaller size range. Apart from increased number concentration of aerosols, another reason for obtaining higher values of aerosol scattering on foggy days is due to increase in scattering efficiency of a reasonably large fraction of aerosols experiencing hygroscopic growth under increased relative humidity condition prevailing during foggy conditions [Malm and Day, 2001]. Lower values of aerosol scattering were measured on relatively clear days such as 5, 6, 16 and 26 December when surface level aerosol number distribution also showed lower concentration in almost all size ranges.

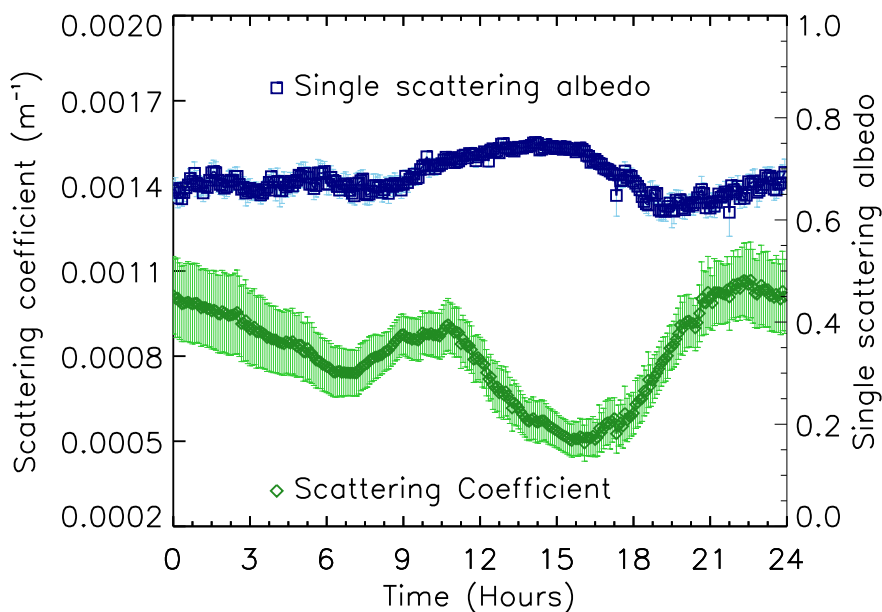


Figure 5.9: Monthly averaged diurnal variation of aerosol scattering coefficient at $0.53 \mu\text{m}$ and single scattering albedo of aerosols at $0.525 \mu\text{m}$. Vertical bars represent $\pm 1\sigma$ variation about the mean value.

Diurnal variation of scattering coefficient showed periods of two maxima and two minima (Figure 5.9). Vertical lines in this figure represents standard error about the mean

value, which is $\pm 1 \sigma / \sqrt{n}$ where n is the total number of measurements made at any particular time during the entire period of campaign. Pattern of diurnal variation in aerosol scattering is almost identical with the variation in number concentration of near surface aerosols [Figure 5.5(a)]. Highest value in scattering coefficient used to occur in the late evening at around 22 hrs. This peak is a result of several contributing factors such as evening peak in traffic level, biomass and wood burning activities going on at several places during late evening hours, increasing trend in relative humidity facilitating hygroscopic growth of aerosols and finally formation of surface based inversion layer inhibiting convecting mixing of air and aerosols present in the atmosphere. However after this time, production of aerosols from many of these sources decreases to a large extent, while their removal from the atmosphere mostly by gravitational settling process remains active. Removal process continues for the whole night and aerosol scattering reaches a local minima around 07 hrs. However after that time, various anthropogenic activities begin and vehicular traffic starts increasing, which releases lot of precursor gases for the production of sub-micron aerosols, causing the scattering coefficient to rise and reach a maxima around 09 hrs. Diurnal variation of aerosol scattering and BC mass concentration match well except that BC mass variation shows a narrow peak in the morning time around 09 hrs whereas scattering coefficient exhibited a relatively flat peak between 09 and 12 hrs. Most of the scattering type aerosols viz. sulfates and nitrates are secondary aerosols formed by gas-to-particle conversion processes and as long as concentration of these gases remain sufficient and other atmospheric conditions remain conducive, their transformation into particles continues. This transformation mechanism is responsible for maintaining the scattering coefficient at high level for some more time even after the peak emission of precursor gases from anthropogenic activities. However with increased insolation, convective mixing of air results in dilution of aerosols near the surface thereby causing the scattering coefficient to decrease and reach lowest value of the day at around 16 hrs. Once again under favorable conditions such as increasing relative humidity, collapsing boundary layer and increased production of aerosols in the evening hours, scattering coefficient of aerosols start rising to reach the evening maxima.

5.2.6 Single scattering albedo

Since absorbing and scattering type of aerosols are together present in the atmosphere, their ultimate effect in terms of cooling or warming of the atmosphere depends on the single scattering albedo (ω) of the mixture of aerosols. Single scattering albedo is the ratio of scattering to extinction coefficient of aerosols and its magnitude is considered as an index for the relative dominance of scattering with respect to absorbing type of aerosols. Single scattering albedo can range from 0 (purely absorbing) to 1 (purely scattering). Exact knowledge of single scattering albedo is very crucial as small error in its magnitude can produce large difference in the estimated values of aerosol radiative forcing [Takemura *et al.*, 2002]. Ganguly *et al.* [2005a] have shown that for the same aerosol optical depth (AOD) and mass loading over Bay of Bengal, atmospheric forcing by aerosols is very sensitive to ω . Over land areas knowledge of ω is even more critical and any small change in its value can have large impact resulting from flux changes within and below the aerosol layer such as differential heating rates, changes in atmospheric stability and even cloud formation [Ackerman *et al.*, 2000; Russell *et al.*, 2002]. Also, satellite retrieval of aerosol optical depth (AOD) intricately depends on the assumption of ω in the aerosol model for any study region [Ignatov *et al.*, 1995; Stowe *et al.*, 1997]. Although there are some reports on measurement of BC mass concentration over the Indian mainland [Babu *et al.*, 2002; Venkataraman *et al.*, 2002; Tripathy *et al.*, 2005; Latha and Badrinath, 2005], measurement of single scattering albedo is almost nil, except during a field campaign over central India [Ganguly *et al.*, 2005c].

In the present study, single scattering albedo of aerosols are estimated by taking the ratio of scattering coefficient measured at $0.53 \mu\text{m}$ using Nephelometer and its sum with the absorption coefficient at $0.52 \mu\text{m}$ measured using Aethalometer. Although there is a difference of $0.01 \mu\text{m}$ between the wavelengths of absorption and scattering coefficient measurements, our error analysis shows that the error in ω due to this difference will be less than 1% even in extreme cases. Measured values of scattering coefficient are associated with some angular truncation loss which is an inherent and unavoidable problem for all Nephelometers [Heintzenberg and Charlson, 1996]. Detailed Mie theory calculation using the simultaneously measured aerosol size distribution shows that an angular truncation of 8° each in the forward and backward direction could result in an underestimation of scattering coefficient by about 15%. This will cause a 3% error in the estimated values of ω

which is ultimately used for the radiative transfer calculations described later in Chapter-6. Similarly a maximum error of 10% in the estimation of absorption coefficient using Aethalometer causes about 2% error in the ω value. Taking into account all possible sources of error, overall uncertainty in the estimated value of ω during the present study is around 6%. Nevertheless, in the estimation of aerosol radiative forcing, discussed in Chapter-6, the daily average ω is used which has a spread of about 15%.

During the present study, ω at $0.525 \mu\text{m}$ is found to vary between 0.6 and 0.8 with an average value close to 0.68 for the entire period of campaign. Comparing results from this campaign with previously published values of single scattering albedo for other regions [Anderson *et al.*, 1999; Jayaraman *et al.*, 2001a; Russel *et al.*, 2002, Bergstrom *et al.*, 2003; Han *et al.*, 2003; Qiu *et al.*, 2004], we find that ω values estimated during the present campaign are much lower due to dominance of absorbing aerosols like BC over the study region. Babu *et al.* [2002] estimated ω ($0.5 \mu\text{m}$) for Bangalore (13°N , 77°E) based on measurements of BC mass fraction and using the OPAC model developed by Hess *et al.* [1998] to be around 0.73. Following the same method Singh *et al.* [2005] and Tripathy *et al.* [2005] reported ω ($0.5 \mu\text{m}$) value for Delhi and Kanpur to be 0.67 and 0.76 respectively. Here we must mention that although ω value reported by Singh *et al.* [2005] matches very well with the average value of this parameter measured during the present study, aerosol types and their concentration contributing towards this value of ω could be quite different as the period of these two studies are not the same. By inverting sun/sky radiometer data, Pandithurai *et al.* [2004] estimated ω ($0.5 \mu\text{m}$) value for Pune (18.53°N , 73.85°E) to be around 0.81. Unlike previous examples, Ramana *et al.* [2004] estimated ω ($0.5 \mu\text{m}$) value for Kathmandu (27.67°N , 85.31°E) to be in the range of 0.7-0.9, combining the actual measurements of scattering and absorption coefficient using a Nephelometer and a Particle Soot Absorption Photometer (PSAP). Similar to present study, Ganguly *et al.* [2005c] reported the single scattering albedo ($0.525 \mu\text{m}$) values estimated using simultaneously operated Nephelometer and Aethalometer measuring scattering and absorption coefficient of aerosols respectively for different locations (mostly rural) over the central Indian region to be in the range of 0.75 – 0.90.

Mean values of ω ($0.525 \mu\text{m}$) measured at Delhi under ambient conditions during the entire month are shown in Figure 5.9 as a function of time of the day. No strong diurnal pattern in the variation of single scattering albedo is observed except for slightly higher

values of ω during afternoon hours. Since single scattering albedo represents the combined property of scattering and absorption, the diurnal variation is determined by the contemporary behavior of scattering and absorbing type of aerosols. We find that ω values start rising very slowly just after 09 hrs which corresponds to the morning peak in BC concentration [Figure 5.7(a)] and also start time for the flat maxima in scattering coefficient. However after this time, BC concentration and hence absorption coefficient start decreasing while scattering coefficient values are maintained at higher level for some more time and starts decreasing only after about 11 hrs or so. While BC aerosols from vehicular exhausts are released directly as particles, most of the scattering type aerosols viz. sulfates and nitrates are secondary aerosols formed by gas-to-particle conversion processes and as long as concentration of these gases remain sufficient and other conditions remain conducive in the atmosphere, their transformation into particles continues. This phenomenon actually widens the gap between scattering and absorption coefficient, with first parameter showing somewhat stable behavior for some time while the second one decreases, causing an increasing trend in ω . Exactly opposite behavior is observed after around 15 hrs when traffic level starts rising along with increase in other types of burning activities causing BC mass and absorption coefficient values to increase in response to the increased production of aerosols from these sources. Although scattering coefficient increases after 15 hrs, a faster increase shown by BC aerosols cause ω value to decrease up to a time when both scattering and absorption coefficient values reach a more or less steady state after around 20 hrs.

5.2.7 Aerosol vertical profiles

For the first time, vertical profile of aerosol extinction coefficients are measured over Delhi. Micro Pulse Lidar (MPL) observations were carried out for almost 24 hours in a day and for the whole month with some breaks on clear days around noontime to avoid direct sunlight being incident on the telescope. Differences in vertical distribution of aerosols are seen at different times of a day as well as on different types of days. Figure 5.10 shows 24-hour averaged aerosol extinction profiles for three different days, each one being representative for either clear, hazy or foggy day. Since MPL signals were averaged and stored at 1 minute interval, each profile shown in figure 5.10 is an average of nearly 1440 individual profiles. The inset in figure 5.10 shows a magnified view of these extinction profiles be-

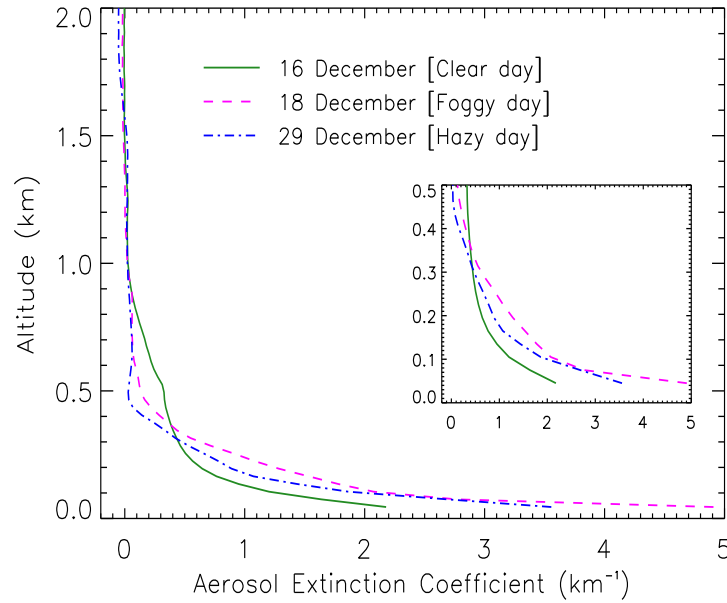


Figure 5.10: 24-hour averaged aerosol extinction profiles for three different days, each one being representative of either clear, hazy or foggy day.

low 0.5 km altitude. Major differences in vertical distribution of aerosols are seen in lower altitudes. We find that extinction coefficients below 0.2 km are almost two to three times higher on foggy days compared to their value on clear days. All profiles show a sharp decrease in extinction values from surface to nearly 0.2 km. On hazy and foggy days, aerosol extinction becomes almost negligible above 0.5 km from ground level while on clear days it asymptotically approaches zero value above this height. Due to presence of a strong inversion close to Earth's surface, lasting for nearly 15 hours or even longer time in a day, all locally produced aerosols remain trapped within this surface layer, causing higher values of extinction at lower heights. Extinction coefficients from MPL observations exhibit similar behavior as seen in other surface measurements discussed earlier. Also, extinction values at lower heights are lesser on clear days, while their corresponding values at higher altitudes are larger than observed on hazy or foggy days. Extinction coefficients on clear days show opposite trend above and below 0.3 km relative to their values on hazy or foggy days. Also, we find that aerosol extinction values at almost all altitudes are only slightly higher on foggy days compared to those on hazy days. This happens because before the onset of fog, we find very little difference between hazy and foggy day in terms of aerosol

concentration and only slightly higher relative humidity condition turns a hazy day into a foggy day. Most of the foggy mornings were preceded by hazy conditions in the evening hours on previous day. Thus compared to a hazy day, higher values of aerosol extinction observed on foggy days is primarily due to increased absorption and scattering efficiency of numerous aerosols present at all these altitudes undergoing hygroscopic growth due to higher relative humidity.

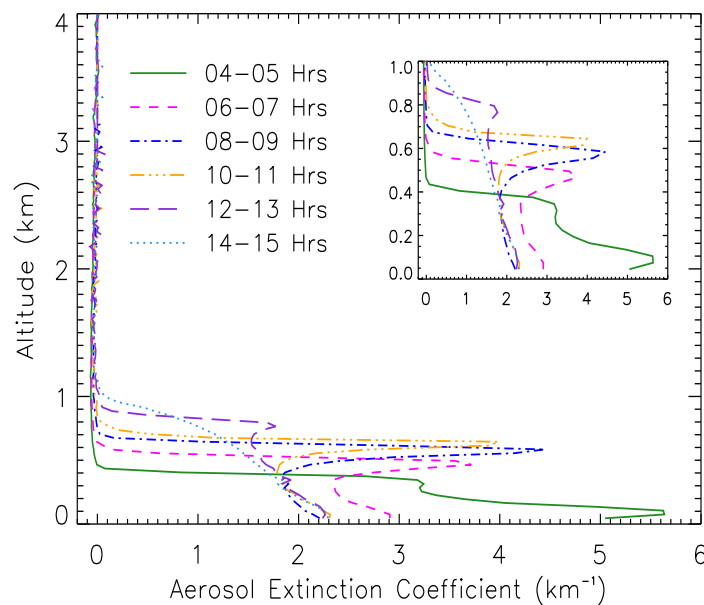


Figure 5.11: Sequence of changes observed in hourly mean extinction profiles from 04 hrs to 15 hrs obtained on 23 December 2004. The pattern of variation shows redistribution of aerosols with altitude where aerosols from lower levels get lifted to form an aerosol layer at an elevated altitude.

The only other measurement of vertical distribution of aerosols from North Indian region were made by *Ramana et al.* [2004] during a field campaign at Kathmandu ($27.67^{\circ}N$, $85.31^{\circ}E$, 1.35 km above msl), in winter 2003. Most striking difference between the extinction profiles reported by *Ramana et al.* [2004] and those observed during the present study is seen at lower altitudes below 0.5 km where we find that aerosol extinction values measured over Delhi are almost an order of magnitude higher than those from Kathmandu. Also, unlike the occurrence of a second peak in extinction coefficient at a height of around 1.3 km as observed by *Ramana et al.* [2004], in most of the cases we find extinction values decreasing almost monotonically with increase in altitude. However, from 22-24 December, when

high values of AOD are observed during daytime, most of the other parameters measured at surface level did not show a corresponding increase in their values. Figure 5.11 shows the sequence of changes observed in hourly mean extinction profiles between 04 and 15 hrs obtained on 23 December. The pattern of variation suggests a kind of redistribution of aerosols occurring in the atmosphere. Early morning (before sunrise) profiles for this day are similar to those observed under foggy conditions, suggesting that there might have been a fog like condition around that time. However, due to increased insolation after sunrise, surface based inversion becomes weak, which then triggers convective process and aerosols from surface level are lifted to higher altitudes. At this time, we observe a decrease in extinction values near the surface but the corresponding values keep rising at higher altitudes. However unlike other days, horizontal wind speed at these altitudes (above 0.4 km) was very weak during this period. This prevented a regular ventilation of aerosols from these altitudes to surrounding places beyond city limits. Thus although vertical transport of aerosols from surface level continued in a regular manner due to convective lifting, lower horizontal wind caused stacking of aerosols at elevated altitudes and resulted in an anvil shaped distribution of aerosols in the atmosphere. As time progressed, due to continued convective pressure from below, this elevated aerosol layer is slowly pushed upwards. And after sufficiently long time, as shown by the mean profile of 14 – 15 hrs, this layer vanishes and aerosols are distributed in the atmosphere in a monotonically decreasing fashion. Gravitational settling of aerosols being the only active mechanism for removal of aerosols in absence of regular transport and dispersal of aerosols occurring at higher levels, extinction coefficients remain significant upto 1 km unlike other days when the contribution of aerosol extinction becomes practically negligible above 0.6 km.

All measured parameters have been used to make estimates of aerosol radiative forcing for the region, details of which are presented and discussed in *Chapter-6*.

5.3 Alterations in aerosol properties during a fog episode

Continuous measurements were made throughout the month of December 2004 at New Delhi, when we encountered an intense fog event on 18 December followed by a very hazy and misty day on 19 December. Formation of dense fog in the morning hours of 18 December was triggered by conditions which became favorable just after the sunset hours

on previous day evening. Rapid infra red cooling of the earth surface helped in cooling the surface atmospheric layer from below and calm wind conditions prevented mixing of this shallow layer of cool and heavy air. Figure 5.12(a) shows the NCEP reanalyzed vertical wind speed data from surface to 500 mbar pressure level on all days in December 2004. A sudden anticyclonic movement of air created the much needed condition for the fog event to trigger in the early hours of December 18 by suppressing the surface level winds and drying the air aloft through subsidence and facilitating radiative cooling at the surface. During the winter season, North India is affected by the western disturbances which are a series of alternate low and high pressure belts moving from west to east and leading to intense fog events in this region [Pasricha *et al.*, 2003]. Among other factors which favored the occurrence of this fog event is the presence of large concentration of aerosols in the atmosphere together with high relative humidity which helped in bringing the dew point temperature close to the ambient air temperature. Relative humidity values were maintained above the 80% mark for nearly 12 Hrs, starting prior to midnight on 17 December and continuing almost up to local noon on 18 December [Figure 5.12(b)].

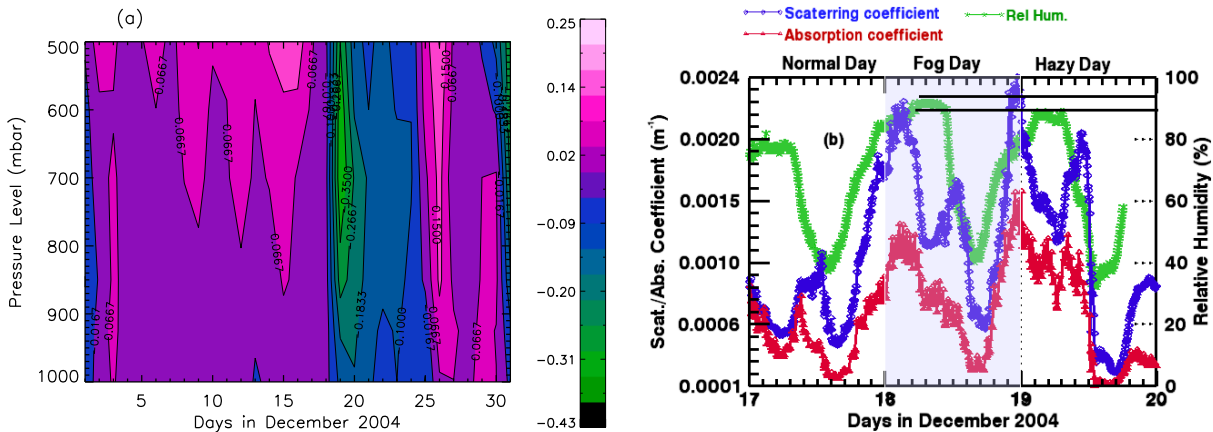


Figure 5.12: (a) Distribution NCEP reanalysis data on vertical wind speed from surface to 500 mbar pressure level on all days in December 2004. (b) Temporal variation of scattering and absorption coefficients of aerosols together with ambient relative humidity measured during the fog event and for comparison, data for previous day and one day after the fog event are also shown.

Figure 5.12(b) shows the temporal variation of the scattering and absorption coefficients (β_{sca} , β_{abs}) of aerosols measured during the fog event and for comparison, data for previous day and one day after the fog event are also shown. Just as any other day, both β_{sca} and β_{abs} started increasing in the afternoon hours of 17 December, however the build

up of aerosols was very rapid on this day and continued almost up to 2 a.m. in the night when both parameters reached maxima nearly twice in magnitude compared to their corresponding values around the same time on earlier days. This augmentation in β_{sca} values is due to combined effect of a collapsing boundary layer and increase in scattering efficiency of a reasonably large fraction of aerosols experiencing hygroscopic growth under increased relative humidity conditions. Previously, *Malm and Day* [2001] reported the values of aerosol scattering as a function of RH in terms of $f(RH) = b_{scat}(RH)/b_{scat,dry}$, where $b_{scat}(RH)$ is the scattering coefficient at relative humidity equal to RH and $b_{scat,dry}$ is the scattering coefficient at $RH < 20\%$. They found $f(RH)$ to vary between 1.53 – 2.75 at Great Smoky in Tennessee and between 1 – 4 at Grand Canyon in Arizona. Most of the inorganic species such as sulfates and nitrates which constitute a major fraction of the ambient aerosol are hygroscopic in nature and exhibit the property of deliquescence under humid conditions [*Tang and Munkelwitz, 1993; Tang, 1996*]. *Tang, [1996]* has shown that there occurs a spontaneous phase transition from solid particles to saline droplets and an associated increase in their scattering efficiency at the deliquescence point when RH value crosses a threshold level, specific to the chemical composition of the aerosols. While increase in b_{scat} with increase in RH is expected, exact quantitative details were not available for Delhi. It is interesting to observe an increase in b_{abs} with increase in RH. This observation is particularly important from the point of view of estimation of single scattering albedo at ambient conditions which are often based on absorption measurements at low RH ($< 30\%$) conditions with the assumption that aerosol absorption does not change with humidification and result in an overestimation of ω [*Redemann et al., 2001*]. In fact our observations show a gradual decrease in ω value during the fog episode with increase in absorption capability of the distribution of particles in the ambient atmosphere which later helps in a rather rapid dissipation of the fog layer with increased insolation. Using a core-shell model with the core being soot and the shell made up of hygroscopic species such as sulfates, *Redemann et al., [2001]* have shown that for a monomodal aerosol distribution, RH enhancement factors can reach upto 1.35 for RH greater than 90%. In a more recent study, *Nessler et al. [2005]* have shown using concentric core/coating particle model applied on particles representative of the alpine station Jungfraujoch that RH enhancement factors of absorption by aerosols could vary anywhere between 0.84 to 1.78.

Although β_{sca} and β_{abs} both exhibited rapid increase in the evening of 18 December,

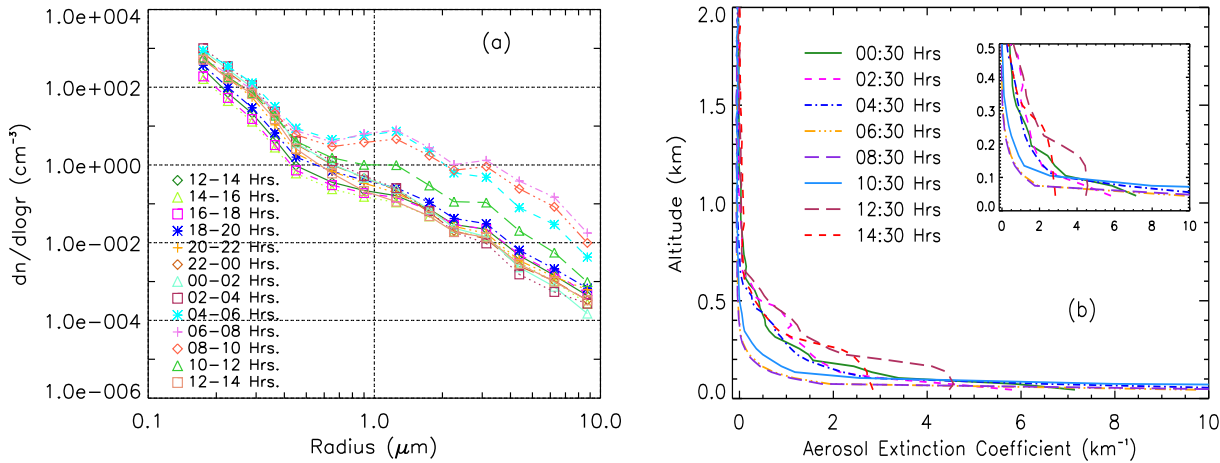


Figure 5.13: (a) Evolution of number size distribution of aerosols through the formation and dissipation of the fog layer on 18 December. (b) Hourly mean aerosol extinction profiles for 18 December, depicting the sequence of changes observed in the structure of lower atmosphere from a time just before onset of fog, continuing through the fog time and till it dissipates.

reaching much higher values compared to a normal day, accompanying drop in air temperature and increase in RH was just not sufficient to trigger a fog event and resulted in hazy conditions with poor visibility on 19 December. While scattering and absorption characteristics of aerosols were similar on 18 and 19 December [Figure 5.12(a)], we have observed distinctly different features in the size distribution of aerosols measured on foggy, hazy and normal days [Ganguly *et al.*, 2006]. Figure 5.13(a) shows the evolution of number-size distribution of aerosols through the formation and dissipation of the fog layer on 18 December. Although the fog event was marked by increase in number concentration of aerosols of all size ranges, it was more pronounced for particles of size larger than 1 μm . Effective radius for the distribution of aerosols, estimated by taking the ratio of total volume to the surface area distribution of the particles, showed a sharp rise in its value marking the onset of fog formation at around 05 hrs, with a rapid increase in the number of larger particles with respect to smaller ones [Figure 5.14(a)]. Actually the growth of fog droplets is governed by *Köhler* equation describing the equilibrium state for individual droplets as a function of supersaturation level and droplet diameter [Seinfeld and Pandis, 1998]. If the supersaturation level or relative humidity exceeds a critical value, droplet undergoes an activation when it is no longer in an equilibrium state and grows indefinitely by

condensation of more and more water vapor onto it. The critical relative humidity and also the critical diameter for the activation of droplet depends very specifically on the size and chemical composition of individual particles which later turn into droplets [Svenningsson *et al.*, 1997]. Effective radii for the distribution of aerosol showed similar asymptotically decreasing trend from the previous day evening to around 05 hrs on both 18 and 19 December [Figure 5.14(a)]. However after this time, a slight increase in RH on 18 December [Figure 5.12(b)] caused activation of droplets and resulted in fog formation on 18 while 19 remained hazy. Also, since only a small fraction of nucleation particles got activated, the observed increase in number concentration of larger sized particles was not accompanied by any detectable decrease in the concentration of smaller size particles.

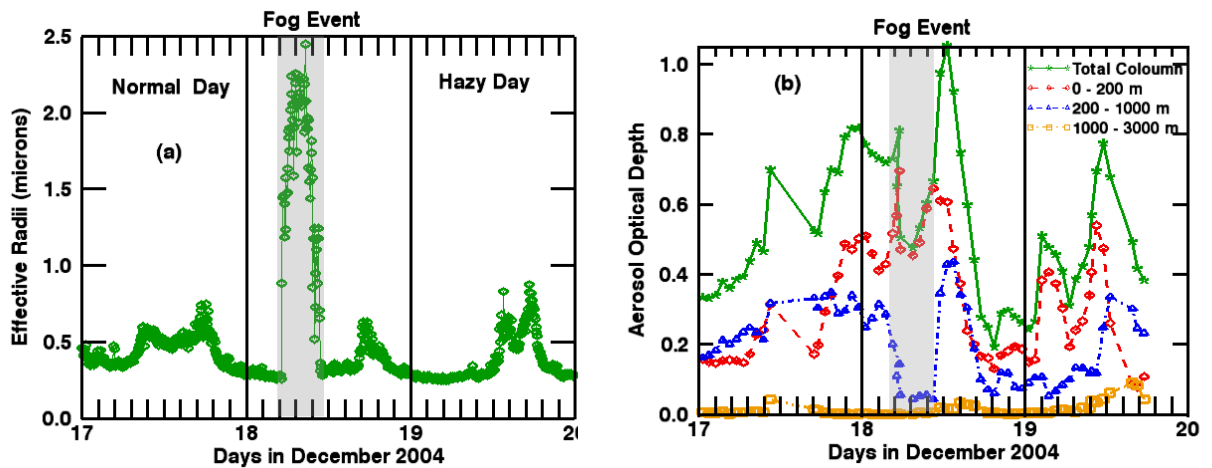


Figure 5.14: (a) Time series of effective radius for the distribution of aerosols showing a sharp peak in its value and marking the onset of fog at around 05 hrs which lasted almost upto 11 hrs on 18 December 2004. (b) Time series of hourly averaged aerosol optical depths estimated by integrating the aerosol extinction profiles for different atmospheric layers.

Figure 5.13(b) shows the hourly mean aerosol extinction profiles obtained from Lidar measurements on 18 December, depicting the sequence of changes observed in the structure of lower atmosphere from a time just before onset of fog, continuing through the fog time and till it dissipates. Since the fog formation is initiated by cooling of the surface layer from below, fog droplets are also formed first near the ground and the process builds up rapidly in vertical direction. As a result during the initial phase of fog formation, extinction values at lower altitude start increasing first as shown by the profiles of 00 : 30 and 02 : 30 hrs. Within a short time there was a large increase in the extinction values at lower altitude

marking the development of dense fog building up from the surface. As time progressed, fog intensified at lower levels and there was a total collapse in the vertical distribution of aerosols with all of them getting accommodated in an extremely dense and shallow atmospheric layer of merely 200 m height from the surface. The situation worsened further after around 09 : 00 hrs when city life starts even under foggy condition with traffic level increasing on roads. Exhausts from these vehicles added to the already high aerosol levels in the atmosphere in the form of fog droplets. This caused the extinction values at lower levels to increase further as evident from the profile of 10 : 30 hrs and the fog turns into a smog (smoke + fog) with further reduction in visibility. However, this situation could not continue for long time as the Solar radiation heated up the Earth's surface and led to the dissipation of fog. Soon after the fog dissipation, a large drop in the extinction values is observed at lower altitudes along with increase in the extinction values at slightly higher altitude. Figure 5.14(b) shows the time series of hourly averaged aerosol optical depths estimated by integrating the aerosol extinction coefficients derived from the Lidar data for three different layers and also for the total atmospheric column. It shows almost a collapse in the vertical distribution of aerosols during the fog event and their subsequent re-distribution with the breakdown of temperature inversion at the top of boundary layer, facilitating dispersal of aerosols from surface to higher altitudes during the dissipation of fog.

Implications of the occurrence of such fog episodes on the regional level aerosol radiative forcing are discussed separately in the *Chapter-6*.

5.4 Summary

Results from complementary measurements of optical and physical parameters of aerosols made at the urban megacity New Delhi, during a period characterized by intermittent foggy, hazy and clear sky conditions in December 2004 are presented. Important aerosol parameters measured during this campaign include: column AOD spectra, wavelength dependent aerosol absorption, aerosol scattering coefficient, single scattering albedo, number size distribution and vertical profile of aerosols. Most of the parameters showed large variability over the campaign period with their values being particularly higher during hazy and foggy periods. Average AOD value at $0.5 \mu m$ is found to be 0.91 ± 0.48 . In-

crease in AOD on hazy and foggy days are found spectrally non-uniform with percentage increase in AOD at shorter wavelengths being higher on hazy days compared to clear days. Although foggy days were marked with increased concentration of aerosols of all size ranges, the addition was more pronounced in case of coarse particles of size greater than $1 \mu\text{m}$. In general surface level aerosol parameters showed good correlation with column integrated properties. However, unusually high values of AOD with considerably lower concentration of near surface aerosols during a special event revealed the presence of aerosol layer present at an elevated altitude. During the campaign, diurnally averaged values of BC mass concentration varied between a low value of $15 \mu\text{g}/\text{m}^3$ measured on clear days to a high value close to $65 \mu\text{g}/\text{m}^3$ on hazy days. Wavelength dependence of aerosol absorption shows signatures of the presence of absorbing aerosols produced from biofuel/biomass burning. Single scattering albedo at $0.525 \mu\text{m}$ is found to vary between 0.6 and 0.8 with an average value of 0.68 for the entire period of measurement. Our results show that carbonaceous aerosols over Delhi has its source from both fossil fuel and biomass burning activities. A sudden anticyclonic movement of air created the much needed condition for the fog event to trigger in the early hours of December 18, 2004. Both scattering and absorption coefficient of aerosols exhibited nearly two fold increase during the fog episode. While scattering and absorption characteristics of aerosols were not much different on the 18 and 19 December, slightly higher relative humidity helped in the activation of droplets and resulted in fog formation on the first day while it remained hazy on the second day. LIDAR observations during the fog event reveal a total collapse of the vertical distribution of aerosols in an extremely dense and shallow atmospheric layer of merely 200 m height from the surface.

Model estimates of aerosol radiative forcing and its sensitivity to various parameters

Atmospheric aerosols from both natural and anthropogenic sources directly affect the radiative balance of the Earth-atmosphere system by scattering and absorbing the incoming Solar and outgoing terrestrial radiation besides producing other indirect effects such as modifying the cloud properties etc. [IPCC, 2001 and references therein]. Actual implications of diverse aerosol types in terms of their potential ability to perturb the radiative balance of the Earth-Atmosphere system are quantified in terms of model estimates of aerosol radiative forcing [Ramaswamy *et al.*, 2001]. Variations in aerosol composition affect climate through variations in the abundance and distribution of these radiatively active species which alter the energy balance of the Earth-Atmosphere system at various levels in the atmosphere. Different aerosols interact with radiation in different ways, eg. soot is highly absorbing while sulfate is highly scattering, however their combined impact on global climate need not be additive because of inhomogeneity in the distribution of different aerosol types over both space and time, differences in their mixing states, differences in albedo of the underlying surface, differences in the vertical distribution of aerosols in the atmosphere and several other factors [Haywood and Ramaswamy, 1998; Haywood and Boucher, 2000; Jacobson, 2001; Ramaswamy *et al.*, 2001; Chung *et al.*, 2005].

However, robustness of these model evaluations demand comparison with long-term measurements of various aerosol parameters from various stations spread all across the globe. It is necessary that observations and modelling studies should complement each

other for further improvement in our understanding of climate change occurring in recent times (post-industrial period) and help reducing uncertainties involved in future projections of how aerosols influence climate.

In order to understand the implications of the observed variabilities in aerosol parameters measured over our study locations in terms of perturbation created to the radiative balance of the Earth-Atmosphere system, we used the measured aerosol parameters as input in a radiative transfer model and estimated the aerosol radiative forcing for each of these locations. We have also carried out further studies to see the sensitivity of various parameters used as input for model estimates of aerosol direct radiative forcing over our study region. This chapter first describes the basic methodology and approach for the estimation of aerosol radiative forcing over the region. A brief description of the radiative transfer model used in the present study along with necessary inputs required for running the model are presented. This is followed by separate discussions on important results from model estimates of aerosol radiative forcing carried out over different study locations presented in earlier chapters. We also present results from some of the sensitivity tests carried out for each of these studies.

6.1 Methodology and Approach

In our study, we have used the radiation code SBDART (Santa Barbara DISORT Atmospheric Radiative Transfer), developed by *Ricchiazzi et al.* [1998] to perform the radiative transfer calculations in the SW (Short Wave, $0.25 - 4.0 \mu m$) and LW (Long Wave, $4.0 - 40.0 \mu m$) regions. SBDART is a radiative transfer model which computes plane-parallel radiative transfer both in clear and cloudy sky conditions within the Earth's atmosphere and at the surface. However, in the present study, radiative transfer computations are performed only for clear sky conditions. The model is well suited for a wide variety of problems in atmospheric radiative energy balance and remote sensing studies. For molecular absorption part, SBDART uses the low-resolution band models of *LOWTRAN - 7* atmospheric transmission code. These band models take into account the effects of all radiatively active molecular species found in the Earth's atmosphere and has wavelength resolution of about 5 nm in the visible and about 200 nm in the thermal infrared. Radiative transfer equations are numerically integrated using DISORT (Discrete Ordinate Radiative Transfer) module

developed by *Stamnes et al.* [1988]. The intensity of both scattered and thermally emitted radiations can be computed at different heights and directions. Presently, SBDART is configured to allow up to 65 atmospheric layers and 40 radiation streams (40 zenith angles and 40 azimuthal modes). For our study over Ahmedabad, we have used 65 atmospheric layers with 0.25 km resolution in the lower troposphere and eight radiation streams (to save computational time at the cost of very small difference in accuracy) in the radiative transfer calculations.

The main input parameters required for DISORT module include spectral values of solar radiation incident at the top of the atmosphere, aerosol optical depths, single scattering albedo (ω) and asymmetry parameter (g) of the aerosol distribution. In the present work, we have followed two different approaches to generate the spectral values of various aerosol parameters which are used as input for the radiative transfer calculations. In the first method (method-1), we have used the OPAC (Optical Properties of Aerosols and Clouds) model developed by *Hess et al.* [1998], to make estimates of aerosol components which possibly contributed towards the measured properties of aerosols over the study location. OPAC model provides optical properties of various atmospheric particulate matter in the solar and terrestrial spectral range (0.25 to 40 μm). This model consists of ten major aerosol components viz. insoluble, water soluble (including sulfate), soot, mineral dust (coarse, accumulation and nucleation), mineral-transported, sea salt (coarse and accumulation) and sulfate droplets. Using different combinations of these aerosol components, ten different aerosol types are defined viz. continental clean, continental average, continental polluted, urban, desert, maritime clean, maritime polluted, maritime tropical, Arctic and Antarctic. Each of these aerosol types are representative of climatologically different environments. In addition to this, OPAC model also allows users to define new mixtures out of given aerosol components to best fit the observations and to derive different microphysical and optical properties, such as aerosol optical depths, scattering and extinction coefficients, single scattering albedo, asymmetry factor etc. for the prescribed combination. As some of the aerosol components are able to uptake water from the atmosphere under favorable conditions, which may in turn change their optical properties, OPAC outputs are available for eight different relative humidity (0%, 50%, 70%, 80%, 90%, 95%, 98% and 99%) conditions.

In method-1, we first select a suitable aerosol model appropriate for the study location

and use different combinations of aerosol components from that model such as sulfates, nitrates, water soluble constituents, organics, soot, sea salts, mineral dusts etc. to best fit the AOD spectrum observed over the study region. These aerosols are assumed to be distributed in the atmosphere according to certain scale height applicable for the study location. Output parameters from the model are derived for the nearest relative humidity conditions available in OPAC. Model derived optical parameters are obtained by varying the number concentration of individual components in small steps until maximum of the following criteria are satisfied. (1) Angstrom parameter α for the observed and the model estimated AOD spectra are consistent with each other. (2) Sum of root mean square difference between model estimated and observed AOD values at all the six wavelength channels of Microtops is minimum (for the present study, we have constrained this sum within 0.1 AOD). (3) Total mass for the model estimated aerosol mixture is comparable with aerosol mass concentration measured using QCM (Quartz Crystal Microbalance) impactor. (4) BC mass used in the model is almost the same as its measured value using Aethalometer (5) Mass fraction of BC in the total aerosol mass are also constrained close to their actual values derived from simultaneous and co-located measurements using Aethalometer and QCM impactor. (6) Model derived values of single scattering albedo at 500 nm closely matches with ω at $0.525 \mu m$ estimated using simultaneous measurements of absorption and scattering coefficient of aerosols. Figure 6.1(a) shows a comparison of aerosol mass measured using QCM impactor during four year study over Ahmedabad and the total mass for all the components estimated using OPAC model. From the same study, figure 6.1(b) shows the comparison between single scattering albedo of aerosols estimated from simultaneous measurements of their absorption and scattering coefficients using Aethalometer and Nephelometer respectively and the model derived values of ω at $0.5 \mu m$. However, there have been situations when we could not find any suitable combination of aerosol components which satisfied all the above criteria. For our study over Ahmedabad, such conditions mostly appeared during Pre-Monsoon and Monsoon seasons. This happens mostly due to presence of elevated aerosol layers above the atmospheric boundary layer. We have detected presence of such layers at altitudes above ~ 2 km using simultaneously operated Micro Pulse Lidar (MPL) system from our study location. Such elevated layers form when aerosols from neighboring land regions are lifted to higher altitudes by convective processes and then get transported to much longer distances

in the free troposphere. In most of the cases, such layers are constituted by mineral dust aerosols originating from arid and semiarid regions. During our study, we have seen that on many of the days, air parcels reaching our measurement location at higher altitudes, cross large portions of arid and semiarid regions of north Africa, west Asia and western India [Figure 2.6(a)]. Thus probability of any such transported mineral dust layer being present above the atmospheric boundary layer can not be ruled out. Also, we find that incorporation of such mineral transported aerosol layer in the OPAC model, whenever necessary, with typical number concentrations up to 10 particles cm^{-3} at altitude levels between 2 and 4 km better fits the observed AOD spectra.

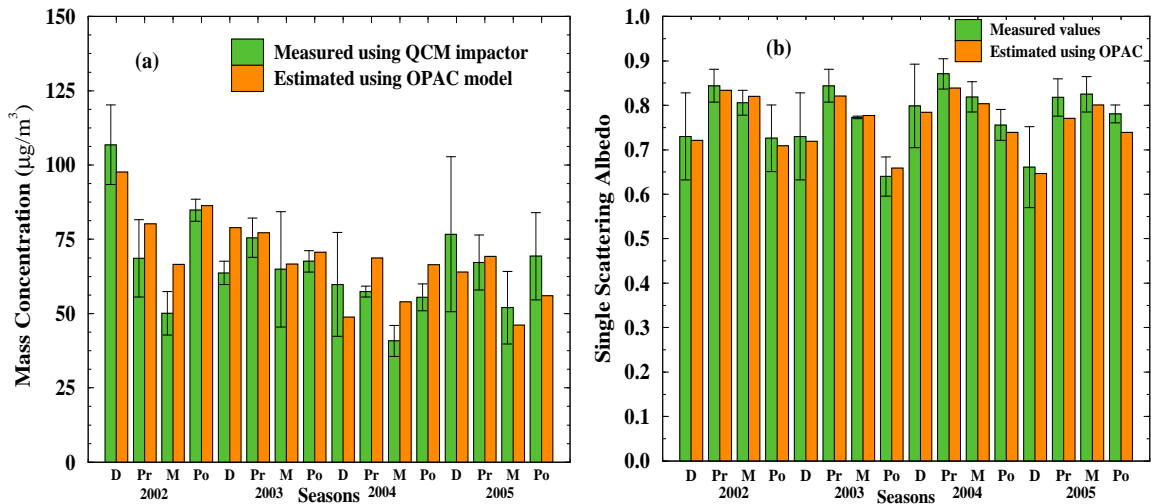


Figure 6.1: (a) Comparison of aerosol mass measured using QCM impactor and total mass for all aerosol components estimated using the OPAC model. (b) Comparison of measured values of ω at $0.525 \mu m$ with the values of ω at $0.5 \mu m$, estimated using OPAC model.

The second method (method-2) is more straight forward in the sense that it avoids the iterative method of best fitting the observations using OPAC model to derive the basic inputs required for the radiative transfer calculations. Instead, in method-2, simultaneously measured AOD values at six wavelength channels ($0.38, 0.44, 0.5, 0.675$ and $0.87 \mu m$) of Microtops sun-photometer are first used to calculate the Angstrom parameters α and β for the AOD spectrum. These parameters are then used to generate AOD values for the entire SW region using the well known Angstrom relation ($\tau = \beta\lambda^{-\alpha}$, where τ is the AOD at wavelength λ). Next, in the absence of spectral dependent values of single scattering albedo (ω), we performed theoretical estimation of ω for suitable aerosol models like conti-

mental clean, continental average, continental polluted, marine [d'Almeida, 1991] etc. using software package OPAC, based on measured ω at $0.525 \mu\text{m}$ and Angstrom parameters. The spectrum of ω for the chosen aerosol model is multiplied by a suitable scaling factor in such a way that the model derived single scattering albedo matches with ω at $0.525 \mu\text{m}$ estimated using simultaneous measurements of absorption and scattering coefficient of aerosols. Figure 6.2(a) shows a comparison of spectral ω values derived for the Dry season in 2004, using both the methods. For further comparison, this figure also shows the spectral ω values for the continental polluted aerosol type of OPAC model. We find aerosols over Ahmedabad to be more of continental polluted type. In method-2, asymmetry parameter required for the radiative forcing calculations are computed using Mie theory [Bohren and Hoffman, 1983] for the measured aerosol size distribution. For the calculation of asymmetry parameter, we have used a weighted refractive index for the aerosols assuming them to be an internal mixture of various components present in the model atmosphere appropriate for the study location. Weighted refractive index for the mixture of aerosols at a particular wavelength is estimated by summing products of mass mixing ratios and the refractive index for individual components at that particular wavelength [d'Almeida *et al.*, 1991; Hess *et al.*, 1998]. Figure 6.2(b) shows two sets of asymmetry parameter values corresponding to station-9 of our study over central India being compared with the asymmetry parameter values for some of the standard aerosol models prescribed in OPAC.

Thus both methods of deriving aerosol related input parameters for the radiative transfer calculations are different from each other and each approach involves different assumptions and approximations of its own. However, it will be shown later in this chapter that in spite of taking two different approaches for generating the basic aerosol parameters, estimated values of aerosol radiative forcing are comparable. Previously, there are quite a few reports on estimation of aerosol radiative forcing over selected locations in the Indian sub-continent as well its surrounding ocean regions [Babu *et al.*, 2002; Satheesh, 2002; Ganguly *et al.*, 2005a; Ramachandran, 2005; Singh *et al.*, 2005; Tripathy *et al.*, 2005]. In all these studies, aerosol radiative forcing are estimated using the SBDART model and basic aerosol related input parameters required for the radiative transfer calculations are derived by following almost the same procedure as method-1, described earlier in this section. However, most of these studies were limited by measurements of only few aerosol parameters, except AOD which in any case is essential for calculations of aerosol radiative forcing. As a result, the

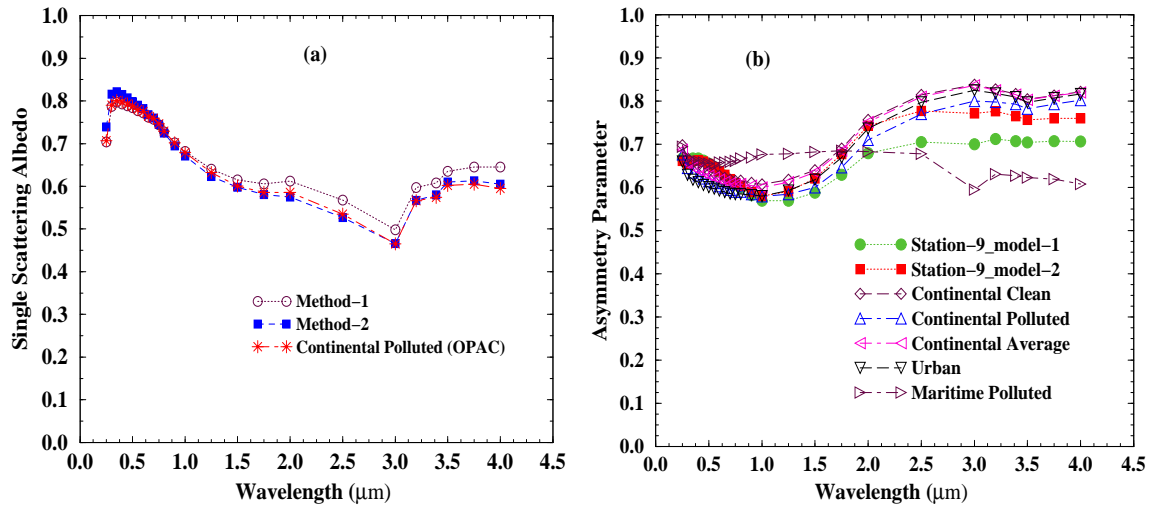


Figure 6.2: (a) Spectral values of ω for Dry season in Ahmedabad, derived using two different methods discussed in the text are compared with the corresponding values for continental polluted aerosols as prescribed in OPAC model of Hess *et al.* [1998]. (b) Two sets of asymmetry parameter values corresponding to station-9 of our study over central India are compared with the asymmetry parameter values for some of the standard aerosol models prescribed in OPAC.

OPAC model fitting carried out in all these studies are either subjected to fewer rigorous constraints or involve more assumptions and approximations. For example, besides AOD, Babu *et al.* [2002] had measurements of total aerosol mass using QCM and BC mass concentration using Aethalometer over their study location in Bangalore ($13^{\circ}N$, $77^{\circ}E$). Tripathy *et al.* [2005] has largely followed the work of Babu *et al.* [2002] at a different location in India, Kanpur ($23.43^{\circ}N$, $80.33^{\circ}E$), but advantage of this work is that Tripathy *et al.* [2005] could compare their OPAC estimated ω values with the AERONET (Aerosol RObotic NETwork) data available for the same location. Similarly, radiative forcing values over Bay of Bengal region, estimated by Ganguly *et al.* [2005a], are mainly based on simultaneous measurements of AOD and size segregated aerosol mass using QCM impactor. However, unlike all previous studies listed above, Ganguly *et al.* [2005b] estimated SW aerosol radiative forcing over different locations in Central India, avoiding OPAC fitting of aerosol optical properties but following a procedure similar to method-2 described above.

Another very important aerosol parameter required for radiative transfer calculations, is the knowledge on vertical distribution of aerosols in the atmosphere. Several researchers have emphasized on the importance of measuring vertical distribution of aerosols as they have pointed out that one major contributor to the uncertainty in atmospheric forcing

comes from uncertainty in the vertical distribution of aerosols and the aerosol single scattering albedo [Haywood and Ramaswamy, 1998; Chung *et al.*, 2005]. Differences in vertical profiles of aerosols affect the distribution of forcing within atmosphere and depending on the type of aerosols (scattering or absorbing) dominating in the atmosphere, it can produce different patterns of cooling or heating as a function of altitude in the atmosphere. This can have further implications for precipitation in the tropics, which occurs mostly due to convective processes in the atmosphere over these regions [Chung and Zhang, 2004]. Except over the Bay of Bengal, all radiative transfer calculations discussed in the present work are carried out using the actual profiles of aerosol extinction coefficient obtained from co-located MPL (Micro Pulse Lidar) measurements and normalized for the AOD value at the lidar wavelength ($0.523 \mu\text{m}$ in this case).

Other atmospheric profiles are constructed using the FNL [Results obtained from the final run in the series of National Center for Environmental Prediction (NCEP)] data available for the lower atmosphere and merged with the standard tropical atmospheric profiles above 26 km . For column ozone, we have used the TOMS (Total Ozone Mapping Spectrometer) data available for our study period and study location. Another important parameter which can introduce large errors in the estimated values of aerosol radiative forcing over land regions is the surface albedo of the location for which forcing estimates are being determined [Wielciki *et al.*, 2005]. For our study, we have used MODIS (Moderate Resolution Imaging Spectroradiometer) derived surface reflectance data available for the study region. In this we have used the 'Nadir BRDF-Adjusted Reflectance 16-Day L3 Global 1km SIN Grid' product derived at the mean solar zenith angle of Terra overpass for every successive 16-day period, calculating surface reflectance as if every pixel in the grid are viewed from nadir direction. Figure 6.3(a) shows the seasonal variation of surface reflectance over Ahmedabad, obtained by MODIS at seven different wavelength bands for the period from 2002 to 2005. Vertical lines in this figure represent $\pm 1\sigma$ variation about the mean value of surface reflectance measured during that season. Surface reflectance data available at seven wavelength bands of MODIS centered around $0.47, 0.56, 0.65, 0.86, 1.24, 1.64$ and $2.13 \mu\text{m}$ are further used to reproduce the spectral dependence of surface albedo for the entire SW range using a combination of three different surface types viz. vegetation, sand and water [Figure 6.3(b)]. On an average, surface reflectance values are found to be higher during Pre-Monsoon and Monsoon seasons while the corresponding values

are low during Dry and Post-Monsoon seasons.

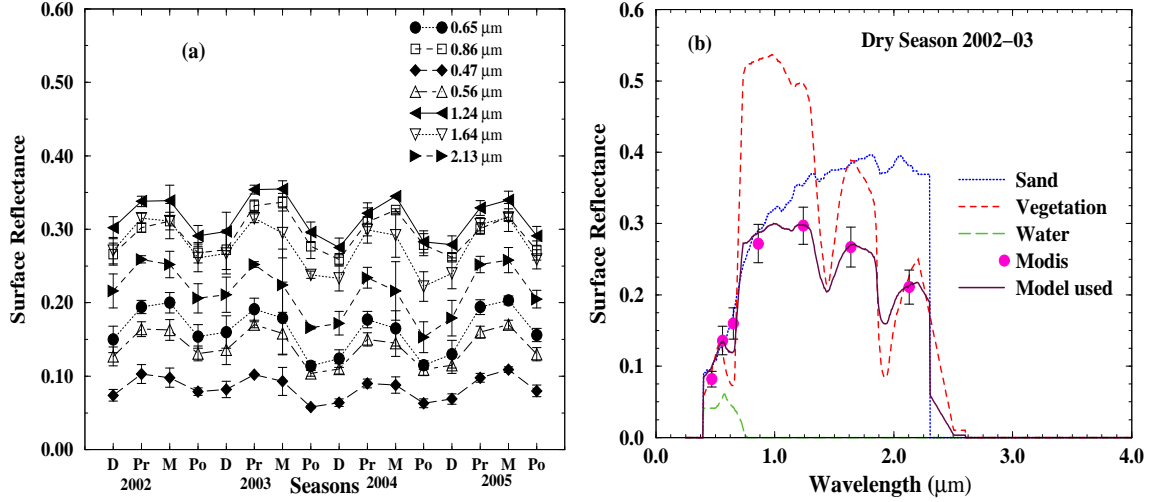


Figure 6.3: (a) Seasonal variation of surface reflectance over Ahmedabad, measured by MODIS at seven wavelength bands centered around 0.47, 0.56, 0.65, 0.86, 1.24, 1.64 and 2.13 μm for the entire period of our study from 2002 to 2005. Vertical lines in this figure represent $\pm 1\sigma$ variation about the mean value of surface reflectance measured during that season. (b) Surface reflectance data available at seven wavelength bands of MODIS centered around 0.47, 0.56, 0.65, 0.86, 1.24, 1.64 and 2.13 μm are used to reproduce the spectral dependence of surface albedo for the entire SW range using a combination of three different surface types viz. vegetation, sand and water.

6.2 Model estimates and Aerosol Radiative Forcing

Radiative forcing due to aerosols (ARF) are estimated by taking differences of results obtained by running the radiative transfer model with and without aerosol loading in the atmosphere under clear sky conditions.

6.2.1 ARF over Ahmedabad

Calculations of radiant fluxes integrated over entire SW region for all atmospheric layers are carried out at every 15 minute interval and for 24 hours period. Figure 6.4 shows the average values of SW aerosol direct radiative forcing at the surface level and TOA (Top Of the Atmosphere, 100 km in this case) for the entire period of our study from 2002 to 2005. Radiative forcing calculations have been carried out separately for each season (described in Chapter-2) in all years and also repeated for aerosol inputs derived using both methods

1 and 2. Vertical line on top of each bar represents $\pm 1\sigma$ variation about the mean value of radiative forcing for a particular season over four years of our study period from 2002 to 2005, representing the inter-annual variability in the forcing estimates for a particular season. One important observation to be made from figure 6.4 is that, although we followed two different approaches for generating basic aerosol input parameters, estimated values of aerosol radiative forcing at both levels are comparable in both these methods and this is true for every season. This proves the robustness of both methods used to generate the basic aerosol input parameters required for radiative transfer calculations. Another interesting observation is that radiative forcing values during Dry and Post Monsoon seasons are found to be negative at surface as well as at TOA in all years of our study, while during Pre-Monsoon and Monsoon seasons, the forcing at TOA flips sign to become positive. Comparing the values for surface level, we find aerosol radiative forcing to be the highest during Post-Monsoon season ($-63 \pm 10 \text{ W/m}^2$) and slightly less during Dry season ($-54 \pm 6 \text{ W/m}^2$). Surface level radiative forcing are found to be comparable during Pre-Monsoon and Monsoon seasons with their values being $-41.4 \pm 5 \text{ W/m}^2$ and $-41 \pm 11 \text{ W/m}^2$ respectively. In the case of TOA, aerosol forcing are found to be negative during Dry ($-26 \pm 3 \text{ W/m}^2$) and Post-Monsoon ($-22 \pm 3 \text{ W/m}^2$) seasons, while positive values of forcing are obtained during Monsoon ($14 \pm 4 \text{ W/m}^2$) and Pre-Monsoon seasons ($8 \pm 2 \text{ W/m}^2$). Aerosol radiative forcing over any location is very intricately dependent on several parameters such as total column burden of aerosols, their vertical distribution in the atmosphere, single scattering albedo, their size distribution, scattering phase functions, reflectance of the underlying surface, relative humidity in the atmosphere, solar insolation and many more [Haywood and Boucher, 2000]. Later in this section, we discuss the sensitivity of the estimated aerosol radiative forcing on some of the factors mentioned above. The difference between the TOA and surface level forcing is taken as atmospheric forcing. It represents the amount of energy trapped within the atmosphere by aerosols and mostly results in heating of the atmosphere [Ramanathan et al., 2001a]. Atmospheric forcing will increase if aerosol forcing at the TOA is more towards positive side while there is a large negative forcing at surface level. Over the period of our study, average values of atmospheric forcing are found to be 28 ± 9 , 48 ± 7 , 55 ± 15 and $40 \pm 11 \text{ W/m}^2$ during Dry, Pre-Monsoon, Monsoon and Post-Monsoon seasons respectively. Importantly, the aerosol atmospheric forcing is in addition to the well known heating caused by the con-

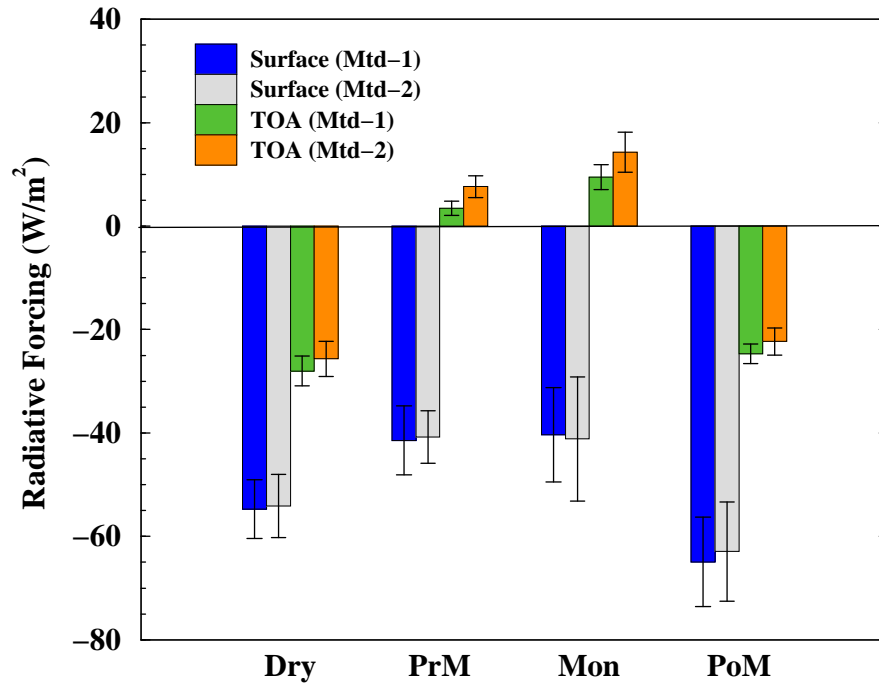


Figure 6.4: Average values of SW aerosol direct radiative forcing at the surface and TOA for the entire period of our study from 2002 to 2005 and for aerosol inputs derived using both methods 1 and 2 discussed in the text. Vertical lines on top of each bar represents $\pm 1\sigma$ variation about the mean value of radiative forcing for a particular season.

ventional greenhouse gases (naturally as well as anthropogenically produced) and water vapor. Our model estimates show that atmospheric forcing occurs in all seasons, but much more strongly during Pre-Monsoon and Monsoon seasons. This can have much larger implications for the regional scale dynamical processes such as wind flow, convection scheme and even precipitation patterns [Menon *et al.*, 2002]. It is essential to understand how the Earth-Atmosphere system responds to such large scale perturbations with regional cooling at the surface accompanied by a warming of the lower troposphere. Under normal equilibrium conditions, surface absorbed radiation energy is balanced by evaporation (latent heat flux) and sensible heat flux from the surface. In order to compensate for the reduction in surface reaching solar flux due to aerosols, either one or both these heat fluxes released from the surface must decrease. For the observed reduction in surface reaching solar flux over the Indian Ocean region, Ramanathan *et al.* [2001a] hinted on a greater possibility of this reduction being balanced by reduction in evaporation. Also, Ramanathan *et al.* [2001b] have pointed out that the reduction in evaporation could in turn result in reduction of

rainfall amount and hence effectively slow down the hydrological cycle.

Although large difference between the TOA and surface forcing is itself sufficient to prove the trapping of energy occurring in the atmosphere, it is of great importance to know how this heating is distributed within the atmosphere. This is useful to better understand how various components of the Earth-Atmosphere system could respond to such large scale heating perturbations imposed on it. We have observed large variabilities in aerosol loading, their vertical distribution, their physical and optical properties during different seasons of the year (see *Chapter-2*). In addition to these, there are large seasonal differences in meteorological parameters (important one being the vertical distribution of water vapor in the atmosphere) and reflectance of the underlying surface [figure 6.3(a)]. We show how these factors contribute in producing different amounts of radiative forcing at different levels of the atmosphere. Figure 6.5(a) shows the average patterns of SW aerosol direct radiative forcing values estimated for different levels in the atmosphere from surface to TOA. It is seen that radiative forcing values remain negative throughout the atmosphere (at all levels) during Post-Monsoon and Dry seasons, showing that there is a net reduction of downwelling flux in the SW region at each of these levels due to aerosols. The magnitude of aerosol forcing is found to decrease with increasing height in the lower troposphere but initially this decrease is very rapid in the first few hundred meters from the surface during Post-Monsoon and Dry seasons. This is related to variations in the vertical distribution of aerosols during these seasons. Aerosol profiles for Dry and Post-Monsoon seasons are characterized by very high values of extinction coefficient within first few hundred meters (~ 0.2 km) from the surface where there is a sharp decrease in the extinction values with increase in height. However, above the surface layer, aerosol concentration decreases rather slowly and approaches zero, almost asymptotically, at a height of around 4 km from the surface. As a result of this, forcing values also decrease rather slowly from the top of this surface layer to about 3-4 km altitude and thereafter remains almost constant up to TOA. Another important observation is that although surface forcing is more negative during Post-Monsoon compared to Dry seasons, forcing values for Post-Monsoon smoothly crosses over the corresponding values of Dry season at an altitude close to 2 km and then remains less negative up to the TOA. This effect causes trapping of more energy within the atmosphere during Post-Monsoon compared to Dry seasons. Forcing values remain constant above about ~ 4 km altitude because there is very little aerosol to scatter or

absorb either the downwelling or upwelling flux available at these levels. Negative values of forcing during Dry and Post-Monsoon season, representing decrease in net SW radiation flux at altitudes above 4 km are actually due to higher upscattering of radiation by aerosols at lower altitudes (discussed later in this chapter). It is already shown that surface

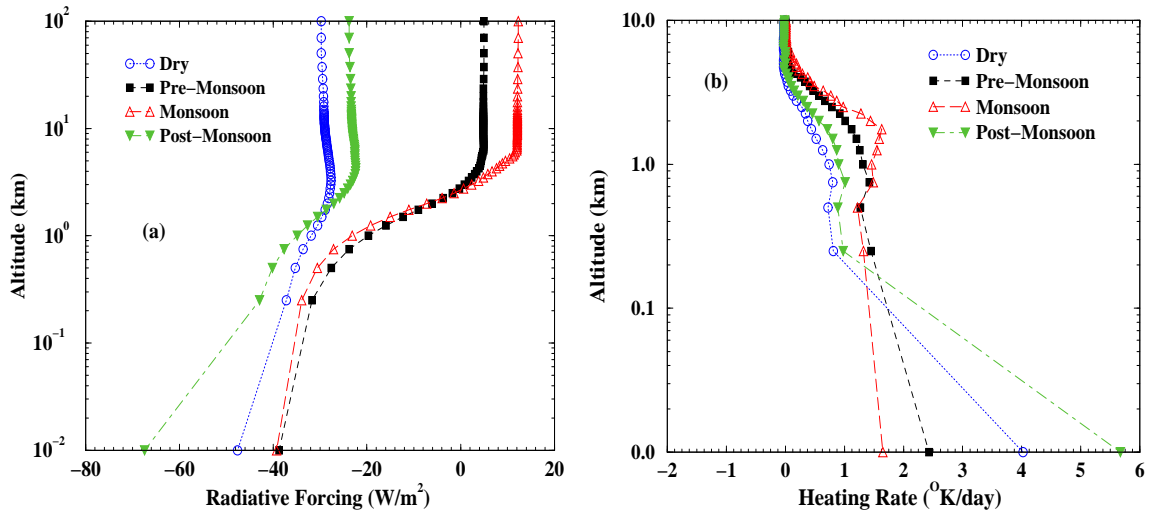


Figure 6.5: (a) Average seasonal patterns of SW aerosol direct radiative forcing estimated for different altitudes from surface to TOA. (b) Average profiles of heating rate due to aerosols in the atmosphere from surface to TOA for four major seasons occurring over the study region.

forcing during Pre-Monsoon and Monsoon seasons are less negative compared to their values during other two seasons. However we find large atmospheric forcing accompanied by trapping of energy within the atmosphere during these seasons. Hence it is of great interest to know how this atmospheric forcing and the associated heating is distributed in the atmosphere. As some of the earlier studies have shown that the atmospheric heating by absorbing aerosols can evaporate some of the low level clouds, resulting a decrease in cloud cover and planetary albedo, which in turn can lead to a net warming at the surface whose magnitude can exceed the cooling due to direct effect [Hansen *et al.*, 1997; Ackerman *et al.*, 2000]. Unlike Dry and Post-Monsoon seasons, magnitude of aerosol radiative forcing during Pre-Monsoon and Monsoon seasons decrease rather slowly in the first few hundred meters (~ 0.2 km) from the surface. However above ~ 0.5 km, magnitude of aerosol forcing decreases much rapidly and even flips sign to become positive at altitudes beyond 2.5 km. Similar to Dry and Post-Monsoon seasons, aerosol forcing during Pre-Monsoon and Monsoon seasons become almost constant above certain maximum altitude between 5 – 6

km from the surface. However it is of interest to examine how the loss or gain in SW radiation flux is translated into heating or cooling of the atmosphere at different levels. In our model, spectral irradiance at various atmospheric levels are used to estimate the net heating rate due to radiative heating or cooling caused by the aerosols. Figure 6.5(b) shows the average heating rate profiles in the atmosphere, obtained for different seasons of a year. At surface level, we get maximum heating rate during Post-Monsoon season and this is followed by values during Dry, Pre-Monsoon and Monsoon seasons in the decreasing order. The heating of the atmosphere is mainly caused by absorbing aerosols produced due to fossil fuel combustion and biomass burning activities. Over Ahmedabad, highest values of BC mass are measured during Post-Monsoon season ($7.3 \pm 3.7 \mu\text{g}/\text{m}^3$) which decreases slightly during Dry season ($5.5 \pm 2.8 \mu\text{g}/\text{m}^3$) and comparatively much lower values of BC mass are obtained in Pre-Monsoon ($2.2 \pm 1.0 \mu\text{g}/\text{m}^3$) and Monsoon seasons ($1.5 \pm 0.8 \mu\text{g}/\text{m}^3$). We also find that not only the absolute values of BC mass concentration are high in Post-Monsoon and Dry seasons, mass fraction of BC in the total aerosol concentration also remains high during these seasons. In addition to these, absorbing capability of the aerosols (particularly at shorter wavelengths) also increase during Post-Monsoon and Dry seasons (see *Chapter-2*). Therefore, the large heating rate at the surface level obtained during Post-Monsoon season is an effect caused by several contributing factors but more related to increased absorption of SW radiation close to surface by the dominant presence of soot particles in the atmosphere. This heating up of the lower atmosphere can in turn amplify the formation of winter time inversion layer and hence impact on the dispersal of aerosols [Ramana *et al.*, 2004].

Although during Post-Monsoon and Dry seasons we find large heating rates at the surface level, it decreases very sharply in the first two hundred meters from the surface itself. On the other hand, even though heating rates at the surface level are lower during Pre-Monsoon and Monsoon seasons compared to their values during Dry and Post-Monsoon season, its decrease with increase in height occurs at a much slower rate during Pre-Monsoon and Monsoon seasons. Almost in all seasons, after an initial decrease, heating rate values remain more or less constant from 0.25 to 0.50 km and above this height, we find a heated atmospheric layer although the actual heating, its maxima as well as its vertical extent differs from season to season [Figure 6.5(b)]. One important observation is that although heating rates are relatively small at lower altitudes during Pre-Monsoon

and Monsoon seasons, the values are high at higher altitudes during these seasons. During Monsoon seasons, heating rate at altitudes between 1 and 2 km are as high as its value near the surface. We find the average heating rates for the lowest 0.5 km thick surface atmospheric layer to be 1.9, 1.7, 1.4 and 2.5 $^{\circ}K/day$ during Dry, Pre-Monsoon, Monsoon and Post-Monsoon seasons respectively. Whereas, if we compare the average heating rates for the atmospheric layer from surface to 4 km altitude, the maximum heating of the atmosphere occurs during Monsoon season which is followed by Pre-Monsoon, Post-Monsoon and Dry seasons in the decreasing order with values 1.13, 1.0, 0.8 and 0.6 $^{\circ}K/day$ respectively. This heating up of the atmosphere at higher altitudes during Monsoon seasons can have large implications for the regional climate. In an earlier work, *Ackerman et al.* [2000] have shown that the atmospheric heating by absorbing aerosols can evaporate some of the low level clouds, resulting a decrease in cloud cover and planetary albedo. Such cloud burnings can produce much adverse consequences for the Indian region where the maximum annual rainfall is received during Monsoon season. In another work related to climate effects of black carbon aerosols over China and India, *Menon et al.* [2002] have shown that large amounts of black carbon (soot) particles and other pollutants are responsible for causing the observed changes in precipitation patterns and temperature trends over China in particular.

As mentioned earlier, aerosol radiative forcing over any location depends on several parameters such as total column burden of aerosols (AOD), their vertical distribution in the atmosphere, single scattering albedo, their size distribution, scattering phase functions, reflectance of the underlying surface, relative humidity in the atmosphere, solar insolation and many more [*Haywood and Boucher, 2000*]. In order to know the relative importance of each of these parameters in determining the radiative forcing values over our study location, we have performed several sensitivity tests in which we change one or more input parameters required for the radiative forcing calculations and estimate its effect on the model output. Most of the aerosol parameters exhibit extreme characteristics during Dry and Monsoon seasons and their characteristics remain by and large confined between these two extremes for rest of the year. Even other factors which play a deciding role in the estimation of aerosol radiative forcing such as reflectance of the underlying surface, relative humidity in the atmosphere, solar insolation or the total sun duration also exhibit extreme and opposite types of behavior during Dry and Monsoon seasons. For these rea-

sons, we carried out sensitivity study using various input parameters belonging to these two extreme seasons and using the measured input parameters for the year 2004. At first, all input parameters corresponding to Dry season of the year 2004 are selected and the radiative transfer computations are performed with and without aerosol loading to derive aerosol radiative forcing values at various levels of the atmosphere. Then we replace the AOD spectrum for Dry season with that of Monsoon season of the same year while keeping all other input parameters same and repeat radiative transfer calculations. Comparing the radiative forcing values for these tests we find that on replacing Dry season AODs with those of Monsoon season, which are actually higher, surface forcing becomes further negative (from -47.6 to -66.0 W/m^2) while magnitude of TOA forcing decreases slightly (from -29.8 to -28.4 W/m^2) and results in almost two fold increase in the atmospheric absorption (~ 20 W/m^2). Table 6.1 summarizes the results of aerosol radiative forcing obtained from twenty five sensitivity tests carried out using various combinations of input parameters for Dry and Monsoon seasons. Figure 6.6(a,b) shows the aerosol radiative forcing values at various atmospheric levels for the first six and next six sensitivity tests respectively, as listed in table 6.1. In the next sensitivity test (*Test-3*), we use ω values for Monsoon season and rest all input parameters are kept same as of *Test-1*. Result from this sensitivity test shows that on replacing the original ω values of Dry season with comparatively higher values corresponding to Monsoon season, forcing estimates at the surface and TOA both increase towards more negative side. Also, we find the shift in TOA forcing to be slightly more than the corresponding shift observed in surface forcing. It can be seen from figure 6.6(a) that the shift not only occurs at the surface and TOA, but we observe similar shift in the forcing values towards more negative side, at all atmospheric levels. This means that compared to a case where purely Dry season parameters are used, in the present combination of input parameters, there is a greater reduction of net SW radiation flux available at all levels in the atmosphere. However, due to nearly equal shift in radiative forcing values at all levels, we do not observe any significant difference in the atmospheric absorption with the present set of input parameters with respect to what is obtained in *Test-1* carried out using all input parameters for Dry season alone. In *Test-4*, all input parameters are kept same as that of Dry season (*Test-1*), except the surface albedo is replaced by the corresponding value for Monsoon season of the same year. Now, comparing the model outputs for *Test-4* and *Test-1*, we find that due to change in surface

albedo, forcing values at all levels in the atmosphere from surface to TOA shift almost uniformly by an amount of $2 - 3 \text{ W/m}^2$ towards the positive side. This shows that keeping all other parameters fixed and slightly raising the surface albedo increases the net SW flux available at various atmospheric levels. In another sensitivity test (*Test-5*), we replaced the set of asymmetry parameter values corresponding to Dry season by that of Monsoon season and allowed all other parameters to remain same as of original Dry season. Forcing results from this particular sensitivity test showed least deviation from the results of *Test-1*, showing that for the range of asymmetry parameter values obtained over our study location, aerosol radiative forcing is sensitive within a range of only $1 - 2 \text{ W/m}^2$. Further, in order to see the effect of vertical distribution of aerosols on estimates of aerosol radiative forcing, we perform another sensitivity test (*Test-6*) in which all input parameters are kept same as that of *Test-1*, except the vertical distribution of aerosols for Dry season is replaced by that of Monsoon season. Most interestingly, result from this sensitivity test shows that aerosol radiative forcing at surface level as well as at TOA exhibit almost same values in all model runs using any pattern of aerosol vertical profile but all other input parameters remaining same. However, it can be seen from figure 6.6(a) that there can be large differences in the radiative forcing values at intermediate atmospheric levels between surface and TOA for model runs carried out using different vertical profiles of aerosols but with all other input parameters remaining same. Heating rate perturbations for this particular test shows when the vertical distribution of aerosols for Dry season is replaced by that of Monsoon season, during which aerosols are spread up to much higher altitudes in the atmosphere, air temperature increases by a large magnitude over a sufficiently thick atmospheric layer from the surface due to increased radiative heating caused by absorbing aerosols predominant during Dry season.

For the next six sensitivity tests (*Test-7* to *Test-12*), we first performed the radiative transfer calculations using all original input parameters for Monsoon season (*Test-7*) and in the subsequent tests, we changed one out of the first five input parameters listed in table-1 to see the sensitivity of aerosol forcing for individual parameters. For example, *Test-8* is performed using all input parameters corresponding to Monsoon season except that the AOD values for Monsoon season are replaced by those of Dry season (relatively lower values at all wavelengths). Result of this sensitivity test shows that if the AOD values are decreased by a certain amount, magnitude of surface forcing decreases to become less

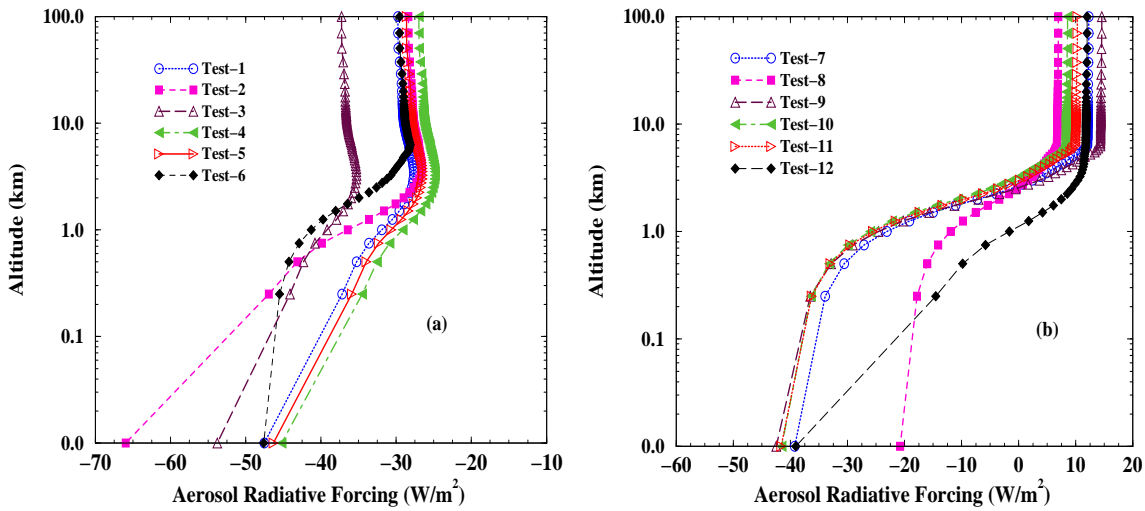


Figure 6.6: Aerosol radiative forcing at various atmospheric heights for (a) the first six and (b) next six sensitivity tests, mentioned in table 1.

negative while TOA forcing also decreases to become less positive. In fact, such decrease in radiative forcing values are observed throughout the atmosphere at all levels. Finally, both these favorable factors cause atmospheric forcing to decrease by a substantial amount. In *Test-9*, we used the ω spectrum corresponding to Dry season and performed radiative transfer calculations for the Monsoon period. We find that for the present combination of input parameters, forcing values at all altitudes below 1 km shift towards more negative side, while it remains almost unchanged between 1 – 2 km and increase towards more positive side above 2 km [figure 6.6(b)]. Overall effect of these changes in forcing values is to increase the amount of atmospheric trapping of energy from 51.5 W/m^2 for the case with all Monsoon season parameters (*Test-7*) to 57 W/m^2 for the present combination of parameters. In *Test-10*, we replaced the more reflective surface albedo of Monsoon season with slightly less reflective albedo of Dry season and performed model calculations of aerosol forcing using all other input parameters corresponding to Monsoon season. Model results for this particular test show a shift in the forcing values at lower altitudes (less than 1 km) towards more negative side with respect to corresponding values obtained in *Test-7*. Like the previous sensitivity test, aerosol forcing is not much affected by the new combination of input parameters (change of albedo in the present case) at atmospheric layers between 1 and 2 km. However, at altitudes more than 2 km, aerosol forcing shifts toward less positive values if its earlier value (corresponding to *Test-7*) is positive while

the same shifts toward less negative value if its earlier (corresponding to *Test-7*) value is negative. Another important point to be noticed from this particular sensitivity test is that, TOA forcing is more sensitive to changes in surface albedo compared to any effect seen in forcing estimates at surface level. *Test-11* is performed to see the changes in forcing values for Monsoon season, when among several input parameters, only the asymmetry factor for Monsoon season is replaced by its corresponding values from Dry season. The relative changes in surface and TOA forcing for this particular test with respect to results from *Test-7* are similar to that obtained in the case of *Test-10*. Due to change in asymmetry factor value, surface forcing becomes further negative from -39 to -42 W/m^2 while TOA forcing becomes less positive from 12 to 10 W/m^2 with negligible amount of change in atmospheric absorption. Now we examine the changes in aerosol radiative forcing for Monsoon season when the vertical distribution of aerosols is replaced by that of the Dry season. The result shows that both surface and TOA forcing remain almost unchanged even when the aerosol vertical profile for Monsoon season is completely replaced by that of Dry season, but forcing at intermediate atmospheric levels change substantially due to change in vertical distribution of aerosols. The altitudes at which forcing values are negative in *Test-1*, shift towards positive side while the forcing values which are already positive, increase in magnitude but these values reach their saturation at altitude close to 4 km, where its value becomes same as that of TOA.

Besides the twelve sensitivity tests discussed so far, we have carried out additional tests in which at least two out of six major input parameters required for radiative transfer calculations, listed in table 6.1, are replaced by their corresponding values from the opposite season. For *Test-13* to *Test-24*, we first selected the same combination of input parameters as used for *Test-1* to *Test-12* but changed an additional parameter by its value for the opposite season. In all sensitivity tests, we obtained different values of aerosol radiative forcing at different levels in the atmosphere for different combinations of basic input parameters required for radiative transfer calculations and summarized results of various model runs are listed in table 6.1. It is interesting to note that in all sensitivity tests which are performed for the Monsoon period, TOA forcing has been always positive, irrespective of any other combination of input parameters. On the other hand, in all sensitivity tests which are performed for the period of Dry season, TOA forcing values are always negative. In order to confirm our finding, we performed two more sensitivity tests viz. *Test-25*

and *Test-26*. In *Test-25*, we used all input parameters corresponding to Dry season but the model was run for the middle of Monsoon season. Interestingly, result from this sensitivity test came in favor of our earlier observation with forcing values at the surface and TOA being -25.9 and 5.0 W/m^2 respectively. Lastly, in *Test-26*, we used all input parameters corresponding to Monsoon season but carried out model calculations for the middle of Dry season. Once again, model results from this sensitivity test supported our earlier observation as the forcing values obtained in *Test-26* are -55.2 and -20.9 W/m^2 at the surface and TOA respectively. The basic difference in the radiative transfer calculations carried out for Monsoon and Dry season arises due to differences in insolation and diurnal variation of solar zenith angle during these two extreme type of seasons. Thus results from several sensitivity tests show that besides other parameters like columnar burden of aerosols (AOD), their vertical distribution in the atmosphere, single scattering albedo, aerosol size distribution, scattering phase functions, reflectance of the underlying surface, relative humidity in the atmosphere etc., one crucial parameter which plays a major role in determining both magnitude as well as sign of diurnally averaged aerosol radiative forcing at TOA is related with the amount of insolation and other allied factors.

Thus over Ahmedabad, we find TOA forcing to be always positive during Monsoon and negative during Dry season, for any combinations of different input parameters varied within limits of their measured values over our study period [Table 6.1]. We also see that over an annual cycle, most of the aerosol parameters exhibit extreme and opposite type of behavior during Dry and Monsoon seasons and for rest of the year, values remain mostly confined between these two extreme seasons. Therefore, in order to find the maximum variation in aerosol radiative forcing that can be expected for our study location over a full annual cycle, additional sensitivity studies were made. In these tests, aerosol parameters for the two extreme type of seasons (viz. Dry and Monsoon) are used in the radiative transfer calculations to get the diurnally averaged values of aerosol radiative forcing for all months of a year. Figure 6.7(a,b) gives the summary of aforementioned sensitivity studies, showing the monthly variation of aerosol radiative forcing at the surface level and TOA, using both (Dry and Monsoon) sets of input parameters. From the results, we find that aerosol forcing at the surface level is always negative in all months and shows a consistent pattern of variation over an annual cycle with more negative values during Dry (December to March) and Post-Monsoon (October-November) seasons and less nega-

tive values during Pre-Monsoon (April-May) and Monsoon (June to September) seasons. Pattern of variation is found to be same for both sets of input parameters. For the same set of input parameters (either Dry or Monsoon), less negative values of surface forcing during Pre-Monsoon and Monsoon months while large negative values during Dry and Post Monsoon months, clearly indicates that differences in surface insolation and diurnal range of solar zenith angle variation plays a major role in modulating the aerosol radiative forcing values over our study location. However, most interesting results from the current series of sensitivity tests are in regards to TOA forcing values. It can be seen from figure 6.7(b) that TOA forcing corresponding to both set of input parameters show negative values in model run for the months of January to March and from September to December. Month of April is a transition period when model results of TOA forcing carried out using input parameters corresponding to Dry season remains negative while the results obtained using Monsoon season input parameters flip sign to become positive. Thereafter, TOA forcing for both sets of input parameters exhibit positive values from May to August. Once again, month of August acts as a transition period when forcing values estimated using Dry season input parameters remain positive but much close to zero. Our study shows that for the same set of input parameters, radiative transfer calculations carried out for different months of a year, can produce much different results and it can even flip the sign of aerosol forcing at TOA. Thus through our results, we have emphasized the importance of diurnal variations in the amount of insolation, solar zenith angle and other related factors in controlling the values of aerosol radiative forcing over any location. Reasons for getting large negative values of surface radiative forcing during Dry season for any combination of aerosol parameters is that during this season Earth's northern hemisphere is tilted away from the Sun and therefore over our study location, solar zenith angles remain mostly high (minimum is $\sim 45^\circ$) over a diurnal cycle. As a result of this, solar radiations has to traverse a longer slant path in the Earth's atmosphere, during which its chances of getting absorbed or scattered by aerosols are high. Due to this increased scattering of incoming radiation by aerosols, we find a large reduction in the downward flux at lower altitudes of the atmosphere. Moreover, due to higher values of average solar zenith angle within a day during Dry season, same amount of energy becomes spread over a larger area. This reduction in down-welling flux caused by aerosols in the atmosphere is manifested as large negative aerosol radiative forcing at the surface. On the contrary, during

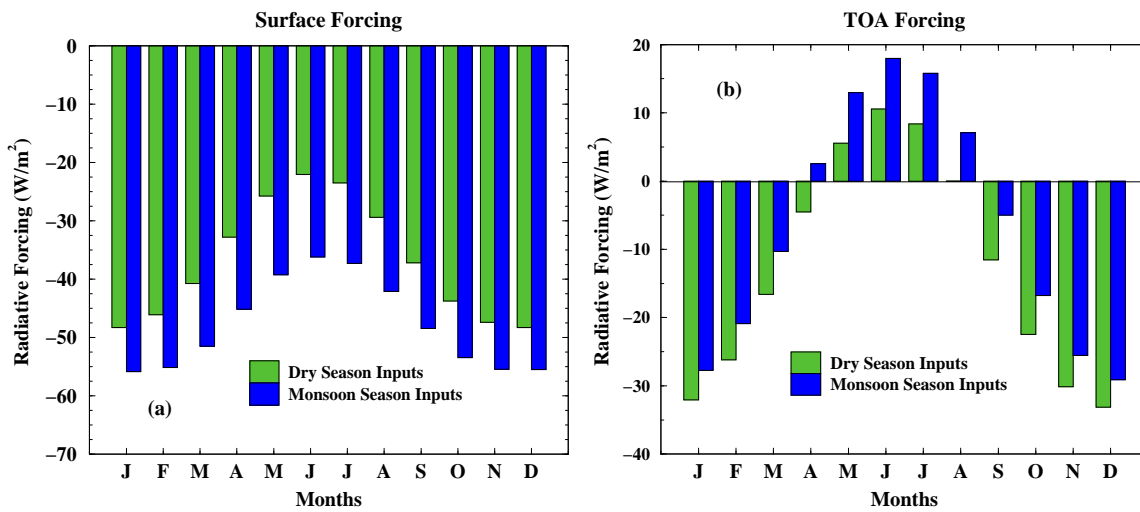


Figure 6.7: Results of sensitivity study on the monthly variation of diurnally averaged values of shortwave aerosol direct radiative forcing at (a) surface level and (b) TOA, estimated using Dry and Monsoon season input parameters.

summer months or Pre-Monsoon and Monsoon seasons, Earth's northern hemisphere is tilted towards the Sun and we get a large diurnal variation of solar zenith angle with its minima much closer to zero degree over our study location. The Sun is close to overhead for significantly longer time in a day, during which the incoming radiation crosses shorter path through the atmosphere before reaching the Earth's surface. This means that for all other conditions such as aerosol types and their distribution in the atmosphere remaining same, incoming radiations from the Sun traverse through shorter path length in summer months compared to winter months and therefore encounter lesser aerosols in their path, reducing its chances of getting scattered away on their transit through the atmosphere during summer months. Thus, even when all the input parameters are kept same, aerosol radiative forcing at the surface is less negative during summer months while large negative surface forcing is observed during winter months. Difference between the two bars of every month in figure 6.7(a) represents the difference in aerosol radiative forcing due to differences in aerosol parameters occurring during Dry and Monsoon seasons. For any particular month, higher values of aerosol forcing are obtained using the Monsoon season inputs due to higher loading of aerosols in the total atmosphere during this season compared to Dry season.

Aerosol forcing at TOA is more dependent on upscatter fraction of radiation, denoting

the fraction of radiation scattered into the upward hemisphere relative to the local horizon [Pilinis *et al.*, 1995]. This upscatter fraction of radiation depends on solar zenith angle and angular phase function of the distribution of aerosols. While studying the dependence of upscatter fraction of radiation on solar zenith angle, Nemesure *et al.* [1995] found that upscatter fraction is high for larger zenith angles and it shows maxima when the Sun is at horizon. This happens because at higher solar zenith angles, large portion of scattering in the forward hemisphere contributes to this upscatter fraction. During winter months, solar zenith angle remains mostly high (minimum is $\sim 45^\circ$) in a full diurnal cycle over our study location, which result in a higher upscatter fraction of radiation during Post-Monsoon and Dry seasons. As a result of this increased upscattering of radiation during winter months, atmosphere loses a large fraction of the incoming radiation at almost all levels, which ultimately results in negative aerosol forcing at the TOA. If we compare the TOA forcing values estimated using two different sets of input parameters, for a particular month during Dry and Post-Monsoon season, we find that TOA forcing is more negative for model run using Dry season inputs compared to that obtained using Monsoon season inputs. Nemesure *et al.* [1995] have also shown that except for very large solar zenith angles (Sun is close to horizon), upscatter fraction of radiation decreases with increase in particle size. This decrease in upscatter fraction is more strongly realized when the Sun approaches closer to zenith. It is also shown that, smaller size particles exhibit larger upscattering of radiation at all solar zenith angles. Our study shows the dominance of smaller size particles during Dry and Post-Monsoon seasons while increase in coarser particles during Pre-Monsoon and Monsoon seasons. Due to increased dominance of smaller size particles during Dry season, we find more upscatter fraction of radiation in model computations performed using Dry season aerosol inputs than using Monsoon season aerosol parameters. In addition to this, during Monsoon season, aerosols are present up to much higher altitudes in the atmosphere and chances of incoming radiations from the Sun getting absorbed by aerosols in the atmosphere is higher during Monsoon season. As a result, computed values of outgoing SW flux at the TOA are found higher and atmosphere losses more energy when the model is run using Dry season inputs rather than using Monsoon season parameters.

During Pre-Monsoon and Monsoon seasons, there is a larger variation in solar zenith angle over a diurnal cycle, with its minima coming much closer to zenith. Previously,

Nemesure et al. [1995] have shown that upscatter fraction of radiation decreases substantially with decrease in solar zenith angle and at times when Sun is close to zenith. Therefore, during summer months when Sun stays near the zenith for a relatively longer time, decrease in upscatter fraction of radiation by aerosols in the atmosphere causes upwelling flux at the TOA to decrease to such an extent that we get large differences between net downward and net upward flux, almost at all altitudes above ~ 5 km. In addition to the reduction in upscatter fraction, absorption by aerosols in the lower atmosphere further decreases the net upward SW flux at TOA, resulting in trapping of energy within the atmosphere and rendering the TOA forcing to be positive. Another important observation to be made from figure 6.7(b) is that, although magnitude of TOA forcing during months corresponding to Dry and Post-Monsoon seasons are smaller when the model computations are performed using Monsoon season inputs. But during summer months, when TOA forcing shows a tendency to attain positive values, its magnitude is found to be higher for model runs performed using Monsoon season inputs compared to those performed using inputs from Dry season. Reasons for getting more positive values of TOA forcing during summer months when the model computations are performed using Monsoon season inputs is due to dominance of coarser particle in the atmosphere during Pre-Monsoon and Monsoon seasons (see *Chapter-2*). When Sun remains closer to zenith, predominant forward scattering by larger particles causes upscatter fraction to decrease by a large amount. In addition, during Monsoon season, aerosols are present up to much higher altitudes in the atmosphere and this increases chances of getting radiations absorbed in the atmosphere even at higher altitudes.

Table 6.1: Results from various sensitivity tests of Aerosol Radiative Forcing to different parameters used as input in radiative transfer calculations.

Test	AOD	ω	Albedo	g	Profile	Period	Aerosol Radiative Forcing		
							Surface	TOA	Atmosphere
1	Dry	Dry	Dry	Dry	Dry	Dry	-47.6	-29.8	17.8
2	Mon	Dry	Dry	Dry	Dry	Dry	-66.0	-28.4	37.6
3	Dry	Mon	Dry	Dry	Dry	Dry	-53.8	-37.3	16.5
4	Dry	Dry	Mon	Dry	Dry	Dry	-45.2	-27.0	18.2
5	Dry	Dry	Dry	Mon	Dry	Dry	-46.3	-28.6	17.7
6	Dry	Dry	Dry	Dry	Mon	Dry	-47.6	-29.6	18.0
7	Mon	Mon	Mon	Mon	Mon	Mon	-39.3	12.3	51.6
8	Dry	Mon	Mon	Mon	Mon	Mon	-20.8	6.9	27.7
9	Mon	Dry	Mon	Mon	Mon	Mon	-42.5	14.5	57.0
10	Mon	Mon	Dry	Mon	Mon	Mon	-41.4	8.5	49.9
11	Mon	Mon	Mon	Dry	Mon	Mon	-41.7	10.3	52.0
12	Mon	Mon	Mon	Mon	Dry	Mon	-39.1	12.0	51.1
13	Mon	Dry	Dry	Dry	Mon	Dry	-66.1	-28.2	37.9
14	Dry	Mon	Dry	Dry	Mon	Dry	-53.9	-37.1	16.8
15	Dry	Dry	Mon	Dry	Mon	Dry	-45.3	-26.8	18.5
16	Mon	Dry	Dry	Mon	Dry	Dry	-64.0	-26.5	37.5
17	Dry	Mon	Dry	Mon	Dry	Dry	-44.9	-29.5	15.4
18	Dry	Dry	Mon	Mon	Dry	Dry	-44.1	-25.9	18.2
19	Dry	Mon	Mon	Mon	Dry	Mon	-20.7	6.7	27.4
20	Mon	Dry	Mon	Mon	Dry	Mon	-42.3	14.2	56.5
21	Mon	Mon	Dry	Mon	Dry	Mon	-41.4	8.3	49.7
22	Dry	Mon	Mon	Dry	Mon	Mon	-22.2	5.7	27.9
23	Mon	Dry	Mon	Dry	Mon	Mon	-44.8	12.6	57.4
24	Mon	Mon	Dry	Dry	Mon	Mon	-44.1	6.3	50.4
25	Dry	Dry	Dry	Dry	Dry	Mon	-25.9	5.0	30.9
26	Mon	Mon	Mon	Mon	Mon	Dry	-55.2	-20.9	34.3

6.2.2 ARF over Bay of Bengal

It is a challenge for the climate research community to express the direct aerosol radiative forcing separately in terms of major anthropogenic and natural aerosol components. For the estimation of ARF over BoB, we have followed procedures described as method-1 in previous section. OPAC model has been used to make estimates of number concentration of different aerosol components which contribute to the observed AODs over the study region. As the mean relative humidity during the measurement period was in the range of 50 to 70%, number concentration of aerosols are computed for both these limiting relative humidity cases. Previously, *Satheesh et al.* [2001] and *Satheesh* [2002] reported the single scattering albedo for the Arabian Sea and Bay of Bengal region to be around 0.90 and 0.85 respectively. *Vinoj et al.* [2004] estimated the single scattering albedo of aerosols over the BoB as 0.88, taking into account the black carbon (BC) aerosol data collected from the island station Port Blair (11.63° N, 92.71° E). In another study, *Salam et al.* [2003] found the BC concentration over Bhola (22.17° N, 90.75° E) island located south of Bangladesh to be in the range of 1.4 to 4.2 $\mu\text{g m}^{-3}$. In the absence of simultaneous measurements of absorption and scattering coefficient of aerosols and considering the range of published results for the region, we estimated two sets of aerosol model for each day, satisfying all other constraints and single scattering albedo for the mixture being 0.90 and 0.85. For the Bay of Bengal region, estimates of radiative forcing have been carried out for both SW and LW bands. Aerosol forcing in LW region is sensitive to the columnar content of water vapor and ozone. For ozone value, we have used the TOMS data which was not varying much during the cruise period. However, column water vapor is a highly varying constituent in the atmosphere and the value for this has been obtained from the Microtops measurements made onboard the cruise. It may be noted that the typical total column water content prescribed in the SBDART model for the tropical atmosphere is 4.1 cm while our measurements show that the values are in the range from 1.5 to 2.5 cm which is also corroborated by the FNL data [Figure 6.9(a)]. In order to study the sensitivity of aerosol radiative forcing to changes in the aerosol composition, we have estimated the forcing values for each day corresponding to two different sets of aerosol mixture with single scattering albedo for the combination being close to 0.85 and 0.90. We found that SW forcing is negative at the surface as well as at TOA while LW forcing is always positive for both these cases. Moreover, the magnitude of LW forcing is much less ($\sim 10\%$) compared to its SW

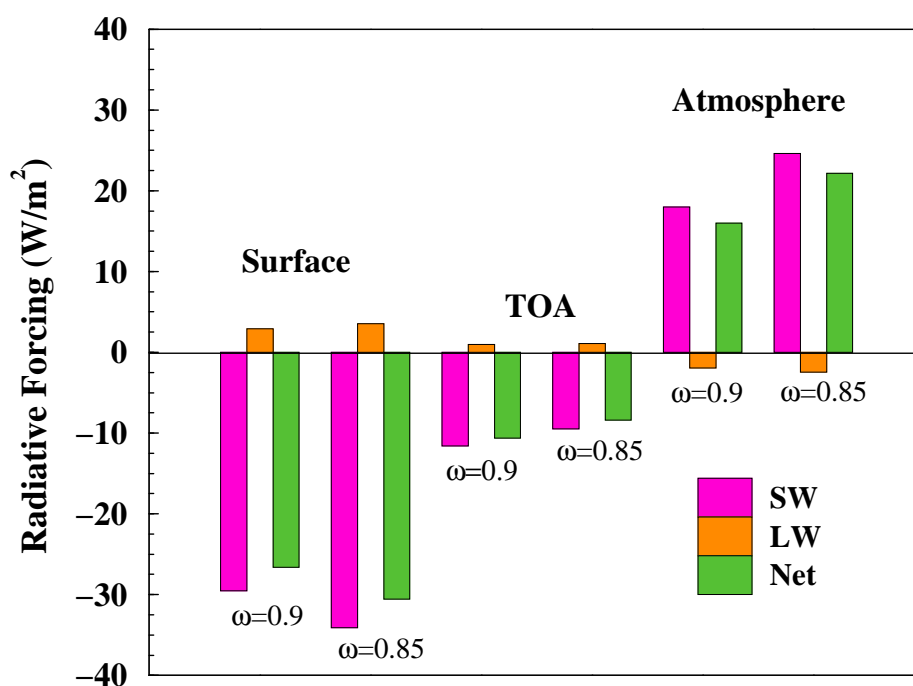


Figure 6.8: Spatially and diurnally averaged aerosol direct radiative forcing estimated over the Bay of Bengal for the cruise period.

counterpart, meaning, only about 10% of the SW forcing is compensated by the LW forcing both at surface and TOA. The difference of the forcing values at the surface and TOA represents the energy trapped within the atmosphere by aerosols and results in heating of the atmosphere. We found that for the same optical depth values and same aerosol mass loading over BoB, a decrease in the single scattering albedo for the mixture of aerosols from 0.90 to 0.85 can increase the radiation flux trapped within the atmosphere from 16.1 to 22.2 W/m^2 . With the increase in the amount of absorbing aerosols, magnitude of short-wave forcing increases at the surface level and decreases at the TOA (Figure 6.8). We also observe that the column water vapor amount as well as its vertical distribution obtained from FNL data showed large variations during the cruise period. A sensitivity test of LW aerosol radiative forcing is performed for different values of water vapor concentration and it is found that the magnitude of LW aerosol forcing at the surface level decreased with the increase in column water vapor while the TOA aerosol forcing is not much sensitive to variation in water vapor [Figure 6.9(b)]. A similar test conducted for the SW region shows no significant correlation between the SW aerosol radiative forcing and water vapor concentration in the atmosphere. Table 6.2 shows a comparison between the forcing val-

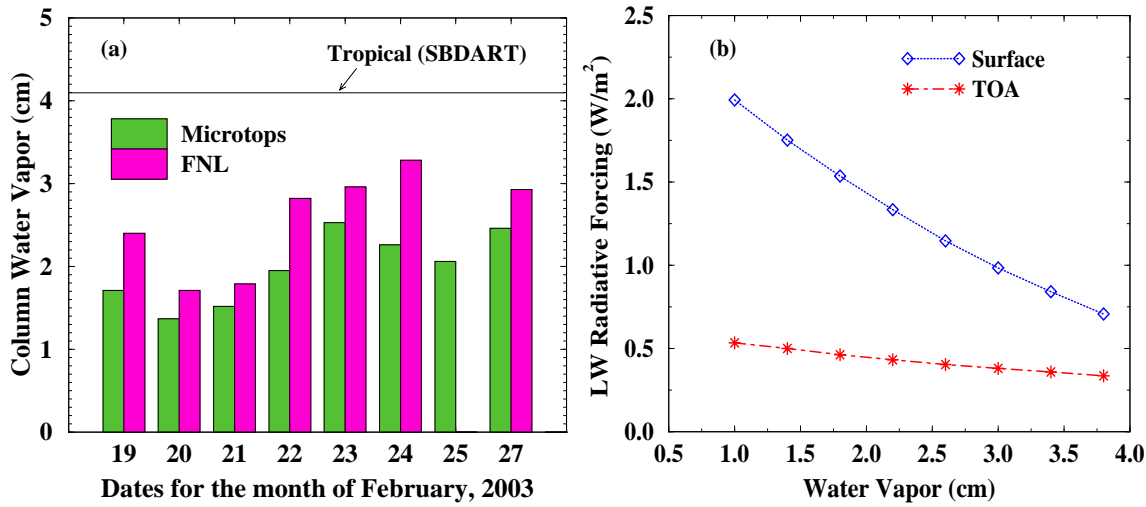


Figure 6.9: (a) Comparison between column water vapor measured using Microtops, that obtained from FNL and as prescribed for tropical atmosphere in SBDART (default value). FNL data for 25 February could not be obtained. (b) LW aerosol radiative forcing sensitivity to water vapor concentration shown as an example for the 19th Feb data.

Table 6.2: Average values of aerosol radiative forcing obtained in the present study for two different values of ω and those reported by *Vinoj et. al* [2004] and *Satheesh* [2002] for the same region.

Source	Surface			TOA			Atmosphere
	SW	LW	Net	SW	LW	Net	Net
Present Study ($\omega \sim 0.85$)	-34.09	+3.52	-30.57	-9.50	+1.08	-8.42	22.15
Present Study ($\omega \sim 0.90$)	-29.55	+2.94	-26.62	-11.58	+0.97	-10.61	16.01
<i>Vinoj et. al</i> , [2004]	-34.20	+9.8	-24.4	-6.3	+2.7	-3.6	20.8
<i>Satheesh</i> , [2002]	-38	+11	-27	-7	+3	-4	23.0

ues obtained from the present study with those reported by *Vinoj et al.* [2004] for the same region and for the same period of observation and *Satheesh* [2002] for a cruise conducted over BoB in March 2001. We found that at the surface level, SW aerosol forcing over BoB closely matches with the forcing values reported by *Vinoj et al.* [2004] and *Satheesh* [2002]. However, the major difference between our results and those of *Vinoj et al.* [2004] as well as *Satheesh* [2002] lies in the LW forcing values. We have found a low value of about +3.52 W/m^2 and +1.08 W/m^2 for the LW forcing at the surface and TOA respectively for the case when ω is close to 0.85. Similarly for the case when ω is close to 0.90, we still get low LW forcing values of about +2.94 W/m^2 and +0.97 W/m^2 at the surface and TOA respectively. The corresponding values reported by *Vinoj et al.* [2004] and *Satheesh* [2002] are +9.8, +2.7

W/m^2 and $+11, +3 W/m^2$ respectively. The present results are more realistic as we have used the measured column water vapor concentration and the actual vertical profiles of water vapor, temperature etc. obtained from FNL data for the cruise period.

6.2.3 ARF over Central India

In our study over Central India, we generated the basic input parameters required for the radiative transfer computations by following the procedures described as method-2 in a previous section of this chapter. In the absence of spectral dependent values of single scattering albedo (ω), we performed theoretical estimation of ω for standard aerosol models such as continental clean, continental average, continental polluted, marine [d'Almeida, 1991] etc. using software package OPAC [Hess *et al.*, 1998]. Out of these aerosol models, two nearest ones were chosen for each station based on observed values of ω and Angstrom parameters and scaled to match the measured ω at $0.525 \mu m$. Since the scaling factor could be different at different wavelengths, we repeated the radiative transfer calculations for every station with two sets of ω spectrum corresponding to the two nearest matching aerosol models. Asymmetry parameter required for the radiative forcing calculations are derived by applying Mie theory to the measured aerosol size distribution constructed by merging the data obtained from two different but simultaneously operated instruments, viz. the QCM cascade impactor and an aerosol size spectrometer. Further, we have also used the MODIS derived surface reflectance available at seven wavelength bands centered around $0.47, 0.56, 0.65, 0.86, 1.24, 1.64$ and $2.13 \mu m$ separately for all the stations. Figure 6.10 shows the computed values of shortwave aerosol radiative forcing at the surface level, at TOA and within the atmosphere over various stations in the Central Indian region. Vertical line on top of each bar represents the range of radiative forcing values obtained using different sets of ω and asymmetry parameter values as discussed earlier. We find that over the study region and during the period of our measurements, there is a large negative forcing at the surface level in the range of -15 to $-40 W/m^2$, while forcing at the TOA varied between $+0.7$ to $-11 W/m^2$. Atmospheric forcing, which is the difference between TOA and surface forcing, represents the absorption within the atmosphere and it is very large over this region. Comparing figures 4.11 and 6.10, we find that the surface level radiative forcing is primarily governed by the magnitude of AOD values which varied mostly between 0.2 and 0.6 at $0.5 \mu m$ during the campaign. Whereas the TOA forcing is

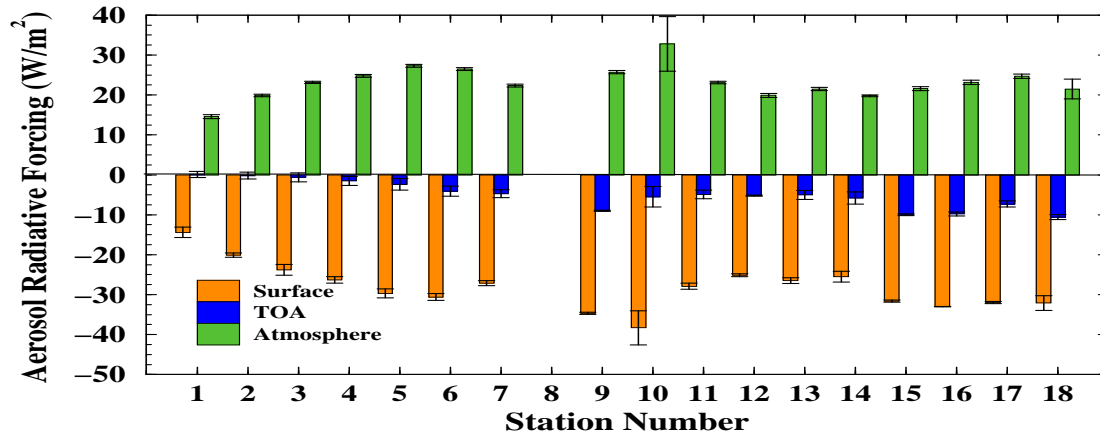


Figure 6.10: Clear sky direct shortwave aerosol radiative forcing at the surface level, at TOA and in the atmosphere over various stations in the Central Indian region. Error bar shows the range of radiative forcing values obtained using different sets of ω and asymmetry parameter values.

very intricately dependent on several aerosol parameters such as AOD, surface albedo, ω etc. Previously *Ramana et al.* [2004] have reported the ARF over the Himalayan region for the winter season to be around $-25 W/m^2$ at the surface level and about $0 W/m^2$ at TOA. In another study, *Pandithurai et al.* [2004] reported the average ARF over Pune ($18.3^\circ N$, $73.5^\circ E$) for dry seasons (Nov-Apr) to be around $-33 W/m^2$ at the surface and almost $0 W/m^2$ at TOA. Negative values of ARF at the TOA over the study region and its increasing trend indicates the presence of significant amount of scattering type aerosols and their increasing relative dominance along the period of our observation. This could be possible due to decline in the biomass burning activities, a major source of absorbing BC aerosols, towards the end of dry winter season. Comparing our present estimates on SW aerosol radiative forcing with earlier results obtained over the surrounding ocean regions on both sides of peninsular India for the winter season, we find that the mean atmospheric forcing of about $22 \pm 4 W/m^2$ over the study region is higher than $7.8 W/m^2$ reported by *Jayaraman* [2001b] for the Arabian Sea. However the atmospheric forcing values reported over Bay of Bengal region is in the range of $25-31 W/m^2$ [*Ganguly et al., 2005a*]. Since majority of the aerosols are confined within first 2 km of the atmosphere, our forcing estimate translates into a heating rate of about $0.8^\circ K/day$ for this layer.

6.2.4 ARF over New Delhi

In this study, OPAC model [Hess *et al.*, 1998] is used to make estimates of aerosol components which contributed towards the measured aerosol properties over New Delhi. Firstly we used different combinations of aerosol components from the urban model, which are sulfates, nitrates, organics, soot and mineral dust particles, to best fit the mean AOD spectrum observed on each individual day. As the mean relative humidity during the measurement period is found to vary between 50% to 70%, output parameters of the model are computed for these two limiting relative humidity cases. Model derived optical parameters are obtained by varying the number concentration of individual components in small steps until they satisfy several stringent conditions described earlier as method-1 in section-6.2. Finally, radiation code SBDART is used to perform radiative transfer calculations in the shortwave region. Among other input parameters, we have used the actual aerosol extinction profiles obtained from MPL measurements and normalized for the observed AOD value at the MPL wavelength. Other atmospheric profiles are constructed using the FNL data available for the campaign period for the lower atmosphere and merged with the standard tropical atmospheric profiles above 26 km. For column ozone, we have used the TOMS data available for the campaign period. In this study, we have used the MODIS derived surface reflectance data for the study region, available at seven wavelength bands centered around 0.47, 0.56, 0.65, 0.86, 1.24, 1.64 and 2.13 μm to reproduce the spectral dependence of surface albedo for the entire shortwave range using a combination of three different surface types viz. vegetation, sand and water. Calculations of irradiance were carried out at 15 minute interval and for 24 hours period and diurnally averaged radiative forcing were estimated for the surface and top of the atmosphere. Figure 6.11 shows the average values of shortwave aerosol radiative forcing at the surface level and TOA computed separately for individual days and then grouped into three categories viz. clear, hazy and foggy days. Over the period of our study, we find a large negative forcing at the surface level in the range of -40 to -86 W/m^2 , while forcing at the TOA varied between -2 and $+3 \text{ W/m}^2$. At the surface level, forcing estimates are found to be highest on hazy days (-75 W/m^2) followed by those during foggy days (-71 W/m^2) and comparatively lower values are obtained on clear days (-51 W/m^2). Similarly, average forcing at TOA is found to be highest on hazy days ($+1.9 \text{ W/m}^2$), followed by foggy days ($+1.4 \text{ W/m}^2$) and lowest on clear days ($+0.9 \text{ W/m}^2$). Comparing the forcing estimates with AOD

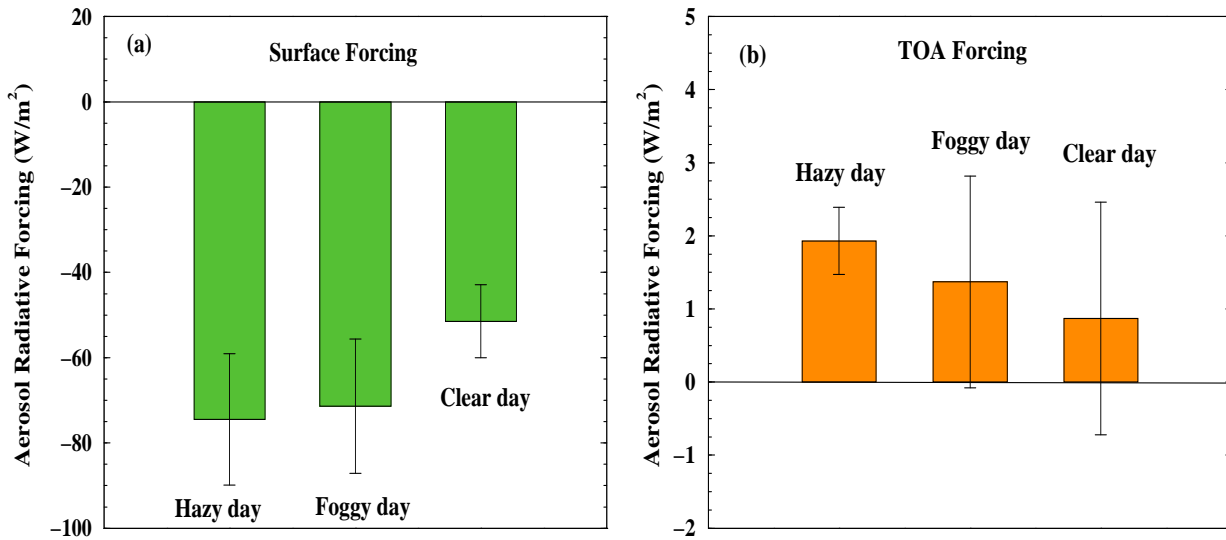


Figure 6.11: Average values of SW aerosol radiative forcing at (a) surface level and (b) TOA computed separately for individual days and then grouped into three categories viz. clear, hazy and foggy days.

values, we find that the surface level radiative forcing is primarily governed by the magnitude of AODs which varied from a low value of 0.37 to high values above 2 at $0.5 \mu\text{m}$ during the campaign. But TOA forcing is very intricately dependent on several parameters such as AOD, ω , surface albedo etc. Large difference between the forcing values at the surface and TOA cause large amount of energy to remain trapped within the atmosphere resulting in heating up of the lower atmosphere which in turn amplifies the formation of winter time inversion layer and limit the dispersal of aerosols to long distances [Ramana *et al.*, 2004]. High values of atmospheric forcing estimated over Delhi is alarming as earlier studies have shown that widespread aerosol haze over this region can even slow down the hydrological cycle and thereby producing global consequences [Ramanathan *et al.*, 2001b, 2005].

6.3 Summary

Implications of variabilities in aerosol parameters to the regional scale aerosol radiative forcing are presented. Measured aerosol parameters are used as input in a radiative transfer model and aerosol radiative forcing values are estimated for all study locations. A discrete ordinate radiative transfer model, SBDART, is used to carry out radiative transfer calculations in the SW and LW regions. Two different approaches are followed to gener-

ate spectral values of various input aerosol parameters required for the radiative transfer model and the computed values of aerosol radiative forcing are found comparable in both methods. Over Ahmedabad, magnitude of surface forcing are found to be the highest during Post-Monsoon ($-63 \pm 10 \text{ W/m}^2$), followed by Dry season ($-54 \pm 6 \text{ W/m}^2$) and lower values during Pre-Monsoon ($-41.4 \pm 5 \text{ W/m}^2$) and Monsoon ($-41 \pm 11 \text{ W/m}^2$) seasons. In the case of TOA, aerosol forcing are found to be negative during Dry ($-26 \pm 3 \text{ W/m}^2$) and Post-Monsoon ($-22 \pm 3 \text{ W/m}^2$), while positive values of forcing are obtained during Monsoon ($14 \pm 4 \text{ W/m}^2$) and Pre-Monsoon ($8 \pm 2 \text{ W/m}^2$) seasons. Different properties of aerosols and differences in their vertical distribution give rise to different heating rates within the atmosphere during different seasons. Using several sensitivity studies we have emphasized the importance of diurnal variations in the amount of insolation, solar zenith angle and other related factors in modulating the values of aerosol radiative forcing. Average value of net ($LW + SW$) direct aerosol radiative forcing over Bay of Bengal region, computed using the measured values of AOD, are in the range of -30.6 to -26.6 W/m^2 at the surface and -8.4 to 10.6 W/m^2 at the TOA. Magnitude of LW forcing is found to be less ($\sim 10\%$) compared to its SW counterpart, both at the surface and TOA. Result of a sensitivity test shows that LW aerosol forcing decreases with the increase in column water vapor. Over Central India, we find the diurnally averaged SW forcing at the surface to be negative in the range of -15 to -40 W/m^2 and $+0.7$ to about -11 W/m^2 at the TOA. Our results indicate towards a possible gradient in the atmospheric forcing due to aerosols during Indian winter season from Arabian Sea in the west, peninsular India in the middle and Bay of Bengal in the east. During a field campaign over New Delhi, we find a large negative forcing at the surface, in the range of -40 to -86 W/m^2 , while forcing at the TOA varied between -2 and $+3 \text{ W/m}^2$.

Summary and Scope for Future Work

The present study has been carried out to characterize the physical and optical properties of aerosols that are mainly present over urban regions. Major part of this research work is devoted to understand the seasonal and inter-annual variabilities in various aerosol parameters measured over Ahmedabad, an industrialized urban location in western India. Two cases of long range transport of aerosols have been studied. First one refers to transport of naturally produced dust aerosols from various arid and semi arid regions of west Asia, Northern Africa and North West India to our study location which is an urban site in western India. This provided us a unique opportunity to study the behavior of urban aerosols, mainly characterized by presence of anthropogenic aerosols such as soot, sulfates etc., which get influenced by the transported dust particles from western arid regions. Other transport pathway which has been studied during the present work involves transport of anthropogenic aerosols from highly populated urban and industrialized areas of Indo-Gangetic plain to the otherwise clean oceanic region of Bay of Bengal as well as transport of aerosols from North Indian regions to central India during the Dry winter season. Finally, implications of variabilities in aerosol parameters in terms of their potential capability to perturb the radiation budget of the Earth-Atmosphere system are quantified in terms of model estimates of aerosol radiative forcing at all the study locations. We have carried out further model estimates to know the sensitivity of aerosol radiative forcing to various parameters required as input to the radiative transfer calculations. Important results obtained from the present study are summarized below.

- Major aerosol parameters studied include: column AOD spectra, aerosol mass concentration, their number size distribution, BC mass concentration, wavelength de-

pendency in absorption by aerosols, scattering coefficient, single scattering albedo and vertical distribution of aerosols in the atmosphere.

- The four years data obtained over Ahmedabad are classified into four major seasons viz. Dry (December to March), Pre-Monsoon (April-May), Monsoon (June-September) and Post-Monsoon (October-November).
- Results from size distribution measurements show the dominance of smaller size particles during Dry and Post-Monsoon seasons while increase in coarser particles during Pre-Monsoon and Monsoon seasons, a signature of the long range transport of dust particles from the west.
- Average clear sky AOD at $0.5 \mu\text{m}$ is found to be 0.31 ± 0.07 , 0.41 ± 0.09 , 0.43 ± 0.12 and 0.42 ± 0.07 during Dry, Pre-Monsoon, Monsoon and Post-Monsoon seasons respectively. Higher AODs during Monsoon is a combined effect of increased dust transported from the west as well as increased boundary layer height which could accommodate more aerosols.
- Vertical distribution of aerosol for Dry and Post-Monsoon seasons are characterized by high values of extinction coefficients within first few hundred meters from the surface while Monsoon season profiles show presence of a thick and stable aerosol layer between 0.5 and 2.0 km, contributing significantly to the columnar AODs.
- Seasonal variation in near surface aerosol number concentration is found to be maximum for nucleation mode aerosols (60% spread about the mean), followed by accumulation (26%) and coarse (17%) mode aerosols.
- Highest value of surface level BC mass concentration is obtained during Post-Monsoon ($7.3 \pm 3.7 \mu\text{g}/\text{m}^3$) while lowest value is measured during Monsoon season ($1.5 \pm 0.8 \mu\text{g}/\text{m}^3$). Large production of soot particles from waste burning activities, having increased absorption efficiency, in addition to the fossil fuel and industrial emissions brings down the single scattering albedo to 0.73 during Post-Monsoon and Dry season compared to relatively higher values around 0.85 during Pre-Monsoon season.
- Bay of Bengal cruise study shows higher aerosol number concentrations as well as higher extinction values over northern and coastal areas of Bay of Bengal, indicat-

ing transport of anthropogenic aerosols from the Indo-Gangetic plain during winter season.

- Estimated value of aerosol scale height is found to be low over northern Bay of Bengal due to relatively larger contribution of boundary layer aerosols to the total columnar AOD values, showing that majority of transport takes place within the planetary boundary layer over BoB in contrast to the western region where free tropospheric transport is found to be important.
- We find an excess absorption of about 30% compared to what is expected from equivalent mass of BC from fossil fuel burning over the central Indian region, indicating presence of significant quantities of other absorbing aerosols from biofuel/biomass burning. During winter, the central and peninsular India is influenced by the fine soot particles of fossil fuel origin from the north which gets mixed with the locally produced soot particles mainly produced from biofuel/biomass burning.
- An overall increasing trend in single scattering albedo is observed towards the end of dry winter season, indicating unequal changes in source strength or removal processes of absorbing and scattering type aerosols.
- In order to study the wintertime haze and fog over Indo-Gangetic belt, complementary measurements of various physical and optical parameters of aerosols were made from New Delhi in December 2004. Average clear sky AOD at $0.5 \mu\text{m}$ is 0.91 ± 0.48 , which is higher than AOD values reported for most other cities in India during the same season. Single scattering albedo at $0.525 \mu\text{m}$ varied between 0.6 and 0.8 with an average value of 0.68 for the period of our study in New Delhi.
- Lidar observations during a Fog event reveal a collapse of the vertical distribution of aerosols to an extremely dense and shallow atmospheric layer of merely 200 m height from the surface. While scattering and absorption characteristics remain almost same prior to the formation of fog, slightly higher Relative humidity resulted in fog formation on 18 December while 19th remained hazy.
- Two different approaches are followed to generate spectral values of various aerosol parameters required as input to the radiative transfer calculations, and the computed aerosol radiative forcing values are found comparable for both methods.

- Magnitude of surface forcing are found to be highest during Post-Monsoon ($-63 \pm 10 W/m^2$), which is followed by Dry season (-54 ± 6) and lower values during Pre-Monsoon (-41.4 ± 5) and Monsoon (-41 ± 11) seasons, over Ahmedabad.
- In the case of TOA, aerosol forcing is found to be negative during Dry ($-26 \pm 3 W/m^2$) and Post-Monsoon ($-22 \pm 3 W/m^2$), while positive values are obtained during Monsoon ($14 \pm 4 W/m^2$) and Pre-Monsoon ($8 \pm 2 W/m^2$) seasons.
- Different properties of aerosols and differences in their vertical distribution give rise to different heating rates within the atmosphere for different seasons. Surface level heating rates are found to be highest during Post-Monsoon ($5.6^0 K/day$) while higher atmospheric heating is observed between 1 – 2 km altitudes during Monsoon season.
- Results from several sensitivity studies have emphasized the importance of diurnal variations in the amount of insolation, solar zenith angle and other related factors in modulating the values of aerosol radiative forcing over our location.
- Result from a sensitivity study showed LW aerosol forcing to decrease with increase in water vapor column content in the atmosphere
- In the study over central India, a large negative forcing at the surface in the range of -15 to $-40 W/m^2$ is found, while forcing at the TOA varied between $+0.7$ to $-11 W/m^2$. Negative ARF at the TOA over central India and its increasing trend towards the end of Dry winter season indicates the presence of significant amount of scattering type aerosols and their increasing relative dominance over the period of our study.
- Our results indicate towards a possible gradient that exists in the atmospheric forcing due to aerosols from the Arabian Sea in the west ($7.8 W/m^2$), peninsular India in the middle ($22 \pm 4 W/m^2$) and the BoB in the east ($25 - 31 W/m^2$), during the winter season.

For semi-arid region like Ahmedabad, rainfall and aerosol loading in the atmosphere are intricately related to each other. This is because on the one hand, amount and type of aerosols which act as cloud condensation nuclei (CCN) together with the available moisture in the atmosphere decides the amount of rainfall that occurs over the region, while

on the other hand, more frequent rainfall leads to moist soil and helps vegetation to grow, which in turn curtails the amount of soil derived dust aerosol loading in the atmosphere and can have possible impacts on subsequent weather patterns. Besides this, we observe in our study that, due to large difference between TOA and surface forcing values, larger amount of heat is trapped by aerosols within the atmosphere during Monsoon and Pre-Monsoon seasons. This can have much larger implications for the regional scale dynamical process such as wind flow, convection scheme and even precipitation patterns [Ramanathan *et al.*, 2005]. It is very much essential to understand how the Earth-Atmosphere system responds to such large scale perturbations with cooling at the surface and warming in the lower troposphere. Since aerosols are key to the formation of CCN required for rainfall, seasonal and inter-annual variabilities of major aerosol parameters measured over this site will be very useful for the future studies related to the role of aerosols on monsoon rainfall over the region. The monsoon rain serves as a source of fresh water and helps millions of farmers across the country whose livelihood depends on agriculture. So, it is of great interest to study, using regional scale climate model (RegCM), how the seasonal and inter annual variabilities in aerosol parameters measured over different regions are correlated with the spatial distribution of the monsoon rainfall and affect other climate parameters in general. Finally, it is necessary that observations and modelling studies should complement each other for further improvement in our understanding of climate change occurring in recent times (post-industrial period) as this will help in reducing uncertainties in the future projections of how aerosols influence climate.

References

- Ackerman, A. S., O. B. Toon, D. E. Stevens, A. J. Heymsfield, V. Ramanathan, and E. J. Welton (2000), Reduction of tropical cloudiness by soot, *Science*, 288, 1042-1047.
- Anderson, T. L., D. S. Covert, J. D. Wheeler, J. M. Harris, K. D. Perry, B. E. Trost, D. J. Jaffe, J. A. Ogren (1999), Aerosol backscatter fraction and single scattering albedo: Measured values and uncertainties at a coastal station in the Pacific Northwest, *J. Geophys. Res.*, 104(D21), 26793-26808, 10.1029/1999JD900172.
- Angstrom, A. (1964), techniques of determining the turbidity of the atmosphere, *Tellus*, 13, 214.
- Akimoto, H. (2003), Global Air Quality and Pollution, *Science*, 302, 1716–1719.
- Andreae, M.O., (1995), Climatic effects of changing atmospheric aerosol levels. In: Henderson Sellers, A. (Ed.), *World Survey of Climatology*, vol. 16, *Future Climates of the World*, Elsevier, NewYork, pp. 341-392.
- Babu, S. S., S. K. Satheesh, and K. K. Moorthy (2002), Aerosol radiative forcing due to enhanced black carbon at an urban site in India, *Geophys. Res. Lett.*, 29(18), 1880, doi:10.1029/2002GL015826.
- Babu, S. S., and K. K. Moorthy (2002), Aerosol black carbon over a tropical coastal station in India, *Geophys. Res. Lett.*, 29(23), 2098, doi:10.1029/2002GL015662.
- Bates, T. S, et al. (1998), Processes controlling the distribution of aerosol particles in the lower marine boundary layer during the First Aerosol Characterization Experiment (ACE-1), *J. Geophys. Res.*, 103, 16,369-16,383.

- Bergstrom, R. W., P. B. Russell and P. Hignett (2002), Wavelength dependence of the absorption of Black Carbon particles: predictions and results from the TARFOX experiment and implications for the aerosol single scattering albedo, *J. Atmos. Sci.*, 59, 567–577.
- Bergstrom, R. W., P. Pilewskie, B. Schmid and P. B. Russell (2003), Estimates of the spectral aerosol single scattering albedo and aerosol radiative effects during SAFARI 2000, *J. Geophys. Res.*, 108, D13, 8474, DOI:10.1029/2002JD002435.
- Bodhaine, B. A. (1995), Aerosol absorption measurements at Barrow, Mauna Loa and the south pole, *J. Geophys. Res.*, 100, 8967–8975.
- Bohren, C. F., and D. R. Hoffman (1983), Absorption and Scattering of Light by Small Particles, Wiley, New York, pp. 530.
- Bond, T. C. (2001), Spectral dependence of visible light absorption by carbonaceous particles emitted from coal combustion, *Geophys. Res. Lett.*, 28, 4075–4078.
- Cachorro, V. E., R. Vergaz, and A. M. de Frutos (2001), A quantitative comparison of α -Angstrom turbidity parameter retrieved in different spectral ranges based on spectroradiometer solar radiation measurements, *Atmos. Environ.*, 35, 5117–5124.
- Campbell, J. R., D. L. Hlavka, E. J. Welton, C. J. Flynn, D. D. Turner, J. D. Spinhirne, V. S. Scott, and I. H. Hwang (2002), Full-time, eye-safe cloud and aerosol lidar observation at Atmospheric Radiation Measurement Program sites: Instrument and data processing, *J. Atmos. Oceanic Technol.*, 19, 431–442.
- Charlson, R. J., N. C. Ahlquist and H. Horvath (1968), On the generality of correlation of atmospheric aerosol mass concentration and light scatter, *Atmos. Environ.*, 2, 455–464.
- Charlson, R. J., S. E. Schwartz, J. M. Hales, R. D. Cess, J. A. Coakley, J. E. Hansen, and D. J. Hoffmann (1992), Climate forcing by anthropogenic aerosols, *Science*, 255, 423–430.
- Chung, C. E., and G. J. Zhang (2004), Impact of absorbing aerosol on precipitation: Dynamic aspects in association with convective available potential energy and convective parametrization closure and dependence on aerosol heating profile, *J. Geophys. Res.*, 109, D22103, doi:10.1029/2004JD004726.

- Chung, C. E., V. Ramanathan, D. Kim, and I. A. Podgorny (2005), Global anthropogenic aerosol direct forcing derived from satellite and ground-based observations, *J. Geophys. Res.*, *110*, D24207, doi:10.1029/2005JD006356.
- Crutzen, P. J. (2004), New Directions: The growing urban heat and pollution island effect impact on chemistry and climate, *Atmos. Environ.*, *38*, 3539–3540.
- d’Almeida, G. A., P. Koepke and E. P. Shettle (1991), Atmospheric Aerosols: Global Climatology and Radiative Characteristics, A. Deepak, Hampton, Va., pp. 559.
- Devara, P.C.S., Maheskumar R.S., Raj P.E., Dani K.K., Pandithurai G. and Rao Y.J. (1999), Correlative measurements of aerosol optical depth and size distribution around INDOEX-IFP98 from multi-spectral solar radiometry, *Current Science*, *76*, 977–980.
- Devara, P. C. S., R. S. Maheskumar, P. E. Raj, G. Pandithurai, K. K. Dani (2002), Recent trends in aerosol climatology and air pollution as inferred from multi-year lidar observations over a tropical urban station, *Int. J. Clim.*, *22*, 435–449.
- Eck, T. F., B. N. Holben, J. S. Reid, O. Dubovik, A. Smirnov, N. T. O’Neill, I. Slutsker, and S. Kinne (1999), Wavelength dependence of the optical depth of biomass burning, urban, and desert dust aerosols, *J. Geophys. Res.*, *104*, 31,333–31,349.
- Exton, H. J., Latham, J., P. M. Park, S. J. Perry, M. H. Smith and R.R. Allan (1985), The production and dispersion of marine aerosols, *Q. J. Meteorol. Soc.*, *III*, 817–837.
- Fitzgerald, J. W. (1991), Marine aerosols: A review, *J. Atmos. Sci.*, *39*, 1838–1852.
- Frank, G., et al. (1998), Droplet Formation and Growth in Polluted Fogs, *Contr. Atmos. Phys.*, *71*(1), 65–85.
- Franke, K., A. Ansmann, D. Müller, D. Althausen, C. Venkataraman, M. S. Reddy, F. Wagner, and R. Scheele (2003), Optical properties of the Indo-Asian layer over the tropical Indian Ocean, *J. Geophys. Res.*, *108*(D2), 4059, doi:10.1029/2002JD002473.
- Gadhavi, H. (2005), Experimental investigation of aerosol properties and modelling its impact on radiation budget, Ph.D. Thesis, Gujarat University, Ahmedabad.
- Gaffney, J.S. and N. A. Marley (2003), ‘Atmospheric Chemistry and Air Pollution,’ *Scientific World* (invited mini review) *3*:199-234.

- Ganguly, D., A. Jayaraman and H. Gadhavi (2005a), In situ ship cruise measurements of mass concentration and size distribution of aerosols over Bay of Bengal and their radiative impacts, *J. Geophys. Res.*, 110, D06205, doi:10.1029/2004JD005325.
- Ganguly, D., A. Jayaraman, H. Gadhavi and T. A. Rajesh (2005b), Features in wavelength dependence of aerosol absorption observed over central India, *Geophys. Res. Lett.* 32, L13821, doi:10.1029/2005GL023023.
- Ganguly, D., H. Gadhavi, A. Jayaraman, T. A. Rajesh and A. Misra (2005c), Single scattering albedo of aerosols over the central India: Implications for the regional aerosol radiative forcing, *Geophys. Res. Lett.* 32, L18803, doi:10.1029/2005GL023903.
- Ganguly, D., A. Jayaraman, T. A. Rajesh and H. Gadhavi (2006), Wintertime aerosol properties during foggy and non-foggy days over urban center Delhi and their implications to Short Wave radiative forcing, *J. Geophys. Res.*, doi:10.1029/2005JD007029 [In Press].
- Gundel, L. A., R. L. Dod, H. Rosen and T. Novakov(1984), The relationship between optical attenuation and black carbon concentrations for ambient and source particles, *Sci. Total Environ.*, 36, 197–202.
- Gong, S. L., L. A. Barrie and J. P. Blanchet (1997), Modelling of sea salt aerosols in the atmosphere, 1, model development, *J. Geophys. Res.*, 102, 3805–3818.
- Grey, H. A., G. R. Cass, J. J. Huntzicker, E. K. Heyerdahl and J. A. Rau (1986), Characteristics of Atmospheric Organic and Elemental Carbon Particle Concentrations in Los Angeles, *Environ. Sci. Technol.*, 20(6), 580–589.
- Han, Z., D. C. Montague, J. R. Snider (2003), Airborne measurements of aerosol extinction in the lower and middle troposphere over Wyoming, USA, *Atmos. Environ.*, 37, 789–802.
- Hansen, A. D. A., H. Rosen and T. Novakov (1982), Real-time measurement of the absorption coefficient of aerosol particles, *Appl. Opt.*, 21, 3060–3062.
- Hansen, A. D. A., H. Rosen and T. Novakov(1984), The Aethalometer - an instrument for the real-time measurement of optical absorption by aerosol particles, *Sci. Total Environ.*, 36, 191–196.

- Hansen, J., M. Sato, and R. Ruedy (1997), Radiative forcing and climate response, *J. Geophys. Res.*, *102*, 6831-6864.
- Haywood, J. M., and V. Ramaswamy (1998), Global sensitivity studies of the direct radiative forcing due to anthropogenic sulfate and black carbon aerosols, *J. Geophys. Res.*, *103*, 6043-6058.
- Haywood, J., O. Boucher (2000), Estimates of the direct and indirect radiative forcing due to tropospheric aerosols: A review, *Rev. Geophys.*, *38(4)*, 10.1029/1999RG000078, 513-543.
- Heintzenberg, J. and R. J. Charlson (1996), Design and applications of the Integrating Nephelometer: A Review, *J. Atmos. Oceanic Technol.*, *13*, 987-1000.
- Hess, M., P. Keopke and I. Schult (1998), Optical Properties of aerosols and clouds: The software package OPAC, *Bull. Am. Meteorol. Soc.*, *79*, 831-844.
- Hoppel, W.A., J.W. Fitzgerald, G.M. Frick, R.E. Larson (1990), Aerosol size distributions and optical properties found in the marine boundary layer over Atlantic Ocean, *J. Geophys. Res.*, *95*, 3659-3686.
- Ichoku, C., R. Levy, Y. J. Kaufman, L. A. Remer, R. R. Li, V. J. Martins, B. N. Holben, N. Abuhassan, I. Slutsker, T. F. Eck, C. Pietras (2002), Analysis of the performance characteristics of the five-channel Microtops II Sun photometer for measuring aerosol optical thickness and precipitable water vapor, *J. Geophys. Res.*, *107(D13)*, 4179, doi:10.1029/2001JD001302.
- Ignatov, A. M., L. L. Stowe, S. M. Sakerin and G. K. Korotaev (1995), Validation of NOAA/NESDIS satellite aerosol product over North Atlantic in 1989, *J. Geophys. Res.*, *100*, D3, 5123-5132.
- Intergovernmental Panel on Climate Change (IPCC) (2001), *Climate Change 2001: The Scientific Basis, Contribution of Working Group I to the Third Assessment Report of the Intergovernmental Panel on Climate Change*, edited by J. T. Houghton et al., 944 pp., Cambridge Univ. Press, New York.
- Jacobson, M. Z. (2000), A physically-based treatment of elemental carbon optics: implications for global direct forcing of aerosols, *Geophys. Res. Lett.*, *27(2)*, 217-220.

- Jacobson, M. Z. (2001), Strong Radiative heating due to the mixing state of black carbon in the atmospheric aerosols, *Nature*, 409, 695–697.
- Jacobson, M. Z. (2002), Control of fossil-fuel particulate black carbon and organic matter, possibly the most effective method of slowing global warming, *J. Geophys. Res.*, 107(D19), 4410, doi:10.1029/2001JD001376.
- Jaenicke, R. (1993), Tropospheric aerosols in aerosol-cloud-climate interactions, edited by P. V. Hobbs, Academic, San Diego, Calif. pp. 1–31.
- Jayaraman, A., S. Ramachandran and Y.B. Acharya (1995), Pinatubo volcanic aerosol layer observed at Ahmedabad (23.03⁰N, 72.55⁰E) India, using Nd:YAG backscatter lidar, *J. Geophys. Res.*, 100, 23209-23214.
- Jayaraman, A., D. Lubin, S. Ramachandran, V. Ramanathan, E. Woodbridge, W. D. Collins and K. S. Zalpuri (1998), Direct observations of aerosol radiative forcing over tropical Indian Ocean during the January-February 1996 pre-INDOEX cruise, *J. Geophys. Res.*, 103, 13827-13836.
- Jayaraman, A., S. K. Satheesh, A. P. Mitra and V. Ramanathan (2001a), Latitude gradient in aerosol properties across the Inter Tropical Convergence Zone: Results from the joint Indo-US study on board Sagar Kanya, *Curr. Sci.*, 80, 128-137.
- Jayaraman, A. (2001b), Aerosol Radiative Forcing over the Tropical Indian Ocean, *Proc. Ind. Nat. Sci. Acd. (Phy. Sci.)* 67, 385-394.
- Jayaraman, A., H. Gadhavi, D. Ganguly, A. Misra, S. Ramachandran and T. Rajesh (2006), Spatial variation in aerosol characteristics over central India observed during the February 2004 road campaign experiment, *Atmos. Environ.*, doi:10.1016/j.atmosenv.2006.01.034 [In Press].
- Jin, M., J. M. Shepherd, and M. D. King (2005), Urban aerosols and their variations with clouds and rainfall: A case study for New York and Houston, *J. Geophys. Res.*, 110, D10S20, doi:10.1029/2004JD005081.
- Kaestner M., (1986), Lidar inversion with variable backscatter/extinction ratios: comment, *Appl. Opt.*, 25, 833–835.

- Kaufman, Y. J., D. Tanre and O. Boucher (2002), A satellite view of aerosols in the climate system, *Nature*, 419, 215–223.
- Kiehl, J. T. and B. P. Briegleb (1993), The radiative roles of sulphate aerosols and greenhouse gases in climate forcing, *Science*, 260, 311–314.
- Kiehl, J. T., and H. Rodhe (1995), Modeling geographical and seasonal forcing due to aerosols in *Aerosol Forcing of Climate*, edited by R. J. Charlson and J. Heintzenberg, Wiley, New York, pp. 281–296.
- Kirchstetter, T. W., T. Novakov and P. V. Hobbs (2004), Evidence that the spectral dependence of light absorption by aerosols is affected by organic carbon, *J. Geophys. Res.*, 109, D21208, doi:10.1029/2004JD004999.
- King, M. D., D. M. Byrne, B. M. Herman and J. A. Regan (1978), Aerosol size distributions obtained by inversion of spectral optical depth measurements, *J. Atmos. Sci.*, 35, 2153–2167.
- King, M. D. (1982), Sensitivity of constrained linear inversions to the selection of the Lagrange multiplier, *J. Atmos. Sci.*, 39, 1356–1369.
- Klett J. D., (1985), Lidar inversion with variable backscatter/extinction ratios, *Appl. Opt.*, 24, 1638–1643.
- Koponen, I. K., A. Virkkula, R. Hillamo, V. M. Kerminen, M. Kulumala (2002), Number size distributions and concentrations of marine aerosols: Observations during a cruise between the English Channel and coast of Antarctica, *J. Geophys. Res.*, 107(D24), doi:10.1029/2002JD002533.
- Koponen, I. K., A. Virkkula, R. Hillamo, V. M. Kerminen, M. Kulumala (2003), Number size distributions and concentrations of continental summer aerosols in Queen Maud Land, Antarctica, *J. Geophys. Res.*, 108(D18), doi:10.1029/2003JD003614.
- Krishnamurti, T. N., B. Jha, J.M. Prospero, A. Jayaraman and V. Ramanathan (1998), Aerosol and pollutant transport over the tropical Indian Ocean during the 1996 north-east monsoon and the impact on radiative forcing, *Tellus*, 50(B), 521–542.

- Krishnan, P. and P. K. Kunhikrishnan (2004), Temporal variations of ventilation coefficient at a tropical Indian station using UHF wind profiler, *Curr. Sci.*, 86(3), 447–451.
- Latha, K. M. and K. V. S. Badrinath (2005), Seasonal variations of black carbon aerosols and total aerosol mass concentrations over urban environment in India, *Atmos. Environ.*, 39, 4129–4141.
- Lawless, P. A., C. E. Rodes, D. S. Ensor (2004), Multiwavelength absorbance of filter deposits for determination of environmental tobacco smoke and black carbon, *Atmos. Environ.*, 38, 3373–3383.
- Leon, J.-F., and M. Legrand, Mineral dust sources in the surroundings of the north Indian Ocean (2003), *Geophys. Res. Lett.*, 30(6), 1309, doi:10.1029/2002GL016690.
- Li, F. and V. Ramanathan (2002), Winter to summer monsoon variation of aerosol optical depth over the tropical Indian Ocean, *J. Geophys. Res.*, 107(D16), 4284, doi:10.1029/2001JD000949.
- Lillis, D., C. N. Cruz, J. Collett Jr., L. W. Richards, S. N. Pandis (1999), Production and removal of aerosol in a polluted fog layer: model evaluation and fog effect on PM, *Atmos. Environ.*, 33, 4797–4816.
- Lindberg, J. D. (1993), Carbon and the optical properties of atmospheric dust, *Applied Optics*, 32, 6077–6081.
- Lubin, D., S. K. Satheesh, G. McFarquar and A. J. Heymsfield (2002), Longwave radiative forcing of Indian Ocean tropospheric aerosol, *J. Geophys. Res.*, 107(D19), 8004, doi:10.1029/2001JD001183.
- McClatchey, R. A., R. W. Fenn, J. E. A. Selby, F. E. Volz, and J. S. Garing (1972), Optical properties of the atmosphere, 3rd ed., *Environ. Res. Pap.* 411, 108 pp., Air Force Cambridge Res. Lab., Cambridge, Mass.
- Malm, W. C., D. E. Day (2001), Estimates of aerosol species scattering characteristics as a function of relative humidity, *Atmos. Environ.*, 35, 2845–2860.
- Menon, S., J. Hansen, L. Nazarenko, and Y. Luo (2002), Climate effects of black carbon aerosols in China and India, *Science*, 297, 2250–2253.

- Monkkonen, P., R. Uma, D. Srinivasan, I. K. Koponen, K. E. J. Lehtinen, K. Hameri, R. Suresh, V. P. Sharma, and M. Kulmala (2004), Relationship and variations of aerosol number and PM10 mass concentrations in a highly polluted urban environment New Delhi, India, *Atmos. Environ.*, *38*, 425-433.
- Moorthy, K. K., K. Niranjana, B. Narasimhamurthy, V. V. Agashe, and B. V. Krishna Murthy (1999), Aerosol climatology over India: 1. ISRO GBP MWR Network and database, ISRO-GBP Sci. Rep. 03-99, Indian Space Res. Organ., Bangalore.
- Moorthy, K. K., A. Saha and K. Niranjana (2001), Spatial variation of aerosol spectral optical depth and columnar water vapor content over the Arabian Sea and Indian Ocean during the IFP of INDOEX, *Curr. Sci.*, *80*, 145–150.
- Moorthy, K. K., S. S. Babu and S. K. Satheesh (2003), Aerosol spectral optical depths over Bay of Bengal: Role of transport, *Geophys. Res. Lett.*, *30*(5), 1249, doi:10.1029/2002GL016520.
- Moorthy, K. K., S. S. Babu, S. V. Sunilkumar, P. K. Gupta and B. S. Gera (2004), Altitude profiles of aerosol BC, derived from aircraft measurements over an inland urban location in India, *Geophys. Res. Lett.*, *31*, L22103, doi:10.1029/2004GL021336.
- Moorthy, K. K., et al. (2005), Wintertime spatial characteristics of boundary layer aerosols over peninsular India, *J. Geophys. Res.*, *110*, D08207, doi:10.1029/2004JD005520.
- Moosmuller, H., W. P. Arnott, C. F. Rogers, J. C. Chow, C. A. Frazier, L. E. Sherman and D. L. Dietrich (1998), Photoacoustic and filter measurements related to aerosol light absorption during the Northern Front Range Air Quality Study (Colorado 1996/1997) *J. Geophys. Res.*, *103*, 28,149–28,157.
- Morys, M., F. M. Mims III, S. Hagerup, S. E. Anderson, A. Baker, J. Kia and T. Walkup (2001), Design calibration, and performance of MICROTOPS II handheld ozone monitor and sun photometer, *J. Geophys. Res.*, *106*(D13), 14,573-14,582.
- Nemesure, S., R. Wagner and S. E. Schwartz (1995), Direct shortwave forcing of climate by the anthropogenic sulfate aerosol: Sensitivity to particle size, composition, and relative humidity. *J. Geophys. Res.*, *100*(D12), 26105–26116.

- Nessler, R., E. Weingartner, U. Baltensperger (2005), Effect of humidity on aerosol light absorption and its implications for extinction and the single scattering albedo illustrated for a site in the lower free troposphere, *J. Aerosol Sci.*, 36, 958–972.
- Niranjan, K., B. Malleswara Rao, Auromeet Saha, and K.S.R. Murty (2004), Aerosol spectral optical depths and size characteristics at a coastal industrial location in India effect of synoptic and mesoscale weather, *Ann. Geophys.*, 22, 1851–1860.
- Niranjan, K., B. Malleswara Rao, P. S. Brahmanandam, B. L. Madhavan, V. Sreekanth, and K. Krishna Moorthy (2005), Spatial characteristics of aerosol physical properties over the northeastern parts of peninsular India, *Ann. Geophys.*, 23, 3219–3227.
- Novakov, T., M. O. Andreae, R. Gabriel, T. W. Kirchstetter, O. L. Mayol-Bracero and V. Ramanathan (2000), Origin of carbonaceous aerosols over the tropical Indian Ocean: Biomass burning or fossil fuel, *Geophys. Res. Lett.*, 27(24), 4061–4064.
- Novakov, T., S. Menon, T. W. Kirchstetter, D. Koch, and J. E. Hansen (2005), Aerosol organic carbon to black carbon ratios: Analysis of published data and implications for climate forcing, *J. Geophys. Res.*, 110, D21205, doi:10.1029/2005JD005977.
- Pandis, S. N. and J. H. Seinfeld (1990), The Smog-Fog-Smog cycle and acid deposition, *J. Geophys. Res.*, 95(D11), 18,489–18,500.
- Pandithurai, G., R. T. Pinker, T. Takamura and P. C. S. Devara (2004), Aerosol radiative forcing over a tropical urban city in India, *Geophys. Res. Lett.*, 31, L12107, doi:10.1029/2004GL019702.
- Pasricha, P. K., B. S. Gera, S. Shastri, H. K. Maini, A. B. Ghosh, M. K. Tiwari, and S. C. Garg (2003), Role of the water vapor greenhouse effect in the forecasting of fog occurrence, *Boundary Layer Meteorol.*, 107(2), 469–482.
- Pearce, F. (1992), Back to the days of deadly smogs, *New Scientist*, 136(1850), 24–28.
- Penner, J.E., R.J. Charlson, J.M. Hales, N.S. Laulainen, R. Leifer, T. Novakov, J. Ogren, L.F. Radke, S.E. Schwartz, and L. Travis (1994), Quantifying and minimizing uncertainty of climate forcing by anthropogenic aerosols. *Bull. Amer. Meteor. Soc.*, 75, 375–400.

- Pilinis, C., S. N. Pandis, J. H. Seinfeld (1995), Sensitivity of direct climate forcing by atmospheric aerosols to aerosol size and composition, *J. Geophys. Res.*, 100(D9), 18739-18754, 10.1029/95JD02119.
- Porter, J. N., and A. D. Clarke (1997), Aerosol size distribution models based on in situ measurements, *J. Geophys. Res.*, 102, 6035-6045.
- Prospero, J.M. (1979), Mineral and sea salt aerosol concentrations in various ocean regions, *J. Geophys. Res.*, 84, 725-731.
- Qiu, J., L. Yang and X. Zhang (2004), Characteristics of imaginary part and single-scattering albedo of urban aerosols in northern China, *Tellus*, 56B, 276-284.
- Quinn, P. K., V. N. Kasputin, T. S. Bates and D.S. Covert(1996), Chemical and optical properties of marine boundary layer aerosol particles of the mid-Pacific in relation to sources and meteorological transport , *J. Geophys. Res.*, 101(D3), 6931-6952.
- Rajeev, K., V. Ramanathan, and J. Meywerk (2000), Regional aerosol distribution and its long-range transport over the Indian Ocean, *J. Geophys. Res.*, 105(D2), 2029-2044.
- Ramachandran, S. and A. Jayaraman (2002), Premonsoon aerosol loading and size distribution over the Arabian Sea and the Tropical Indian Ocean, *J. Geophys. Res.*, 107(D24), 4738, doi:10.1029/2002JD002386.
- Ramachandran, S. and A. Jayaraman (2003a), Spectral aerosol optical depths over Bay of Bengal and Chennai: I - Measurements, *Atmos. Environ.*, 37, 1941-1949.
- Ramachandran, S. and A. Jayaraman (2003b), Spectral aerosol optical depths over Bay of Bengal and Chennai: II - sources, anthropogenic influence and model estimates, *Atmos. Environ.*, 37, 1951-1962.
- Ramachandran, S. (2005), Premonsoon shortwave aerosol radiative forcings over the Arabian Sea and tropical Indian Ocean: Yearly and monthly mean variabilities, *J. Geophys. Res.*, 110, D07207, doi:10.1029/2004JD005563.
- Ramana, M., V. Ramanathan, I. A. Podgorny B. B. Pradhan and B. Shrestha (2004), The direct observations of large aerosol radiative forcing over the Himalayan region, *Geophys. Res. Lett.*, 31, L05111, doi:10.1029/2003GL018824.

- Ramanathan, V., et al. (2001a), Indian Ocean Experiment: An integrated analysis of the climate and the great Indo-Asian haze, *J. Geophys. Res.*, 106(D22), 28,371–28,398.
- Ramanathan, V., P. J. Crutzen, J. T. Kiehl and D. Rosenfeld (2001b), Aerosols, climate and the hydrological cycle, *Science*, 294, 2119–2124.
- Ramanathan, V. and P. J. Crutzen (2003), New Directions: Atmospheric Brown Clouds, *Atmos. Environ.*, 37, 4033–4035.
- Ramanathan, V., C. Chung, D. Kim, T. Bettge, L. Buja, J. T. Kiehl, W. M. Washington, Q. Fu, D. R. Sikka and M. Wild (2005), Atmospheric brown clouds: Impacts on South Asian climate and hydrological cycle, *PNAS*, 102, 5326–5333.
- Ramaswamy, V., et al. (2001), Radiative forcing of climate change, in *Climate Change 2001: The Scientific Basis*, by H. T. Houghton et al., chap. 6, pp. 349–416, Cambridge Univ. Press, New York.
- Rao, Y. J. and P. C. S. Devara (2001), Characterization of aerosols over Indian Ocean and Arabian Sea during INDOEX I/P-99, *Curr. Sci.*, 80, 120–122.
- Rastogi, N. and M. M. Sarin (2005), Long-term characterization of ionic species in aerosols from urban and high-altitude sites in western India: Role of mineral dust and anthropogenic sources, *Atmos. Environ.*, 39, 5541–5554.
- Reddy, M. S. and C. Venkataraman (2002), Inventory of aerosol and sulphur dioxide emissions from India: II-Biomass combustion, *Atmos. Environ.*, 36, 699–712.
- Redemann, J., P. B. Russell and P. Hamill (2001), Dependence of aerosol light absorption and single-scattering albedo on ambient relative humidity for sulfate aerosols with black carbon cores, *J. Geophys. Res.*, 106(D21), 27,485–27,495.
- Reid, J.S., T. F. Eck, S. A. Christopher, P. V. Hobbs, B. N. Holben (1999), Use of the Angstrom exponent to estimate the variability of optical and physical properties of aging smoke particles in Brazil. *J. Geophys. Res.*, 104, 27473–27489.
- Ricchiazzi, P., S. Yang, C. Gautier and D. Sowle (1998), SBDART, A research and teaching tool for plane-parallel radiative transfer in the Earth's atmosphere, *Bull. Am. Meteorol. Soc.*, 79, 2101–2114.

- Russell, P. B. et al. (2002), Comparison of aerosol single scattering albedos derived by diverse techniques in two North Atlantic experiments, *J. Atmos. Sci.*, *59*, 609–619.
- Sagar, R., B. Kumar, U. C. Dumka, K. K. Moorthy, and P. Pant (2004), Characteristics of aerosol spectral optical depths over Manora Peak: A high-altitude station in the central Himalayas, *J. Geophys. Res.*, *109*, D06207, doi:10.1029/2003JD003954.
- Salam, A., H. Bauer, K. Kassin, S. M. Ullah and H. Puxbaum (2003), Aerosol chemical characteristics of an island site in the Bay of Bengal (Bhola - Bangladesh), *J. Environ. Monit.*, *5*, 1–9
- Satheesh, S. K., K. K. Moorthy and B. V. Murthy (1998), Spatial gradients in aerosol characteristics over the Arabian Sea and Indian Ocean, *J. Geophys. Res.*, *103*(D20), 26,183–26,192.
- Satheesh, S. K., V. Ramanathan, Xu Li-Jones, I. A. Podgorny, J. M. Prospero, B. N. Holben and N. G. Loeb (1999), A model for the natural and anthropogenic aerosols over the tropical Indian Ocean derived from Indian Ocean Experiment, *J. Geophys. Res.*, *104*(D22), 27,421–27,440.
- Satheesh, S. K. and V. Ramanathan (2000), Large differences in tropical aerosol forcing at the top of the atmosphere and at the Earth's surface, *Nature*, *405*, 60–62.
- Satheesh, S. K., K. K. Moorthy and I. Das (2001), Aerosol spectral optical depths over Bay of Bengal, Indian Ocean and Arabian Sea, *Current Sci.*, *81*, 1617–1625.
- Satheesh, S. K. (2002), Radiative forcing by aerosols over Bay of Bengal region, *Geophys. Res. Lett.*, *29*(22), 2083, doi:10.1029/2002GL015334.
- Satheesh, S. K. and K. Krishna Moorthy (2005), Radiative effects of natural aerosols: A review, *Atmos Environ*, *39*, 2089-2110.
- Schnaiter, M., H. Hovath, O. Mohler, K. H. Naumann, H. Saathoff and O. W. Schock (2003), UV-VIS-NIR spectral optical properties of soot and soot-containing aerosols, *J. Aerosol Sci.*, *34*, 1421–1444.
- Seinfeld, J. H. and S. N. Pandis (1998), Atmospheric chemistry and physics: From air pollution to climate change, *Wiley-Interscience*, USA, pp. 1326.

- Shepherd, J. M., H. Pierce, and A. J. Negri (2002), Rainfall modification by major urban areas: Observations from spaceborne rain radar on the TRMM satellite. *J. Appl. Meteor.*, *41*, 689-701.
- Singh, R. P., S. Dey, S. N. Tripathi, V. Tare, and B. Holben (2004), Variability of aerosol parameters over Kanpur, northern India, *J. Geophys. Res.*, *109*, D23206, doi:10.1029/2004JD004966.
- Singh, S., S. Nath, R. Kohli, and R. Singh (2005), Aerosols over Delhi during pre-monsoon months: Characteristics and effects on surface radiation forcing, *Geophys. Res. Lett.*, *32*, L13808, doi:10.1029/2005GL023062.
- Smirnov, A., B. N. Holben, D. Savoie, J. M. Prospero, Y. J. Kaufman, T. F. Eck and I. Slutsker (2000), Relationship between column aerosol optical thickness and in situ ground based dust concentrations over Barbados, *Geophys. Res. Lett.*, *27*(11), 1643–1646.
- Stamnes, K., S. C. Tsay, W. Wiscombe, and K. Jayaweera (1988), Numerically stable algorithm for discrete-ordinate-method radiative transfer in multiple scattering and emitting layered media, *Appl. Opt.*, *27*, 2502–2509.
- Stowe, L. L., A. M. Ignatov and R. R. Singh (1997), Development, validation and potential enhancements to the second generation operational aerosol product at the National Environmental satellite, data and information service of the National Oceanic and Atmospheric Administration, *J. Geophys. Res.*, *102*, D14, 16,923–16,934.
- Svenningsson, B. et al. (1997), Cloud droplet nucleation scavenging in relation to the size and hygroscopic behaviour of aerosol particles, *Atmos. Environ.*, *31*, 2463–2475.
- Takemura, T., T. Nakajima, O. Dubovik, B. N. Holben and S. Kinne (2002), Single scattering albedo and radiative forcing of various aerosol species with a global three dimensional model, *J. Climate*, *15*(4), 333–352.
- Tang, I. N. and H. R. Munkelwitz (1993), Composition and temperature dependence of the deliquescence properties of hygroscopic aerosols, *Atmos. Environ.*, *27A*, 467–473.
- Tang, I. N. (1996), Chemical and size effects of hygroscopic aerosols on light scattering coefficients, *J. Geophys. Res.*, *101*(D14), 19,245–19,250.

- Tomasi, C. and F. Prodi(1982), Measurements of atmospheric turbidity and vertical mass loading of particle matter in marine environments, *J. Geophys. Res.*, *87*, 1279-1286.
- Tripathi, S. N., S. Dey, V. Tare, and S. K. Satheesh (2005), Aerosol black carbon radiative forcing at an industrial city in northern India, *Geophys. Res. Lett.*, *32*, L08802, doi:10.1029/2005GL022515.
- UNDP, cited 2001: World Urbanization Prospects: The 2001 Revision. [Available online at www.un.org/esa/population/publications/wup2001.]
- UNEP Assessment Report (2002), The Asian Brown Cloud: Climate and Other Environmental Impacts, UNEP/DEWA/RS.02-3; Available at www.rrcap.unep.org/abc/impactstudy/.
- Venkataraman, C., K. Reddy, S. Josson, and M. S. Reddy (2002), Aerosol size and chemical characteristics at Mumbai, India, during the INDOEX-IFP (1999), *Atmos. Environ.*, *36*, 1979-1991.
- Venkataraman, C., G. Habib, A. E. Fernandez, A. H. Miguel, S. K. Friedlander (2005), Residential biofuels in South Asia: Carbonaceous aerosol emissions and climate impacts, *Science*, *307*, 1454–1456.
- Villevalde, Y.V., A.V. Smirnov, N.T. O'Neill, S.P. Smyshlyaev, V.V. Yakovlev (1994), Measurement of aerosol optical depth in the Pacific Ocean and North Atlantic, *J. Geophys. Res.*, *99*, 20,983–20,988.
- Vinoj, V., S. S. Babu, S. K. Satheesh, K. Krishna Moorthy and Y. J. Kaufman(2004), Radiative forcing by aerosols over the Bay of Bengal region derived from shipborne, island-based, and satellite (Moderate-Resolution Imaging Spectroradiometer) observations, *J. Geophys. Res.*, *109*, D05203, doi:10.1029/2003JD004329.
- Voss, K. J., E. J. Welton, P. K. Quinn, J. Johnson, A. M. Thompson and H. R. Gordon, (2001), Lidar Measurements during Aerosol99, *J. Geophys. Res.*, *106*, 20821–20831.
- Weingartner, E., H. Saathoff, M. Schnaiter, N. Streit, B. Bitnar and U. Baltensperger (2003), Absorption of light by soot particles; determination of the absorption coefficient by means of aethalometers, *J. Aerosol Sci.*, *34*, 1445–1463.

- Welton, E. J., et al. (2000), Ground-based Lidar Measurements of Aerosols during ACE-2: Instrument description, Results, and comparisons with other ground-based and airborne measurements, *Tellus*, 52B, 635–650.
- Welton E. J., K. J. Voss, P. K. Quinn, P. J. Flatau, K. Markowicz, J. R. Campbell, J. D. Spinhirne, H. R. Gordon and J. E. Johnson, (2002), Measurements of aerosol vertical profiles and optical properties during INDOEX 1999 using micro pulse lidars, *J. Geophys. Res.*, 107, 8019, doi:10.1029/2000JD000038.
- Wielicki, B. A., T. Wong, N. Loeb, P. Minnis, K. Priestley and R. Kandel (2005), Changes in Earth's Albedo Measured by Satellite, *Science*, 308, 825.
- Young, S. A., D. R. Cutten, M. J. Lynch and J. E. Davies (1993), Lidar-derived variations in the backscatter-to-extinction ratio in southern hemisphere coastal maritime aerosols, *Atmos. Environ.*, 27, 1541–1551.
- Young, A. T. (1994), Air mass and refraction, *Appl. Opt.*, 33(6), 1108–1110.

List of Publications

I. In Refereed Journals:

- Ganguly, D., A. Jayaraman, T. A. Rajesh, H. Gadhavi (2006), Wintertime aerosol properties during foggy and non-foggy days over urban center Delhi and their implications to Short Wave radiative forcing, *J. Geophys. Res.*, doi:10.1029/2005JD007029 [In Press].
- Jayaraman, A., H. Gadhavi, D. Ganguly, A. Misra, S. Ramachandran and T. Rajesh (2006), Spatial variation in aerosol characteristics over central India observed during the February 2004 road campaign experiment, *Atmos. Environ.*, doi:10.1016/j.atmosenv.2006.01.034 [In Press].
- Ganguly, D., H. Gadhavi, A. Jayaraman, T. A. Rajesh and A. Misra (2005c), Single scattering albedo of aerosols over the central India: Implications for the regional aerosol radiative forcing, *Geophys. Res. Lett.* 32, L18803, doi:10.1029/2005GL023903.
- Ganguly, D., A. Jayaraman, H. Gadhavi and T. A. Rajesh (2005b), Features in wavelength dependence of aerosol absorption observed over central India, *Geophys. Res. Lett.* 32, L13821, doi:10.1029/2005GL023023.
- Ganguly, D., A. Jayaraman and H. Gadhavi (2005a), In situ ship cruise measurements of mass concentration and size distribution of aerosols over Bay of Bengal and their radiative impacts, *J. Geophys. Res.*, 110, D06205, doi:10.1029/2004JD005325.

II. In Proceedings/Abstracts of Symposium/Conference:

- Ganguly D., A. Jayaraman, T. A. Rajesh and H. Gadhavi, Wintertime aerosol properties during foggy and non-foggy days over urban centre Delhi and their implications to aerosol radiative forcing, *14th National Space Science Symposium*, Vishakhapatnam, India, 9-12 Feb., 2006.
- Ganguly D., A. Jayaraman, T. A. Rajesh and H. Gadhavi, Modulation of aerosol physical properties during a fog episode in Delhi, *4th Asian Aerosol Conference*, Mumbai, India, 13-16 Dec., 2005.
- Ganguly D., A. Jayaraman and H. Gadhavi, Observational study on aerosol optical properties over the Indian region and estimation of their radiative forcing, *European Research School on Atmospheres*, Grenoble, France, Jan-Feb 2005.
- Ganguly D., A. Jayaraman, H. Gadhavi and T. A. Rajesh, Spatial variation in aerosol characteristics studied during the ISRO-GBP land campaign-1: Feb 2004, *IASTA Meeting and International Conference on: Aerosols Clouds and Indian Monsoon*, Kanpur, India, vol. 16 (1 & 2), 15-17 November, 2004.
- Jayaraman, A., H. Gadhavi and D. Ganguly, Lidar observations of inter and intra annual variations in aerosol profiles over an urban site in India, *8th International Global Atmospheric Chemistry Conference*, Christchurch, New Zealand, 4-9 Sep., 2004.
- Jayaraman, A., H. Gadhavi, D. Ganguly and A. Misra, Lidar, sun-photometer and QCM studies of summertime variation in aerosol characteristics over Ahmedabad, *13th National Space Science Symposium*, Kottayam, India, 17-20 Feb., 2004.
- Ganguly, D. and A. Jayaraman, Cruise study of aerosol size distribution over Bay of Bengal, *13th National Space Science Symposium*, Kottayam, India, 17-20 Feb., 2004.
- Ganguly, D., H. Gadhavi and A. Jayaraman, Pre monsoon aerosol characteristics over Ahmedabad, Proceedings of the conference on *Aerosol remote sensing in global change and atmospheric pollution* organized by IASTA, Thiruvananthapuram, India, vol. 14(1), 18-20 Sep., 2002.